DOCTORAL THESIS

The Gutzwiller Approach to out-of-equilibrium correlated fermions

Author:

Matteo SANDRI

Supervisor:

Prof. Michele FABRIZIO

ma per seguir virtute e canoscenza

SISSA

Thesis submitted for the degree of Doctor of Philosophy

Contents

Summary

The Gutzwiller Approach to out-of-equilibrium correlated fermions

by Matteo SANDRI

Correlated electron systems represent a wide class of materials which at equilibrium display fascinating properties. Several recent experimental breakthroughs in the field of femtosecond spectroscopy and cold atomic gases allow nowadays to investigate the real time dynamics of these many-body quantum systems. Since strongly correlated systems usually escape single particle approaches, the theoretical study of their dynamics constitutes a formidable problem which necessitates the development of novel techniques.

In this Thesis we investigate the out-of-equilibrium physics of simple paradigmatic models that are believed to capture some essential physics of interacting fermions by means of the time dependent extension of the Gutzwiller Variational Approach.

After an introductory Chapter on the recent results in this field, in Chapter 2 we present the Gutzwiller Approach in-and-out of equilibrium.

In Chapter 3 we investigate the dynamics for the single band Hubbard model after a linear ramp of the Coulomb interaction. We will show that a dynamical transition appears for any duration of the ramp; this dynamical point is adiabatically connected to the zero temperature Metal-to-Insulator transition. We will then consider the role of quantum fluctuations beyond mean field.

In Chapter 4 we consider the dynamics of an initial antiferromagnetic state under a quench of the interaction in the single band fermionic Hubbard model. We will show that non-thermal ordered states survive more than expected and that two different nonequilibrium antiferromagnets can be distinguished. Finally in Chapter 5 we will consider a two-band Hubbard model which we believe captures the main physics of the paradigmatic compound vanadium sesquioxide, V_2O_3. After an investigation of the equilibrium properties for this model, we will provide evidences that non-thermal metallic phases can emerge upon an excitation of a Mott insulator.

. . .

Chapter 1

Introduction

The behavior of a generic system when driven out-of-equilibrium represents one of the fundamental questions in physics. In particular, the dynamics of quantum systems with a large number of interacting particles is of primarily interest since, in principle, it is necessary to interpret and predict experiments where matter is excited by an external perturbation.

Electronic materials with partially filled d and f bands constitute a wide class of quantum many-body systems which deserve particular attention. These compounds are usually characterized by the strong Coulomb interaction between electrons which, in many cases, is responsible for very unusual physical properties and fascinating phase transitions, such as high temperature superconductivity in cuprates and the Mott transition in oxides. Intuition would suggest a likewise rich counterpart when these strongly correlated materials are excited out-of-equilibrium.

In the last decade several experimental breakthroughs in the field of femtosecond spectroscopy and cold atomic systems rendered this expectation a concrete scenario, providing access to the unitary out-of-equilibrium dynamics of quantum many-body systems. This new characterization of materials, which was not accessible through common experimental probes due to the extremely short timescale of electrons in solids, introduces nowadays a complementary point of view with respect to the usual equilibrium or near-to-equilibrium one of the past. Equilibrium phase diagrams, in fact, are enriched with a novel and "orthogonal" *time axis* dimension. Transitions between different thermodynamic phases can be observed *in real time* or, even more fascinating, the emergence of novel phases of matter with no equilibrium counterpart can be discovered and manipulated.

The comprehension of quantum nonequilibrium physics therefore, apart from awakening old theoretical problems which still wait for a solution, has become a today's fundamental step forward that we should reach in order to govern matter for future technologies.

This necessity calls for the development of novel theoretical techniques which, differently from the common near-to-equilibrium methods adopted in the past, can deal with strongly correlated electrons far-from-equilibrium.

In the following paragraphs we will briefly recapitulate the main experimental and theoretical advances on this front which motivated the scope of the present Thesis.

1.1   Correlated systems out-of-equilibrium

The simplest experimental setup to investigate ultrafast dynamics in solids is by means of a pump-probe experiment. In this setup a sample is excited by a first ultrafast *pump* pulse while a second delayed pulse is used to *probe* the system after a given interval of time Δt. Refined solid state laser techniques allow nowadays to excite out-of-equilibrium bulk materials and control the interval Δt on timescales of the order of femtoseconds [1–3], thus smaller than the typical relaxation time of the system. On these very short timescales, the system can be considered isolated from the environment. Pumping-and-probing repeatedly the sample with different delays, dynamical processes can then be recorded in real time. This technique has been recently used to study the out-of-equilibrium dynamics of Mott or Charge-Transfer insulators [1, 2, 4] and unconventional superconductors [5, 6], just to mention some.

The relaxational dynamics in a solid is in general characterized by the interplay of several excitations at different energy scales. Femtosecond spectroscopy, accessing different timescales, opens the possibility to dynamically disentangle multiple degrees of freedom, thus providing an orthogonal point of view in cases where several competing mechanisms determine rich equilibrium phase diagrams [4, 7, 8].

An example is given by the electronic and phononic degrees of freedom, which are usually characterized by two well separated energy scales. In this case, a two temperature model can often be used. It assumes that electrons rapidly thermalize on timescales of the order of femtoseconds to an effective temperature much higher than the temperature of the lattice. This is due to electron-electron interactions. Subsequently, electron-phonon interactions mediate a slower relaxation of the hot electron gas. This approximation has recently been applied with success in [5] for example, where electronic contributions could be disentangled from phononic ones in a high-T_c superconductor.

This picture however becomes useless whenever the true relaxation dynamics of the electrons has to be resolved. Such circumstance is particularly relevant for photo-excited materials in vicinity of a Mott transition [8]. An example is the photo-induced

Insulator-to-Metal transition observed in 1T-TaS2, in which the breakdown of the electronic energy gap, attributed to a purely electronic process, is directly measured on a timescale shorter than $100 fs$ [2].

Moreover, the two temperature model becomes questionable when the relaxation time of electrons is not much faster than the typical energy scale of phonons [9]. This might be caused by strong correlation which, in some cases, prevents a thermal relaxation of the electronic degrees of freedom up to very long times [10]. Such scenario is of extreme interest for systems that are excited through an equilibrium phase transition in which some kind of long-range order is formed or destroyed. Long-lived phases with no thermal counterpart can indeed emerge in this circumstance, as predicted for example in [11], where an antiferromagnetic ordered state survives well above the corresponding Néel temperature.

The description of such situations inevitably requires theoretical methods that do not rely on a quasi-equilibrium approximation.

Apart from solid state materials, which historically provided a "nature-given" class of quantum many-body systems, a second one that has emerged in the last two decades is represented by cold atomic gases. Since the first experimental realization in 1995 of Bose-Einstein condensation, there has been an enormous progress in the engineerization of these artificial macroscopic quantum many-body systems [12]. Three main aspects have revealed to be crucial in the development of this field. First of all these systems are almost perfectly isolated from the environment, which leads to the possibility to observe truly quantum unitary evolution. Moreover, optical lattices and trapping potentials allow to artificially create almost arbitrary lattice structures and reduced dimensionalities. Finally, the development of the Feshbach resonance technique allows to tune (even in time) the interaction strength between the atoms.

Combining together these unprecedented degrees of tunability, cold atomic systems, differently from solid state materials, provide a clean realization of simple model Hamiltonians which for some decades have been considered popular toy-models to capture low energy physics of more complex systems.

The ability to change the Hamiltonian parameters together with the long observational times attainable[1] has *de facto* opened the path towards the real time observation of paradigmatic models that have been the subject of intensive theoretical studies since the introduction of quantum mechanics. A milestone in this context is the seminal experiment of *Greiner et al.* in which they succeeded in observing collapse and revival oscillations of the matter wave interference pattern for a Bose-Einstein condensate after

---

[1]In cold atomic systems typical relaxation times can be of the order of milliseconds.

a sudden change of the strength of the lattice depth in a Bose Hubbard model [13].
A second landmark experiment by *Kinoshita et al.* established that trapped Rb condensates thermalize rapidly when confined in three-dimensional geometries, while they show a slow relaxation in quasi-one-dimensional traps [14]. The difference in the one-dimensional case has been attributed to the vicinity of an integrable model, a one-dimensional hard core bosons system, thus starting a (still open) debate on the role of integrability in quantum dynamics.

Although the energy scales and the microscopic degrees of freedom in solid state materials and cold atomic systems are very different, the physical mechanisms which govern the time evolution of these many-body systems follow similar lines, thus representing a fascinating example of universality [15]. Not surprisingly, these experiments inevitably boosted a fervid theoretical discussion regarding the dynamics of quantum systems.

1.2   Theoretical implications

From a theoretical point of view, the main framework of quantum dynamics and quantum statistical physics was formulated at the beginning of the last century. However, the experimental progresses described in the previous paragraphs posed a serious challenge both for a deeper comprehension of such thematic and for a practical implementation of predictive methods necessary to describe the out-of-equilibrium behavior of quantum matter.

Regarding these issues, a great effort so far has been concentrated on the old debate on the dynamics of a *closed* quantum system [16]. In fact, although oversimplified, a first theoretical framework to describe the out-of-equilibrium physics in cold atoms and femtosecond spectroscopy experiments is to assume that the effect of the external perturbation is to leave the system in an isolated initial highly excited state. A simple theoretical rephrasing of this excitation scheme is the paradigm of a *quantum quench*[2] [17]. In practice one considers a closed quantum system initially in the ground state $|\Psi\rangle_0$ of an Hamiltonian $\mathcal{H}(u_i)$ that depends on a global parameter u_i; at a certain time t, this parameter is changed to a new one resulting in the final Hamiltonian $\mathcal{H}(u_f)$. In this way one can parametrize an initial state that corresponds to an excited state of the final Hamiltonian.
Having in mind the experimental situations aforementioned, important questions on the

---

[2]In the following the quantum quench has to be intended as a variation of a global (not local) parameter of the Hamiltonian.

dynamics of this excited state rise. Does the system relax towards thermal equilibrium or non-thermal long-lived or stationary states? On which timescales does relaxation occur?

For classical systems with many degrees of freedom the concept of thermalization is connected to the concept of *ergodicity*. In general one expects that the high complexity of the Hamilton's equations of motion leads to a chaotic dynamics of the orbits which eventually covers uniformly all the available phase space and redistribute the injected energy among the different degrees of freedom. In this case the long time average of an observable coincides with its statistical average over the phase space so that the details of the initial configuration are "washed away" at long times with the solely exception of few integrals of motions, *in primis* the internal energy and the number of particles. Many cases are also known in which ergodicity is broken, the easiest and extreme scenario being represented by integrable models. In this circumstance the system is characterized by a number of integrals of motion equal to the number of degrees of freedom, so that the complete coverage of the phase space is prohibited.

A direct transposition of classical ergodicity and ergodicity breaking to the quantum case is not an obvious task. This is clear if one realizes that thermalization cannot be attributed solely to a property of the evolving state through its time dependent density matrix operator $\hat{\rho}(t) = |\Psi(t)\rangle\langle\Psi(t)|$. An initial pure state remains pure during time evolution, i.e. $\text{Tr}[\hat{\rho}^2(t)] = 1$, therefore there is no way for the initial density matrix to relax into the Boltzmann-Gibbs thermal distribution[3] characterized by $\text{Tr}[\hat{\rho}_{eq}^2] < 1$. One may still define thermalization in a weaker sense requiring that the long time average of common local observables relaxes to the Boltzmann-Gibbs prediction

$$\lim_{\tau \to \infty} \frac{1}{\tau} \int_0^\tau dt \langle\Psi(t)|\hat{O}|\Psi(t)\rangle = \text{Tr}[\hat{\rho}_{eq}\hat{O}]$$

at an effective temperature such that the internal energy (constant in time) equals the thermal one.

For non-integrable models the wisdom is that thermalization, in this sense, takes place, even though the mechanism beyond it remains still unclear. A widely known scenario which accounts for thermalization is the so called *Eigenstate Thermalization Hypothesis*, which states that thermalization occurs eigenstate by eigenstate, in the sense that the average value of certain observables on a single energy eigenstate is equal to the microcanonical one [18, 19]. If this is the case, provided the initial condition is sufficiently narrow in energy, thermalization would occur.

---

[3]For finite size systems one should consider the microcanonical ensemble. In the limit of large system sizes, the two ensembles are equivalent.

Indeed there have been works supporting this expectation [10, 20–22] even though several numerical evidences suggest the contrary, with a lack of thermalization at least for the longest times reached in simulations [11, 23–25]. In this situation it is of particular relevance the role played by strong interaction and spatial dishomogeneities which might be responsible for trapping the dynamics in long-lived metastable states that show no relaxation towards thermal equilibrium [23, 26, 27].

As in classical physics, thermalization is instead expected to fail for quantum integrable systems where many constants of motion constrain the dynamics. For these systems an intuitive generalization of the Boltzmann-Gibbs distribution has been proposed, the so called *Generalized Gibbs Ensemble*, which is constructed from a maximum information entropy ensemble compatible with the constants of motion [28]. The GGE has proven to reproduce correctly the long-time stationary values for simple observables in several cases [28–31], however there is yet no conclusive proof regarding the validity of this ansatz [32] and some results even indicate a failure of GGE for specific observables and initial states [33–35].

The crossover from integrable to non-integrable systems arises further important questions. Recent analyses indicate that nearly-integrable systems display a two-stage relaxation towards equilibrium, characterized by a short time relaxation to a non-thermal state known as *prethermalization*, followed by a much slower decay towards thermal equilibrium [36–39]. The concept of prethermalization might however be more general and connected to the presence of non-thermal fixed points which do not necessary require the existence of an integrable limit, [40, 41].

Overall, these studies highlight that, apart from the characterization of the long time dynamics, the approach to the stationary state in many cases is not characterized by a simple relaxation, but instead reveals relevant features, with the appearance of different timescales that might be even separated by sharp singularities, i.e. *dynamical transitions*. The characterization of these dynamical critical points, their nature and their possible universal behavior represents a current important issue, as we shall see in the rest of this Thesis.

1.3 Interacting fermions and the Gutzwiller Approach

A complete understanding of the problems introduced above is a challenging task, as witnessed by the amount of questions that, almost one hundred years after the introduction of quantum mechanics, are still unsolved. The main difficulty resides in the fact that novel theoretical approaches have to be developed which can deal with both

interaction and nonequilibrium dynamics for large systems. Most of the theoretical results aforementioned have been found by analyzing the dynamics of simple paradigmatic one-dimensional or finite size models, also triggered by their realization in cold atomic experiments. For these systems, exact solutions or effective analytical approximations are in some cases available; otherwise, exact diagonalization methods and the time-dependent Density Matrix Renormalization Group (DMRG) [42] represent a valid and in principle exact numerical approach, although they are bounded to small system sizes and finite simulation times.

Quantum quench in the fermionic Hubbard model

Calculations in more realistic multi-dimensional models, which are necessary in order to describe real solid state materials, are much more difficult to tackle and indeed they pose a formidable numerical problem even at equilibrium. This motivated historically the introduction of simpler minimal models capable of reproducing the main physical mechanisms of strong correlation in electronic systems. The paradigmatic example in this case is the single band fermionic Hubbard model, which entails the competition between the itinerant and atomic nature of electrons in a solid. This model is commonly used to provide a simple interpretation of femtosecond experiments in correlated materials, see for example Ref. [2], but it has recently been realized also by means of cold atomic systems [43].
The Hubbard model, although being already a simplification of real materials, is generally not solvable analytically. Several approximation and numerical schemes therefore have been developed in the past in order to deal with strong correlation at equilibrium. The recent interest in nonequilibrium problems has driven the extension of most of these techniques to treat time dependent situations and, not surprisingly, the Hubbard model has represented the test-bed system to address quantum dynamics in correlated fermions [44].

The time evolution under the Hubbard Hamiltonian has been firstly studied by a perturbative approach, the flow equation method, in [45]. Later, similar results have been found by Keldish diagrammatic expansion technique [37]. These works considered the evolution of an initial non-interacting state subject to a sudden quench of the Coulomb strength U. The picture that emerged is that, for small values of the interaction quench, the short-to-intermediate times regime displays the build-up of a prethermal state characterized by a non-thermal Fermi-liquid behavior of the momentum distribution, with thermalization that was argued to occur only on much larger times [45]. The trapping into non-thermal states was also observed in the limit of very large quenches, for which

the final Hamiltonian approaches the opposite integrable atomic limit and shows collapse and revival oscillations [10].

Apart from perturbative calculations, these results were confirmed by the time dependent extension of Dynamical Mean Field Theory (DMFT). This method maps a lattice model into a local impurity problem coupled to a self-consistent determined bath and, becoming exact in the limit of infinite coordination number, represents the state of the art technique to treat correlated fermions in dimensions higher than one[4] [15].

Non-equilibrium DMFT reproduced the presence of two different prethermal regimes which trap the dynamics in metastable states and delay thermalization. Moreover, DMFT results highlighted that these two regimes are separated by a critical region at which one-time observables, and also correlation functions, display a fast thermalization [10]. This critical region was argued to identify a *dynamical phase transition*. The presence of a dynamical critical point has been subsequently discovered within the time-dependent Gutzwiller Approach (t-GA) [49] and recently sustained in *one* and *two dimensions* by means of high order perturbative calculations [46, 50]. Similar dynamical critical points have been found within mean field theories in various models [51–55].

The Gutzwiller Variational Approach

The single band fermionic Hubbard model already displays much of the paradigmatic properties that drove the out-of-equilibrium discussions in the last years. In fact, many concepts, such as the dynamical phase transition, originated from the dynamics of the Hubbard model. Apart from the relaxation dynamics after a quench of the interaction, in several recent works the dynamics for the Hubbard model coupled to an external electromagnetic field has also been considered in order to achieve a more realistic description of experiments, [9, 56, 57].

Being the simplest scenario to describe correlated compounds, the results so far obtained for the Hubbard Hamiltonian encourage both a deeper understanding of some issues that remain still open (i.e. the nature of the dynamical transition) and the analysis of more realistic extensions of the model which eventually are suitable to describe with greater accuracy real correlated materials. Non-equilibrium DMFT has recently been extended in several directions, such as to treat the coupling with an external electromagnetic field, inhomogeneous systems, ordered phases, electron-phonon interactions (for a detailed review see [15]). Although in many cases a perturbative solution of the impurity problem renders the numerical computation affordable [58, 59], this method quickly becomes very demanding.

---

[4]Only few works in dimensions greater than one and smaller than infinity are known [46–48], hence leaving the regime between these two extremes far from being theoretically understood.

On the contrary, less expensive methods played an important historical role in describing the equilibrium physics of correlated materials. Among them it is not exaggerated to say that the Gutzwiller Variational Approach [60, 61] has proven to be a fundamental *non perturbative* tool for the understanding of strong correlation effects, with the most famous example being probably represented by the Brinkmann-Rice scenario for the Mott-transition [62].

At zero temperature, the Gutzwiller Variational Approach introduces a variational wavefunction which has to be optimized in order to minimize the ground state energy of the system. An analytical approximation to compute average values on this wavefunction, known as the Gutzwiller Approximation, greatly simplifies calculations and has shown to become exact in the limit of infinite coordination number [63]. Thenceforth this method has benefited from continuous improvements and nowadays represents a flexible tool which can be integrated with Density Functional Theory (DFT) to give results even in quantitative agreement with DMFT+DFT [64–66].

The agility of the Gutzwiller Approximation, combined with the important role played at equilibrium, motivated its recent extension by Schiró and Fabrizio [49] to treat the quantum dynamics of pure states. This technique has been applied with success to investigate the dynamics for the aforementioned quench in the single band Hubbard model, showing to be in agreement with the weak and strong interaction regimes found by other methods. Moreover, the Gutzwiller dynamics predicts a dynamical transition at an intermediate value of quench in very good agreement with the DMFT result [49]. These successes enlighten the intuition that t-GA may represent a fast and reliable numerical method to disclose non trivial dynamical effects where other approaches become prohibitive, thus generating interest in possible applications of the method to more elaborate models and further improvements beyond the Gutzwiller Approximation [67].

In this direction goes the work presented in the Thesis in which we shall present various extensions and applications of the Gutzwiller Approach to treat the time evolution of correlated fermionic systems.

1.4   Plan of the Thesis

The work presented in this Thesis is structured in the following.

Chapter 2 is devoted to present the state of the art of Gutzwiller Approach. We first introduce the Gutzwiller technique for ground states calculations in a general formalism which is suitable to treat generic multiband models. In many situations however, a proper generalization of the method to finite temperatures is necessary, both for a more

realistic description of the phase diagrams of correlated compounds and for a comparison between long time averages obtained from quantum dynamics and the corresponding thermal ones. These reasons motivated our recent extension of the Gutzwiller Approach to finite temperature that we present here.

Finally, we conclude this Chapter by presenting the time dependent extension of the method as introduced by Schiró and Fabrizio [49] and further elaborated in [68]. This Chapter provides the necessary background to analyze different models.

We begin by considering two extensions of the paramagnetic quench in the fermionic Hubbard model. In **Chapter 3** we consider the out-of-equilibrium dynamics induced by a linear ramp of the repulsive interaction U. We study the degree of adiabaticity for this excitation protocol and we investigate the fate of the dynamical transition encountered in the sudden quench case. Finally, we go beyond the Gutzwiller Approach by discussing the role of quantum fluctuations on the mean-field dynamics.

At low temperature, the single band Hubbard model at half filling displays an antiferromagnetic ordered phase [69]. This motivates the work presented in **Chapter 4** in which we investigate the dynamics of an antiferromagnetic state evolved after a sudden change of the repulsion strength U. The energy injected into the system, in the thermalization hypothesis, would allow to dynamically move across the *Temperature vs U* phase diagram and eventually cross the equilibrium phase transition. We find that magnetic order survives more than what is expected on the basis of thermalization arguments and that two different types of out-of-equilibrium antiferromagnets are separated by a dynamical critical point.

In the last Chapter of the Thesis we consider an application of the Gutzwiller Approach to multiband systems, which eventually allows for a more refined description of physical materials. To this extent in **Chapter 5** we introduce a two-orbital model that we believe captures some essential features of V_2O_3. We first apply the finite temperature Gutzwiller approximation to this model and we indeed find that its phase diagram bears many similarities to that of real vanadium sesquioxide. In the final part of the Chapter we investigate the out-of-equilibrium dynamics for this model evidencing the existence of metastable metallic phases which have no equilibrium counterpart.

The results presented in this Thesis are contained in the following publications:

1. Ch. 2, 5 : M. Sandri, M. Capone, and M. Fabrizio, Phys. Rev. B 87, 205108 (2013)

2. Ch. 3   : M. Sandri, M. Schiró, and M. Fabrizio, Phys. Rev. B 86, 075122 (2012)

3. Ch. 4   : M. Sandri and M. Fabrizio, Phys. Rev. B 88, 165113 (2013)

Chapter 2

The Gutzwiller Variational Approach

2.1 The Gutzwiller Approach for ground state calculations

In 1963 Hubbard [70], Gutzwiller [60] and Kanamori [71] proposed independently a model to treat strongly correlated s-electrons in transition metal materials. Thenceforth, the Hubbard model represents a minimal description of electron conduction in metals and can be considered one of the simplest Hamiltonians which displays a competition between the kinetic energy of electrons and the Coulomb interaction. Its form is given by

$$\mathcal{H} = -t \sum_{\langle \mathbf{R},\mathbf{R}' \rangle, \sigma} \left(c^\dagger_{\mathbf{R}\sigma} c_{\mathbf{R}'\sigma} + H.c. \right) + \frac{U}{2} \sum_{\mathbf{R}} (n_{\mathbf{R}} - 1)^2, \tag{2.1}$$

where the operator $c_{\mathbf{R}\sigma}$ annihilates a spin-σ electron at site $\mathbf{R}$, t is the hopping strength between nearest-neighbors, U is the interaction strength and $n_{\mathbf{R}} = \sum_\sigma c^\dagger_{\mathbf{R}\sigma} c_{\mathbf{R}\sigma}$ is the onsite total density.

Despite its innocent looking the Hubbard model describes many landmark phenomena for correlated materials such as the Mott Metal-to-Insulator transition. Apart from the special case of one dimension, the Hamiltonian (2.1) cannot be solved exactly. This motivated a huge theoretical effort in the years with the development of Dynamical Mean Field Theory being probably the main success [69].

A more intuitive and less demanding approximation to the ground state of (2.1) was proposed by Martin Gutzwiller himself immediately after the introduction of the Hubbard model. The main idea beyond this method relies on the observation that the value of double occupancies has to decrease as a function of U, i.e. strong correlation disfavors doubly occupied states and freeze charge fluctuations. Thus, in order to implement this

constraint without breaking any symmetry of the ground state, Gutzwiller introduced a variational wavefunction starting from an uncorrelated metallic state $|\psi\rangle$ (e.g. a Slater determinant) on which double occupancies are projected out depending on a variational parameter $g \in [0, 1]$

$$|\Psi\rangle_G = \prod_{\mathbf{R}} \left(1 - (1 - g)\, n_{\mathbf{R}\uparrow} n_{\mathbf{R}\downarrow}\right) |\psi\rangle. \tag{2.2}$$

The case $g = 1$ corresponds to the non-interacting uncorrelated state, while the case $g = 0$ describes the full suppression of the states with two electrons on the same site. Despite these opposite limits, even on this simplified ansatz it is in general not possible to calculate exactly average values. For this reason Gutzwiller introduced an approximation scheme, which goes under the name of Gutzwiller Approximation, that turns out to be exact in the infinite coordination limit [63], as we shall show below.

Brinkmann and Rice showed that in this limit a Metal-to-Insulator transition is predicted for a finite value of U_c, characterized by the vanishing of double occupancies and of the quasiparticle residue Z. Although the insulating solution within the GA is trivial and misses any description of the incoherent Hubbard bands, the metallic solution can be interpreted in terms of a non-interacting renormalized Hamiltonian whose excitations are usually denoted as Landau-Gutzwiller quasiparticles and give access to the low energy coherent part of the spectrum. This description in terms of renormalized quasiparticles provides a good representation of the Metal-to-Insulator transition from the metallic side. This is completely missed in single particle methods such as the Hartree-Fock approximation, which are therefore unable to predict a transition to an insulating state without breaking translational symmetry.

Such result motivated the success of the Gutzwiller Approach and its further reformulation and application to more complex multiband systems in the years. In this Section we shall present the nowadays most popular form of the Gutzwiller approach as proposed by Bünemann and coworkers and further developed by Fabrizio and Lanatà.

We shall consider a generic tight binding Hamiltonian

$$\mathcal{H} = \sum_{\mathbf{R},\mathbf{R}'} \sum_{ab} \left(t^{ab}_{\mathbf{R}\mathbf{R}'}\, c^{\dagger}_{\mathbf{R}a} c_{\mathbf{R}'b} + H.c.\right) + \sum_{\mathbf{R}} \mathcal{H}_{\mathbf{R}}, \tag{2.3}$$

defined on a lattice with coordination number z, and hopping parameters $t^{ab}_{\mathbf{R}\mathbf{R}'}$ such that their contribution to the total energy is well behaved also in the limit $z \to \infty$. $\mathcal{H}_{\mathbf{R}}$ includes on-site potential and interaction terms.

Starting from the original Gutzwiller ansatz (2.2) we introduce a generic variational wavefunction

$$|\Psi\rangle = \prod_{\mathbf{R}} \mathcal{P}_{\mathbf{R}} |\psi\rangle \tag{2.4}$$

where both the Slater determinant $|\psi\rangle$ and the local *Gutzwiller projector* $\mathcal{P}_{\mathbf{R}}$ must be variationally optimized by requiring the minimization of the total energy

$$E = \frac{\langle \Psi | \mathcal{H} | \Psi \rangle}{\langle \Psi | \Psi \rangle}. \tag{2.5}$$

The computation of the total energy E is in general inaccessible analytically; however Bünemann and collaborators realized that in the limit of infinite coordination number, $z \to \infty$, average values on the Gutzwiller wavefunction can be computed exactly provided that the following constraints are satisfied

$$\langle \psi | \mathcal{P}_{\mathbf{R}}^{\dagger} \mathcal{P}_{\mathbf{R}} | \psi \rangle \stackrel{!}{=} 1 \tag{2.6}$$

$$\langle \psi | \mathcal{P}_{\mathbf{R}}^{\dagger} \mathcal{P}_{\mathbf{R}} \, \mathcal{C}_{\mathbf{R}} | \psi \rangle \stackrel{!}{=} \langle \psi | \mathcal{C}_{\mathbf{R}} | \psi \rangle \tag{2.7}$$

where $\mathcal{C}_{\mathbf{R}}$ is a any single particle operator $c_{\mathbf{R}a}^{\dagger} c_{\mathbf{R}b}$[1]. To show this one starts realizing that, since Wick's theorem can be applied to calculate average values on $|\psi\rangle$, it follows that

$$\langle \psi | \mathcal{P}_{\mathbf{R}}^{\dagger} \mathcal{P}_{\mathbf{R}} \, \mathcal{C}_{\mathbf{R}} | \psi \rangle = \overbrace{\langle \psi | \mathcal{P}_{\mathbf{R}}^{\dagger} \mathcal{P}_{\mathbf{R}} | \psi \rangle}^{=1} \langle \psi | \mathcal{C}_{\mathbf{R}} | \psi \rangle$$
$$+ \; \langle \psi | \mathcal{P}_{\mathbf{R}}^{\dagger} \mathcal{P}_{\mathbf{R}} \, \mathcal{C}_{\mathbf{R}} | \psi \rangle_{\text{connected}}. \tag{2.8}$$

From the constraints (2.6-2.7) we have that the sum of all Wick's contractions of a pair of single fermionic operator with $\mathcal{P}_{\mathbf{R}}^{\dagger} \mathcal{P}_{\mathbf{R}}$ vanishes, $\langle \psi | \mathcal{P}_{\mathbf{R}}^{\dagger} \mathcal{P}_{\mathbf{R}} \, \mathcal{C}_{\mathbf{R}} | \psi \rangle_{\text{connected}} = 0$. This is true also for the contractions of $\mathcal{P}_{\mathbf{R}}^{\dagger} \mathcal{P}_{\mathbf{R}}$ with a pair of fermionic operators at different sites. Moreover in the Appendix we show that in the limit of $z \to \infty$ also the contractions where more than two lines are extracted from the term $\mathcal{P}_{\mathbf{R}}^{\dagger} \mathcal{P}_{\mathbf{R}}$ and contracted with fermionic operators at a different site $\mathbf{R}'$ disappear. This determines a great simplification in the calculation of expectations values.

Indeed, given a local observable $\mathcal{O}_{\mathbf{R}}$, its average value on the Gutzwiller wavefunction becomes

$$\langle \psi | \mathcal{P}^{\dagger} \mathcal{O}_{\mathbf{R}} \mathcal{P} | \psi \rangle = \prod_{\mathbf{R}' \neq \mathbf{R}} \overbrace{\langle \psi | \mathcal{P}_{\mathbf{R}'}^{\dagger} \mathcal{P}_{\mathbf{R}'} | \psi \rangle}^{=1} \langle \psi | \mathcal{P}_{\mathbf{R}}^{\dagger} \mathcal{O}_{\mathbf{R}} \mathcal{P}_{\mathbf{R}} | \psi \rangle$$
$$+ \; \langle \psi | \prod_{\mathbf{R}' \neq \mathbf{R}} (\mathcal{P}_{\mathbf{R}'}^{\dagger} \mathcal{P}_{\mathbf{R}'}) \, \mathcal{P}_{\mathbf{R}}^{\dagger} \mathcal{O}_{\mathbf{R}} \mathcal{P}_{\mathbf{R}} | \psi \rangle_{\text{connected}}$$
$$= \; \langle \psi | \mathcal{P}_{\mathbf{R}}^{\dagger} \mathcal{O}_{\mathbf{R}} \mathcal{P}_{\mathbf{R}} | \psi \rangle \tag{2.9}$$

with the connected term that vanishes because of the constraint (2.7) and the limit $z \to \infty$. Hence the average value of $\mathcal{O}_{\mathbf{R}}$ can be computed considering only the effect of

---

[1] We shall not consider in the following the presence of a superconducting order parameter, so that we can avoid terms of the form $c_{\mathbf{R}a}^{\dagger} c_{\mathbf{R}b}^{\dagger}$.

the local projector $\mathcal{P}_{\mathbf{R}}$, a great simplification in the calculations.

Similarly, the average value of intersite hopping operators reads

$$\langle\psi| \, \mathcal{P}^{\dagger} \, c^{\dagger}_{\mathbf{R}a} c_{\mathbf{R}'b} \, \mathcal{P} \, |\psi\rangle = \langle\psi| \, \mathcal{P}^{\dagger}_{\mathbf{R}} \, c^{\dagger}_{\mathbf{R}a} \, \mathcal{P}_{\mathbf{R}} \; \mathcal{P}_{\mathbf{R}'} \, c_{\mathbf{R}'b} \, \mathcal{P}_{\mathbf{R}'} \, |\psi\rangle \tag{2.10}$$

and making use of the Wick's theorem it can be written as

$$\langle\psi| \, \mathcal{P}^{\dagger} \, c^{\dagger}_{\mathbf{R}a} c_{\mathbf{R}'b} \, \mathcal{P} \, |\psi\rangle = \sum_{c,d} R^*_{\mathbf{R}ac} \, R_{\mathbf{R}'bd} \, \langle\psi| \, c^{\dagger}_{\mathbf{R}c} c_{\mathbf{R}'d} \, |\psi\rangle \tag{2.11}$$

where the *Gutzwiller renormalization factors* R_{ab} are defined through

$$\langle\psi| \, \mathcal{P}^{\dagger}_{\mathbf{R}} \, c^{\dagger}_{\mathbf{R}a} \, \mathcal{P}_{\mathbf{R}} \, c_{\mathbf{R}b} \, |\psi\rangle = \sum_{c} R^*_{\mathbf{R}ac} \langle\psi| \, c^{\dagger}_{\mathbf{R}c} c_{\mathbf{R}b} \, |\psi\rangle. \tag{2.12}$$

The best variational estimation of the ground state amounts then to find the Slater determinant $|\psi\rangle$ and the projector $\mathcal{P}$ which minimize the energy functional

$$E = \min_{|\psi\rangle, \mathcal{P}} \left[\langle\psi| \, \mathcal{H}_* \, |\psi\rangle + \langle\psi| \, \mathcal{P}^{\dagger}_{\mathbf{R}} \mathcal{H}_{\mathbf{R}} \mathcal{P}_{\mathbf{R}} \, |\psi\rangle \right] \tag{2.13}$$

subject to the Gutzwiller constraints. $\mathcal{H}_*$ is the initial non-interacting part of the Hamiltonian with a renormalized hopping strength $t^{ab}_{\mathbf{R}\mathbf{R}'} \to \sum_{cd} R^*_{\mathbf{R}ca} R_{\mathbf{R}'db} \, t^{cd}_{\mathbf{R}\mathbf{R}'}$.

The mixed-basis representation

In order to perform a numerical minimization of (2.13) we have to introduce a proper parametrization for the Gutzwiller projector. To this extent we follow the proposal of Lanatà *et al.* and we introduce the *natural basis* operators $d^{\dagger}_{\mathbf{R}a}$, $d_{\mathbf{R}a}$ which have the property to diagonalize the local non-interacting density matrix,

$$\langle\psi| \, d^{\dagger}_{\mathbf{R}a} d_{\mathbf{R}b} \, |\psi\rangle = \delta_{ab} \, n^{(0)}_{\mathbf{R}a}. \tag{2.14}$$

Quite generically, the operators $d^{\dagger}_{\mathbf{R}a}$ are related to the original basis $c^{\dagger}_{\mathbf{R}a}$ through a unitary transformation. However, the importance of the mixed-basis formulation relies on the fact that, as we shall show, all calculations can be carried without specifying this unitary transformation. Moreover, since in this representation the local density matrix is diagonal, (2.14), the Gutzwiller constraints are much simplified, thus reducing the complication of the numerical optimization problem.

Upon introducing a basis for the local Fock space

$$|\mathbf{R}; n\rangle = \prod_a \left(d^\dagger_{\mathbf{R}a}\right)^{n_a} |0\rangle \qquad (2.15)$$

and equivalently a set of local states in the original basis $|\mathbf{R}; \Gamma\rangle$, we can parametrize the local Gutzwiller projector in the mixed-basis representation as

$$\mathcal{P}_{\mathbf{R}} = \sum_{\Gamma n} \frac{\Phi_{\mathbf{R};\Gamma n}}{\sqrt{P^{(0)}_{\mathbf{R};n}}} \, |\mathbf{R}; \Gamma\rangle\langle\mathbf{R}; n|, \qquad (2.16)$$

where $P^{(0)}_{\mathbf{R};n}$ is the uncorrelated occupation probability matrix, which is diagonal by definition,

$$P^{(0)}_{\mathbf{R};n} = \langle\psi \, |\mathbf{R}; n\rangle\langle\mathbf{R}; n| \, \psi\rangle = \prod_a \left(n^{(0)}_{\mathbf{R}a}\right)^{n_{\mathbf{R}a}} \left(1 - n^{(0)}_{\mathbf{R}a}\right)^{1-n_{\mathbf{R}a}}. \qquad (2.17)$$

The Gutzwiller variational parameters $\Phi_{\mathbf{R};\Gamma n}$ constitute the elements of a matrix $\hat{\Phi}_{\mathbf{R}}$ and actually correspond to the rotationally invariant slave boson mean field introduced by Lechermann *et al.* [72].

A very effective computation on the Gutzwiller wavefunction can be achieved by introducing a matrix representation also for the creation/annihilation operators and for a given local observable $\mathcal{O}_{\mathbf{R}}$ [64]

$$
\begin{aligned}
\left(\hat{d}^\dagger_{\mathbf{R}a}\right)_{n_1 n_2} &= \langle\mathbf{R}; n_1|d^\dagger_{\mathbf{R}a}|\mathbf{R}; n_2\rangle \\
\left(\hat{c}^\dagger_{\mathbf{R}a}\right)_{\Gamma_1 \Gamma_2} &= \langle\mathbf{R}; \Gamma_1|c^\dagger_{\mathbf{R}a}|\mathbf{R}; \Gamma_2\rangle \\
\left(\hat{O}^\dagger_{\mathbf{R}a}\right)_{\Gamma_1 \Gamma_2} &= \langle\mathbf{R}; \Gamma_1|\mathcal{O}_{\mathbf{R}}|\mathbf{R}; \Gamma_2\rangle.
\end{aligned}
\qquad (2.18)
$$

Within this reformulation one can easily verify that the Gutzwiller constraints (2.6-2.7) can be rewritten as

$$
\begin{aligned}
\langle\psi| \, \mathcal{P}^\dagger_{\mathbf{R}}\mathcal{P}_{\mathbf{R}} \, |\psi\rangle &= \mathrm{Tr}(\hat{\Phi}^\dagger_{\mathbf{R}}\hat{\Phi}_{\mathbf{R}}) \\
&\overset{!}{=} 1
\end{aligned}
\qquad (2.19)
$$

$$
\begin{aligned}
\langle\psi| \, \mathcal{P}^\dagger_{\mathbf{R}}\mathcal{P}_{\mathbf{R}} \, d^\dagger_{\mathbf{R}a}d_{\mathbf{R}b} \, |\psi\rangle &= \mathrm{Tr}(\hat{\Phi}^\dagger_{\mathbf{R}}\hat{\Phi}_{\mathbf{R}} \, \hat{d}^\dagger_{\mathbf{R}a}\hat{d}_{\mathbf{R}b}) \\
&\overset{!}{=} \delta_{ab} \langle\psi| \, d^\dagger_{\mathbf{R}a}d_{\mathbf{R}a} \, |\psi\rangle.
\end{aligned}
\qquad (2.20)
$$

Seemingly, the average value of a local operator $\mathcal{O}_{\mathbf{R}}$ is equal

$$\langle\psi| \, \mathcal{P}^\dagger\mathcal{O}_{\mathbf{R}}\mathcal{P} \, |\psi\rangle = \mathrm{Tr}(\hat{\Phi}^\dagger_{\mathbf{R}}\hat{O}_{\mathbf{R}}\hat{\Phi}_{\mathbf{R}}) \qquad (2.21)$$

and repeating the reasoning that conducted to eq. (2.11), the average value of the intersite hopping operator becomes

$$\langle\psi|\, \mathcal{P}^{\dagger}\, c^{\dagger}_{\mathbf{R}a} c_{\mathbf{R}'b}\, \mathcal{P}\, |\psi\rangle = \sum_{c,d} R^{*}_{\mathbf{R}ac}\, R_{\mathbf{R}'bd}\, \langle\psi|\, d^{\dagger}_{\mathbf{R}c} d_{\mathbf{R}'d}\, |\psi\rangle, \qquad (2.22)$$

where the renormalization factors R_{ab} are defined in this case

$$\langle\psi|\, \mathcal{P}^{\dagger}_{\mathbf{R}}\, c^{\dagger}_{\mathbf{R}a}\, \mathcal{P}_{\mathbf{R}}\, d_{\mathbf{R}b}\, |\psi\rangle = \sum_{c} R^{*}_{\mathbf{R}ac}\langle\psi|\, d^{\dagger}_{\mathbf{R}c} d_{\mathbf{R}b}\, |\psi\rangle = R^{*}_{\mathbf{R}ab}\, n^{(0)}_{\mathbf{R}b}. \qquad (2.23)$$

The last equality follows from the property of the natural basis (2.14). We can arrive to a more compact form for the renormalization factor adopting the matrix representation. Indeed eq. (2.23) is equal to (we use Einstein's convention for index summations and discard site index $\mathbf{R}$)

$$
\begin{aligned}
\langle\psi|\, \mathcal{P}^{\dagger}\, c^{\dagger}_{a}\, \mathcal{P}\, d_{b}\, |\psi\rangle &= \langle\psi|\, \frac{\hat{\Phi}^{\dagger}_{n_1\Gamma_1}}{\sqrt{P^{(0)}_{n_1}}} |n_1\rangle\langle\Gamma_1|\, \hat{c}^{\dagger}_{a\Gamma_2\Gamma_3}|\Gamma_2\rangle\langle\Gamma_3|\, \frac{\hat{\Phi}_{\Gamma_4 n_2}}{\sqrt{P^{(0)}_{n_2}}}|\Gamma_4\rangle\langle n_2|\, \hat{d}_{bn_3n_4}|n_3\rangle\langle n_4|\, \psi\rangle \\
&= \sqrt{\frac{P^{(0)}_{n_1}}{P^{(0)}_{n_2}}} \hat{\Phi}^{\dagger}_{n_1\Gamma_1} \hat{c}^{\dagger}_{a\Gamma_1\Gamma_3} \hat{\Phi}_{\Gamma_3 n_2} \hat{d}_{bn_2n_1}. \qquad (2.24)
\end{aligned}
$$

Since the matrix element $\hat{d}_{bn_2n_1}$ are different from zero only between Fock states $|n_1\rangle$ and $|n_2\rangle$ that differ from the application of the operator d_b, from eq. (2.17) we have that

$$\sqrt{\frac{P^{(0)}_{n_1}}{P^{(0)}_{n_2}}} = \sqrt{\frac{n^{(0)}_{b}}{(1 - n^{(0)}_{b})}}, \qquad (2.25)$$

hence also the renormalization factor acquires an effective form suitable for computation

$$R^{*}_{\mathbf{R}ab} = \frac{1}{\sqrt{n^{(0)}_{\mathbf{R}b}\,(1 - n^{(0)}_{\mathbf{R}b})}}\, \mathrm{Tr}(\, \hat{\Phi}^{\dagger}_{\mathbf{R}} \hat{c}^{\dagger}_{\mathbf{R}a} \hat{\Phi}_{\mathbf{R}} \hat{d}_{\mathbf{R}b}\,). \qquad (2.26)$$

From eq. (2.26) and (2.21) we see that all average values on the Gutzwiller wavefunction can be conveniently computed as matrix multiplications. The matrix $\hat{\Phi}$ will constitute a variational matrix of dimensions 2^{2n}, where n is the number of orbitals, but in general it can be reduced by exploiting the symmetries of the problem. Instead, the matrix elements of the creation/annihilation operators $\hat{c}_a$, $\hat{d}_a$ can be computed and stored ones for all, since they depend only on the definition of the relative basis states. One then realizes that the unitary transformation which connects the original basis to the natural one does not need to be known at any stage in the computation with a great simplification in the method.

Overall the best estimation of the ground state has to be computed by minimizing an energy functional that depends on the Slater determinant $|\psi\rangle$ and the matrix $\hat{\Phi}$ subject to the Gutzwiller constraints (2.19,2.20)

$$E = \min_{|\psi\rangle, \hat{\Phi}} \left[\sum_{\mathbf{R},\mathbf{R}'} \sum_{ab} \left(t_{\mathbf{R}\mathbf{R}'}^{*ab} \langle\psi| d_{\mathbf{R}a}^\dagger d_{\mathbf{R}'b} |\psi\rangle + H.c. \right) + \text{Tr}(\hat{\Phi}_{\mathbf{R}}^\dagger \mathcal{H}_{\mathbf{R}} \hat{\Phi}_{\mathbf{R}}) \right] \qquad (2.27)$$

where the hopping strength is renormalized accordingly to eq. (2.22) as

$$t_{\mathbf{R}\mathbf{R}'}^{*ab} = \sum_{cd} R_{\mathbf{R}ca}^* R_{\mathbf{R}'db} \, t_{\mathbf{R}\mathbf{R}'}^{cd}. \qquad (2.28)$$

The minimization of this energy functional naturally leads to the identification of the renormalized single particle Hamiltonian $\mathcal{H}_*$

$$\mathcal{H}_* = \sum_{\mathbf{R},\mathbf{R}'} \sum_{ab} t_{\mathbf{R}\mathbf{R}'}^{*ab} d_{\mathbf{R}a}^\dagger d_{\mathbf{R}'b} + H.c. - \sum_{\mathbf{R}} \sum_{ab} \mu_{\mathbf{R}ab} d_{\mathbf{R}a}^\dagger d_{\mathbf{R}b} \qquad (2.29)$$

where μ_{ab} are Lagrange multipliers that enforce the constraint $\langle\psi|d_{\mathbf{R}a}^\dagger d_{\mathbf{R}b}|\psi\rangle = \delta_{ab} n_a^{(0)}$.

The Hamiltonian (2.29) has a rigorous meaning only for its ground state which provides the best estimation of the Slater determinant, $|\psi_0\rangle$, in the construction of the Gutzwiller wavefunction. However, following the reasoning beyond Landau's theory of Fermi liquids, it is common to construct coherent excitations within the GA starting from the Gutzwiller ground state, [73]. Indeed, we can consider the Gutzwiller projector $\mathcal{P}$ as the operator which adiabatically constructs the Fermi liquid ground state from the non-interacting one. Therefore, upon diagonalizing (2.29)

$$\mathcal{H}_* = \sum_{\mathbf{k},\alpha,\sigma} \epsilon_{\mathbf{k}\alpha\sigma}^* \zeta_{\mathbf{k}\alpha\sigma}^\dagger \zeta_{\mathbf{k}\alpha\sigma} \qquad (2.30)$$

so that $|\psi_0\rangle$ is the corresponding Fermi sea, we can identify with $\langle\psi_0|\zeta_{\mathbf{k}\alpha\sigma}^\dagger \zeta_{\mathbf{k}\alpha\sigma}|\psi_0\rangle$ the quasiparticle occupation probability and with $|\zeta_{\mathbf{k}\alpha\sigma}\rangle = \mathcal{P}\zeta_{\mathbf{k}\alpha\sigma}^\dagger|\psi_0\rangle$ the quasiparticle excited state.

The renormalization factors are thence connected to the weight on the quasiparticle excitation of the original fermionic operators,

$$\langle\zeta_{\mathbf{k}\alpha\sigma}|c_{\mathbf{R}a}^\dagger\mathcal{P}|\psi_0\rangle = \langle\psi_0|\zeta_{\mathbf{k}\alpha\sigma}\mathcal{P}^\dagger c_{\mathbf{R}a}^\dagger\mathcal{P}|\psi_0\rangle = \sum_b R_{\mathbf{R}b}^* \langle\psi_0|\zeta_{\mathbf{k}\alpha\sigma} d_{\mathbf{R}b}^\dagger|\psi_0\rangle \qquad (2.31)$$

which in general gives access to the coherent part of the spectral function that can be used to compare with ARPES experiments [74]. In the Appendix we show that for the single band paramagnetic Hubbard model, the square of the renormalization factor is indeed equal to the jump at the Fermi surface of the momentum distribution, thus

identifying in the GA an approximate method to derive a Landau's description of a normal metal.

The Metal-to-Insulator transition is therefore correctly captured from the metallic side, where the coherent part of the spectrum vanishes. However, from this analysis, it is also clear that the Gutzwiller Approach cannot properly describe the insulating side of the transition, since a description of the incoherent part of the spectrum is completely missed.

2.2   Extension at finite temperature

The formulation of the Gutzwiller approach presented in the previous Section represents a powerful and efficient method to deal with strongly correlated electrons in complex multiband lattice models. In order to access quantitative agreement with real compounds more recently several attempts have been made to combine efficiently and self-consistently the Gutzwiller approach with ab initio methods such as the Density Functional Theory (DFT)[64–66]. DFT+GA has shown to be a much less demanding method than DFT+DMFT and in several cases has reproduced quantitatively well physical properties of real compounds.

So far, these attempts have been restricted to ground state properties with the main success being the prediction of a Mott Metal-to-Insulator transition. However, a genuine Mott insulator, where the insulating character is due exclusively to charge localization, is a very useful concept but never realized in the ground state of known correlated materials. Indeed, no system can sustain at zero temperature the residual entropy that would be associated with all other electronic degrees of freedom different from charge. As a result, Mott localization is always accompanied at low temperature by other phenomena that freeze those degrees of freedom, for instance magnetic ordering or structural distortions, which effectively turn the Mott insulator into a conventional band insulator. By this we mean the possibility of reproducing low-temperature static and often also dynamic properties of a supposed Mott insulator by an independent-particle scheme, no matter how sophisticated it is [75]. However, even though it provides satisfactory results, an independent-particle scheme, like Hartree-Fock or DFT within LDA and its extensions, has a drawback: it can describe only the simultaneous locking of charge and other degrees of freedom, like spin or lattice, while in a Mott insulator the charge freezes at a much higher energy scale than any other degree of freedom. A tool that can reveal this hierarchy of energy scales typical of a Mott insulator is the temperature, which unveils the profound difference between the excited states of a Mott insulator and those of its "band-insulator" counterpart [76].

Apart from a more reliable characterization of equilibrium phase diagrams, finite temperature calculations are essential if one intends to compare the long time dynamics with the corresponding thermal state, which is crucial to establish if thermalization occurs or if possible long-lived phases with no equilibrium counterpart emerge. To verify the thermalization hypothesis one should compare the long time expectation value of an observable $\mathcal{O}$ with the corresponding thermal value $\text{Tr}[e^{-\mathcal{H}/T_*}\mathcal{O}]/Z_*$, where the effective temperature T_* is such that the internal energy $\langle\Psi(t)|\mathcal{H}|\Psi(t)\rangle$ (which is conserved in the unitary evolution for a time independent Hamiltonian) equals the thermal one,

$\mathrm{Tr}[e^{-\mathcal{H}/T_*}\mathcal{H}]/Z_*$.

It is therefore desirable to dispose of a method which allows to compute thermal values in a Gutzwiller-like Approach.

These reasons motivated the work presented in this Section in which we introduce an extension to finite temperature of the Gutzwiller Approach that we recently proposed [77].

First of all we start by deriving a rigorous upper-bound estimate of the free-energy of a many-body Hamiltonian within the class of Gutzwiller- and Jastrow-like variational density matrices. Next, we specialize to the case of Gutzwiller-like density matrices and introduce the Gutzwiller approximation at finite temperature extending the zero temperature mixed-basis formulation so far adopted.

2.2.1   Variational estimation of the free energy

In this Section we shall repeatedly use some known trace inequalities, for which we refer to Ref. [78]. Let us consider an interacting many-body system described by the Hamiltonian $\mathcal{H}$ at finite temperature $T > 0$. It is known that the free-energy functional

$$F(X) = \mathrm{Tr}\big(X\,\mathcal{H}\big) + T\,\mathrm{Tr}\big(X \ln X\big), \tag{2.32}$$

with the matrix $X > 0$ and such that $\mathrm{Tr}\,X = 1$, is minimized by the Boltzmann distribution function

$$X_{\min} = \frac{\mathrm{e}^{-\beta\mathcal{H}}}{\mathrm{Tr}\,\mathrm{e}^{-\beta\mathcal{H}}}, \tag{2.33}$$

where $\beta = 1/T$. Therefore, any variational ansatz for the density matrix X provides an upper bound of the actual free energy

$$F \equiv F\big(X_{\min}\big) \leq F(X), \quad \forall X > 0 \text{ with } \mathrm{Tr}\,X = 1. \tag{2.34}$$

It is also known that, for any positive matrix Y, the entropy of the distribution X satisfies the inequality [78]

$$
\begin{aligned}
S(X) &= -\mathrm{Tr}\big(X \ln X\big) \geq -\mathrm{Tr}\big(X \ln Y\big) \\
&\quad -\mathrm{Tr}\Big(X \ln \big(X\,Y^{-1}\big)\Big) \equiv S_{\mathrm{var}}(X,Y).
\end{aligned} \tag{2.35}
$$

It then follows that, for any positive Y and X such that $\mathrm{Tr}\,X = 1$,

$$F \leq \min_{X,Y}\Big\{\mathrm{Tr}\big(X\mathcal{H}\big) - T\,S_{\mathrm{var}}(X,Y)\Big\}. \tag{2.36}$$

Eq. (2.36) provides a variational principle for the free energy in terms of the distribution X and the matrix $Y > 0$. Let us assume the variational ansatz

$$X = \mathcal{P} \, \rho_* \, \mathcal{P}^\dagger, \tag{2.37}$$

where

$$\rho_* = \frac{e^{-\beta \mathcal{H}_*}}{\operatorname{Tr} e^{-\beta \mathcal{H}_*}}, \tag{2.38}$$

is the Boltzmann distribution corresponding to a variational non-interacting Hamiltonian $\mathcal{H}_*$, and $\mathcal{P}$ a many-body operator that we can parametrize as

$$\mathcal{P} = \mathcal{U} \sqrt{\mathcal{Q}}, \tag{2.39}$$

with unitary $\mathcal{U}$ and $\mathcal{Q} > 0$. It follows that the entropy of the distribution X

$$
\begin{aligned}
S(X) &= -\operatorname{Tr}\Big(X \ln X\Big) \\
&= -\operatorname{Tr}\Big(\mathcal{Q}^{1/2} \rho_* \, \mathcal{Q}^{1/2} \ln \big(\mathcal{Q}^{1/2} \rho_* \, \mathcal{Q}^{1/2}\big)\Big),
\end{aligned} \tag{2.40}
$$

is independent of the unitary operator $\mathcal{U}$. By means of Eq. (2.35), setting $Y = \mathcal{Q}$, we obtain

$$
\begin{aligned}
S_{\mathrm{var}}(X, Y) &= -\operatorname{Tr}\Big(\mathcal{Q}^{1/2} \rho_* \, \mathcal{Q}^{1/2} \ln \mathcal{Q}\Big) \\
&\quad - \operatorname{Tr}\Big(\mathcal{Q}^{1/2} \rho_* \, \mathcal{Q}^{1/2} \ln \big(\mathcal{Q}^{1/2} \rho_* \, \mathcal{Q}^{-1/2}\big)\Big) \\
&= -\operatorname{Tr}\Big(\rho_* \, \mathcal{Q} \ln \mathcal{Q}\Big) - \operatorname{Tr}\Big(\rho_* \, \mathcal{Q} \ln \big(\rho_*\big)\Big).
\end{aligned} \tag{2.41}
$$

In conclusion, given the ansatz Eqs. (2.37)-(2.39), one can obtain an upper estimate of the actual free energy

$$
\begin{aligned}
F \leq \quad \min\Big\{ &\operatorname{Tr}\Big(\rho_* \, \mathcal{P}^\dagger \, \mathcal{H} \, \mathcal{P}\Big) + T \operatorname{Tr}\Big(\rho_* \, \mathcal{P}^\dagger \mathcal{P} \ln \mathcal{P}^\dagger \mathcal{P}\Big) \\
&+ T \operatorname{Tr}\Big(\rho_* \, \mathcal{P}^\dagger \mathcal{P} \ln \rho_*\Big) \Big\},
\end{aligned} \tag{2.42}
$$

minimizing with respect to a non-interacting Hamiltonian $\mathcal{H}_*$ and a many-body operator $\mathcal{P}$. This minimization is feasible only for particular choices of $\mathcal{P}$. For instance, if $\mathcal{P} = 1$, Eq. (2.42) reduces to the well-known Hartree-Fock variational estimate of the free energy. Another possibility is that $\mathcal{P}$ is a two-body Jastrow factor, which can be handled by the variational Monte Carlo statistical approach [79]. In the next, we shall consider operators of the Gutzwiller type, $\mathcal{P}$, which can be dealt with analytically in the limit of infinite coordination lattices.

We conclude by noting that, since Eq. (2.42) is based on the lower bound estimate

$S_{\text{var}}(X, Y)$ of the entropy of the distribution X, Eq. (2.41), there is no guarantee that such estimate is positive at any temperature, as the true entropy should be. Therefore, it is more appropriate to state that

$$S(X) \geq \underset{Y > 0}{\text{Max}} \Big\{ S_{\text{var}}(X, Y), 0 \Big\}. \tag{2.43}$$

We further mention that Eq. (2.35) is actually the $p = 1$ case of the more general inequality [78]

$$
\begin{aligned}
S(X) &= -\text{Tr}\big(X \ln X\big) \geq -\text{Tr}\big(X \ln Y\big) \\
&\quad -\frac{1}{p} \text{Tr}\Big(X \ln \big(X^p Y^{-p}\big)\Big),
\end{aligned} \tag{2.44}
$$

which becomes an equivalence as $p \to 0$. We cannot exclude that exploiting Eq. (2.44) one could get a better but still manageable estimate of the entropy, though we did not succeed.

2.2.2 The Gutzwiller approximation at finite T

As for the zero temperature case we assume a generic tight binding Hamiltonian

$$\mathcal{H} = \sum_{\mathbf{R}, \mathbf{R}'} \sum_{ab} \big(t_{\mathbf{R}\mathbf{R}'}^{ab} \, c_{\mathbf{R}a}^\dagger c_{\mathbf{R}'b} + H.c. \big) + \sum_{\mathbf{R}} \mathcal{H}_{\mathbf{R}}, \tag{2.45}$$

with local interaction terms $\mathcal{H}_{\mathbf{R}}$.

Given a variational density matrix of the form as in Eqs. (2.37) and (2.38), i.e.

$$\rho_{\text{G}} = \mathcal{P} \, \rho_* \, \mathcal{P}^\dagger, \tag{2.46}$$

we take the operator $\mathcal{P}$ to be of the Gutzwiller type

$$\mathcal{P} = \prod_{\mathbf{R}} \mathcal{P}_{\mathbf{R}}, \tag{2.47}$$

for which we shall generalize the zero temperature Gutzwiller constraints as

$$\text{Tr}\Big(\rho_* \, \mathcal{P}_{\mathbf{R}}^\dagger \mathcal{P}_{\mathbf{R}}\Big) = 1, \tag{2.48}$$

$$\text{Tr}\Big(\rho_* \, \mathcal{P}_{\mathbf{R}}^\dagger \mathcal{P}_{\mathbf{R}} \, \mathcal{C}_{\mathbf{R}}\Big) = \text{Tr}\Big(\rho_* \, \mathcal{C}_{\mathbf{R}}\Big), \tag{2.49}$$

where $\mathcal{C}_{\mathbf{R}}$ is any single-particle operator at site $\mathbf{R}$. The above conditions replace (2.6-2.7) and allow to analytically compute averages over the distribution function ρ_{G} in the limit of infinite coordination number, $z \to \infty$. The proof follows exactly the same

reasoning we explained for the zero temperature case. Specifically, when $z \to \infty$, the two conditions (2.48) and (2.49) imply that the distribution ρ_G has unit trace, and that all the formulas presented in Sec. 2.1 hold with the only difference that, instead of averaging over a variational Slater determinant, one has to average over the variational non-interacting Boltzmann distribution ρ_*.

Once again it is more convenient to assume that ρ_* identifies a local natural basis, with creation operators $d^\dagger_{\mathbf{R}a}$ such that

$$\mathrm{Tr}\left(\rho_* \, d^\dagger_{\mathbf{R}a} d_{\mathbf{R}b}\right) = \delta_{ab} \, n^0_{\mathbf{R}a}, \tag{2.50}$$

where $n^0_{\mathbf{R}a}$ depends on the variational Hamiltonian $\mathcal{H}_*$ and on the temperature. Using the local Fock states basis introduced in (2.15) and generalizing the local probability distribution as

$$\mathrm{Tr}\left(\rho_* \mid \mathbf{R}; n\rangle\langle\mathbf{R}; n \mid \right) = P^0_{\mathbf{R};n} = \prod_\alpha \left(n^0_{\mathbf{R}\alpha}\right)^{n_{\mathbf{R}\alpha}} \left(1 - n^0_{\mathbf{R}\alpha}\right)^{1 - n_{\mathbf{R}\alpha}}, \tag{2.51}$$

the Gutzwiller projector can be parametrized exactly as in (2.16)

$$\mathcal{P}_{\mathbf{R}} = \sum_{\Gamma n} \frac{\Phi_{\mathbf{R};\Gamma n}}{\sqrt{P^{(0)}_{\mathbf{R};n}}} \mid \mathbf{R}; \Gamma\rangle\langle\mathbf{R}; n|. \tag{2.52}$$

In the matrix representation (2.18) the Gutzwiller constraints, the average of local observables and the average of the hopping terms can be rewritten exactly as in the zero temperature case. With this, we obtain that the expectation value of the Hamiltonian on the variational Gutzwiller canonical distribution is equal to

$$\mathrm{Tr}\left(\rho_G \, \mathcal{H}\right) = \sum_{\mathbf{R},\mathbf{R}'} \sum_{ab} \mathrm{Tr}\left(\rho_* \left(t^{ab}_{*\mathbf{R}\mathbf{R}'} \, d^\dagger_{\mathbf{R}a} d_{\mathbf{R}'b} + H.c.\right)\right) + \sum_{\mathbf{R}} \mathrm{Tr}\left(\hat{\Phi}^\dagger_{\mathbf{R}} \, \hat{H}_{\mathbf{R}} \, \hat{\Phi}_{\mathbf{R}}\right), \tag{2.53}$$

where both $t^{ab}_{*\mathbf{R}\mathbf{R}'}$ and the renormalization factors have the same form as in the zero temperature case (2.28,2.26). In other words, the average over ρ_G of the Hamiltonian (2.45) is equal to the average over the uncorrelated distribution ρ_* of a renormalized hopping Hamiltonian plus the sum of local terms that depend only on the variational matrices $\hat{\Phi}_{\mathbf{R}}$.

We next need to evaluate the entropy. We note that, in the $z \to \infty$ limit, and for any, even non-local, single-particle operator $\mathcal{C}$

$$\mathrm{Tr}\left(\rho_* \, \mathcal{P}^\dagger \mathcal{P} \, \mathcal{C}\right) = \mathrm{Tr}\left(\rho_* \, \mathcal{C}\right).$$

Since it also holds that

$$
\begin{aligned}
\mathrm{Tr}\Big(\rho_* \, \mathcal{P}^\dagger \mathcal{P} \, \ln \mathcal{P}^\dagger \mathcal{P}\Big) &= \sum_{\mathbf{R}} \mathrm{Tr}\Big(\rho_* \, \mathcal{P}_{\mathbf{R}}^\dagger \mathcal{P}_{\mathbf{R}} \, \ln \mathcal{P}_{\mathbf{R}}^\dagger \mathcal{P}_{\mathbf{R}}\Big) \\
&= \sum_{\mathbf{R}} \mathrm{Tr}\bigg[\hat{\Phi}_{\mathbf{R}}^\dagger \hat{\Phi}_{\mathbf{R}} \, \ln \Big(\big(P_{\mathbf{R}}^0\big)^{-1} \, \hat{\Phi}_{\mathbf{R}}^\dagger \hat{\Phi}_{\mathbf{R}}\Big)\bigg]
\end{aligned}
$$

it follows that Eq. (2.41) reads, in the $z \to \infty$ limit,

$$
\begin{aligned}
S_{\mathrm{var}}\big(\rho_*, \hat{\Phi}^\dagger \hat{\Phi}\big) &= S(\rho_*) - \sum_{\mathbf{R}} \mathrm{Tr}\bigg[\hat{\Phi}_{\mathbf{R}}^\dagger \hat{\Phi}_{\mathbf{R}} \, \ln \Big(\big(P_{\mathbf{R}}^0\big)^{-1} \, \hat{\Phi}_{\mathbf{R}}^\dagger \hat{\Phi}_{\mathbf{R}}\Big)\bigg] \\
&= S(\rho_*) + \sum_{\mathbf{R}} S\big(\hat{\Phi}_{\mathbf{R}}^\dagger \hat{\Phi}_{\mathbf{R}} || P_{\mathbf{R}}^0\big),
\end{aligned} \tag{2.54}
$$

where $S\big(\hat{\Phi}_{\mathbf{R}}^\dagger \hat{\Phi}_{\mathbf{R}} || P_{\mathbf{R}}^0\big)$ is the relative entropy between the distribution $\hat{\Phi}_{\mathbf{R}}^\dagger \hat{\Phi}_{\mathbf{R}}$ and the uncorrelated local distribution $P_{\mathbf{R}}^0$. In conclusion, the free energy can be upper estimated through

$$
\begin{aligned}
F \leq \quad \min\bigg\{ &\sum_{\mathbf{R},\mathbf{R}'} \sum_{ab} \mathrm{Tr}\Big(\rho_* \, \big(t_{*\,\mathbf{R}\mathbf{R}'}^{ab} \, d_{\mathbf{R}a}^\dagger d_{\mathbf{R}'b} + H.c.\big)\Big) + \sum_{\mathbf{R}} \mathrm{Tr}\Big(\hat{\Phi}_{\mathbf{R}}^\dagger \, \hat{H}_{\mathbf{R}} \, \hat{\Phi}_{\mathbf{R}}\Big) \\
&- T \, \mathrm{Max}\Big(S_{\mathrm{var}}\big(\rho_*, \hat{\Phi}^\dagger \hat{\Phi}\big), 0\Big)\bigg\},
\end{aligned} \tag{2.55}
$$

hence one just needs to minimize the right-hand side supplemented by the constraints

$$
\mathrm{Tr}\big(\hat{\Phi}_{\mathbf{R}}^\dagger \hat{\Phi}_{\mathbf{R}} \big) = 1 \tag{2.56}
$$

$$
\mathrm{Tr}\big(\hat{\Phi}_{\mathbf{R}}^\dagger \hat{\Phi}_{\mathbf{R}} \, \hat{d}_{\mathbf{R}a}^\dagger \hat{d}_{\mathbf{R}a} \big) = n_{\mathbf{R}a}^{(0)} \tag{2.57}
$$

A possible route is to regard $n_{\mathbf{R}a}^0$ in Eqs. (2.50) and (2.57) as independent minimization parameters, and introduce two Lagrange multipliers terms

$$
\mathrm{Tr}\big(\rho_* \, \mathcal{V}\big) - \sum_{\mathbf{R}} \sum_{ab} \mu_{\mathbf{R}\,ab} \bigg[\mathrm{Tr}\Big(\hat{\Phi}_{\mathbf{R}}^\dagger \hat{\Phi}_{\mathbf{R}} \, d_{\mathbf{R}a}^\dagger d_{\mathbf{R}b}\Big) - \delta_{ab} \, n_{\mathbf{R}a}^0 \bigg],
$$

where the non-interacting potential $\mathcal{V}$ enforces Eq. (2.50), while $\mu_{\mathbf{R}\,ab}$ enforce Eq. (2.57).

When $S_{\mathrm{var}}\big(\rho_*, \hat{\Phi}^\dagger \hat{\Phi}\big) > 0$, minimization with respect to the uncorrelated distribution ρ_*, see Eq. (2.38), leads to the identification

$$
\mathcal{H}_* = \sum_{\mathbf{R},\mathbf{R}'} \sum_{ab} \big(t_{*\,\mathbf{R}\mathbf{R}'}^{ab} \, d_{\mathbf{R}a}^\dagger d_{\mathbf{R}'b} + H.c.\big) + \mathcal{V}, \tag{2.58}
$$

so that, once $\mathcal{V}$ is chosen so as to satisfy Eq. (2.50), Eq. (2.55) reads

$$
\begin{aligned}
F \quad &\leq \min\Bigg\{ F_*\big[\hat{\Phi}, n^0\big] + \sum_{\mathbf{R}} \mathrm{Tr}\Big(\Phi_{\mathbf{R}}^{\dagger}\, \hat{H}_{\mathbf{R}}\, \Phi_{\mathbf{R}} \Big) + S\Big(\Phi_{\mathbf{R}}^{\dagger} \Phi_{\mathbf{R}} || P_{\mathbf{R}}^0 \Big) \\
&\quad - \sum_{\mathbf{R}} \sum_{ab} \mu_{\mathbf{R}\,ab} \bigg[\mathrm{Tr}\Big(\hat{\Phi}_{\mathbf{R}}^{\dagger} \hat{\Phi}_{\mathbf{R}}\, d_{\mathbf{R}a}^{\dagger} d_{\mathbf{R}b} \Big) - \delta_{ab}\, n_{\mathbf{R}a}^0 \bigg] \Bigg\} \\
&\equiv \min_{\hat{\Phi}, n^0, \mu} \Big\{ F\big[\hat{\Phi}, n^0, \mu\big] \Big\},
\end{aligned}
\tag{2.59}
$$

where F_* is the free energy of non-interacting electrons described by the Hamiltonian $\mathcal{H}_*$ in (2.58) that depends on the variational matrices $\hat{\Phi}_{\mathbf{R}}$ and on the parameters $n_{\mathbf{R}\alpha}^0$ through the constraint (2.50) and the Eqs. (2.28) and (2.26).

When instead $S_{\mathrm{var}}\big(\rho_*, \hat{\Phi}^{\dagger}\hat{\Phi}\big) \leq 0$, the r.h.s. of Eq. (2.55) becomes the Gutzwiller energy functional that we would minimize at $T = 0$, in which case the optimized ρ_* is simply the projection onto the ground state of the Hamiltonian $\mathcal{H}_*$ in Eq. (2.58). In other words, the variational estimate of the free energy coincides with that of the ground state energy whenever $S_{\mathrm{var}}\big(\rho_*, \hat{\Phi}^{\dagger}\hat{\Phi}\big)$ is negative, evidently a drawback of the entropy bound that we use. In our experience, this problem may arise only at very low temperature, where the entropy contribution to the free energy is nonetheless negligible

Minimization of $F\big[\hat{\Phi}, n^0, \mu\big]$ therefore provides an upper bound to the actual free energy in lattices with infinite coordination number $z \to \infty$. Seemingly to what it is done at zero temperature, one can keep using the same free-energy functional also when the coordination number is finite, which can be regarded as the finite temperature extension of the Gutzwiller approximation [60, 61, 80]. We mention that, in the simple case of a one-band Hubbard model, the free energy functional $F\big[\hat{\Phi}, n^0, \mu\big]$ coincides with the expression derived by different arguments in Ref. [81].

2.3   The Time-Dependent Gutzwiller Approximation

In this Section we shall conclude this methodological Chapter by presenting the real time extension of the Gutzwiller Approach originally introduced by Schiró and Fabrizio in [49]. This Section therefore concludes the technical panoramic on the Gutzwiller Approach.

We follow its formulation in the mixed-basis representation [68], since it allows a natural generalization of the framework we introduced in the previous sections.

The quantum dynamics of pure state $|\Psi(t)\rangle$ under the effect of a time dependent Hamiltonian is set by the Scrödinger equation

$$i\partial_t|\Psi(t)\rangle = \mathcal{H}(t)\,|\Psi(t)\rangle. \tag{2.60}$$

We have seen that both ground state and finite temperature calculations rely on variational principles, respectively the minimization of energy and the minimization of the free-energy. This provided a way to obtain a systematic optimization of the real ground state and the canonical distribution in a given subspace of Gutzwiller-type wavefunctions. Also the Scrödinger equation can be re-expressed by means of a stationarity principle which allows an effective computation within the Gutzwiller Approach. Indeed, upon introducing the Action functional

$$\mathcal{S}[|\Psi\rangle] = \int_0^{t_f} d\tau\,\langle\Psi(\tau)|\,i\partial_\tau - \mathcal{H}(\tau)\,|\Psi(\tau)\rangle\,, \tag{2.61}$$

the evolving wavefunction $|\Psi(t)\rangle$ which satisfies the Scrödinger equation is the one that stationarizes $\mathcal{S}[|\Psi\rangle]$ [82],

$$\frac{\delta\mathcal{S}[|\Psi\rangle]}{\delta|\Psi(t)\rangle} \overset{!}{=} 0. \tag{2.62}$$

By means of this variational reformulation it is then possible to search systematically the best approximation for the evolving state in a subclass of time-dependent wavefunctions.

For the same reasons that hold at equilibrium, the exact evaluation of the Action $\mathcal{S}$ over a correlated wave function is still a highly non trivial task which, in general, cannot be accomplished exactly. Rather one has to use approximation schemes or evaluate it numerically, using for example a suitable time dependent extension of the variational Monte Carlo algorithm as recently done in Ref. [26] for the bosonic Jastrow wave-function. However it turns out that an exact calculation can be carried out generalizing the zero

temperature Gutzwiller ansatz (2.4) to a time dependent Gutzwiller wavefunction

$$|\Psi(t)\rangle = \mathcal{P}(t) \, |\psi(t)\rangle \, . \tag{2.63}$$

$|\psi(t)\rangle$ is a time dependent Slater determinant and $\mathcal{P}(t)$ is a time dependent generalization of the Gutzwiller projector that we shall properly parametrize in the following.

Imposing, as at equilibrium, that the Gutzwiller constraints are satisfied for any time t,

$$\langle\psi(t)| \, \mathcal{P}_{\mathbf{R}}^{\dagger}(t)\mathcal{P}_{\mathbf{R}}(t) \, |\psi(t)\rangle \overset{!}{=} 1 \tag{2.64}$$

$$\langle\psi(t)| \, \mathcal{P}_{\mathbf{R}}^{\dagger}(t)\mathcal{P}_{\mathbf{R}}(t) \, \mathcal{C}_{\mathbf{R}} \, |\psi(t)\rangle \overset{!}{=} \langle\psi(t)| \, \mathcal{C}_{\mathbf{R}} \, |\psi(t)\rangle \, , \tag{2.65}$$

by the same reasons indicated previously, an analytical computation in the limit of $z \to \infty$ can be performed exactly.

Given the form of the evolving wavefunction (2.63), the Action $\mathcal{S}(t)$ can indeed be evaluated exactly and reads [68]

$$\mathcal{S}[|\Psi\rangle] = \int_0^{t_f} d\tau \, \left[i\langle\psi(\tau)|\partial_\tau\psi(\tau)\rangle + i\sum_{\mathbf{R}}\langle\psi(\tau)| \, \mathcal{P}_{\mathbf{R}}^{\dagger}(\tau)\partial_\tau\big(\mathcal{P}_{\mathbf{R}}(\tau)\big) \, |\psi(\tau)\rangle - E(\tau) \right] \tag{2.66}$$

with $E(t) = \langle\psi(t)| \, \mathcal{P}^{\dagger}(t)\mathcal{H}(t)\mathcal{P}(t) \, |\psi(t)\rangle$ being the total energy.

Eq. (2.66) can be properly evaluated upon parametrizing the Gutzwiller projector. Following the same scheme we applied at equilibrium, we write the local projector $\mathcal{P}_{\mathbf{R}}(t)$ as

$$\mathcal{P}_{\mathbf{R}}(t) = \sum_{\Gamma n} \frac{\Phi_{\mathbf{R};\Gamma n}(t)}{\sqrt{P_{\mathbf{R};n}^{(0)}(t)}} \, |\mathbf{R};\Gamma\rangle\langle\mathbf{R};n| \tag{2.67}$$

where both the variational matrix $\hat{\Phi}_{\mathbf{R}}(t)$ and the local uncorrelated probability $P_{\mathbf{R};n}^{(0)}(t) = \langle\psi(t) \, |\mathbf{R};n\rangle\langle\mathbf{R};n| \, \psi(t)\rangle$ are in this case time dependent and we assume the existence of a natural basis identified by the operators $d_{\mathbf{R}a}^{\dagger}$, $d_{\mathbf{R}a}$ such that

$$\langle\psi(t)| \, d_{\mathbf{R}a}^{\dagger}d_{\mathbf{R}b} \, |\psi(t)\rangle = \delta_{ab}n_{\mathbf{R}a}^{(0)}(t). \tag{2.68}$$

In the matrix representation we obtain the following form for the Action

$$\mathcal{S}[|\Psi\rangle] = \int_0^{t_f} d\tau \quad \left[i\langle\psi(\tau)|\partial_\tau\psi(\tau)\rangle - \langle\psi(\tau)|\mathcal{H}_*(\tau)|\psi(\tau)\rangle \right.$$

$$\left. + i\sum_{\mathbf{R}} \mathrm{Tr}\Big(\hat{\Phi}_{\mathbf{R}}^{\dagger}(\tau)\partial_\tau\hat{\Phi}_{\mathbf{R}}(\tau)\Big) - \sum_{\mathbf{R}} \mathrm{Tr}\Big(\hat{\Phi}_{\mathbf{R}}^{\dagger}(\tau)\hat{H}_{\mathbf{R}}\hat{\Phi}_{\mathbf{R}}(\tau)\Big) \right] \tag{2.69}$$

where the renormalized Hamiltonian $\mathcal{H}_*(t)$ has the same form as at equilibrium, with the only difference that it acquires a time dependence through the renormalization factors

$$R^*_{\mathbf{R}ab}(t) = \frac{1}{\sqrt{n^{(0)}_{\mathbf{R}b}(t)\,(1-n^{(0)}_{\mathbf{R}b}(t))}}\,\mathrm{Tr}(\,\hat{\Phi}^\dagger_{\mathbf{R}}(t)\hat{c}^\dagger_{\mathbf{R}a}\hat{\Phi}_{\mathbf{R}}(t)\hat{d}_{\mathbf{R}b}\,). \tag{2.70}$$

Since the derivation of (2.66) and (2.69) follows the same philosophy as in the equilibrium case, we report it in the Appendix.

The best approximation of the real evolving state within the subclass of Gutzwiller wavefunction can be then calculated by requiring the stationarity of (2.69) with respect to the Slater determinant $|\psi(t)\rangle$ and the Gutzwiller variational matrix $\hat{\Phi}(t)$. Taking the functional derivative of (2.70) with respect to $|\psi(t)\rangle$ and $\hat{\Phi}^\dagger_{\mathbf{R}}(t)$ one obtains,

$$i\partial_t|\psi(t)\rangle = \mathcal{H}_*[\hat{\Phi}(t)]\,|\psi(t)\rangle$$
$$i\partial_t\hat{\Phi}_{\mathbf{R}}(t) = \hat{H}_{\mathbf{R}}(t)\hat{\Phi}_{\mathbf{R}}(t) + \langle\psi(t)|\frac{\partial\mathcal{H}_*[\hat{\Phi}(t)]}{\partial\hat{\Phi}^\dagger_{\mathbf{R}}(t)}|\psi(t)\rangle. \tag{2.71}$$

One can then recognize that, in analogy to the equilibrium case, the uncorrelated part of the Gutzwiller wavefunction evolves accordingly to a renormalized single-particle Hamiltonian, which is self-consistently coupled through the renormalization coefficients (2.70) to the dynamics of the variational matrix $\hat{\Phi}(t)$. As at equilibrium, the dynamics of the Slater determinant can be interpreted as the the dynamics for the Gutzwiller quasiparticles, whilst the Gutzwiller parameters $\hat{\Phi}(t)$, describing the local degrees of freedom can be associated to the dynamics of atomic-like excitations. The two are coupled in a mean-field like fashion.

Overall this constitutes a set of non-linear differential equation that has to be solved numerically in most of the cases. A simple calculation shows that, for time-independent Hamiltonians, energy is conserved.

Before concluding this Section we remark that the equations of motion (2.71) have to be solved subject to the time dependent Gutzwiller constraints (2.64) and (2.65), which in the matrix notation read

$$\mathrm{Tr}\big(\hat{\Phi}_{\mathbf{R}}(t)\hat{\Phi}_{\mathbf{R}}(t)\big) = 1 \tag{2.72}$$
$$\mathrm{Tr}\big(\hat{\Phi}_{\mathbf{R}}(t)\hat{\Phi}_{\mathbf{R}}(t)d^\dagger_{\mathbf{R}a}d_{\mathbf{R}a}\big) = \langle\psi(t)|\,d^\dagger_{\mathbf{R}a}d_{\mathbf{R}a}\,|\psi(t)\rangle = n^{(0)}_{\mathbf{R}a}(t). \tag{2.73}$$

However in Ref. [68] it was shown that these constraints are automatically satisfied during the dynamics, that is, once the variational matrix $\hat{\Phi}$ and the Slater determinant are set at $t = 0$ in a way to satisfy the Gutzwiller constraints, then (2.72,2.73) are automatically satisfied for any $t > 0$. This result drastically simplifies the solution of the Gutzwiller dynamics, since a constrained minimization problem is needed only at

the initial time and in most of the cases amounts to a groundstate calculation problem for which the procedure presented in Sec. 2.1 can be applied.

In this Chapter we presented the recent extensions of the Gutzwiller Approach necessary in order to attack the dynamics of strongly correlated systems. In particular the dynamics of an initial pure state can be simulated through the time dependent GA and its long time behavior can be compared to the corresponding thermal value by means of the finite-T GA. However, it has to be stressed that t-GA, as we shall show in the rest of the Thesis, remains essentially a mean-field approach, hence, although it improves the time-dependent Hartree-Fock approximation simply because of the larger number of variational parameters, it misses dissipative processes that in reality bring the system to a stationary or thermal state. A comparison with thermal values is therefore meaningless *a priori* if intended to verify thermalization hypothesis. In spite of that, the Gutzwiller Approach seems to reproduce quite satisfactorily the main results obtained by exact DMFT calculations, whenever a comparison is possible and even when time-dependent Hartree-Fock fails completely, like in the case of quantum quenches within the paramagnetic sector [49]. In particular t-GA captures well short time properties of the dynamics, so that, in this case, a comparison with the corresponding thermal state can lead to the identification of possible long-lived non-thermal phases. In this sense the Gutzwiller Approch is very useful for a first analysis of complicated multiband models where other methods become excessively demanding.

We conclude this Chapter remarking that all the above treatment is strictly variational only in the limit of infinite coordination number, where the exact averages on the Gutzwiller variational wavefunction (or the thermal averages on the variational canonical distribution) coincide with those we have computed.
In finite coordination lattices the approach is not anymore variational. Nevertheless, it is common to keep using the same expressions also in these more physical cases, which goes under the name of *Gutzwiller Approximation*. Even though to our knowledge there are so far no exact out-of-equilibrium results to compare with in finite coordination lattices, recent high order perturbative calculations in one and two dimensions [46, 50] bring results quite similar to those obtained in Ref. [49] through the Gutzwiller approach.
At equilibrium, instead, the Gutzwiller approximation seems to reproduce well exact variational Monte Carlo calculations on the Gutzwiller wave functions [83], and, when applied in combination with *ab-initio* density functional theory methods, also physical properties of real materials [84].

Chapter 3

Linear Ramps of Interaction in the Fermionic Hubbard Model

3.1 Introduction

In a typical cold atom experiment, microscopic parameters controlling the Hamiltonian of a quantum many body system, for instance the lattice depth or the interparticle interaction, are changed in time between different values following some given protocol [85]. The dynamics during and after this time dependent transformation is recorded.

From a theoretical perspective, if the rate of change is much faster than any typical time scale of the system, one can model such a process as a sudden change of parameters, a *sudden quench*. Although this protocol is far from usual solid state experiments, it generally provides a simple description for an initial excited state, thus allowing the characterization of dynamical features which might be independent on the excitation scheme. To this extent, beside the general issue of thermalization and its relation to integrability [20, 86] and localization [26, 87], an intriguing question which has been recently addressed in a number of works concerns the ways strongly correlated system approach equilibrium, namely the short-to-intermediate time dynamics. Here non trivial behaviors, featuring metastable prethermal states trapping the dynamics for long time scales [45, 88, 89], are likely to emerge as a result of strong correlations. The intriguing possibility of sharp crossovers among different relaxation regimes, or even genuine dynamical transitions, has been firstly argued in a DMFT investigation of the fermionic Hubbard model [10] and then found in a number of mean field models, including the Gutzwiller Approximation. We shall revise these results in the first Section of this Chapter.

A rather different situation may arise if the time dependent protocol is performed in a finite time τ, the simplest example being a linear-in-time increase of some control parameter, a so called ramp. Here the Hamiltonian of the system is explicitly time dependent and one may wonder about new issues concerning, for example, the degree of adiabaticity of the dynamics, namely to which extent an isolated system is able to follow a (slow) time dependent change of its Hamiltonian parameters without being excited [90]. Such a question has been around since the early days of quantum mechanics [91], an example being the Landau Zener process [92–95] where a two level system is driven through an avoided level crossing. In the context of quantum many body systems with a continuum of energy levels, this very basic idea lays the ground for the Landau's phenomenological description of Normal Fermi Liquids [96]. More recently, the interest in the adiabatic dynamics of quantum many body systems has grown stimulated by a debate on quantum computation and mainly in connection with ramps across quantum critical points. In the small excitation energy limit, namely for slow ramps, the possibility of a universal behavior has been discussed in a number of works [97, 98] as a generalization to isolated quantum systems of the classical dynamical behavior.

It is worth noticing at this point that understanding the degree of adiabaticity of a time dependent process in a quantum many body system is not only of theoretical interest but also of practical relevance for cold atoms applications. Indeed, one has to consider that real experiments are always performed at a finite rate which unavoidably induces heating into the system. Hence the challenge one has to face in order to use cold atoms to *simulate* specific low temperature quantum phases is to minimize those heating effects. Recent works address this issue and look for the optimal ramping protocol which produces the minimal heating [99, 100]. Other investigations on the slow quench dynamics in trapped cold gases address the issue of equilibration of local and global quantities [101, 102].

Finally, we note that while those questions mainly address the dynamics during the ramp, there are interesting issues as well that concern the evolution of the system once the ramp is over, namely for times $t > \tau$. Here the system is again isolated, initialized with the excitation energy acquired during the ramp, and it is let evolve with its unitary dynamics. One can see that this set up is very similar to the quench case, with the ramp process affecting the initial condition of the dynamics. As we discussed, an interesting question in this case is to understand how the excitation energy due to the ramp affects the relaxation toward equilibrium and the possible existence of non trivial dynamical behaviors.

In this Chapter we address some of these questions in the context of the fermionic Hubbard model already introduced by using the time dependent Gutzwiller Approach. We start with the preliminary Section 3.2 where we show how the t-GA is applied to the single band Hubbard model and we recall the main results regarding the dynamical phase transition for a sudden quench of the interaction [49, 103]. Next in Sec. 3.3 we move to consider the case of linear ramps of the Hubbard interaction across the Mott transition. We will first discuss the issue of adiabaticity of the dynamics. Then we will show that a dynamical phase transition occurs also for finite values of the ramping time τ and, for very large values of τ, this dynamical critical point is continuously mapped into the zero temperature phase transition point.

Finally in Sec. 3.4 we shall discuss a slave spin formulation which allows to go beyond the mean field nature of the Gutzwiller approximation for both regimes of slow and very fast ramps.

3.2 Interaction quench in the single band Hubbard model

In this Section we give some details regarding the implementation of the t-GA introduced so far to investigate the dynamics for the single band Hubbard model after a sudden quench of the interaction strength. As already discussed, the out-of-equilibrium dynamics of this model encodes many non trivial effects that enlighten theoretical debates in the recent years, such as the presence of prethermal regimes and a dynamical phase transition. Moreover, many concepts introduced in this Section will be used in the rest of the Thesis.

We consider the time dependent Hubbard Hamiltonian

$$\mathcal{H} = -t \sum_{\langle \mathbf{R},\mathbf{R}' \rangle,\sigma} \left(c^\dagger_{\mathbf{R}\sigma} c_{\mathbf{R}'\sigma} + H.c. \right) + \frac{U(t)}{2} \sum_{\mathbf{R}} (n_{\mathbf{R}} - 1)^2, \tag{3.1}$$

where the time dependence is set by $U(t) = U_f \theta(t)$, with $\theta(t)$ being the Heaviside function. We shall restrict the dynamics to paramagnetic states and work at half-filling, i.e. $n_{\mathbf{R}\sigma} = 0.5$. Upon introducing the local Fock states for the natural basis $|0\rangle, |\uparrow\rangle, |\downarrow\rangle$, $|\uparrow\downarrow\rangle$ (which corresponds in this case with the original one), the most general variational

matrix $\hat{\Phi}_{\mathbf{R}}$ compatible with the Gutzwiller constraints can be chosen as

$$
\begin{pmatrix}
\Phi_{\mathbf{R};0} & 0 & 0 & 0 \\
0 & \Phi_{\mathbf{R};\uparrow} & 0 & 0 \\
0 & 0 & \Phi_{\mathbf{R};\downarrow} & 0 \\
0 & 0 & 0 & \Phi_{\mathbf{R};\uparrow\downarrow}
\end{pmatrix}.
\tag{3.2}
$$

Spin symmetry and particle-hole symmetry reduce the number of variables since $\Phi_0 = \Phi_{\uparrow\downarrow}$ and $\Phi_\uparrow = \Phi_\downarrow \equiv \Phi_1$. We do not consider translational invariance breaking, so that the renormalization factor is site (and spin) independent and from (2.70) reads

$$
R(t) = 2\big(\Phi_0^*(t)\Phi_1(t) + \Phi_1^*(t)\Phi_0(t)\big).
\tag{3.3}
$$

During the dynamics the Gutzwiller constraints are satisfied, which in this simple case reduce to a normalization condition

$$
2|\Phi_0(t)|^2 + 2|\Phi_1(t)|^2 = 1.
\tag{3.4}
$$

We shall briefly consider the zero temperature ground state solution within the Gutzwiller approximation. At equilibrium the variational parameters can be chosen to be real so that we are left with only one degree of freedom which is usually chosen to be the expectation value of the double occupation operator, $D = |\Phi_2|^2$. The best estimation of the ground state has then to be computed minimizing

$$
\min_{D,|\psi\rangle} \left\{ -R^2(D)\, t \sum_{\langle \mathbf{R},\mathbf{R}'\rangle,\sigma} \left(\langle\psi|\, c_{\mathbf{R}\sigma}^\dagger c_{\mathbf{R}'\sigma} \,|\psi\rangle + H.c. \right) + U \sum_{\mathbf{R}} D \right\}
\tag{3.5}
$$

where $R^2(D) \equiv Z = 8D(1-2D)$ represents the quasiparticle weight (see Appendix A.3). The best Slater determinant for the renormalized non-interacting Hamiltonian is simply a Fermi sea at half filling, $|\psi\rangle_{FS}$. Upon defining the average hopping energy,

$$
\epsilon = \frac{t}{L} \sum_{\langle \mathbf{R},\mathbf{R}'\rangle,\sigma} \left({}_{FS}\langle\psi|\, c_{\mathbf{R}\sigma}^\dagger c_{\mathbf{R}'\sigma} \,|\psi\rangle_{FS} + H.c. \right)
\tag{3.6}
$$

we obtain that the ground state energy is equal to (L being the number of sites)

$$
\frac{E(D)}{L} = -\epsilon\, 8D(1-2D) + UD.
\tag{3.7}
$$

The minimum is given by

$$
\begin{cases}
D = \frac{1}{4}\left(1 - \frac{U}{8\epsilon}\right) & U < 8\epsilon \\
D = 0 & U \geq 8\epsilon
\end{cases}
\tag{3.8}
$$

with a corresponding quasiparticle renormalization factor

$$\begin{cases} Z = 1 - \left(\frac{U}{8\epsilon}\right)^2 & U < 8\epsilon \\ Z = 0 & U \geq 8\epsilon \end{cases}. \tag{3.9}$$

We hence recover the Metal-to-Insulator transition in the Brinkmann-Rice scenario at the critical value $U_c = 8\epsilon$; within the Gutzwiller approximation this transitions is characterized by the vanishing of double occupancies and the quasiparticle residue Z due to a full suppression of charge fluctuations. The Gutzwiller Approach therefore describes correctly the Mott transition in the metallic side, with a vanishing of the quasiparticle weight and consequently of the coherent part of the spectrum. However, since the method is unable to capture the incoherent one (i.e. the existence of the Hubbard bands), it gives a wrong description on the insulating side.

We remark that all the above and following derivation (i.e. the average values on the Gutzwiller wavefunction) is strictly exact in the limit of infinite coordination number [1].

We move next to consider the dynamics of an initial non-interacting ground state subject to a quench of the interaction. The initial conditions for the dynamics are simply given by $D = 1/4$ and $|\psi(0)\rangle = |\psi\rangle_{FS}$. First of all from (2.71) we easily recognize that the Slater determinant $|\psi(t)\rangle$ has a trivial time evolution determined uniquely by an overall phase factor, therefore the occupation probability in momentum space, $\langle\psi(t)| c_{\mathbf{k}\sigma}^\dagger c_{\mathbf{k}\sigma} |\psi(t)\rangle$, does not evolve in time. In this simple circumstance it is then instructive to compute directly the Lagrangian (2.69) in terms of the Gutzwiller parameters that we can rewrite as $\Phi_a = \rho_a e^{-i\phi_a}$. We obtain

$$\mathcal{L}(t) = 2\rho_0^2(t)\,\partial_t\phi_0(t) + 2\rho_1^2(t)\,\partial_t\phi_1(t) - \overbrace{\epsilon 8\rho_0^2(t)\rho_1^2(t)\cos^2(\phi_0(t) - \phi_1(t)) + U\rho_0^2(t)}^{E(t)} \tag{3.10}$$

where $E(t)$ is the total energy. This latter is conserved during the dynamics together with the Gutzwiller constraint

$$2\rho_0^2(t) + 2\rho_1^2(t) = 1. \tag{3.11}$$

This allows to express $\rho_1^2(t)$ as a function of $\rho_0^2(t)$; moreover, since in the total energy the angle variables appear only through the combination $\phi_0(t) - \phi_1(t) \equiv \phi(t)$, we arrive at system of equations for ϕ and $\rho_0^2 \equiv D$ only,

$$\begin{cases} \partial_t\phi(t) = \frac{1}{2}\frac{\partial E}{\partial D} = \frac{U_f}{2} - 4\epsilon(1 - 4D(t))\cos^2(\phi) \\ \partial_t D(t) = -\frac{1}{2}\frac{\partial E}{\partial \phi} = 4\epsilon D(1 - 2D)\sin(2\phi) \end{cases}. \tag{3.12}$$

---

[1]Indeed the Brinkmann-Rice transition does not exist in any finite dimension [104].

The entire dynamics for the Hubbard model is mapped into that of two classical conjugate variables where $E/2$ plays the role of a classical Hamiltonian. Hence, being the total energy a constant of motion

$$E(t) = -\epsilon Z(t) + UD(t) = E_i = -\epsilon + \frac{U_f}{4} \tag{3.13}$$

the dynamics can be recast in an equation of motion for a single degree of freedom. From (3.12) we chose the angle variable ϕ as the only coordinate since this choice will become useful in the rest of the Thesis. The equation of motion for the phase reads

$$2\partial_t\phi(t) = \pm\sqrt{U_f^2 - 16\epsilon^2 \sin^2(2\phi(t))}. \tag{3.14}$$

Therefore the angle ϕ shows a characteristic pendulum-like dynamics, with finite amplitude oscillations for $U_f \leq U_c^{dyn} = U_c/2$ and full precessions around the unit circle for greater values of the quench.

Exactly at U_c^{dyn} the value of the total energy coincides with that of a ground state Mott insulator, $E = 0$. At this critical point the dynamics displays a relaxation towards a stationary solution of (3.12) characterized by the vanishing of the double occupation and consequently of the quasiparticle weight, see Fig. 3.1.

For values of the quench different from U_c^{dyn} the dynamics of $D(t)$ and $Z(t)$ displays instead an undamped oscillatory behavior. The oscillation period increases approaching U_c^{dyn} both from below and above the critical point and diverges logarithmically at U_c^{dyn}, $\tau \sim 1/\log|u_c^{dyn} - u_f|$ [49] (we use the notation $u = U/U_c$). In the limit of very large quenches the oscillating period approaches the atomic limit $\tau = 2\pi/U_f$.

The Gutzwiller approach is a simple mean field approximation and, as evident from the resulting equations of motion (3.12), it lacks enough dissipation channels to predict thermalization or even stationarization. However, some useful insights can be recovered considering long time average of an observable O

$$\langle O \rangle_t = \lim_{\tau \to \infty} \frac{1}{\tau} \int_0^\tau dt\, O(t). \tag{3.15}$$

In particular the long time average for the double occupation and the quasiparticle residue has been computed in the limit of weak and large values of the quench [49]. For small values of the quench $\langle D \rangle_t(u_f) = (1 - u_f)/4$, which corresponds to the zero temperature equilibrium value $D_{eq}(u_f)$. Therefore, no heating effect is expected at leading order in U, and both the kinetic and potential energy thermalize. Instead, the quasiparticle renormalization factor differs from the corresponding $T = 0$ equilibrium
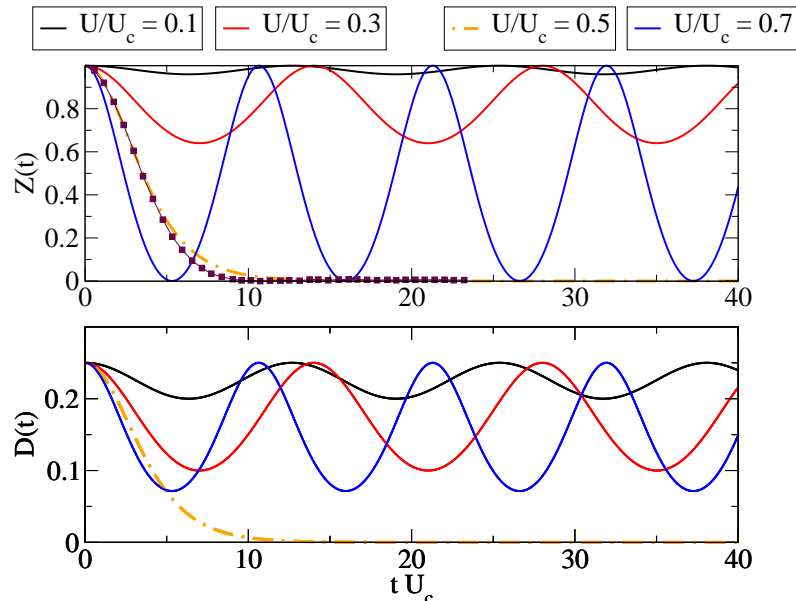
FIGURE 3.1: Dynamics of the quasiparticle weight $Z(t)$ (upper panel) and of the double occupation $D(t)$ (lower panel) for different values of the final value of the interaction. The dynamical transition point can be recognized for $U/U_c = 0.5$. We plot for comparison the DMFT result of Ref. [10] in proximity of the transition.

one

$$\langle Z \rangle_t(u_f) = 2Z_{eq}(u_f) - 1. \tag{3.16}$$

This result is in agreement with the dynamics being trapped in a metastable prethermal regime, where momentum-integrated quantities (such as the double occupation) thermalize, while k-dependent quantities show a much slower thermalization which is deferred to later times. Since the Slater determinant does not evolve in time, extending the concepts explained in Appendix A.3, the evolving state can be interpreted as a zero-temperature correlated state with well defined quasiparticles and a jump in the momentum occupation distribution given by (3.16). Remarkably, these results are in agreement with the prethermalization regime described by perturbative calculations [37, 45]. In particular, in those works, the momentum occupation probability $n_k = \langle \Psi(t) | \, c^\dagger_{k\sigma} c_{k\sigma} \, | \Psi(t) \rangle$ has shown to stationarize to a non-equilibrium zero temperature distribution with enhanced correlation given by (3.16).

The presence of a prethermal regime in the limit of weak quenches has later been ascribed to the vicinity of the integrable non-interacting limit of the Hubbard Hamiltonian. This allows to construct a Generalized Gibbs Ensemble in terms of approximate integrals of motions which reproduces the long time averages of the prethermal state [38, 105].

The t-GA predicts correctly also the long time behavior in the limit of large quenches, where $2\pi/U$ collapse and revival oscillations are present. The long time average of the

double occupation is equal in this case to $\langle D \rangle_t(U_f) = D_i - \frac{\epsilon}{2U_f}$, which agrees with the perturbative result found in [10].

These two opposite regimes are separated in the intermediate region of the quench by the critical point U_c^{dyn}, (Fig. 3.2), at which the time averages of the double occupation and of the quasiparticle residue vanishes as

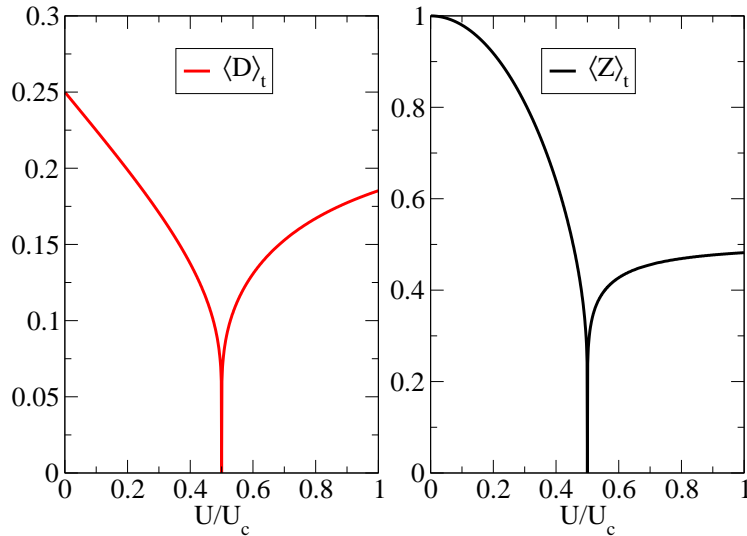$$\langle D \rangle_t(u_f), \langle Z \rangle_t(u_f) \sim 1/\log\left(|u_c^{dyn} - u_f|\right). \tag{3.17}$$

FIGURE 3.2: Long time average of the double occupation D and the quasiparticle weight Z as a function of the final values of U_f. At U_c^{dyn} both the values vanish logarithmically.

The logarithmic singularity is suggestive of a dynamical transition occurring at U_c^{dyn}. This is confirmed considering the behavior of the renormalization factor that from eq. (3.3) reads $R(t) = 4\rho_0(t)\rho_1(t)\cos(\phi)$. Due to the precession of the phase ϕ above U_c^{dyn}, it is immediate to recognize that the long time average of R can be associated to a dynamical order parameter with a finite long time average below the transition point and a vanishing one above,

$$\begin{cases} \langle R \rangle_t & > & 0 & U < U_c^{dyn} \\ \langle R \rangle_t & = & 0 & U \geq U_c^{dyn} \end{cases}. \tag{3.18}$$

U_c^{dyn} therefore distinguishes two different *dynamical phases* and for this reason has been advocated as a dynamical counterpart of the zero temperature Mott transition.

This can be corroborated by introducing the two-times local retarded Green's function (we discard spin index)

$$G^R(t+s,t) = -i\theta(s)\langle\Psi(0)|\{c_{\mathbf{R}}(t+s), c_{\mathbf{R}}^{\dagger}(t)\}|\Psi(0)\rangle \qquad (3.19)$$

and considering the spectral function $A(\omega,t) = -(1/\pi)\Im\int ds e^{i\omega s}G^R(t+s,t)$. Although this spectral function does not have the same meaning as at equilibrium, it was shown in Ref. [106] that it represents a useful quantity to distinguish the weak from the strong coupling quench regime. In particular, for large values of U, the spectrum is characterized by well defined Hubbard bands and a minimum at $\omega = 0$, thus indicating the buildup of a Mott insulator, or more properly of a bad metal.

We can try to estimate (3.19) within the Gutzwiller Approach. For this purpose we notice from the equations of motions (2.71) that the coherent part of the dynamics is described in terms of a non-interacting renormalized Hamiltonian $\mathcal{H}_*(t)$ obtained replacing the original Fermi operator $c_{\mathbf{R}\sigma}$ by its quasiparticle content that, after projection, reads

$$\mathcal{P}_{\mathbf{R}}(t)c_{\mathbf{R}}\mathcal{P}_{\mathbf{R}}(t) \rightarrow R_{\mathbf{R}}(t)c_{\mathbf{R}}. \qquad (3.20)$$

In the same spirit we can assume that the time-evolving operator $c_{\mathbf{R}}(t)$ becomes

$$c_{\mathbf{R}}(t) \rightarrow R_{\mathbf{R}}(t)c_{\mathbf{R}}^*(t) \qquad (3.21)$$

where $c_{\mathbf{R}}^*(t)$ is the time evolved operator through $\mathcal{H}_*(t)$, and the average in (3.19) is computed on the initial Slater determinant $|\psi(0)\rangle$. Within this assumption, eq. (3.19), in the homogeneous case, reads

$$G^R(t+s,t) = -i\theta(s)R(t)R(t+s)\int d\epsilon\rho(\epsilon)e^{-i\int_t^{t+s}d\tau R^2(\tau)\epsilon} \qquad (3.22)$$

where we have replaced the momentum summation with an integral over the density of states. We can compute therefore the spectral function $A(w,t)$ after a quench of the interaction. Since t-GA cannot capture relaxation we consider the time average $\bar{A}(\omega,t) = 1/t\int_0^t A(\omega,\tau)d\tau$. Its behavior is shown in Fig. 3.3 for two different values of the final interaction that lie respectively below and above the dynamical critical point U_c^{dyn}.

As shown in the Figure, below the dynamical transition a well defined peak is centered at $\omega = 0$, thus indicating a coherent metallic nature of the state. Instead, for values of the final quench above the dynamical transition, two well separated Hubbard bands are recognizable, which lie approximately at $\pm U/2$. This confirms the picture that the dynamical transition separates two different dynamical regimes that can be interpreted as the nonequilibrium counterpart of the Brinkmann-Rice transition.

This will be even more clear in the rest of the Chapter, where we shall see that the Gutzwiller dynamics can be mapped into that of an infinitely connected Ising model in presence of a transverse field. In this case, the dynamical transition separates two phases with different symmetry, [54].
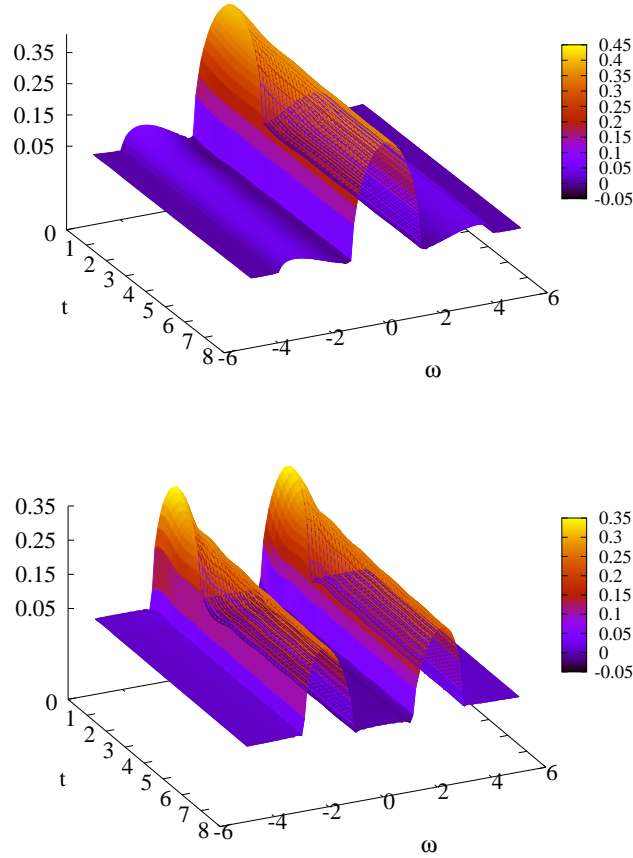

FIGURE 3.3: Time average of the spectral function $\bar{A}(w, t)$ as a function of the time and the frequency, for $U/U_c = 0.4$ (upper panel) and $U/U_c = 0.7$ (lower panel). We used a semicircular density of states $\rho(\epsilon) = \sqrt{4 - \epsilon^2}/2\pi$ where the hopping sets the unit energy.

The existence of a dynamical separation between two different regimes for the Hubbard model has been firstly discovered by means of non-equilibrium DMFT [10] which, being exact in infinite dimensions, provides a correct and non-perturbative (although limited in time) dynamics in this limit. Figure 3.4 summarizes the main picture obtained: for small values of U_f, DMFT results confirmed a prethermal regime, with the jump in the momentum occupation that displays a plateau in agreement with (3.16) and only at later times shows a slow decrease towards zero (which would correspond to the thermal value at finite temperature). In the limit of strong quenches instead, $2\pi/U_f$ oscillations dominate the dynamics and preclude thermalization on the short times reachable by

numerics.

Non-equilibrium DMFT firstly evidenced how these two different regimes are separated by a narrow critical region around $U_f \approx 3.2$ (not easily identifiable as a single value) at which the jump at Fermi surface shows a fast vanishing (in very good agreement t-GA, Fig. 3.1) and common observables, such as the double occupation or the momentum occupation distribution, thermalize very fast.

However, the effective temperature of the corresponding thermal state turned out to be much higher than the equilibrium end-point critical temperature for the Mott transition in the Hubbard model (see sketch in Fig. 3.5). Such evidence suggested that the dynamical critical region is a purely out-of-equilibrium effect not connected to an equilibrium criticality, which motivated the authors of [10] to refer it as *dynamical phase transition*. Remarkably enough, the value for the dynamical critical region within DMFT, $U_{c,DMFT}^{dyn} \approx 3.2$ (for a semicircular density of states $\rho(\epsilon) = \sqrt{4 - \epsilon^2}/2\pi$), is in a good quantitative agreement with that predicted by t-GA for the same density of states, $U_{c,GA}^{dyn} = 4\epsilon \approx 3.4$.
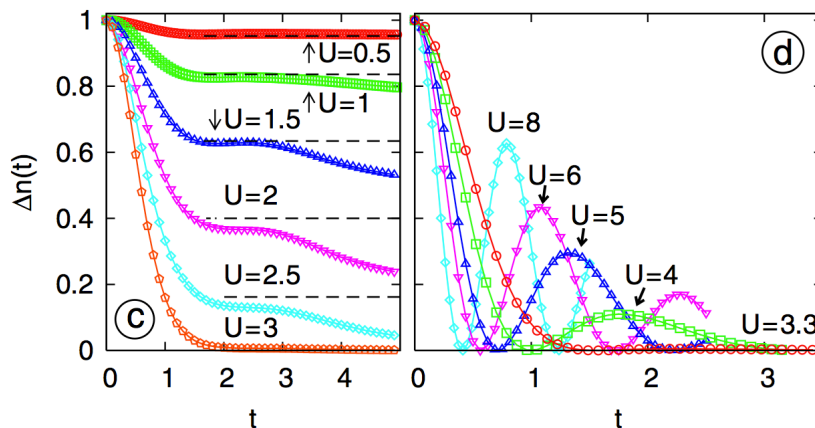

FIGURE 3.4: Discontinuity of the momentum occupation probability at the Fermi surface for different values of final interaction U_f. The dashed lines mark the prethermal plateau of eq. (3.16). Taken from [10].

We see therefore that t-GA, although being a crude approximation, is able to describe with qualitative and also quantitative agreement the main aspects that characterize the dynamics of the Hubbard model after a quench in the interaction. In particular it predicts the existence of a dynamical critical point which separates two well distinct phases that can be reconduced to zero temperature Metal-to-Insulator transition. However, although t-GA helps clarifying the picture that emerged from DMFT, it raises very important questions which remain still unsolved, the main one related to the nature of the dynamical phase transition. Indeed, the existence of a dynamical transition

analogous to that encountered within t-GA has been later observed in a series of different mean field models [51, 53–55] [2] and in all these mean field analysis, the dynamical transition is characterized by two distinct features:

- disappearance of the long time average of an order parameter, with a consequent separation between two distinct nonequilibrium phases;

- absence of thermalization, due to the lack of relaxation mechanisms in the models considered.

These evidences leave then open the debate on the nature of the transition for the Hubbard model in the limit of infinite dimensions as found by DMFT. Is it a transition between two thermodynamic distinct phases (as t-GA would suggest) or is it just a dynamical separation (or even a sharp crossover) between two different prethermal regimes?

If one believes that thermalization occurs within the dynamical critical region, the second scenario would seem the most probable. In fact, since the corresponding equilibrium phase at which the dynamics thermalizes is far away from the equilibrium Metal-to-Insulator transition line [10], (see sketch in Fig. 3.5), this would rule out the possibility that the dynamical transition separates two distinct thermodynamic phases and would rather point towards the interpretation in terms of a dynamical transition (or even a sharp crossover limited to intermediate times) between two different prethermal regimes, maybe due to the vicinity of a non-thermal fixed point (which in this case could be represented by the Gutzwiller dynamical critical point).

However, due to the numerical difficulty in exploring this dynamics within DMFT, non conclusive answer has been given so far, thus leaving the connection between the two phenomena and consequently the nature of the dynamical transition an open debate.

A relevant step forward that would help clarifying this issue requires a better understanding of the possible link between the dynamical transition and the equilibrium phase transition. This could be investigated in two manners. The first would be considering a quench from a finite initial value of the interaction U_i to larger values $U_f < U_c$. For large enough U_i, the effective temperature should eventually cross the phase transition line, provided thermalization occurs (at least it would occur if U_i is greater than the corresponding value for the end-point of the Mott transition, as shown in Fig. 3.5).

---

[2]It is worth to remark that whenever an analytical solution of the equation of motion is not feasible, it is in general not possible to identify the dynamical transition as a single point. In reference [55] indeed the dynamical transition has rather been characterized as an extended region. This issue will be further encountered in the rest of the Thesis.

Within t-GA the dynamical phase transition occurs also in this case at a value [49]

$$\frac{U_c^{dyn}}{U_c} = \frac{1}{2}\left(1 + \frac{U_i}{U_f}\right)$$

which however is unrelated to the thermal one, since thermalization is missed in the Gutzwiller dynamics. It would be interesting to see if a dynamical transition appears within DMFT in this case and if it is related or not to the crossing of the equilibrium transition line.

A second alternative, which we shall consider in rest of this Chapter, is to ramp the interaction adiabatically from the non-interacting limit. We will see that within t-GA a dynamical transition will appear for any value of the ramping time τ and will connected to the zero temperature equilibrium critical point for $\tau \to \infty$. This confirms that within the GA the dynamical phase transition is the nonequilibrium counterpart of the zero temperature Brinkmann-Rice transition.
Unfortunately, also in this case, DMFT results are not available due to the finite time restrictions imposed by numerics, which leaves the puzzle still unsolved.
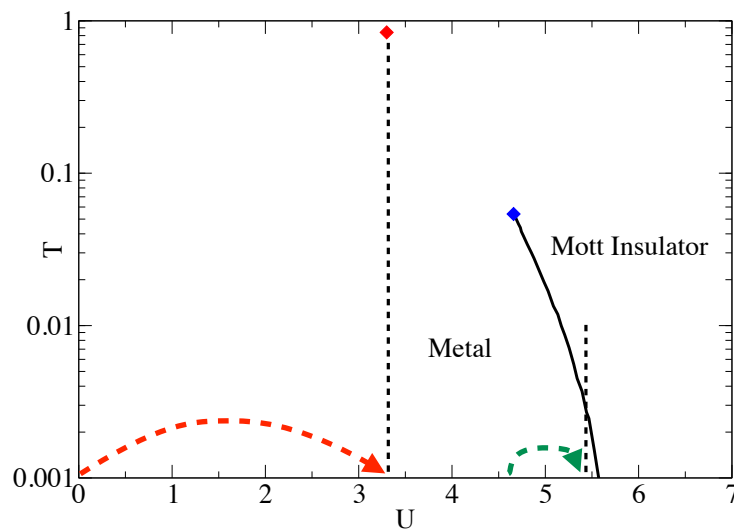

FIGURE 3.5: Sketch diagram representing the dynamical transition as found by DMFT (in units of the hopping, for a semicircular density of states, [10]). The red arrow represents the quench to U_c^{dyn} for which the corresponding effective temperature (red diamond) lies far above the end-point of the Metal-to-Insulator transition (blue diamond). The green arrow sketches the quench proposed in the main text. In this case, for U_f big enough, provided thermalization occurs, the effective temperature should cross the equilibrium phase transition line.

A final important issue to address regards the fate of the dynamical phase transition beyond mean field approximation with particular emphasis on the role of quantum fluctuations. This latter question has been recently tackled in Ref. [107] where leading order corrections beyond mean field were considered in the investigation of quantum N-component ϕ^4 model and a dynamical transition was established characterized by the vanishing of the order parameter.

We mention that recently the qualitative existence of two different dynamical regimes resembling the results presented in this Section has been established also for the one- and two-dimensional Hubbard model by means of high order perturbative schemes [46, 50], thus enforcing the guess that a dynamical critical region might indeed be more general than what expected on the basis of mean field calculations.

In the next sections we will report the attempts we made to address these problems within t-GA.

3.3 Ramping the interaction in the Hubbard Model

In this Section we consider the dynamics of the fermionic Hubbard model (3.1) extending the sudden quench introduced so far and considering a linear ramp of the interaction $U(t)$ between U_i and $U_f = U_i + \Delta U$, namely we shall assume

$$
\begin{aligned}
U(t) &= U_i + \Delta U \, t/\tau &\quad 0 < t < \tau \\
U(t) &= U_f &\quad t \geq \tau.
\end{aligned}
\tag{3.23}
$$

We note that, experimentally, it turns to be easier to change in time the optical lattice depth, which controls the hopping strength $t_{\mathbf{RR'}}$, rather than the local interaction. However, we can safely assume that the same effect can be modeled by tuning in time the local interaction, since the physics will only depend on the ratio between $U(t)$ and the bandwidth. In the following, we shall only focus on the half filled case and, for the sake of simplicity, consider a non interacting initial state ($U_i = 0$), even though the extension to finite U_i is straightforward.

The problem of linear ramps in a strongly correlated fermionic system has been addressed in a number of recent works. The crossover from adiabatic to sudden quench regimes and in particular the scaling of the excitation energy with the ramp time τ has been studied in the Falikov Kimball model by nonequilibrium DMFT [108]. For what concerns the Hubbard model, (3.1) the problem has been tackled in the perturbative small U_f regime and arbitrary ramp-time using Keldysh perturbation theory [37], and in

the non-perturbative regime but short ramp times by nonequilibrium DMFT in combination with CTQMC [99]. Here we will make use of the mean field theory we presented for the sudden quench case to address the problem of ramps and we will compare with the results available whenever this is possible.

Since the time dependent interaction $U(t)$ introduces a new time scale contrary to the sudden quench case, namely the rate τ at which the ramp is performed, one can ask oneself three separate questions: (i) what is the dynamics during the ramp, i.e. for times $t \leq \tau$; (ii) what is the state the system is left once the ramp is terminated (excitation energy, degree of adiabaticity); and finally (iii) what is the nonequilibrium dynamics for times larger than the ramp time, i.e. for $t > \tau$.

3.3.1 Dynamics during the ramp and degree of adiabaticity

In Figure 3.6 we plot the dynamics of the quasiparticle weight $Z(t)$ for different values of the final quench $u_f = U_f/U_c$ in units of U_c, the critical value for the equilibrium Mott transition that will be our unit of energy hereafter, at two different fixed ramp times, $\tau = 100$ (top panel) and $\tau = 20$ (bottom panel). In the same figure we plot, for the sake of comparison, the adiabatic dynamics obtained assuming the system stays in its instantaneous ground state, namely that

$$Z_{ad}(t) = 1 - u^2(t)\,.$$

A quick look to this figure reveals that, as one could expect, the degree of adiabaticity depends strongly on the duration of the ramp τ and on the final value of the interaction u_f. In order to be more quantitative on this issue it is useful to introduce a measure of the adiabaticity of the process. A possible criterion amounts to calculate the excitation energy which is left into the system once the ramp is completed. This quantity is defined as

$$\Delta E_{exc}\left(\tau, u_f\right) = E\left(\tau, u_f\right) - E_{gs}(u_f(\tau))\,, \tag{3.24}$$

where $E(t, u(t)) = \langle H(t) \rangle$ is the time dependent expectation value of the Hamiltonian, while $E_{gs}(u_f)$ is the ground state energy at the final value of the interaction u_f. Based on very general grounds one expects that if the system behaves adiabatically then the excitation energy ΔE_{exct} should go to zero as the ramp duration diverges. Since one expects the process to be more and more adiabatic as τ increases, the expectation for ΔE_{exc} is to show a monotonic decreasing behavior as a function of the ramp time τ.

In Figure 3.7 (top panels) we plot the excitation energy as a function of τ for quenches from the non interacting case $u_i = 0$ to different values of u_f. We notice that
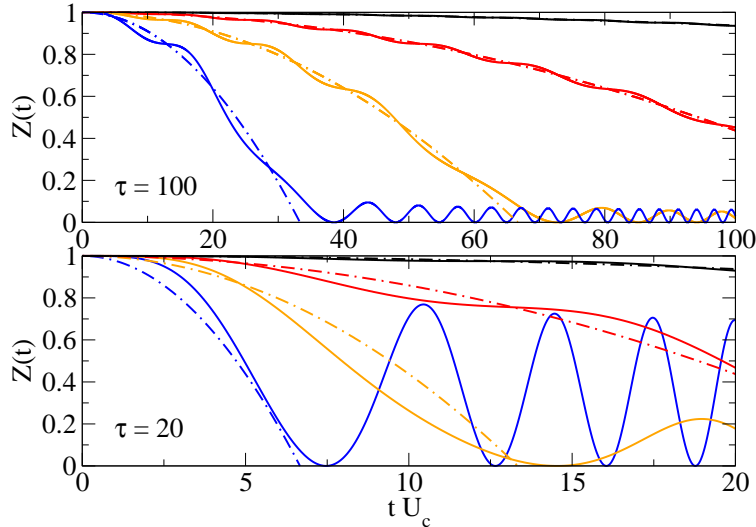
FIGURE 3.6: Gutzwiller mean field dynamics at half-filling for quasiparticle weight $Z(t)$ for quantum quenches from $u_i = 0$ to $u_f = 0.25, 0.75, 1.5, 3.0$ (from top to bottom) for a ramp time $\tau = 100$ (top panel) and $\tau = 20$ (bottom panel). For comparison we plot the adiabatic dynamics $Z_{ad}(t)$ (see dashed lines), obtained assuming the system stays in its instantaneous variational ground state.

the excitation energy does indeed decreases toward zero with τ, although with some small oscillations, thus confirming that the time dependent Gutzwiller approximation is able to capture the crossover from the sudden quench to the adiabatic regime.

It is particularly interesting to study the regime of very long ramp times $\tau \to \infty$, where one expects universal behavior to emerge as a function of the ramp speed. This universality translates into power-laws and scaling relations for the relevant physical observables which have been recently attracting a lot of attention in the literature, starting with the seminal work by Kibble and Zurek on classical phase transitions and its generalization to the quantum case [97, 109, 110]. More recently the issue of universality in the Kibble-Zurek problem has attracted a renewed interest and first steps toward a scaling theory have been performed [111, 112]. Here we focus on the scaling of the excitation energy ΔE_{exc} which is very sensitive to the nature of the elementary excitations in the systems [90]. This question, in the context of the correlated fermionic systems, has been addressed in the Falikov-Kimball model using DMFT [108] and in the fermionic Hubbard model, that is of interest here, mainly using pertubation theory [37, 108].

We perform such a scaling analysis (see bottom panel of figure 3.7) and find that to a very good extent the behavior of ΔE_{exc} is consistent with a power law, possibly with a pre-factor that depends on the interaction u_f and displays in general an extra oscillating behavior in τ

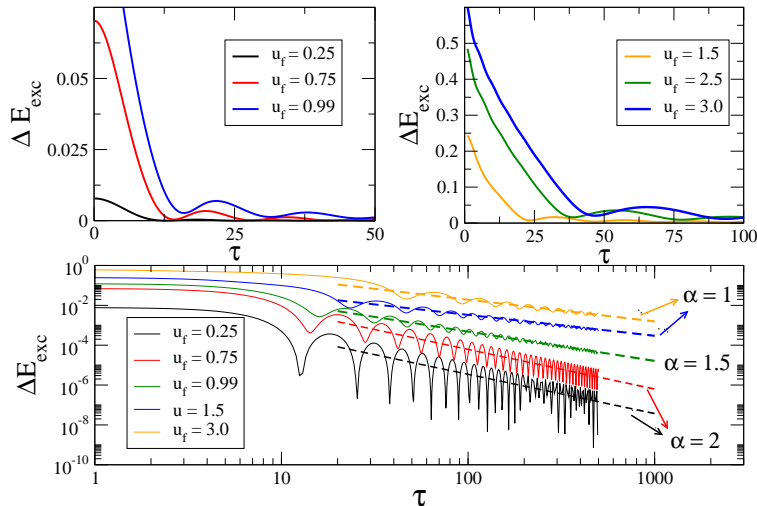$$\Delta E_{exc}(\tau) = \frac{\gamma(\tau, u_f)}{\tau^{\alpha}} \qquad (3.25)$$

FIGURE 3.7: Excitation energy $\Delta E(\tau)$ as a function of the ramp time for quenches starting from the metallic phase ($u_i = 0$) and ending into the metallic (left panel) or insulating (right panel) phase. We see in the former case a fast transient to zero occurs, with some residual oscillations which die out as τ increases. As opposite for quenches which crosses the Mott transition the transient seems much more longer and sensitive to the final value of u_f, namely stronger quenches seems to require longer ramps to achieve a fixed amount of excitation energy.

At small values of the final interaction u_f we find $\Delta E_{exc} \sim \tau^{-2}$. We notice that, in this small quench regime, oscillations are more pronounced (and result into the noisy scaling of figure 3.7), nevertheless the power law scaling with $\alpha = 2$ works very well for the envelope of local maxima. This scaling appears to be consistent with perturbative results [37, 108] and with linear response arguments [90]. We notice that for the Falikov-Kimball model the DMFT analysis gives a different exponent, $\alpha = 1$, for ramps ending in the metallic phase, but this result has been understood as a consequence of the Non-Fermi Liquid ground state of that model [108]. Within our time dependent Gutzwiller approximation we find that the "Fermi Liquid scaling" works up to rather large values of the interaction but appears to break down close to the Mott transition, $u_f = 1$, where the exponent crosses over to $\alpha \simeq 1.5$. Finally, for ramps ending deep inside the Mott phase, we find very small oscillation in the long time behavior of ΔE_{exc} and power law scaling suggests an exponent $\alpha = 1$. In order to get more insights into the behavior of the excitation energy ΔE_{exc} for large τ it is useful to step back for a moment to the Gutzwiller semi-classical dynamics given by equations (3.12). In the limit of very slow ramps, $\tau \to \infty$, one can analyze the deviations from adiabaticity using techniques borrowed from classical mechanics. This is described in great detail in a recent work
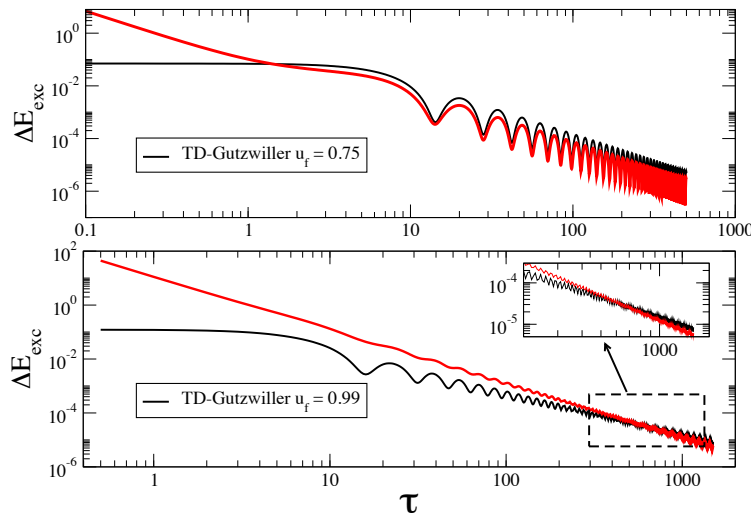
FIGURE 3.8: Excitation energy $\Delta E(\tau)$ as a function of the ramp time for quenches starting ($u_i = 0.0$) and ending ($u_f = 0.75$ top panel, $u_f = 0.99$ bottom panel) in the metallic phase. We compare the Gutzwiller results with the scaling Eq. (3.25-3.26) obtained from the adiabatic classical dynamics (red curve). The agreement for $u_f < 1$ is excellent but worsen upon approaching the critical point.

by Bapst and Semerjain that addresses the ramp dynamics in a fully connected $p-$spin model with a transverse field [113]. For ramps ending in the metallic phase, $u_f < 1$, one can expand the classical Hamiltonian around its instantaneous minimum [114] (see appendix B.1), $D_*(t) = (1 - u(t))/4$, up to a quadratic order with frequency $\omega(t) \sim \sqrt{1 - u(t)^2}$ and obtain for the excitation energy the result (3.25) with $\alpha = 2$ and γ

$$
\begin{aligned}
\gamma(\tau, u_f) &= \frac{u_f^2 \sqrt{1 - u_f^2}}{4} \sin^2 \omega(u_f)\tau + \\
&+ \frac{1 - u_f^2}{4} \left(\frac{u_f}{1 - u_f^2} - \frac{u_f}{(1 - u_f^2)^{1/4}} \cos \omega(u_f)\tau \right)^2
\end{aligned}
\tag{3.26}
$$

with $\omega(u_f) = \frac{1}{4} \left(\arcsin(u_f)/u_f + \sqrt{1 - u_f^2} \right)$. In figure 3.8 we compare this expression with the numerics and find an excellent agreement, in particular we notice the frequency of the oscillations is correctly captured by $\omega(u_f)$. We also notice that upon approaching the critical point $u_f \to 1$ the agreement deteriorates. Indeed for ramps ending in the insulating phase, i.e. $u_f > 1$, the situation is more tricky as the frequency of oscillations $\omega(t)$ vanishes during the ramp at $t = t_\star = \tau/u_f$ and one cannot extend the above analysis to the regime $t_\star < t < \tau$. Still one can proceed by mapping the classical dynamics onto a suitable limit of the Painlevé equation and using the well known results on its asymptotic. This has been discussed in Refs [113, 115] for the fully connected

Ising model in a transverse field, which is relevant for the Hubbard model within the Gutzwiller approximation (as we shall see later), where a power law $\alpha = 1$ has been found for ramps across the critical point, in agreement with our numerical results. In light of this analysis an interesting question, that we leave open for future investigations, is to understand whether a different power law exponent may arise for ramps ending right at the critical point (as our numerics would suggest) or if the quadratic scaling (3.26) expected in the metallic phase eventually sets in on a sufficiently longer time scale.

We finally conclude this Section by briefly discussing whether the above findings can be put into the framework of the Kibble-Zurek scaling theory [97, 109, 110]. For a ramp from the ordered to the disordered phase across a critical point scaling arguments would predict for the excitation energy a power-law decay [98, 116] $\Delta E_{exc} \sim 1/\tau^{d\nu/z\nu+1}$. Indeed, by using the mean field exponents $\nu = 1/2, z = 1$ for the Ising critical point and setting d to the upper-critical dimension $d = 3$ for a quantum Ising model we get $\Delta E_{exc} \sim 1/\tau$, namely $\alpha = 1$, which matches our results. While this observation may suggest a positive answer to this question we notice that the validity of such a scaling theory for fully connected models (or finite-connectivity models treated within mean-field as it is the case here) is not obvious a priori (in particular the identification of d with the upper critical dimension is generally dangerous when dealing with scaling) and it has been not fully addressed in the literature to the best of our knowledge. For this reason and since this is not the main focus of the present paper we refrain from conclusive statements on this issue and leave this question for future investigations.

3.3.2 Dynamics after the ramp

We now turn our attention on the dynamics *after* the ramp is completed, namely for $t > \tau$. Here the system is isolated, i.e. the energy is conserved, and the evolution starts from the state the system is left once the ramp is over. This set-up represents therefore the natural generalization of the sudden quench case (which is indeed recovered in the limit $\tau \to 0$): once the ramp is completed, the system has some excitation energy above its ground state and one is interested in the relaxation dynamics for longer time scales.

Interestingly enough this issue has been only partially addressed in the literature, which mostly focused on the dynamics during the ramp, but it looks particularly intriguing in light of the results obtained on the sudden quench case. As we explained in Sec. 3.2, a dynamical transition characterized by a fast relaxation has been found, quite generically, in mean field models for bosons and spins [51, 53] and in the fermionic case, too, both at the variational level [49] and within DMFT [10].

A natural question we would like to address here is therefore what is the effect of the finite ramp duration on the mean field dynamical transition found in the sudden quench case. A recent investigation using non equilibrium DMFT with the CTQMC impurity solver [99] addressed this same issue for very small ramps and found signatures of a sharp crossover in the dynamics, much similar to what found in the sudden quench limit. While this result seems to suggest that a dynamical transition survives also for small finite τ, it is difficult from numerical data, which are limited to short times, to conclude what happens for a generic speed ramp, and eventually in the adiabatic limit $\tau \to \infty$. Here we will address again this point using mean field theory and study the fate of the dynamical transition after a ramp of arbitrary speed.

As we mentioned earlier, the classical dynamics (3.12) for $t > \tau$ admits an integral of motion which is the total energy,

$$E(t) = u_f\, D(t) - \frac{1}{8}\, Z(t) \equiv E_R(u_f, \tau)\,, \qquad t > \tau\,. \tag{3.27}$$

Hence we can use it to reduce the problem to a one dimensional dynamics, much in the same way we did for the quench case. A simple calculation gives the equation of motion is term of the solely double occupation,

$$\dot{D} = \sqrt{\Gamma(D)}\,, \tag{3.28}$$

with the effective potential $\Gamma(D)$ given by

$$\Gamma(D) = (u_f\, D - E_R)\left(E_R - u_f\, D + 2\, D\,(1/2 - D)\right). \tag{3.29}$$

The energy $E_R(u_f, \tau)$ after the ramp depends on the initial (u_i) and final (u_f) values of the interaction and from the ramp time τ. In the general case, its value has to be determined from the solution of the dynamics for $t < \tau$, but it reduces in the sudden quench limit $(\tau \to 0)$ to the value

$$E_R(u_f, 0^+) = \frac{u_f}{4} - \frac{1}{8}\,,$$

while for an infinitely slow ramp $\tau \to \infty$ it approaches the ground state energy at the final value of the interaction, namely

$$E_R(u_f, \tau \to \infty) = -\frac{1}{8}\,(1 - u_f)^2 \qquad u_f < 1\,,$$

and zero in the Mott insulator phase $u_f > 1$.

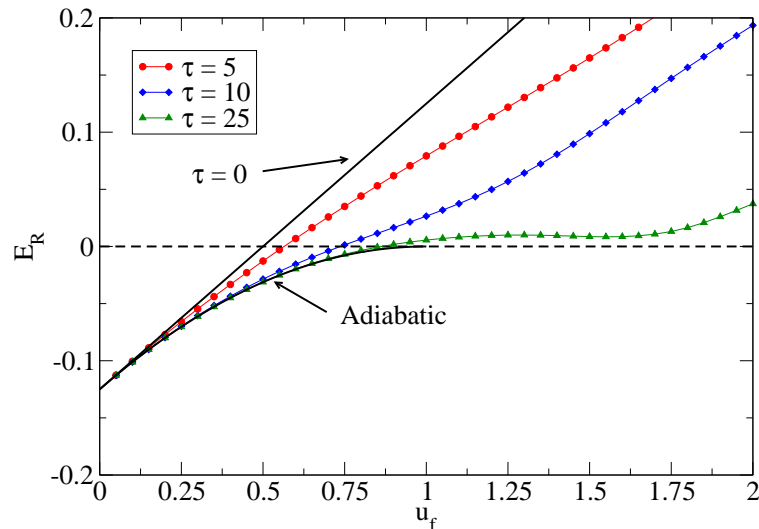In Figure 3.9 we plot the behavior of $E_R(u_f, \tau)$ at different values of τ. The effective

FIGURE 3.9: Average energy after the ramp as a function of the final interaction quench u_f and for different values of the ramp time τ. We see that upon increasing τ the energy crosses over from the sudden quench limit to the adiabatic instantaneous ground state energy $E_{gs}(u_f)$.
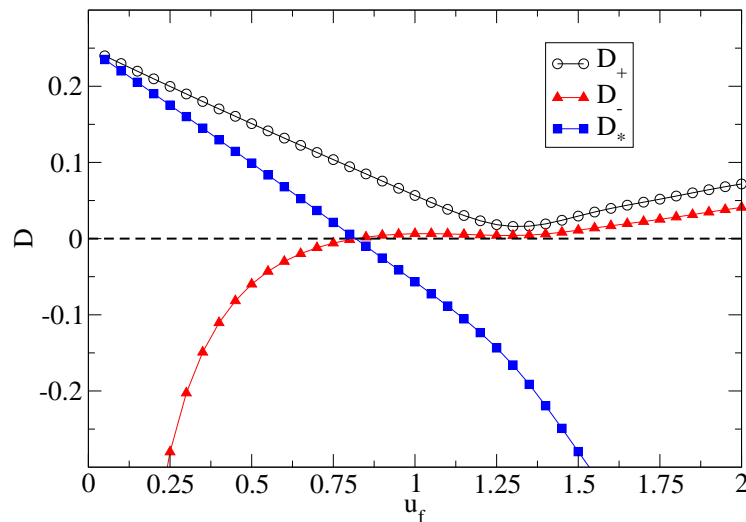

FIGURE 3.10: Behavior of the inversion points $D_\pm, D_\star$ as a function of the final interaction u_f, for a ramp of the interaction of duration $\tau = 20$ and starting from $u_i = 0$. We notice the crossing of roots, occurring at $u_f^c(\tau)$ which signals the onset of a relaxation dynamics.

potential has three roots which read $D_\star = E_R/u_f$ and

$$D_\pm = \frac{1 - u_f \pm \sqrt{(u_f - 1)^2 + 8\,E_R}}{4} \tag{3.30}$$

We immediately see that, much as in the sudden quench case, for a given ramp time τ at which the condition $E_R(u_f, \tau) = 0$ is fulfilled, two of the above roots merge and the
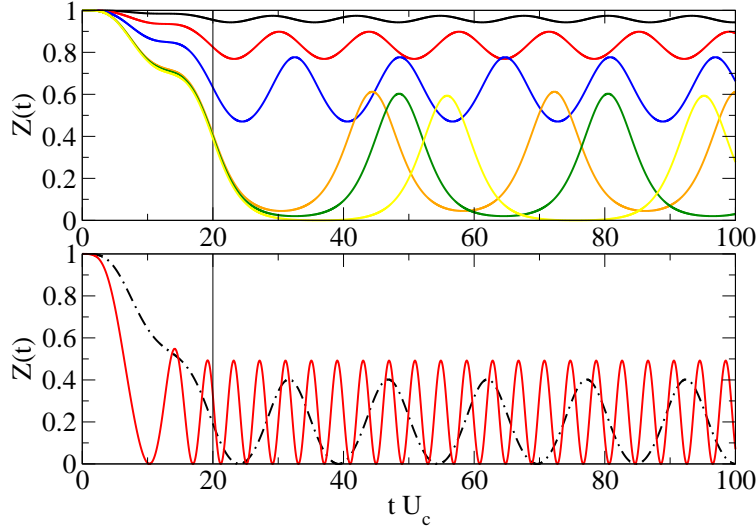
FIGURE 3.11: Gutzwiller mean field dynamics at half-filling for quasiparticle weight $Z(t)$ for a ramp of duration $\tau = 20$ from $u_i = 0$ to $u_f = 0.2, 0.4, 0.6, 0.8, 0.81, 0.82$ (top panel, from top to bottom) and from $u_i = 0$ to $u_f = 1.0$ (dashed) or 2.0 (full red line). The critical value of the interaction quench $u_f^c(\tau = 20) \simeq 0.83$.

dynamics shows an exponentially fast relaxation. The only non vanishing root reads

$$D_- = \frac{1 - u_f^c(\tau)}{2} \qquad (3.31)$$

where $u_f^c(\tau)$ is the value of the final interaction at which $E_R(u_f, \tau) = 0$ (see Figure 3.10). In Figure 3.11 we plot the dynamics of quasiparticle weight $Z(t)$ after a ramp of $\tau = 20$ for different values of the final interaction. We still can distinguish two regimes of slow and fast oscillations with some period $\mathcal{T}(u_f, \tau)$, which turns out to diverge at the transition $u_f^c(\tau)$. Such a diverging time scale is associated to a change in the behavior of the effective potential $\Gamma(D)$, with two inversion points going degenerate at $u_f^c(\tau)$. As a result, the divergence appears to be still logarithmic $\mathcal{T} \sim \log |u_f - u_f^c(\tau)|$. For ramps ending right at $u_f^c(\tau)$ the dynamics approaches exponentially fast the steady state value $Z = 0$. The exact expression for $Z(t)$ can be worked out in this case, but does not look particularly illuminating . The scaling at long times reads

$$Z(t \gg \tau) \sim \exp\left(-t/t_{rel}\right) \qquad (3.32)$$

with $t_{rel} = \sqrt{2\, u_f^c(\tau)}$. We therefore get an exponential scaling at long times, as for the sudden quench case, with a time scale t_{rel} that accounts for the finite duration of the ramp. It is interesting to discuss the dependence of the critical interaction strength u_f^c from the ramp duration τ, which could shed some light on the origin of this putative dynamical critical point, which is still under debate. In addition to that, as we noticed
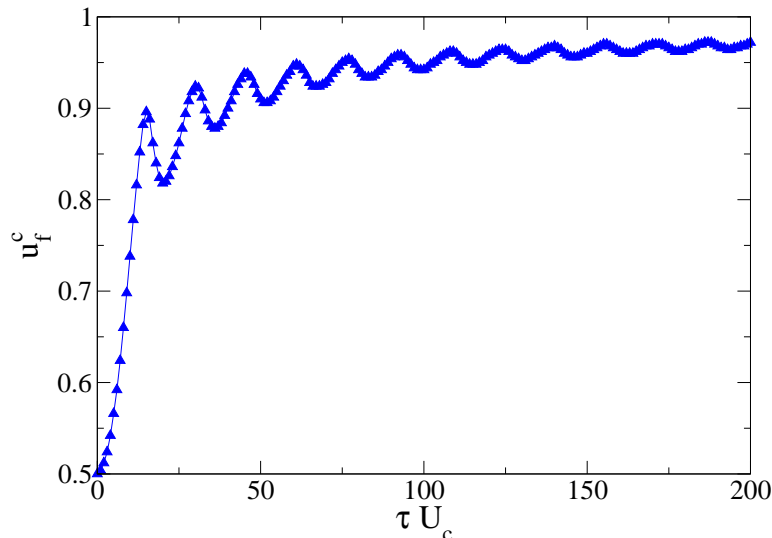
FIGURE 3.12: Mean field dynamical critical point u_f^c as a function of the ramp duration τ. We see that for small τ we recover the sudden quench result $u_f^c = 1/2$ while for longer ramps $\tau \to \infty$ u_f^c approaches the equilibrium Mott critical point $u_f = 1$.

earlier, this quantity (together with the lattice bandwidth) sets the time scale for the relaxation t_{rel}, therefore by tuning properly τ one can arrange protocols where relaxation is faster. This issue was addressed in Ref. [99], although only for short ramps $\tau \simeq 1$, where the authors also discussed the dependence of $u_f^c(\tau)$ upon the ramp protocol.

In Figure 3.12 we plot the behavior of u_f^c as a function of τ for a linear ramp starting at $u_i = 0$. We see that this quantity approaches, for $\tau \to 0$, the sudden quench value $u_f^c(0) = 1/2$. From the behavior of $E_R(u_f, \tau)$ in Figure 3.9 we observe that in the opposite limit of a very long ramp the system is closer and closer to the adiabatic ground state. As a result, the condition $E_R(u_f, \tau) = 0$ suggests that as τ increases the mean field critical point u_f^c smoothly approaches the equilibrium zero temperature Mott transition, namely $u_f^c(\tau \to \infty) = 1$. This is indeed the case, namely u_f^c interpolates between the sudden quench value at small τ and the Mott critical point for long ramps. We also note the presence of small oscillations in its τ dependence, which are likely an artefact of the Gutzwiller mean field dynamics. DMFT data would be required in order to check this point further.

The asymptotic behavior for long ramps, namely for small excitation energies, looks also very intriguing and deserves further investigations. From one side one could have expected this result since the larger is τ the less the system is excited at the time the ramp stops. Hence it is reasonable to expect that some kind of *criticality* or sharp crossover between weak and strong coupling should be visible close to the Mott quantum critical point. On the other hand, one has also to bear in mind that the less the system

is excited above its ground state at the time the ramp ends, the less sharp the signature of the *dynamical* critical point will look. Indeed, as we are going to see and in agreement of what observed by Keldysh perturbation theory, [37] the metastable prethermal states which block the dynamics at small and large quenches become lower and lower in energy as the ramp time increases.

The last issue we would like to discuss here is the dependence from the ramp time τ of long time averages, that we define as

$$\langle O \rangle_t = \lim_{T \to \infty} \frac{1}{T} \int_\tau^T dt\, O\left(t\right) . \tag{3.33}$$

Since the motion for $t > \tau$ is periodic, although as we have seen the initial condition at $t = \tau$ is not an inversion point of the dynamics, one can still express those long time averages as an integral over a period of oscillation. This allows to obtain closed expressions for the double occupation average $\langle D \rangle_t\left(u_f, \tau\right)$ and, through the conservation of energy, for the quasiparticle weight $\langle Z \rangle_t(u_f, \tau)$. The critical behavior is then the same of that obtained for the sudden quench case where both quantities vanish at the dynamical critical point $u_f^c(\tau)$ with the logarithmic divergence,

$$\langle D \rangle_t(u_f, \tau) \sim 1/\log|u_f - u_f^c(\tau)| . \tag{3.34}$$

In other words, as for the period of oscillations $\mathcal{T}(u_f, \tau)$, the only effect of the finite ramp duration is to shift the critical point to $u_f^c(\tau)$, without changing the critical behavior at the transition.

In addition to the behavior close to $u_f^c(\tau)$, also the results at small and large values of u_f are interesting. Indeed, in the sudden quench case it was shown [103] that the long time average of mean field dynamics exactly reproduces the metastable plateau blocking the dynamics, which can be evaluated using perturbation theory. This is consistent with the idea that mean field dynamics is able to capture the short-to-intermediate dynamics, and the trapping occurring on those time scales, but not the final escape toward equilibrium. In light of this results we want now to understand how these metastable plateau move as the ramp time is changed from the sudden to the adiabatic limit.

To this extent we compute the long time average of the quasiparticle weight, $\langle Z \rangle_t(u_f, \tau)$, and define, following Ref. [37], the mismatch function $\mu(\tau)$ as

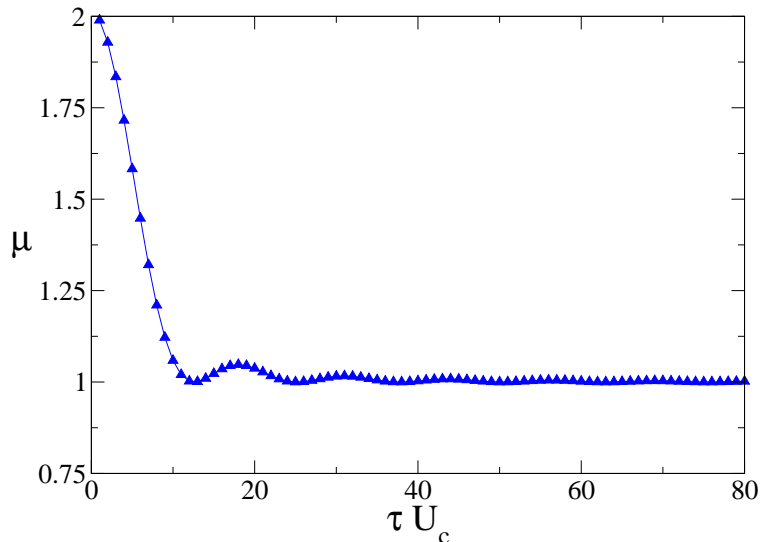$$\mu(\tau) = \frac{1 - \langle Z \rangle_t(u_f \to 0, \tau)}{1 - Z_{eq}(u_f \to 0)} . \tag{3.35}$$

FIGURE 3.13: Mismatch $\mu(\tau)$, as defined in the main text, as a function of the ramp duration τ. We see the crossover from the sudden quench limit $\mu = 2$ to the adiabatic regime $\mu = 1$.

In the sudden quench case this quantity approaches $\mu(0^+) = 2$, consistently with the results obtained with other perturbative methods. In the opposite limit of a very long ramp we expect the mismatch to approach $\mu(\infty) = 1$, namely the dynamics to be adiabatic. We plot in figure (3.13) the behavior of the function $\mu(\tau)$, which shows a smooth crossover from the sudden to the adiabatic regime.

3.4 Quantum Fluctuations Beyond Mean Field

In this Section we discuss the role of quantum fluctuations on the mean field ramp dynamics we have previously presented. To this extent, we reformulate the Hubbard model in the framework of the Z_2 slave spin theory. We give here only the main results of this mapping and refer to Ref. [103, 117, 118]. As in other slave spin approaches [119, 120], we map the local physical Hilbert space of the Hubbard Model onto the Hilbert space of an auxiliary spin model coupled to fermions and subject to a local constraint. In the Z_2 case the formulation is somehow minimal in the sense that auxiliary degrees of freedom are a single Ising spin and a spinful fermion. The Hamiltonian of the original Hubbard model, Eq. (3.1), when written in terms of the auxiliary degrees of freedom

reads

$$H_{Ising} = -t \sum_{<\mathbf{R},\mathbf{R'}>\sigma} \sigma^x_{\mathbf{R}} \sigma^x_{\mathbf{R'}} f^\dagger_{\mathbf{R}\sigma} f_{\mathbf{R'}\sigma} + \frac{U(t)}{4} \sum_{\mathbf{R}} \left(1 - \sigma^z_{\mathbf{R}}\right), \qquad (3.36)$$

where $f_{\mathbf{R}\sigma}, f^\dagger_{\mathbf{R}\sigma}$ are auxiliary fermionic fields while $\sigma^x_{\mathbf{R}}$ is an Ising spin variable. The spin-fermion Hamiltonian (3.36) lives in an enlarged Hilbert space containing on each site a spin-full fermion and an Ising variable. In order to project onto the physical Hilbert space of the original Hubbard model one can introduce the following operator in any quantum average,

$$\mathcal{Q} = \prod_{\mathbf{R}} \left(\frac{1 - \sigma^z_{\mathbf{R}} \Omega_{\mathbf{R}}}{2}\right), \qquad (3.37)$$

where $\Omega_{\mathbf{R}} = e^{i\pi n_{\mathbf{R}}}$ and $n_{\mathbf{R}} = \sum_\sigma f^\dagger_{\mathbf{R}\sigma} f_{\mathbf{R}\sigma}$. The above operator is actually a projector of the enlarged Hilbert space onto the subspace where if $n = 1$ then $\sigma^z = +1$ while, if $n = 0, 2$, then $\sigma^z = -1$. As a matter of fact, $\mathcal{Q}$ is just the constraint introduced in Ref. [118] as a basis of the Z_2 slave-spin representation of the Hubbard model. The constraint holds in general between Hilbert spaces, hence between evolution operators both in imaginary as well as in real time. This allows us to study the dynamics of the original Hubbard model using the Ising spin-fermion Hamiltonian (3.36).

In Ref. [103] it was shown that (i) in infinite dimensions and at particle hole symmetry the constraint is ineffective and (ii) that when gauge fluctuations are neglected, namely a product state between spins and fermions is assumed during the evolution, and when the resulting transverse field Ising model is treated in mean field, the time dependent Gutzwiller results follow. The advantage of this approach is that, once we have formulated the problem in the Ising language, we can attempt to include quantum fluctuations beyond mean field, even though this amounts to move away from infinite coordination lattices where the neglect of the constraint is not anymore justified.

This strategy was pursued in Ref. [118] to study the zero temperature equilibrium Mott transition and then in Ref. [103] to access the dynamics after a sudden quench. Interestingly enough, this latter investigation revealed that quantum fluctuations become dynamically unstable in a region of quenches around the mean field critical line. Such a behavior may be suggestive of an instability toward an inhomogeneous state where translational symmetry (which was implicitly assumed in the mean field dynamics) is broken and may also suggest that the dynamical critical behavior found at the mean field level gets strongly modified in finite dimensions.

Here we would like to apply this mean field plus fluctuation approach to the problem of a finite ramp and revisit in particular the analysis we have done in Section 3.3 on the scaling of excitation energy and the degree of adiabaticity of the process. We expect

that for sufficiently slow ramps, when the system stays close to the instantaneous ground state, no instability in the fluctuation spectrum should arise. This will allow to include gaussian fluctuations in a controlled way and to address questions concerning the Mott insulating state dynamics that otherwise are out of reach within the Gutzwiller mean field theory. Conversely, upon increasing the speed of the ramp, the simple treatment of fluctuations without feedback would again recover the unstable behavior found in the sudden quench case. In order to go beyond this simple treatment, we develop here a self consistent treatment of quantum fluctuations and discuss the results of the coupled quantum-classical dynamics in the sudden quench limit.

3.4.1   Fluctuations above mean field for slow ramps

We start our discussion of fluctuations from the limit of very slow ramps. In this regime when the dynamics is almost adiabatic, the fluctuations are expected to be well behaved, since in the limit of $\tau \to \infty$ we should recover the fluctuation spectrum in the instantaneous ground state of the Ising model which is known to be well behaved [118]. To this extent, we start from the Hamiltonian (3.36) and decouple the slave spins from the fermionic degrees of freedom, namely we assume a time dependent factorized wave function

$$|\Phi(t)\rangle = |\Phi_s(t)\rangle \, |\Phi_f(t)\rangle$$

each component $|\Phi_s(t)\rangle$ and $|\Phi_f(t)\rangle$ being translationally invariant. The electron wavefunction will evolve under the action of a time-dependent hopping, which is however still translationally invariant. Hence, if $|\Phi_f(t = 0)\rangle$ is eigenstate of the hopping at $t < 0$, in particular its ground state state, it will stay unchanged under the time evolution. Therefore we shall only focus on the evolution of the Ising component. Its effective Hamiltonian $H_s = \langle H_{Ising}\rangle_f$ at positive times and in units of U_c is

$$H_s = -\frac{u_f}{4}\sum_{\mathbf{R}}\left(1 - \sigma_{\mathbf{R}}^z\right) - \frac{1}{8}\sum_{<\mathbf{R}\,\mathbf{R'}>}\sigma_{\mathbf{R}}^x\,\sigma_{\mathbf{R'}}^x, \qquad (3.38)$$

We now follow the steps described in Ref. [103] and derive a time dependent spin wave theory for the dynamics of this Ising model. We parametrize the dynamics generated by H_s as a rotation of the spins, namely we choose a trial state in the spin sector of the form

$$|\Phi_s(t)\rangle = \mathcal{U}(t)|\Phi_0(t)\rangle$$

where the unitary operator $\mathcal{U}(t)$

$$\mathcal{U}(t) = e^{i\frac{\alpha}{2}\sum_{\mathbf{R}}\sigma_{\mathbf{R}}^x}\,e^{i\frac{\beta}{2}\sum_{\mathbf{R}}\sigma_{\mathbf{R}}^y}$$

defines a rotation of angles α, β which in general depend on time. By imposing the Scrödinger equation we conclude the state $|\Phi_0(t)\rangle$ evolves with a transformed time dependent effective Hamiltonian $H_{s\star}$ given by

$$H_{s\star}(t) = -i\,\mathcal{U}(t)^\dagger\,\dot{\mathcal{U}}(t) + \mathcal{U}(t)^\dagger\,H_s\,\mathcal{U}(t)$$

This effective Hamiltonian can be treated within a spin-wave approximation in which the spin operators are expressed in terms of bosonic modes. We refer to [103] where this derivation is shown in great detail. The dynamics for the angles α, β is obtained by requiring that the effective Hamiltonian is quadratic in the bosonic operators. It is convenient to express the dynamics in terms of a different set of classical degrees of freedom, θ, ϕ which are related to the angles α, β by

$$\cos\theta = \sin\beta\,\cos\alpha \tag{3.39}$$

$$\sin\theta\,\cos\phi = \cos\beta \tag{3.40}$$

$$\sin\theta\,\sin\phi = \sin\beta\,\sin\alpha. \tag{3.41}$$

The condition of vanishing linear terms gives [103] (for a different derivation see Appendix B)

$$\dot{\theta} = \frac{1}{2}\,\sin\theta\,\cos\phi\,\sin\phi, \tag{3.42}$$

$$\dot{\phi} = -\frac{u(t)}{2} + \frac{1}{2}\,\cos\theta\,\cos^2\phi\,. \tag{3.43}$$

These equations of motion just set the mean field dynamics of the spin average values upon the parametrization

$$
\begin{aligned}
\langle\sigma^x\rangle &= \sin\theta\cos\phi \\
\langle\sigma^y\rangle &= \sin\theta\sin\phi \\
\langle\sigma^z\rangle &= \cos\theta.
\end{aligned}
\tag{3.44}
$$

It is worth stressing that the above dynamics directly translates onto the Gutzwiller mean field one (3.12) for the double occupancy $D(t)$ and its conjugate phase $\phi(t)$ upon posing $D(t) = (1 - \cos\theta)/4$ and $R^2 = \sin^2\theta\,\cos^2\phi = \langle\sigma^x\rangle$. Therefore, in the homogeneous paramagnetic case, a quantum quench in the Hubbard model within the Gutzwiller Approach corresponds to a quantum quench in the Ising model at mean field level. This evidence enforces the interpretation that the dynamical transition is the nonequilibrium equivalent of the Metal-to-Insulator one. In fact, at mean field level the Ising Hamiltonian (3.38) displays an equilibrium quantum phase transition from a ferromagnetic phase $\langle\sigma^x\rangle \neq 0$ to a paramagnetic one $\langle\sigma^x\rangle = 0$ at $u_c = 1$. This transition
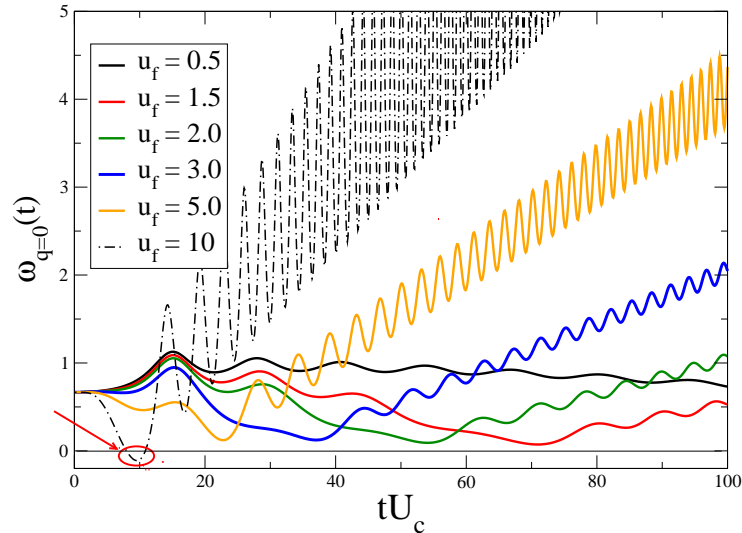
FIGURE 3.14: Evolution of fluctuation spectrum during a slow ramp ($\tau = 100$). Conversely to the sudden quench case which showed an instability ($\omega_{\mathbf{q}=0}^2 < 0$) we find that, beside a small window at short times and for large quenches, fluctuations are generally well behaved.

corresponds to the zero temperature Metal-to-Insulator transition encountered within GA. Out-of-equilibrium, above the dynamical transition, the precession of the phase ϕ is such that $R(t) = \langle \sigma^x(t) \rangle$ oscillates between positive and negative values with a corresponding vanishing average and a consequent restoring of the Z_2 symmetry. In this sense, the dynamical transition separates two distinct phases, and can be interpreted as the non-equilibrium equivalent of the Metal-to-Insulator transition.

While at the mean field level this is just an equivalent formulation, the slave spin framework allows to include quantum fluctuations which are lost in the Gutzwiller approximation. Indeed from the effective Hamiltonian $H_{s\star}$ we have also access to the dynamics of fluctuations around the mean field trajectory described in terms of a quadratic time dependent bosonic Hamiltonian (see Ref. [103]). This reads

$$H_{qf}(t) = \sum_{\mathbf{q}} \frac{1}{2m(t)} \, p_{\mathbf{q}} \, p_{-\mathbf{q}} + \frac{1}{2} \, m(t) \, \omega_{\mathbf{q}}^2(t) \, x_{\mathbf{q}} \, x_{-\mathbf{q}} \tag{3.45}$$

where the mass and the frequency read, respectively, as

$$m(t) = \frac{2 \left(1 - \sin^2 \theta \, \cos^2 \phi \right)}{u(t) \, \cos \theta} \tag{3.46}$$

and

$$\omega_{\mathbf{q}}^2(t) = \left(\frac{u(t) \cos \theta}{2 \left(1 - \sin^2 \theta \, \cos^2 \phi \right)} \right)^2 - \frac{u(t)}{4} \cos \theta \, \gamma_{\mathbf{q}} \tag{3.47}$$

where, in a hypercubic lattice in d-dimensions,

$$\gamma_{\mathbf{q}} = \frac{1}{d} \sum_{i=1}^{d} \cos q_i.$$

We start discussing the behavior of the excitation spectrum $\omega_{\mathbf{q}}(t)$ as a function of time for different values of the final interaction u_f and for a slow ramp $\tau = 100$. In Figure 3.14 we plot in particular the value at $\mathbf{q} = 0$, which was found to be the most unstable mode in the sudden quench case. As we can see, except for very large quenches $u_f \gg 1$ and short times, the spectrum is well behaved. In addition, from the structure of equations (3.47) and the result obtained for the mean field dynamics, we conclude that for an infinitely slow ramp toward a final value of the interaction u_f the out-of-equilibrium dynamics will be close to the instantaneous ground-state manifold, including the fluctuation contribution.

Obviously a finite ramp time induces an excitation in the system and it is particularly interesting to see how the excitation energy $\Delta E_{exc}(\tau)$ scales to zero for very large τ and how the spin wave spectrum affects this decay. To this extent we compute the total energy during the ramp $E(t) = \langle \Psi(t) | H(t) | \Psi(t) \rangle$ and get $\Delta E_{exc}(\tau)$ through the definition

$$\Delta E_{exc}(\tau) = E(t = \tau) - E_{gs}(u_f), \tag{3.48}$$

where the groundstate energy at the final value of the interaction can be computed within an equilibrium spinwave calculation and reads, for $u_f < 1$

$$E_{gs}(u_f) = -\frac{1}{8}(1 - u_f)^2 - \frac{1}{4V} \sum_{\mathbf{q}} \left(1 - \sqrt{1 - u_f^2 \gamma_{\mathbf{q}}} \right) \tag{3.49}$$

while in the Mott Insulating phase $u_f > 1$

$$E_{gs}(u_f) = -\frac{u_f}{4V} \sum_{\mathbf{q}} \left(1 - \sqrt{1 - \gamma_{\mathbf{q}}/u_f} \right). \tag{3.50}$$

The total energy during the ramp is given by the kinetic and potential energy contributions

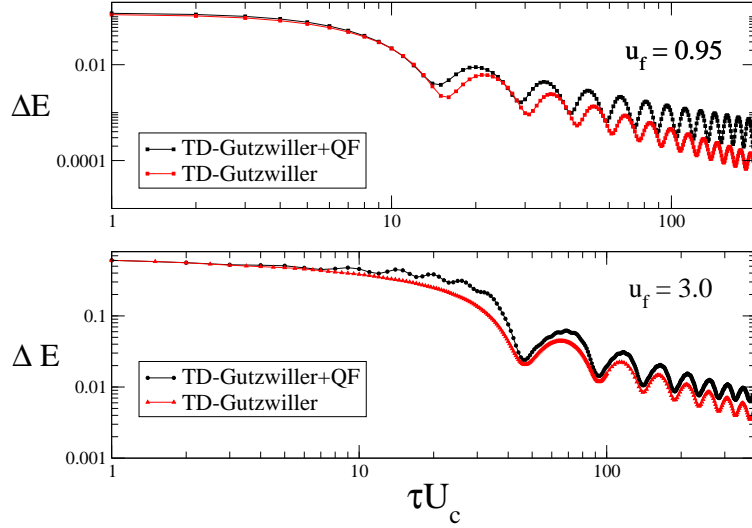$$E(t) = K(t) + u(t) D(t), \tag{3.51}$$

FIGURE 3.15: Excitation Energy $\Delta E(\tau)$ for ramps ending in the metallic phase (top panel) or in the insulating phase (bottom panel). We compare the results of time dependent Gutzwiller with those obtained by including quantum fluctuations at the gaussian level. We notice a sizable effect of these in the metallic case, which turns to be less pronounced for ramps ending in the insulating phase.

which can be easily expressed as a mean field term plus a correction due to quantum fluctuation. In particular, we get for the double occupancy

$$D(t) = \frac{1}{4} \left[1 - \cos\theta \left(\frac{1}{V} \sum_{\mathbf{q}} \left(1 - \langle \Pi_{\mathbf{q}} \rangle_t \right) \right) \right], \qquad (3.52)$$

while the kinetic energy reads

$$
\begin{aligned}
K(t) \;=\; & -\frac{1}{8V} \, \sin^2\theta \, \cos^2\phi \sum_{\mathbf{q}} \left(1 - 2 \langle \Pi_{\mathbf{q}} \rangle_t \right) + \qquad (3.53) \\
& -\frac{1}{4V} \left(1 - \sin^2\theta \, \cos^2\phi \right) \sum_{\mathbf{q}} \gamma_{\mathbf{q}} \langle x_{\mathbf{q}} \, x_{-\mathbf{q}} \rangle_t
\end{aligned}
$$

where $\langle \Pi_{\mathbf{q}} \rangle_t$ measures the strength of quantum fluctuations and is defined by

$$\langle \Pi_{\mathbf{q}} \rangle = \langle x_{\mathbf{q}} \, x_{-\mathbf{q}} + p_{\mathbf{q}} \, p_{-\mathbf{q}} \rangle_t - 1 \,.$$

It is useful at this point to write both the average energy $E(t)$ and its ground state value $E_{gs}(u_f)$ explicitly as a mean field part plus a correction due to quantum fluctuations.

This allows us to disentangle the two contributions to the scaling of the excitation energy

$$\Delta E_{exc}(\tau) = \Delta E_{exc}^{mf}(\tau) + \Delta E_{exc}^{qf}(\tau) \tag{3.54}$$

where the mean field term has been discussed in previous sections while the quantum-fluctuations correction reads

$$
\begin{aligned}
\Delta E_{exc}^{qf}(\tau) &= \frac{1}{4V} \sum_{\mathbf{q}} \left(u_f \, \cos\theta + \sin^2\theta \, \cos^2\phi \right) \langle \Pi_{\mathbf{q}} \rangle_\tau + \\
&- \frac{1}{4V} \sum_{\mathbf{q}} \left(1 - \sin^2\theta \, \cos^2\phi \right) \gamma_{\mathbf{q}} \langle x_{\mathbf{q}} \, x_{-\mathbf{q}} \rangle_\tau
\end{aligned}
$$

We stress that the above quantum averages are taken over the dynamics generated by the time dependent Hamiltonian $H_{qf}(t)$, which is solved numerically step by step together with the mean field dynamics (3.42). To this extent we use a finite grid in momentum space (with typical size $N_{mesh} = 100$) corresponding to a semielliptic density of states

$$\rho(\varepsilon) = \frac{2\sqrt{1 - \varepsilon^2}}{\pi}. \tag{3.55}$$

This makes the evaluation of ΔE_{exc}^{qf} a rather challenging numerical task, in particular for long ramp times where finite size effects become relevant and larger sizes are required to obtain converged results. In figure (3.15) we plot the behavior of the excitation energy $\Delta E_{exc}(\tau)$ as a function of the ramp time τ starting from a non-interacting system and for final values of the interaction corresponding respectively to a metallic (top panel) and insulating (bottom panel) final state. The longest ramp time we were able to achieve, $\tau \sim 200$, although still not enough to obtain a robust scaling, allows us to attempt a discussion of the long time behavior of ΔE_{exc} in presence of quantum fluctuations. As we see from figure (3.15) the numerics suggest that quantum fluctuations do in fact affect the long-time behavior of the excitation energy, particularly in the metallic phase and less strongly in the insulating phase.

In order to rationalize this behavior it is useful to resort to a more analytical approach. Indeed the Hamiltonian of quantum fluctuations $H_{qf}(t)$ describes coupled harmonic oscillators with time dependent parameters (mass $m(t)$ and frequency $\omega_q(t)$). The characteristic time scale for their variation is given by the mean field dynamics of the variational parameters and from Section 3.3 we know we can describe this for long ramps as an adiabatic evolution plus small oscillations. Hence, using Eqs (3.46-3.47) we can write $m(t)$ and $\omega_{\mathbf{q}}(t)$ for large τ as

$$m(t) = m^{gs}(u(t/\tau)) + \frac{\delta m_\tau(t)}{\tau^\delta} \tag{3.56}$$

$$\omega_{\mathbf{q}}(t) = \omega_{\mathbf{q}}^{gs}(u(t/\tau)) + \frac{\delta\omega_{\mathbf{q}\tau}(t)}{\tau^{\delta}} \, , \qquad (3.57)$$

where δ is a mean-field exponent that in general depends on the whether the ramp ends in the metallic or insulating phase, while $\delta m_{\tau}(t), \delta\omega_{\mathbf{q}\tau}(t)$ are pre-factors that can be computed from the mean field dynamics in the adiabatic limit (see appendix B.1 for further details). This argument suggests that we can obtain the dynamics of quantum fluctuations as an expansion around the adiabatic limit [121]. In particular if we define

$$\eta_{\mathbf{q}}(t) = \frac{\dot{m}}{m} + \frac{\dot{\omega}_{\mathbf{q}}}{\omega_{\mathbf{q}}} \qquad (3.58)$$

we can obtain to leading order in $\eta_{\mathbf{q}}$

$$\langle\, x_{\mathbf{q}}\, x_{-\mathbf{q}}\rangle_t \;\; = \;\; \frac{1}{2\, m(t)\omega_{\mathbf{q}}(t)} \left(1 + \int_0^t dt'\, \cos 2\theta_{\mathbf{q}}(t,t')\,\eta_{\mathbf{q}}(t')\right)$$

$$\langle\, p_{\mathbf{q}}\, p_{-\mathbf{q}}\rangle_t \;\; = \;\; \frac{m(t)\omega_{\mathbf{q}}(t)}{2} \left(1 - \int_0^t dt'\, \cos 2\theta_{\mathbf{q}}(t,t')\,\eta_{\mathbf{q}}(t')\right)$$

where

$$\theta_{\mathbf{q}}(t,t') = \int_{t'}^t dt''\, \omega_{\mathbf{q}}(t'')$$

Using this result we can write the excitation energy due to quantum fluctuations ΔE_{exc}^{qf} as the sum of two contributions

$$\Delta E_{exc}^{qf}(\tau) = \Delta E_{exc}^{(1)}(\tau) + \Delta E_{exc}^{(2)}(\tau) \qquad (3.59)$$

that read

$$\Delta E_{exc}^{(1)}(\tau) \;\; = \qquad\qquad\qquad\qquad\qquad\qquad\qquad\qquad\qquad (3.60)$$
$$\frac{1}{4V} \sum_{\mathbf{q}} \left[A(\tau)\left(\frac{m(\tau)\omega_{\mathbf{q}}(\tau)}{2} + \frac{1}{2m(\tau)\omega_{\mathbf{q}}(\tau)} - 1\right) - \frac{B(\tau)\gamma_{\mathbf{q}}}{2m(\tau)\omega_{\mathbf{q}}(\tau)} \right] - E_{gs}^{qf}(u_f)$$

$$\Delta E_{exc}^{(2)}(\tau) \;\; = \qquad\qquad\qquad\qquad\qquad\qquad\qquad\qquad\qquad (3.61)$$
$$\frac{1}{4V} \sum_{\mathbf{q}} \left[A(\tau)\left(\frac{1}{2m(\tau)\omega_{\mathbf{q}}(\tau)} - \frac{m(\tau)\omega_{\mathbf{q}}(\tau)}{2}\right) - \frac{B(\tau)\gamma_{\mathbf{q}}}{2\, m(\tau)\omega_{\mathbf{q}}(\tau)} \right] \int_0^{\tau} dt'\, \cos 2\theta_{\mathbf{q}}(\tau,t')\eta_{\mathbf{q}}(t')$$

where the coefficients $A(\tau), B(\tau)$ read respectively as $A(\tau) = u_f\cos\theta(\tau) + \sin^2\theta(\tau)\cos^2\phi(\tau)$ and $B(\tau) = 1 - \sin^2\theta(\tau)\cos^2\phi(\tau)$. The two terms in Eq. (3.59) have a clear interpretation as the first accounts for excitations produced by a non adiabatic mean field dynamics while assuming quantum fluctuations to follow adiabatically, while the second accounts for deviations from adiabaticity due to quantum fluctuations, with a mean field dynamics following its instantaneous ground state. Interestingly enough one can easily check that this latter contribution vanishes to leading order, (i.e. when $m(\tau) = m^{gs}(u_f)$ and $\omega_{\mathbf{q}}(\tau) = \omega_{\mathbf{q}}^{gs}(u_f)$) namely it only contributes to sub-leading order. The dominant

contribution comes therefore from $\Delta E^{(1)}_{exc}(\tau)$ and quite generically would give rise to corrections of order $1/\tau^{\delta}$. While $\delta = 1$ for ramps in the metallic phase and it is therefore a rather big correction to the mean field power law $\delta = 2$, the situation is milder for ramps in the insulating side and this may explain the behavior in figure (3.15).

3.4.2 Sudden Quench Limit: a self consistent theory of fluctuations

In this Section we address the opposite limit of a sudden quench and formulate a self consistent theory of quantum fluctuations which goes beyond the previous treatment and that of Ref [103]. The crucial ingredient that we include here is the feedback of quantum fluctuations on the mean field dynamics which is expected to be relevant especially close to the mean field dynamical critical line where fluctuations would otherwise start to become unstable. We give a detailed derivation of this new treatment of fluctuations in the Appendix B.2. Here we briefly discuss the key features of this approach and the results of the quench dynamics. In order to couple the mean field dynamics and the fluctuations we took inspiration from the Bogoliubov theory of weakly interacting superfluids. There, a condensate classical order parameter is identified with the quantum degrees of freedom of modes at $\mathbf{q} = 0$ while those modes with $\mathbf{q} \neq 0$ represent the fluctuations out of the condensate. Assuming the classical order parameter to be a macroscopic one can simplify the commutation relations and get a closed set of equations of motion for the classical as well as the quantum components. In the case of present interest there is of course no real condensate as a discrete rather than continuous symmetry is broken in the quantum Ising model. However, we can still consider the modes at $\mathbf{q} = 0$, corresponding to the global magnetization, to be classical and macroscopic with the consequent simplification of the Heisenberg equations of motion for the modes at $\mathbf{q} = 0$ and $\mathbf{q} \neq 0$. The resulting dynamics for the mean field part θ, ϕ will read (see Appendix)

$$
\begin{aligned}
\dot{\theta} &= \frac{N}{2}\sin\theta\cos\phi\sin\phi && (3.62)\\
&\quad + \frac{1}{2NV^2}\sum_{\mathbf{q}\neq 0}\gamma_{\mathbf{q}}\left(\sin\theta\Delta_{xy}(\mathbf{q}) + \cos\theta\sin\phi\Delta_{xz}(\mathbf{q})\right)\\
\sin\theta\dot{\phi} &= -\frac{u}{2}\sin\theta + \frac{N}{2}\sin\theta\cos\theta\cos^2\phi\\
&\quad + \frac{1}{2NV^2}\cos\phi\sum_{\mathbf{q}\neq 0}\gamma_{\mathbf{q}}\Delta_{xz}(\mathbf{q})\\
\dot{N} &= \frac{1}{2V^2}\sum_{\mathbf{q}\neq 0}\gamma_{\mathbf{q}}\left(-\cos\theta\Delta_{xy}(\mathbf{q}) + \sin\theta\sin\phi\Delta_{xz}(\mathbf{q})\right)
\end{aligned}
$$

where $N(t)$ is the magnitude of the classical order parameter while $\Delta_{ab}(\mathbf{q}, t)$ is a (time dependent) average for the modes with $\mathbf{q} \neq 0$ and it is defined as

$$\Delta_{ab}(\mathbf{q}, t) \equiv \frac{1}{2} \langle \sigma_{\mathbf{q}}^a \sigma_{-\mathbf{q}}^b + \sigma_{\mathbf{q}}^b \sigma_{-\mathbf{q}}^a \rangle_t \qquad a, b = x, y, z \qquad (3.63)$$

The above dynamics differs from the conventional mean field Guztwiller dynamics introduced previously in two main respects. First, there is an explicit coupling of the modes at $\mathbf{q} \neq 0$ with the classical dynamics of θ, ϕ. Second, the amplitude N of the order parameter is no more frozen but rather is allowed to change with time. The above dynamical system can be closed by writing the equation of motion for $\Delta_{ab}(\mathbf{q}, t)$. The result takes the form (see Appendix B.2)

$$\partial_t \Delta_{ab}(\mathbf{q}, t) = \sum_{cd} M_{abcd}(\mathbf{q}) \Delta_{cd}(\mathbf{q}, t) \qquad (3.64)$$

where the coefficients $M_{abcd}(\mathbf{q})$ depend in general from both θ, ϕ and N. As we show in the Appendix, the above dynamics conserves the total energy of the system after the quench, a crucial feature that was missing in the spin-wave treatment of fluctuations. We now discuss the numerical solution of the above coupled dynamics for a quantum quench from a non interacting initial state. As in the previous Section in order to solve numerically the coupled dynamics we use a finite grid in momentum space corresponding to the semielliptic density of states (3.55). We expect that in the region where fluctuations are negligible, the time dependent spin wave approximation is recovered and the system will display an oscillatory dynamics with multiple frequencies but no real damping. As opposite, close to the critical region where fluctuations become important and spin wave approximation breaks down, we expect the feedback of the modes at $\mathbf{q} \neq 0$ on the classical dynamics to be extremely relevant in setting the steady state. In Fig. 3.16-3.17 we plot the time dynamics of the double occupation, $D(t)$, and that of the quasiparticle weight, $Z(t)$, for different values of u_f. To enlight the effect of quantum fluctuations, in the same figure we bound with two dashed lines the region where the mean field dynamics for $D(t)$ and $Z(t)$ would display simple oscillations. As expected, we note that approaching the critical region the coupling of fluctuation with the classical sector tends to drive the dynamics of local observables towards stationarity. In particular, one can see that for quenches ranging in a window from $u_f \approx 0.35$ to $u_f \approx 0.9$, the dynamics of $D(t)$ and $Z(t)$ is quickly damped, while for smaller and larger values of u_f fluctuations are less effective in driving the dynamics toward a steady state and some undamped oscillations are still clearly visible.

Another interesting feature emerging from the solution of the coupled dynamics concerns the fate of the mean field dynamical critical point upon including the feedback of fluctuations. This issue was not fully addressed in Ref. [103], since the spin wave
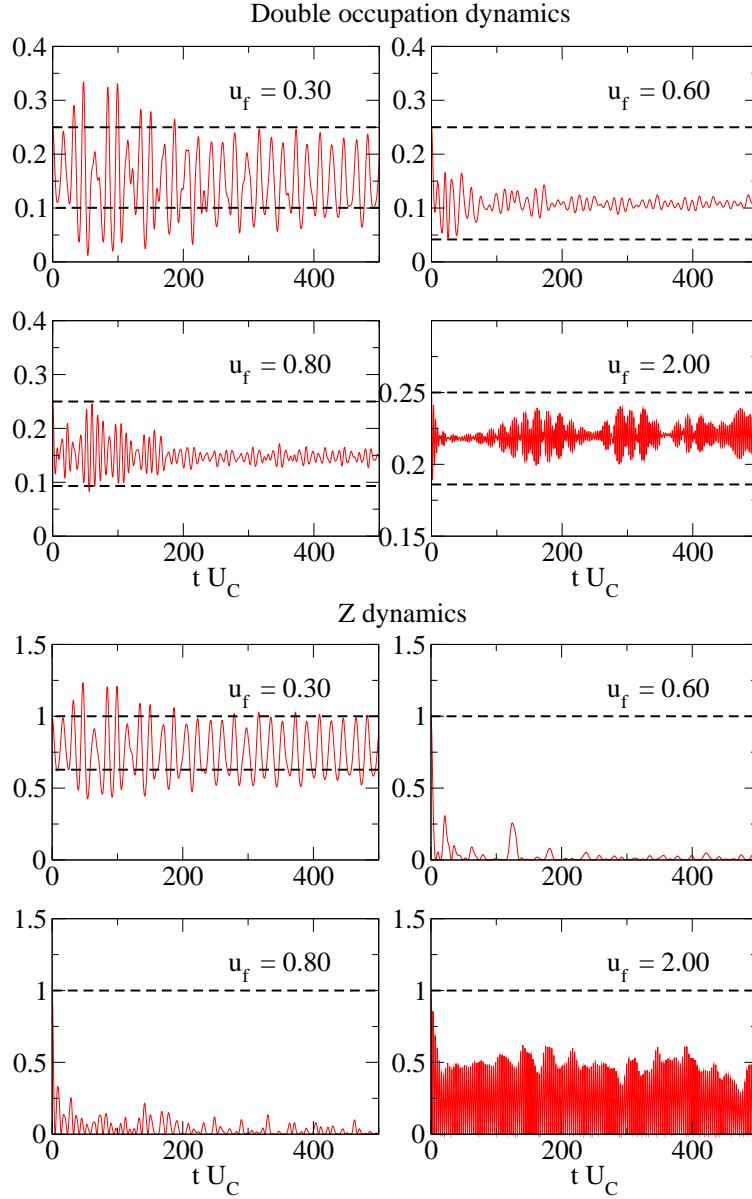
FIGURE 3.16: Time dynamics of the double occupation $D(t)$ (top panel) and of the quasiparticle weight $Z(t)$ (bottom panel). The dashed black lines are guide to eyes and bound the region where the mean field dynamics with no quantum fluctuations would display coherent oscillations. In the last three panels oscillations are between 0 and 1. The red curves are the dynamics obtained from the numerical solution of (B.26-B.27).

approach breaks down before the critical point due to the instability of quantum fluctuations. The solution of the coupled classical-quantum dynamics reveals that a kind of dynamical transition is still present even with quantum fluctuations. This is evident if one looks at the dynamics of the phase ϕ, conjugate to the double occupation $D(t)$. Indeed, such a quantity still features a sharp pendulum-like dynamical instability at a finite value of the interaction u_f^c which now gets modified by fluctuations and renormalized toward a smaller value $u_{f,QF}^c \simeq 0.35$ to be compared with the mean field estimate
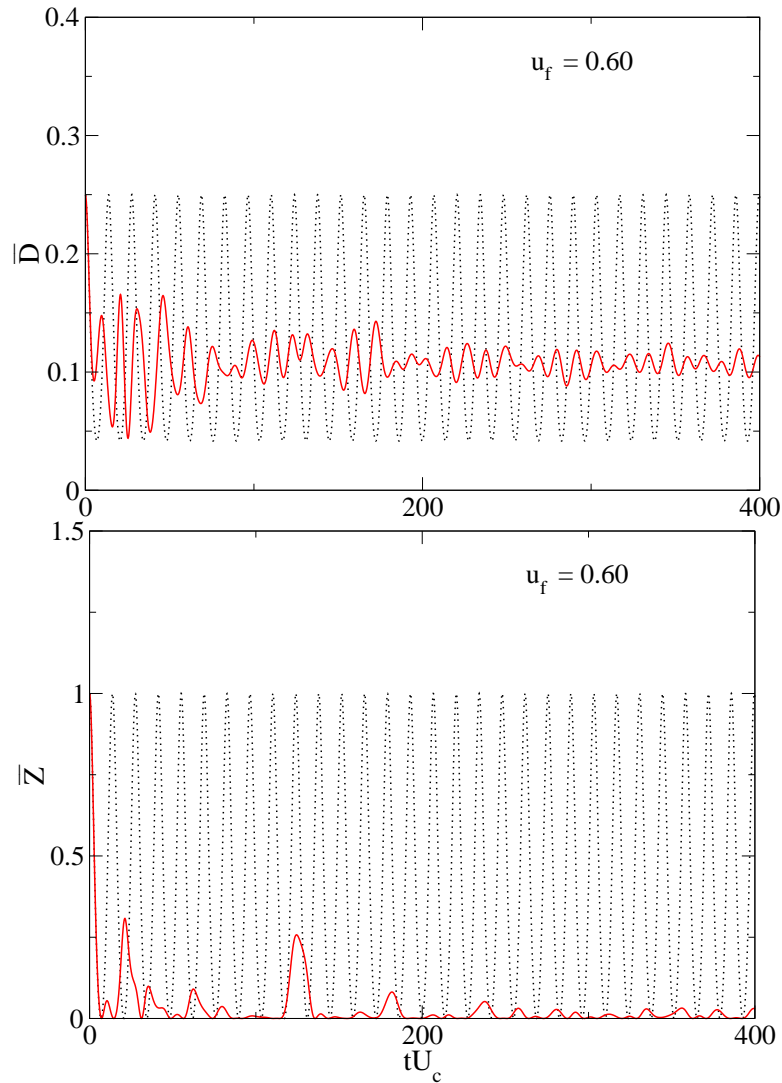
FIGURE 3.17: Short time dynamics with the feedback of quantum fluctuation for double occupation and quasiparticle weight and comparison with the mean field dynamics. We see that the coherent oscillations present at the mean field level are quickly damped out as the contribution of quantum fluctuations is properly taken into account.

$u_{f,MF}^c \simeq 0.5$.

Finally it is interesting to discuss the behavior of the long time averages $\langle D \rangle_t, \langle Z \rangle_t$ as a function of u_f. At the mean field level, those averages contain a clear signature of the dynamical critical point as the special point at which both $D(t)$ and $Z(t)$ relaxes toward zero.

In Fig. 3.18 and 3.19 we plot the behavior of these long time averages with respect to u_f and compare the respective time averages in the mean field dynamics and the results of out-of-equilibrium DMFT [10]. The result of this comparison seems to be consistent with the analysis of the transient dynamics and reveals the presence of three

different regimes. For weak quenches, quantum fluctuations do not play a major role and we recover almost exactly the mean field result. In this regime, time averages capture those predicted by perturbation theory [10] for a pre-thermal state: $\langle D \rangle_t$ tends to the zero-temperature equilibrium value and

$$\langle Z \rangle_t \approx (2Z_{eq} - 1).$$

For quenches that approach the dynamical critical point, which in mean field dynamics corresponds to $u_f = 0.5$, we already saw that the dynamics of $D(t)$ and $Z(t)$ is rapidly driven towards a stationary state; $\bar{Z}$ maintains almost a constant zero value in this interaction window so that it shows a sharp variation with respect to the mean field value. Also $\langle D \rangle_t$ corrects the mean field result which was equal to zero at the dynamical critical point. Finally, for values of $u_f \gtrsim 0.9$, no fast relaxation occurs in the dynamics and time averages recover the mean field results, at least for the double occupation. The coherent part of the kinetic energy gets strongly suppressed with respect to the mean field average, a result that can be understood as due to a transfer of weight to the incoherent modes which are absent at the level of Gutzwiller. Overall, we could say that, upon including the feedback of quantum fluctuations on top of the mean field dynamics, we obtain a picture for the dynamics which is in substantial agreement with DMFT results.
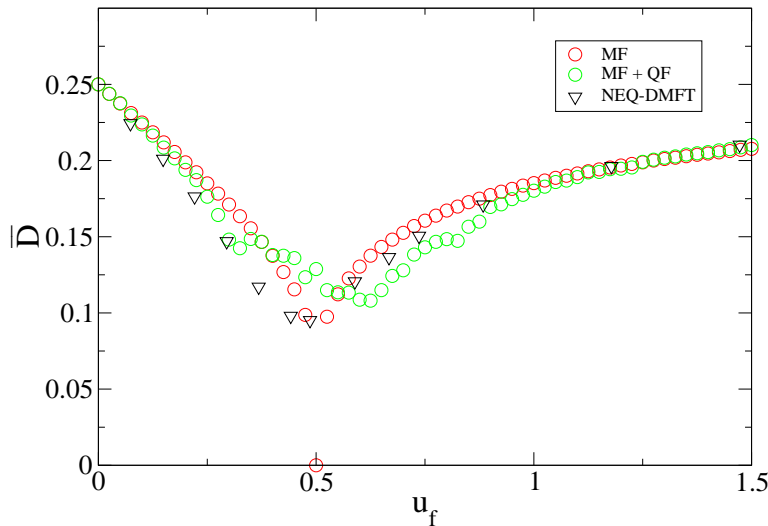

FIGURE 3.18: Long-time average of $D(t)$; one can see that in vicinity of the critical region the inclusion of fluctuation corrects the mean field result. Instead, at weak and large values of u_f the dynamics resembles the mean field one.
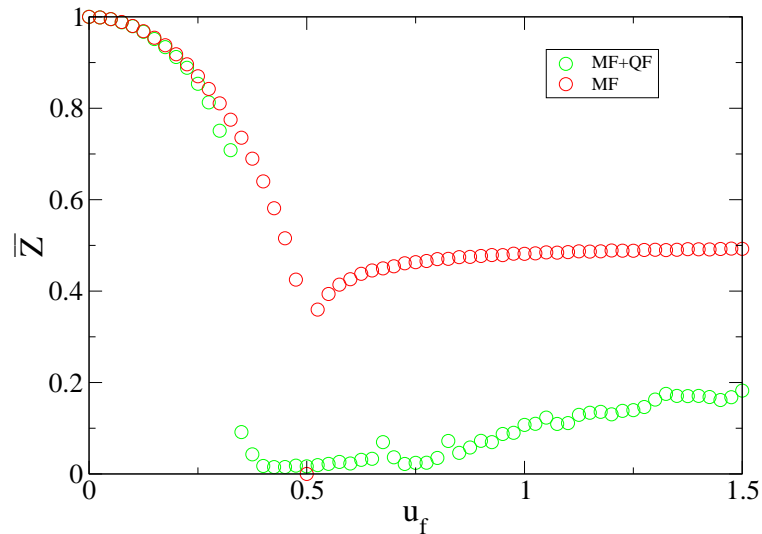
FIGURE 3.19: Long-time average of $Z(t)$. With the inclusion of fluctuations the quasi-particle weight rapidly approaches zero in a region around the dynamical critical point. Such a behavior is only partially catched by mean field dynamics.

3.5   Conclusions

In this Chapter we have discussed the nonequilibrium dynamics of the fermionic Hubbard model after a linear ramp of the interaction U across the Mott transition, starting from the metallic side. Our results are based on a time dependent Gutzwiller variational approach and on a theory of mean field plus fluctuations that we have developed in the framework of the Z_2 slave spin approach. After introducing the results for the sudden quench dynamics previously found by Schiró and Fabrizio, we have discussed the dynamics during the ramp and the issue of adiabaticity of the protocol by computing the excitation energy and studying its scaling for long ramp times. In addition we have discussed the dynamics after the ramp is completed, namely on time scales longer than τ, and identified a dynamical transition at the mean field level which smoothly connects with the one already discussed for the sudden quench case. The properties of this transition as a function of the ramp time have been analyzed. Finally we have discussed the role of fluctuations on top of the mean field dynamics for both regimes of slow and very fast ramps. In the former case a gaussian theory of fluctuations is sufficient as the spectrum of the fluctuating modes is always well defined. Using this gaussian theory we have calculated the scaling of the excitation energy with τ and see how this is affected by the presence of a non trivial spectrum. An interesting extension of this kind of approach could be to look at the evolution of the spectral function in order to understand where the excitation energy due to the ramp is mostly transferred. For what concerns short ramps we have developed a self consistent treatment of quantum fluctuations that goes beyond the simple gaussian theory. By means of this novel approach we have been able

to individuate a dynamical transition which resembles the one described at mean field level. In particular, an intermediate critical region of the quench can be identified, where the role of fluctuations becomes determinant giving a finite and sizable damping and the relaxation to a steady state. This result could be connected to the fast thermalization observed within DMFT at the dynamical critical point.

Chapter 4

Nonequilibrium dynamics in the Antiferromagnetic Hubbard Model

4.1 Introduction

A fundamental issue to address in quantum dynamics for closed systems is the real time dynamics across a phase transition in which symmetry is broken or restored. The ultrafast melting and creation of long range order in transition metal compounds has already been investigated in many experiments [2, 6, 122]. In particular, pump-and-probe spectroscopy on magnetic compounds has attracted a lot of attention motivated by the huge technological advances that could be achieved through an ultrafast control of magnetic phases [123]. On the theoretical side, however, while an equilibrium phase transition is a well established concept, there is yet no clear extension to the out-of-equilibrium case [54]. The common viewpoint is that the initial excess energy ΔE turns into heat, hence the system evolves into a thermal state at a higher effective temperature T_*, higher the bigger ΔE. Should T_* exceed the critical temperature for a order-to-disorder phase transition, the system would dynamically disorder though initially ordered.

However this picture is far from being exhaustive. In the previous Chapter we have seen for example that the dynamics after a quench of the interaction in the paramagnetic single band Hubbard model displays a dynamical transition which seems to be unrelated from the finite temperature Metal-to-Insulator critical line [10, 54]. Furthermore, even in situations where an order parameter can be easily identified, it is unclear how its relaxation time behaves out-of-equilibrium and if it is connected to an equilibrium criticality. This envisages the possibility that non-thermal long-lived phases could emerge

[6], whose manipulation, inaccessible through adiabatic pathways, represents a new and fascinating scenario.

The single-band repulsive Hubbard model that we addressed in the previous Chapter provides a further ideal test-bed to discuss these issues. In fact, when the restriction to paramagnetic states is not enforced, the Hubbard model displays at equilibrium a Néel transition from a low temperature antiferromagnet (AFM) to a high temperature paramagnet (PM)[1]. One immediately recognizes that, upon sudden changing the interaction strength, $U_i \to U_f$, one could dynamically move around the phase diagram and eventually cross the Néel transition (provided thermalization occurs). Recently the dynamics of a symmetry breaking state has been addressed by means of time-dependent DMFT on a Bethe lattice [11, 41]. These works showed that both for $U_f < U_i$ and $U_f > U_i$, long-lived non-thermal ordered states exist even though their expected T_* is above the Néel temperature T_N, thus indicating the presence of very stable phases of matter which cannot be reached by conventional thermal pathways.

Moreover, it was found that for $U_f < U_i$, the melting of the AFM order is related to the existence of a non-thermal critical point with an associated vanishing amplitude mode. Both these features are consequence of pure non-equilibrium effects.

Here we address the same model dynamics by means of the time dependent Gutzwiller variational approach introduced so far. This method, although being less accurate than DMFT, is computationally far less expensive and has already proved its reliability in reproducing the main results of DMFT in the out-of-equilibrium dynamics of paramagnetic states, as shown in the previous Chapter. We find that also in the broken-symmetry dynamics, the time-dependent Gutzwiller technique correctly reproduces both the presence of a critical point at which magnetism disappears as well as the existence of non-thermal ordered states. Moreover, we find evidence of an additional critical point at $U_f > U_i$ between two non-equilibrium antiferromagnetic states that we interpret as the magnetic analogue of a dynamical Mott transition.

This Chapter is organized as follows. In section 4.2 we briefly present how the method works in the specific case of an antiferromagnet. In section 4.3 we move to discuss the results of a quench from an initial magnetic state, ground state of the Hamiltonian at repulsion U_i, evolved with the Hamiltonian at a different value U_f, both for $U_f < U_i$, section 4.3.1, and $U_f > U_i$, section 4.3.2. Finally, section 4.4 is devoted to conclusions.

---

[1]We consider the Hubbard model at half filling for bipartite lattices in dimensions greater than two.

4.2 Time dependent Gutzwiller for AFM states

In this section we briefly show how the time-dependent Gutzwiller technique introduced in 2.3 has to be modified to treat the AFM dynamics within the single band Hubbard model at half filling, with Hamiltonian

$$\mathcal{H} = - \sum_{\langle \mathbf{R}, \mathbf{R}' \rangle, \sigma} \left(c^{\dagger}_{\mathbf{R}\sigma} c_{\mathbf{R}'\sigma} + H.c. \right) + \frac{U(t)}{2} \sum_{\mathbf{R}} (n_{\mathbf{R}} - 1)^2, \tag{4.1}$$

where $c_{\mathbf{R}\sigma}$ annihilates a spin-σ electron at site $\mathbf{R}$, $U(t)$ is the (time dependent) interaction strength and $n_{\mathbf{R}} = \sum_{\sigma} c^{\dagger}_{\mathbf{R}\sigma} c_{\mathbf{R}\sigma}$. The hopping parameter is set equal to one and is our unit of energy.

We have seen that an approximation of the evolving state follows from evaluating the stationary solution of the Action functional

$$\mathcal{L}(t) = \int_0^t d\tau \, \langle \Psi(\tau) | i \partial_\tau - \mathcal{H}(\tau) | \Psi(\tau) \rangle. \tag{4.2}$$

on a Gutzwiller ansatz for the evolving wavefunction

$$|\Psi(t)\rangle = \prod_{\mathbf{R}} \mathcal{P}_{\mathbf{R}}(t) \, |\psi(t)\rangle \tag{4.3}$$

where $|\psi(t)\rangle$ is a generic time-dependent variational Slater determinant. Upon introducing a basis for the local Fock space

$$|\mathbf{R}, \{n\}\rangle = \prod_{\alpha = \uparrow, \downarrow} (c^{\dagger}_{\mathbf{R}\alpha})^{n_\alpha} \tag{4.4}$$

one can parametrize the Gutzwiller projector $\mathcal{P}(t)$ in terms of a set of time dependent variational parameters $\Phi_{\mathbf{R}\,\{n\}}(t)$

$$\mathcal{P}_{\mathbf{R}}(t) = \sum_{\{n\}} \frac{\Phi_{\mathbf{R}\,\{n\}}(t)}{\sqrt{P^{(0)}_{\mathbf{R}\,\{n\}}(t)}} |\mathbf{R}, \{n\}\rangle \langle \mathbf{R}, \{n\}| \tag{4.5}$$

where

$$P^{(0)}_{\mathbf{R}\,\{n\}}(t) = \langle \psi(t)|\mathbf{R}, \{n\}\rangle \langle \mathbf{R}, \{n\}|\psi(t)\rangle. \tag{4.6}$$

The stationarity of (4.2) amounts then solve a set of coupled differential equations that determine the evolution of the uncorrelated wavefunction $|\psi(t)\rangle$ and the variational parameters $\Phi_{\mathbf{R}\,\{n\}}(t)$:

$$i\partial_t |\psi(t)\rangle = \mathcal{H}_*[\hat{\Phi}(t)] \, |\psi(t)\rangle \tag{4.7}$$

$$i\partial_t \hat{\Phi}_{\mathbf{R}}(t) = \hat{U}(t)\hat{\Phi}_{\mathbf{R}}(t) + \langle\psi(t)|\frac{\partial\mathcal{H}_*[\hat{\Phi}(t)]}{\partial\hat{\Phi}_{\mathbf{R}}^\dagger(t)}|\psi(t)\rangle. \tag{4.8}$$

If we assume the magnetization directed along z, then we can choose $\hat{\Phi}_{\mathbf{R}}$ to be a diagonal matrix with diagonal elements $\Phi_{\mathbf{R}\,\{0\}}$, for empty site, $\Phi_{\mathbf{R}\,\{\uparrow\}}$ and $\Phi_{\mathbf{R}\,\{\downarrow\}}$, for singly occupied site with a spin up or down electron, respectively, and finally $\Phi_{\mathbf{R}\,\{\uparrow\downarrow\}}$ for a doubly occupied site.

The Slater determinant evolves according to the renormalized one-body Hamiltonian

$$\mathcal{H}_*[\hat{\Phi}(t)] = -\sum_{\langle\mathbf{R},\mathbf{R}'\rangle,\sigma} \left(R_{\mathbf{R}\sigma}^*(t)c_{\mathbf{R}\sigma}^\dagger R_{\mathbf{R}'\sigma}(t)c_{\mathbf{R}'\sigma} + H.c.\right) \tag{4.9}$$

which is self-consistently coupled to the evolution of the matrix $\hat{\Phi}_{\mathbf{R}}(t)$ through the renormalization factors

$$R_{\mathbf{R}\sigma}(t) = \frac{1}{\sqrt{n_{\mathbf{R}\sigma}(t)(1-n_{\mathbf{R}\sigma}(t))}}\mathrm{Tr}(\hat{\Phi}_{\mathbf{R}}^\dagger(t)\hat{c}_{\mathbf{R}\sigma}\hat{\Phi}_{\mathbf{R}}(t)\hat{c}_{\mathbf{R}\sigma}^\dagger). \tag{4.10}$$

In the presence of Néel AFM order we can separate the bipartite lattice into two sublattices A and B such that Eq. (4.9) becomes

$$\mathcal{H}_*(t) = -\sum_{\langle\mathbf{R}_a,\mathbf{R}_{\bar{a}}\rangle,\sigma} \left(R_{\mathbf{R}_a\sigma}^*(t)R_{\mathbf{R}_a-\sigma}(t)c_{\mathbf{R}_a\sigma}^\dagger c_{\mathbf{R}_{\bar{a}}\sigma} + H.c.\right) \tag{4.11}$$

where if $a = A$ then $\bar{a} = B$ and vice versa, and we make use of

$$R_{\mathbf{R}_a\sigma} = R_{\mathbf{R}_{\bar{a}}-\sigma}, \text{ with } a \in \{A, B\}. \tag{4.12}$$

It is more convenient to work in Fourier space where Eq. (4.11) reads

$$\begin{aligned}
\mathcal{H}_*(t) = \sum_{\mathbf{k}\sigma}\varepsilon(\mathbf{k})\Big[&\Re\big(R_{\mathbf{R}_A\sigma}^*(t)R_{\mathbf{R}_A-\sigma}(t)\big)c_{\mathbf{k}\sigma}^\dagger c_{\mathbf{k}\sigma} \\
&-i\Im\big(R_{\mathbf{R}_A\sigma}^*(t)R_{\mathbf{R}_A-\sigma}(t)\big)c_{\mathbf{k}\sigma}^\dagger c_{\mathbf{k}+\mathbf{Q}\sigma}\Big]
\end{aligned} \tag{4.13}$$

with $\varepsilon(\mathbf{k}) = \frac{1}{N}\sum_{\langle\mathbf{R}_a,\mathbf{R}_{\bar{a}}\rangle}e^{i\mathbf{k}\cdot(\mathbf{R}_a-\mathbf{R}_{\bar{a}})}$ where N is the number of sites, and the vector $\mathbf{Q}$ such that

$$e^{i\mathbf{Q}\cdot\mathbf{R}_a} = \begin{cases} 1 & \text{if } a \in A \\ -1 & \text{if } a \in B \end{cases}. \tag{4.14}$$

The time evolution of the uncorrelated state $|\psi(t)\rangle$ can then be re-casted into that of $\Delta_{\mathbf{k}\mathbf{k}'}^\sigma(t) := \langle\psi(t)|c_{\mathbf{k}\sigma}^\dagger c_{\mathbf{k}'\sigma}|\psi(t)\rangle$ whose equations of motion are

$$i\partial_t\Delta_{\mathbf{k}\mathbf{k}}^\sigma = -i\varepsilon(\mathbf{k})\Im\big(Z^\sigma(t)\big)\Big(\Delta_{\mathbf{k}\mathbf{k}+\mathbf{Q}}^\sigma + \Delta_{\mathbf{k}+\mathbf{Q}\mathbf{k}}^\sigma\Big)$$

$$i\partial_t \Delta^{\sigma}_{\mathbf{kk+Q}} = -2\varepsilon(\mathbf{k})\Re\big(Z^{\sigma}(t)\big)\Delta^{\sigma}_{\mathbf{kk+Q}} \tag{4.15}$$
$$+i\varepsilon(\mathbf{k})\Im\big(Z^{\sigma}(t)\big)\Big(\Delta^{\sigma}_{\mathbf{kk}} - \Delta^{\sigma}_{\mathbf{k+Qk+Q}}\Big).$$

To simplify notations we introduced the quantity $Z^{\sigma}(t) = R^{*}_{\mathbf{R}_A\sigma}(t)R_{\mathbf{R}_A-\sigma}(t)$. By construction it follows that

$$n_{A(B)\sigma}(t) = \frac{1}{N}\sum_{\mathbf{k}} \Delta^{\sigma}_{\mathbf{kk}}(t) \pm \Delta^{\sigma}_{\mathbf{kk+Q}}(t). \tag{4.16}$$

The evolution of the uncorrelated wavefunction is self-consistently coupled to equation (4.8) that, because of (4.12), can be evaluated for a single sublattice and reads

$$\begin{aligned} i\frac{\partial\hat{\Phi}_A}{\partial t} =&\ \hat{U}\hat{\Phi}_A(t) \\ &+ \frac{1}{N}\sum_{k,\sigma}\varepsilon(\mathbf{k})\Big[R_{A-\sigma}\big(\Delta^{\sigma}_{\mathbf{kk}}(t) - \Delta^{\sigma}_{\mathbf{kk+Q}}(t)\big)\frac{\partial R^{*}_{A\sigma}}{\partial\hat{\Phi}^{\dagger}_A} \\ &+ R^{*}_{A-\sigma}\big(\Delta^{\sigma}_{\mathbf{kk}}(t) + \Delta^{\sigma}_{\mathbf{kk+Q}}(t)\big)\frac{\partial R_{A\sigma}}{\partial\hat{\Phi}^{\dagger}_A}\Big]. \end{aligned} \tag{4.17}$$

In conclusion Eqs. (4.15)-(4.17) together with Eqs. (4.10) and (4.16) define a set of coupled non-linear differential equations which must be solved numerically.

In spite of the nonlinearity, the dynamics is still oversimplified and we do not expect to reach thermalization in the long time limit, mainly because the evolution of the Slater determinant still admits an infinite number of integrals of motion. In fact, the dynamics of $|\psi(t)\rangle$ does not mix different $(\mathbf{k}, \mathbf{k}+\mathbf{Q})$ subspaces. Within each subspace, the set of equations (4.15) can be mapped onto the dynamics of a pseudospin-$\frac{1}{2}$ Hamiltonian. Indeed, upon defining

$$\begin{aligned} \Delta^{\sigma}_{\mathbf{kk}} - \Delta^{\sigma}_{\mathbf{k+Qk+Q}} &\equiv \langle\sigma_1\rangle \\ \Delta^{\sigma}_{\mathbf{kk+Q}} + \Delta^{\sigma}_{\mathbf{k+Qk}} &\equiv \langle\sigma_2\rangle \\ \Delta^{\sigma}_{\mathbf{kk+Q}} - \Delta^{\sigma}_{\mathbf{k+Qk}} &\equiv -i\langle\sigma_3\rangle \end{aligned}$$

(where in this case $\mathbf{k}$ is restricted to the Magnetic Brillouin Zone (MBZ)), the set of equations (4.15) is equivalent to solving the dynamics of the pseudo-spin Hamiltonian

$$\mathcal{H}^{S}_{\mathbf{k}\sigma}(t) = \varepsilon(\mathbf{k})\Im\big(Z_{\sigma}(t)\big)\sigma_3 - \varepsilon(\mathbf{k})\Re\big(Z_{\sigma}(t)\big)\sigma_1 \tag{4.18}$$

where $\sigma_{1,2,3}$ are Pauli matrices. Indeed, as we mentioned, the length of the pseudo-spin is a conserved quantity in each subspace.

It is generally believed that the average values of local operators along the unitary

evolution of a wave function $|\Psi\rangle$, generically consisting of a superposition of a macroscopic number of eigenstates, will approach at long times the thermal averages on a Boltzmann-Gibbs distribution at an effective temperature T_* for which the internal energy coincides with the energy of the wave function $|\Psi\rangle$, conserved during the unitary evolution, i.e.

$$\frac{\mathrm{Tr}\left(\mathrm{e}^{-\mathcal{H}/T_*}\,\mathcal{H}\right)}{\mathrm{Tr}\left(\mathrm{e}^{-\mathcal{H}/T_*}\right)} = \langle\Psi|\,\mathcal{H}\,|\Psi\rangle.$$

Therefore it is worth comparing the results of the time-dependent Gutzwiller technique with equilibrium results at finite temperature obtained by a similar technique. For that purpose, we shall make use of the extension to finite temperature of the Gutzwiller variational approach we recently proposed. In brief, as explained in 2.2, the thermal values are computed minimizing the following variational estimate of the free energy,

$$F \leq \min_{\{\rho_*,\hat{\Phi}\}}\left\{\sum_{\langle\mathbf{R},\mathbf{R}'\rangle,\sigma}\mathrm{Tr}\left[\rho_*\left(-R_{\mathbf{R}\sigma}R_{\mathbf{R}'\sigma}c^\dagger_{\mathbf{R}\sigma}c_{\mathbf{R}'\sigma} + H.c.\right)\right] + \sum_{\mathbf{R}}\mathrm{Tr}\left(\hat{\Phi}^\dagger_{\mathbf{R}}\,\hat{U}\,\hat{\Phi}_{\mathbf{R}}\right)\right.$$
$$\left.-T\,\mathrm{Max}\left(S_{\mathrm{var}}\left(\rho_*,\hat{\Phi}^\dagger\hat{\Phi}\right),0\right)\right\}, \tag{4.19}$$

where $\rho_* = \mathrm{e}^{-\beta\mathcal{H}_*}/(\mathrm{Tr}\,\mathrm{e}^{-\beta\mathcal{H}_*})$ is the Boltzmann distribution corresponding to the variational Hamiltonian $\mathcal{H}_*$, and the variational estimate of the entropy reads

$$S_{\mathrm{var}}\left(\rho_*,\hat{\Phi}^\dagger\hat{\Phi}\right) = -\mathrm{Tr}\left(\rho_*\log\rho_*\right) - \sum_{\mathbf{R},\{n\}}|\Phi_{\mathbf{R}n}|^2\log\left(\frac{|\Phi_{\mathbf{R}n}|^2}{P^{(0)}_{\mathbf{R}n}}\right). \tag{4.20}$$

In Fig. 4.1 we plot the finite temperature phase diagram for the model as found by means of this finite temperature extension. The Néel temperature has been computed by comparing the free energy of the AFM solution with the one of the PM solution. We see that the low temperature AFM ordered phase compares qualitatively well with the DMFT results [41]. We also show in the phase diagram the Metal-to-Insulator transition that one finds if a paramagnetic solution is forced. In this case, for a fixed value of the interaction U, the first order Metal-to-Insulator transition is identified by a fast falldown of the renormalization factor R, as previously found in Ref. [81]. A similar computation will be shown in detail for a two-band model in Chapter 5.

Overall, the important aspect that emerges here is that the Gutzwiller wavefunction is able, unlike straight Hartree-Fock, to describe a finite temperature Mott insulating phase devoid of magnetism.
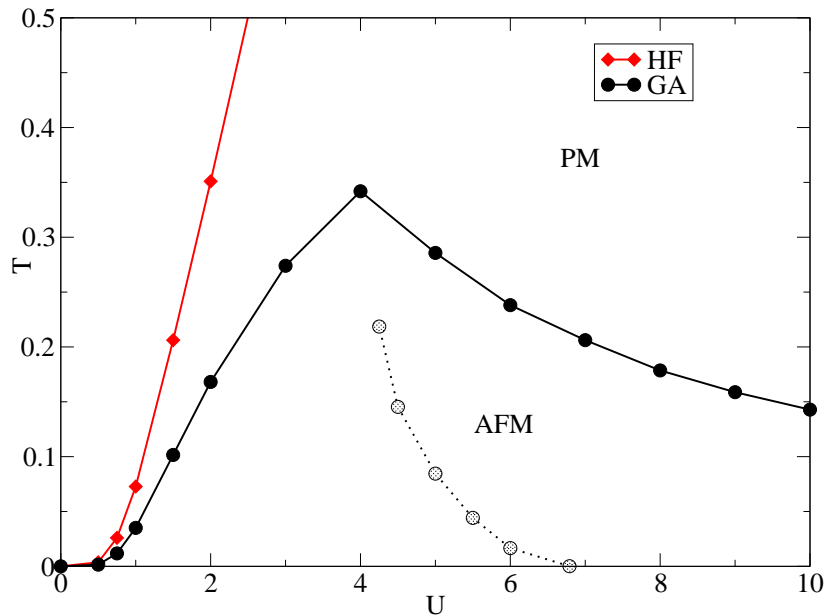
FIGURE 4.1: Finite temperature phase diagram for the single band Hubbard model as obtained by mean of the finite temperature Gutzwiller approach. The solid black line separates the AFM solution from the PM phase. The dotted line indicates the MIT transition when only paramagnetic states are considered. The red line is the Néel temperature within the Hartree-Fock approximation.

4.3 Interaction quench

In this section we apply the time dependent Gutzwiller approach to study the dynamics of (4.1) after a sudden quench of the interaction strength, $U(t) = U_i + (U_f - U_i)\theta(t)$, where $\theta(t)$ is the Heaviside function. Although an instantaneous quench is distant from the real practice in experiments, it is a well-controlled theoretical excitation protocol and suffices well the scope of this work. We assume nearest neighbor hopping on an infinitely branched Bethe lattice, i.e. a semicircular density of states $D(\varepsilon) = \sqrt{4 - \varepsilon^2}/(2\pi)$, in which case the Gutzwiller approximation becomes exact. We remark that the momentum representation we previously adopted is not appropriate for a Bethe lattice but can be easily extended in this case.

4.3.1 $U_f < U_i$ quench

We start by analyzing the dynamics for quenches at $U_f < U_i$. We plot in Fig. 4.2 the time evolution of the AFM order parameter $m = n_\uparrow - n_\downarrow$ for an interaction quench starting from the optimized variational ground state at $U_i = 4.0$. We immediately recognize a pattern which is very similar to that obtained within DMFT and Hartree-Fock dynamics [41]. The order parameter $m(t)$ quickly decreases in time after the quench and

starts oscillating; as U_f decreases below the critical value of $U_c^{U_f < U_i} \approx 1.7$, the order parameter vanishes.

On the same figure we also plot the thermal values m_{th} calculated from the finite temperature Gutzwiller approach [77] at an effective temperature T_* such that the equilibrium internal energy is equal to the average energy on the variational wavefunction, which is conserved by the unitary evolution.

We note that $m(t)$ oscillates around a value which is more and more distant from the thermal one and stays finite even when T_* exceeds the Néel temperature, suggesting that the dynamics stays trapped in a non-thermal ordered state in accordance with DMFT result [41]. From Fig. 4.2 two well separated frequencies are distinguishable in the dynamics, which we extract by a discrete Fourier transform and plot in Fig. 4.5. A high frequency ω_1 sets the fast oscillation and decreases with U_f, although staying finite. A lower frequency ω_2 can instead be associated to the presence of magnetic order and vanishes at the critical point as $\propto |U_f - U_c^{U_f < U_i}|$; the existence of a linearly vanishing mode was found also in Ref. [41].

This two-frequency dynamics reveals the mechanism beyond the disappearance of the AFM order at $U_c^{U_f < U_i}$. This is more clearly shown in Fig. 4.3 where we plot the values of the real and imaginary part of the renormalization factors. We observe that approaching $U_c^{U_f < U_i}$ the renormalization factors show main oscillations with frequency ω_2, on top of which there are much narrower oscillations controlled by ω_1. In proximity of $U_c^{U_f < U_i}$, $\omega_1 \gg \omega_2 \to 0$, so that, within each $(\mathbf{k}, \mathbf{k} + \mathbf{Q})$ subspace, the magnetic field in the pseudo-spin Hamiltonian (4.18) can be effectively taken constant in time. Hence the dynamics of (4.18) is equivalent to that of a spin in the presence of a $\mathbf{k}$-dependent constant magnetic field. The total staggered magnetization then vanishes due to the de-phasing that occurs summing on the entire Brillouin zone, hence the nature of the critical point is essentially that found within the Hartree-Fock approximation by Ref. [41].

Finally, from Fig. 4.6 we see that the long time average of $|R_\sigma|^2$ increases in the limit of $U_f \to 0$, indicating that the AFM insulator actually melts into a PM metal.

4.3.2 $U_f > U_i$ quench

For quenches at $U_f < U_i$ the Gutzwiller dynamics is not very different from the one obtained through single-particle methods such as the Hartree-Fock approximation; the magnetization shows an oscillatory behavior that turns eventually into a fast decay due to dephasing. Differences instead arise when $U_f > U_i$. Here time-dependent Hartree-Fock predicts incorrectly that the magnetic order parameter never vanishes, whatever
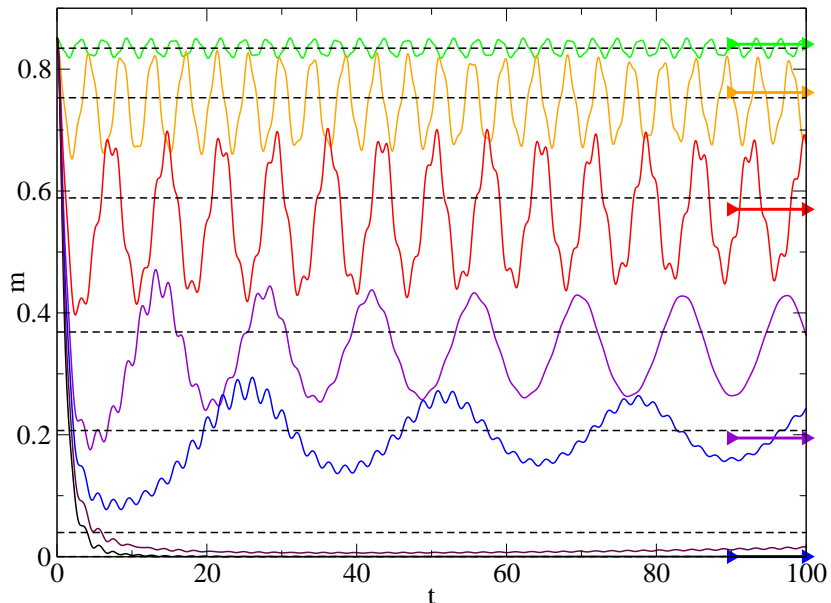
FIGURE 4.2: Time evolution of the staggered magnetization m for quenches $U_i = 4.0 \to U_f = 3.8, 3.2, 2.6, 2.2, 2.0, 1.8, 1.6$. The bold arrows indicate the corresponding thermal values, m_{th}, while the black dashed lines indicate the long time averages.
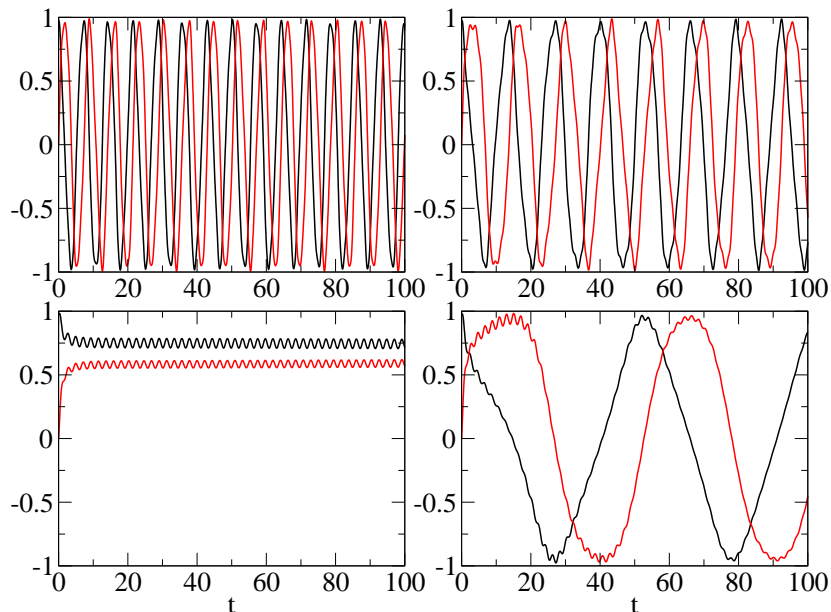

FIGURE 4.3: Time evolution of $\Re(R_{A\uparrow})$ (black) and $\Im(R_{A\uparrow})$ (red) for quenches $U_i = 4.0 \to U_f = 3.2, 2.6, 2.0, 1.6$ (clockwise order from top left).

U_f is. This drawback is directly related to the inadequacy of Hartree-Fock in reproducing a decaying Néel temperature at large values of U, feature that is instead captured by the Gutzwiller approach, see Fig. 4.1. In the assumption that the unitary evolution following the quantum quench brings the system in some thermal configuration at finite temperature, the higher the greater $|U_f - U_i|$, we can not only rationalize why time-dependent Hartree-Fock fails, but also anticipate, within the time-dependent Gutzwiller

technique, a dynamical transition from an antiferromagnetic to a paramagnetic phase. Indeed, in the limit of very large $U_f > U_i$, when the frequency $\omega_1 \sim U_f$ gets much higher than the excitation energies of the Slater determinant, each $(\mathbf{k}, \mathbf{k} + \mathbf{Q})$ pseudo-spin evolves under an effectively slow magnetic field, hence the staggered magnetization averages again to zero due to dephasing.

We find confirmation of this expectation in the time evolution of $m(t)$, see Fig. 4.4, and the main drive frequencies shown Fig. 4.5. In the limit of large U_f, a two frequency oscillation pattern appears again, with a high frequency ω_1 that grows as $\propto U_f$ and a lower frequency associated with a vanishing mode which decays as $\propto |U_f - U_c^{U_f > U_i}|$ with the critical value of $U_c^{U_f > U_i} \approx 21.0$.

We note that also in this regime the long time average of the magnetization differs from the corresponding thermal value. Indeed in Fig. 4.4 we see that for $U_f = 12.0$ the effective temperature has already crossed the Néel temperature, while the long time average of the magnetization stays greater than zero, indicating the persistence of a non-equilibrium ordered state in accordance with the results of Ref. [11].
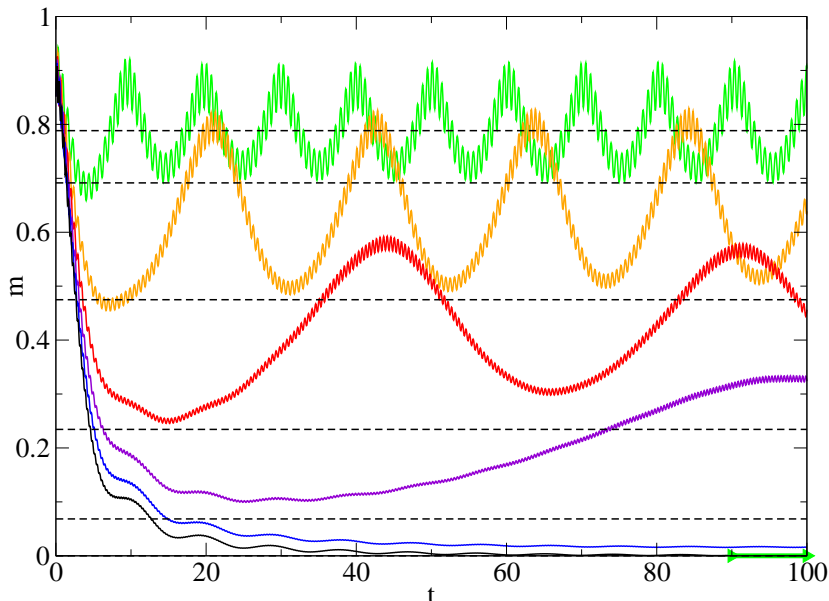

FIGURE 4.4: Time evolution of the staggered magnetization m for quenches $U_i = 4.0 \rightarrow U_f = 12.0, 14.0, 16.0, 18.0, 20.0, 22.0$. The green arrow indicates the thermal values m_{th} for $U_f = 12.0$ and shows that the effective temperature has already crossed the Néel temperature. The black dashed lines indicate the values of the long time average.

For smaller values of U_f instead a less clear scenario appears. Indeed, in the range of values $5.8 \lesssim U_f \lesssim 8.4$ (vertical dashed lines of Fig. 4.5), although the main frequencies ω_1 and ω_2 can be still recognized by continuity from the large and small U_f limits, the Fourier power spectrum loses regularity and shows an increased number of broad peaks. In this interval of U_f, the long time average of the magnetization increases while the
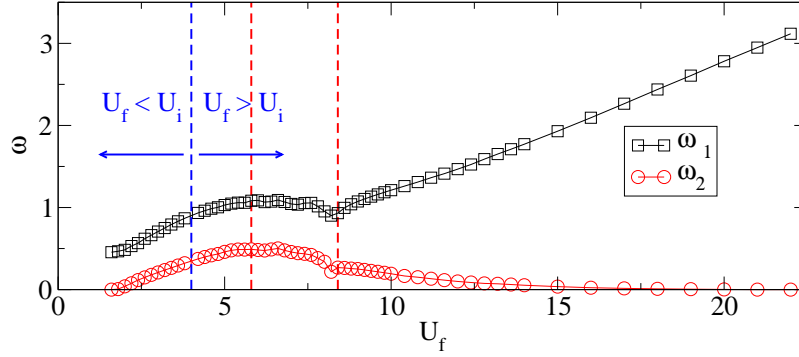
FIGURE 4.5: Behavior of the main drive frequencies ω_1 and ω_2 as a function of U_f. The two dashed red lines indicate the crossover region in which the Fourier power spectrum presents broad peaks.
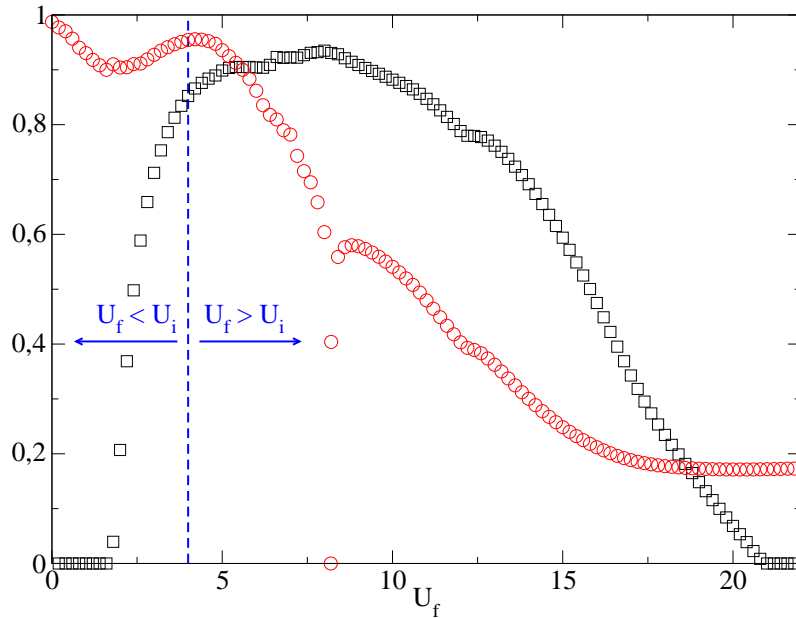

FIGURE 4.6: Long time averages of the magnetization (black squares) and of $|R_\sigma|^2$ (red circles) as a function of U_f. At $U_f^c \approx 8.2$ the renormalization factor time average decays to zero signaling the presence of the dynamical critical point.

renormalization factors diminish, see (Fig. 4.6), suggestive of the systems driven towards a Mott localized regime.

We note that Eqs. (4.15) and (4.17) admit a stationary solution identified by $R_\sigma = 0$ and energy equal to zero, which describes a trivial Mott insulating state. We find that when the conserved energy after the quench is vanishing, which happens at $U_c^{dyn} \approx 8.2$ when $U_i = 4.0$, Eqs. (4.15) and (4.17) flow towards the above stationary solution, see Fig. 4.6, a lot alike what found in the absence of magnetism, see Figure 3.2.

We can shed some light on this dynamical behavior by adopting again the polar representations of the Gutzwiller parameters of Chapter 3

$$\Phi_0 = \Phi_{\uparrow\downarrow} = \rho_0 \, e^{i\phi_0}, \tag{4.21}$$

$$\Phi_\sigma = \rho_\sigma \, e^{i\phi_\sigma}, \tag{4.22}$$

with $\rho_{0(\sigma)} \geq 0$ that, because of normalization, satisfy $2\rho_0^2 + \rho_\uparrow^2 + \rho_\downarrow^2 = 1$. We consider first of all the dynamics for values of the final interaction $U_f < U_c^{U_f < U_i}$ and $U_f > U_c^{U_f > U_i}$, that is the interaction region in which a PM phase is recovered. In the long time limit, since the magnetic order vanishes, it follows that $\rho_\uparrow = \rho_\downarrow \equiv \rho_1$ and the renormalization factor $R_{A\uparrow}$ (4.10) acquires the form

$$R_{A\uparrow}(t) = 2\rho_0(t)\rho_1(t) \, e^{i\phi_D(t)} \cos(\phi(t)) \tag{4.23}$$

where $\phi_D = (\phi_\uparrow - \phi_\downarrow)/2$ and $\phi = \phi_0 - (\phi_\uparrow - \phi_\downarrow)/2$ corresponds to the angle indicative of the dynamical phase transition in the PM quench, (3.12). The renormalized Hamiltonian which sets the dynamics of the Slater determinant (4.9) can be rewritten as

$$\mathcal{H}_*[\hat{\Phi}(t)] = - \sum_{\langle \mathbf{R},\mathbf{R}'\rangle,\sigma} \left(e^{-2i\phi_D(t)\,\sigma e^{i\mathbf{Q}\cdot\mathbf{R}}} R^2 \, c_{\mathbf{R}\sigma}^\dagger c_{\mathbf{R}'\sigma} + H.c. \right) \tag{4.24}$$

where $R = 2\rho_0(t)\rho_1(t) \, \cos(\phi(t))$. We notice that we can absorb the phase by redefining the Slater determinant up to a unitary matrix, $|\psi(t)\rangle \to \mathcal{U} \, |\tilde{\psi}(t)\rangle$. Choosing the unitary operator as

$$\mathcal{U} = e^{-i\phi_D(t)\sum_{\mathbf{R}} e^{i\mathbf{Q}\cdot\mathbf{R}}(n_{\mathbf{R}\uparrow} - n_{\mathbf{R}\downarrow})}, \tag{4.25}$$

the dynamics of the Slater determinant is set by the Scrödinger equation

$$i\partial_t|\tilde{\psi}(t)\rangle = \mathcal{U}^\dagger \mathcal{H}_* \mathcal{U} \, |\tilde{\psi}(t)\rangle - \partial_t\phi_D(t) \sum_{\mathbf{R}} e^{i\mathbf{Q}\cdot\mathbf{R}}(n_{\mathbf{R}\uparrow} - n_{\mathbf{R}\downarrow})|\tilde{\psi}(t)\rangle. \tag{4.26}$$

The second term in (4.26), in the long time limit where magnetic order vanishes, tends to zero. The dynamics of the Slater determinant is then driven by the effective Hamiltonian

$$\mathcal{U}^\dagger \mathcal{H}_* \mathcal{U} = - \sum_{\langle \mathbf{R},\mathbf{R}'\rangle,\sigma} \left(R^2 \, c_{\mathbf{R}\sigma}^\dagger c_{\mathbf{R}'\sigma} + H.c. \right) \tag{4.27}$$

which has actually the same form of the one we encountered in the paramagnetic quench. As for the dynamical phase transition in the paramagnetic quench we find that whenever the final value of the total energy is greater than zero, the angle $\phi(t)$ precesses around the unit circle while it displays finite oscillations below. Therefore, below the critical

point U_c^{dyn}, which is determined by the condition $E = 0$, the antiferromagnet melts into a "coherent" paramagnet, $\langle R \rangle_t > 0$, while the contrary happens above U_c^{dyn}.

For intermediate values of $U_c^{U_f < U_i} < U_f < U_c^{U_f > U_i}$ the magnetic order does not vanish, so that a simple decoupling of the magnetic degrees of freedom from the charge ones is not anymore feasible. However one can see that the out-of-equilibrium antiferromagnetic states above and below U_c^{dyn} have a different nature and can be connected to the respective coherent and incoherent PM phase. This can be seen by considering the quantity

$$
\begin{aligned}
\Re\left(\frac{\Phi_\uparrow \Phi_\downarrow}{\Phi_0^2}\right) &= \frac{\rho_\uparrow \rho_\downarrow}{\rho_0^2} \, \cos\left(2\phi_0 - \phi_\uparrow - \phi_\downarrow\right) \\
&\equiv \frac{\rho_\uparrow \rho_\downarrow}{\rho_0^2} \, \cos\phi
\end{aligned}
\tag{4.28}
$$

which in the paramagnetic case is very sensitive to the dynamical phase transition. Indeed, neglecting magnetism, which is the same as starting from $U_i = 0$, we have seen in Sec. 3.2 that the Mott-localized phase can be identified by the dynamics of the angle ϕ, which reproduces that of a classical pendulum. Below U_c^{dyn}, ϕ undergoes small oscillations around zero, hence Eq. (4.28) is positive. On the contrary, above U_c^{dyn}, $\cos\phi$ starts precessing around the whole unit circle, and, in particular, is negative right in the regions where the double-occupancy probability $|\Phi_{\uparrow\downarrow}|^2 = \rho_0^2$ is lower. It follows that, for $U_f > U_c^{dyn}$, the quantity in Eq. (4.28) is on average negative. Exactly at U_c^{dyn}, ρ_0 vanishes exponentially, so that the long time average of $\Re\left(\frac{\Phi_\uparrow \Phi_\downarrow}{\Phi_0^2}\right)$ diverges and changes sign right at U_c^{dyn}, see Fig. 4.7 left panel. In the right panel of the same figure we show that the same singular behavior persists also when the system is quenched from an AFM state. Even though in this case the angle ϕ is not bounded between $[0 : 2\pi]$ below U_c^{dyn}, due to the dynamics of the AFM order parameter, yet the time average of (4.28) has a well defined sign that changes crossing a singularity at U_c^{dyn}.

This is suggestive of a dynamical Mott localization at $U_c^{dyn} \approx 8.2$, that has no equilibrium counterpart and separates two different antiferromagnetic insulators. We cannot exclude that this transition may be an artifact of the Gutzwiller technique, although we are tempted to give it a physical meaning.

In order to clarify this point, we first introduce a more general definition of the quasiparticle residue $Z_{\mathbf{k}\sigma}$ through

$$
Z_{\mathbf{k}\sigma} = |\langle \mathbf{k}\sigma, N + 1 | c_{\mathbf{k}\sigma}^\dagger |0, N\rangle|^2,
\tag{4.29}
$$

where $|0, N\rangle$ is the ground state with N electrons, assumed to have zero momentum and spin, and $|\mathbf{k}\sigma, N+1\rangle$ the lowest energy state with $N+1$ electrons, momentum $\mathbf{k}$ and spin σ. $Z_{\mathbf{k}\sigma}$ defined by Eq. (4.29) coincides with the jump of the momentum distribution
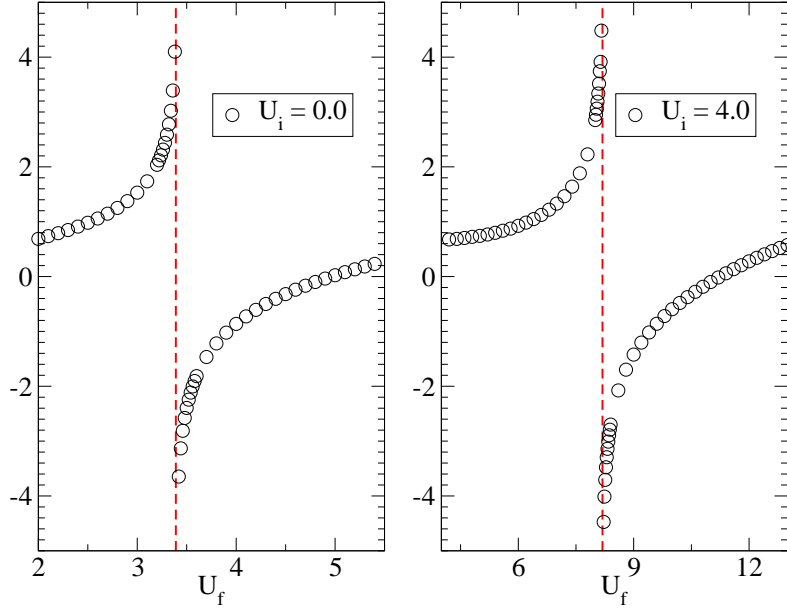
FIGURE 4.7:   Long time average of $\mathcal{O} = \Re\left(\frac{\Phi_\uparrow \Phi_\downarrow}{\Phi_0^2}\right)$ in logarithmic units, i.e. $\mathrm{sgn}\bar{\mathcal{O}}\log(|\bar{\mathcal{O}}|)$, for different values of U_f. Both in the PM case (left panel) and in the AFM one (right panel) the dynamical critical point is evidenced by a sharp singularity.

at the Fermi surface $|\mathbf{k}| = k_F$ for a Landau-Fermi liquid (see A.3), but remains well defined also for an insulator, where it can be used to establish whether well-defined quasiparticles exist above the gap. Indeed, one can readily realize that $Z_{\mathbf{k}\sigma} = 1$ for a non-interacting band-insulator. Therefore, one can in principle distinguish two different insulators: a "coherent" insulator akin to a band insulator with $0 < Z_{\mathbf{k}\sigma} \leq 1$, and an "incoherent" insulator, similar to an idealized Mott insulator, with $Z_{\mathbf{k}\sigma} = 0$ and no well-defined quasiparticles above the gap.

We then observe that, at zero temperature, $|R_\sigma|^2$ defined by Eq. (4.10) is just an estimate, within the Gutzwiller approximation, of $Z_{\mathbf{k}\sigma}$ above. Indeed, one can readily prove that

$$\langle \mathbf{k}\sigma, N+1| \, c_{\mathbf{k}\sigma}^\dagger \, |0, N\rangle \stackrel{GW}{=} \langle \psi_N | \, c_{\mathbf{k}\sigma} \, \mathcal{P} \, c_{\mathbf{k}\sigma}^\dagger \, \mathcal{P} \, |\psi_N\rangle$$
$$= R_\sigma. \tag{4.30}$$

Here we used the fact that the Gutzwiller wavefunction $\mathcal{P}|\psi_N\rangle$ (with $|\psi_N\rangle$ the N-particle Slater determinant that defines the variational wave function in Eq. (4.3)) is the variational estimate of $|0, N\rangle$ and that, within corrections $O(N^{-1})$, the best variational estimate of the $(N+1)$-electron lowest energy wave function with momentum $\mathbf{k}$ and spin σ is just $|\mathbf{k}\sigma, N+1\rangle \simeq \mathcal{P} \, c_{\mathbf{k}\sigma}^\dagger |\Psi_N\rangle$, with the same $\mathcal{P}$ as for N electrons. Eq. (4.30) remains valid also in the time dependent case where the evolution of the ground state, being a pure state, is approximated by Eq. (4.3).

We thence arrive to the conclusion that our dynamical transition separates two different non-equilibrium antiferromagnetic insulators in the above meaning. It is worth mentioning that at equilibrium and zero temperature, all evidences indicate that Z of Eq. (4.29) is everywhere finite in the antiferromagnetic insulating phase of the Hubbard model at any value of U, as confirmed by DMFT [124] and by quantum Monte Carlo simulations on the t-J model [125]. In other words, even at very large U where the Mott's physics dominates and local moments are already well formed, the antiferromagnet has coherent quasiparticles above the gap. We actually believe that, as soon as long-range magnetic order sets in below the Néel temperature, the quasiparticle residue Z becomes finite at equilibrium. In fact, the onset of long-range order is accompanied at large U by a hopping energy gain, through the spin-exchange t^2/U, hence by a raise of lattice coherence that we think has to be associated with an increase of Z. That is why we think that the dynamical transition that we observe has no equilibrium counterpart in the whole U versus temperature phase diagram.

We conclude mentioning that the main results presented above at fixed $U_i = 4$, remain qualitatively the same also at different U_i. We indeed verified the presence of the critical points at which the magnetization vanishes, $U_c^{U_f \lessgtr U_i}$, and the presence of the dynamical critical point, $U_i < U_c^{dyn} < U_c^{U_f > U_i}$, for all values of $U_i < 10.0$.

4.4 Conclusions

In this Chapter we have shown that the time dependent Gutzwiller technique, in spite of its simplicity, is able to reproduce the main features of a quench dynamics from an antiferromagnetic state found by time-dependent DMFT, such as the existence of non-thermal magnetically ordered states that disappears above dynamical critical points, both suddenly decreasing or increasing the value of the Hubbard U. The demagnetization mechanism is reconducting to dephasing rather than thermalization, since this latter is non accessible within the Gutzwiller Approach. Furthermore, we have found evidence of an additional dynamical transition that occurs at large U, which we interpret as a dynamical Mott transition separating two different antiferromagnetic non-equilibrium states. Since the quasiparticle residue Z in an antiferromagnet cannot be extracted by any static property (unlike in a paramagnet where, at zero temperature, Z is the jump of the momentum distribution at the Fermi surface), but requires calculating for instance the full out-of-equilibrium self-energy, its dynamical behavior was not addressed by DMFT in Ref. [11] and Ref. [41]. Although we cannot exclude that the vanishing of Z that we observe could be an artifact of the Gutzwiller technique, nevertheless

this result is intriguing, as it entails the existence in out-of-equilibrium of an incoherent antiferromagnet, hence worth to be further investigated.

Chapter 5

Nonequilibrium dynamics of a toy-model for V_2O_3

5.1 Introduction

Mott insulators potentially represent promising candidates that might enable scalability below the size of conventional semiconductors solid state devices [126]. In fact, a Mott insulator can typically revert to a metal, e.g. under pressure, suddenly releasing the large amount of conduction electrons that were earlier Mott localized. Therefore one may envisage that an external bias could eventually drive a Mott insulator into a metal with a very large carrier concentration of the same order as the inverse of the unit cell volume. Experimental attempts performed so far are indeed encouraging, see e.g. Refs. [127] and [128].

On the contrary, theoretical calculations in the simplest model for a Mott insulator, namely the single-band Hubbard model at half-filling, are not equally promising. For instance, the simulated time evolution of a photo-excited Mott insulator, with holes in the lower Hubbard band and electrons in the upper one, shows that the initial excess energy has a similar effect as heating the system, although the relaxation towards the steady state is slower the stronger the interaction. In other words, the Mott-Hubbard side-bands persist and simply spectral weight is being transferred from the lower to the upper, just as if temperature rises, even though small deviations from the expected thermal behavior are observed [9, 129].

Moreover, theoretical simulations of the dielectric breakdown of a single-band Mott insulator in the presence of a static electric field point towards a conventional Landau-Zener tunneling between lower and upped Hubbard bands, just alike conventional band insulators [56, 57, 130–132]. However these results are not in agreement with actual

experiments [128], thus suggesting the possibility that the single band Hubbard model might not be the appropriate choice to reproduce this effect.

A simple escape route, which we shall follow here, is to abandon the half-filled single-band Hubbard model as the prototypical model to describe real Mott insulators.
The single band Hubbard Hamiltonian is indeed intended to provide a simplification for multiband correlated materials with the main assumption that orbital degeneracy is lifted by strong crystal fields, so that an effective single band theory can be used in proximity of the Fermi surface.
However, in several cases an effective single band description might not be sufficient. An example is given by transition metal oxides with partially filled d-bands, where the crystal field splitting within the t_{2g} orbitals arising from the distortion of the lattice may be of the order of fractions of eV, thus excluding a single band description [133]. In this situation multiple degrees of freedom compete with the result that the interplay between temperature, strong correlation and antiferromagnetic ordering gives rise to very rich equilibrium phase diagrams. In particular the nature of the charge gap in a Mott insulator might be different form the genuine Mott-Hubbard gap that refers to the single band Hubbard model.

The natural question is therefore if and how this feature is going to affect the off-equilibrium response to external perturbations that could drive those materials metallic. It is therefore important to have at disposal theoretical tools able to deal with these situations. At equilibrium, one that is currently adopted is dynamical mean field theory (DMFT) [69] in combination with local-density approximation (LDA) [134] or the GW approximation [135]. These combined methods are extremely reliable for correlated materials, but they can become very cumbersome and numerically demanding, especially if full consistency on the density is required.
Out-of-equilibrium, even though DMFT can be in general applied to multiband problems, its practical implementation has not yet been reached.

In this Chapter we shall approach a more realistic description of real materials within the Gutzwiller Approach. To this extent we introduce here a two-orbital toy-model which we believe captures many features of vanadium sesquioxide, V_2O_3. This compound is characterized by a very rich equilibrium phase diagram and historically has represented a paradigmatic material displaying a Metal-to-Insulator transition in its essential form. Not surprisingly it represents nowadays a test-bed compound for ultrafast manipulation [4, 128] .

In the first part of the Chapter we make use of the extension to finite temperature for the Gutzwiller Approach presented in Sec. 2.2 to investigate the equilibrium properties and the phase diagram of this simple model. We first discuss its results at zero temperature, where we shall point out the importance of a correlation-induced enhancement of the crystal field splitting for the Metal-to-Insulator transition. Then we will consider the finite temperature analysis, and we will show that the phase diagram we obtain indeed resembles the one of V_2O_3 and compares qualitatively well with the exact one obtained by DMFT.

In the second part of the Chapter we shall turn to the out-of-equilibrium properties of this two-band model.

5.2　Equilibrium phase diagram of a toy-model for V_2O_3

The model we are going to analyze is inspired by the physics of V_2O_3. In this compound, the V^{2+} ions have two valence electrons occupying the conduction bands that originate mainly from the t_{2g} atomic d-orbitals. At high temperatures, V_2O_3 is a paramagnetic metal but, upon substituting V with Cr it can turn into a paramagnetic insulator [136]. The transition is first order and ends into a second-order critical point. At low temperature, V_2O_3 is instead an antiferromagnetic insulator, Fig. 5.1. The Néel transition occurs at $T_N \simeq 155$ K and is accompanied by a martensitic transformation from the high-temperature corundum structure to the low-temperature monoclinic one [137]. The magnetic ordering is not a simple G-type, as it could well be in a bipartite lattice, but, in the honeycomb-lattice basal plane, two bonds are antiferromagnetic and one is ferromagnetic [138].

There is wide consensus that the magnetic moment is formed by a spin $S = 1$[139] but it is also contributed by angular momentum [140], signaling a non-negligible spin-orbit coupling. Even though a reliable description of the antiferromagnetic transition requires including electron-lattice and spin-orbit couplings, the main features of the phase diagram can be likely explained ignoring those additional complications. The trigonal field of the corundum structure splits the t_{2g} orbitals into a lower e_g^π doublet and a higher a_{1g} singlet. It is therefore tempting to conclude that the low-temperature insulator describes the two electrons in the e_g^π doublet that, because of Hund's rules, are coupled into a spin-triplet. This conclusion is probably not far from reality. Indeed, although the bare value of the crystal field splitting is too small in comparison with the bare conduction bandwidth [141], strong enough electronic correlations may reverse the situation and stabilize the insulating phase [142]. This scenario has been actually
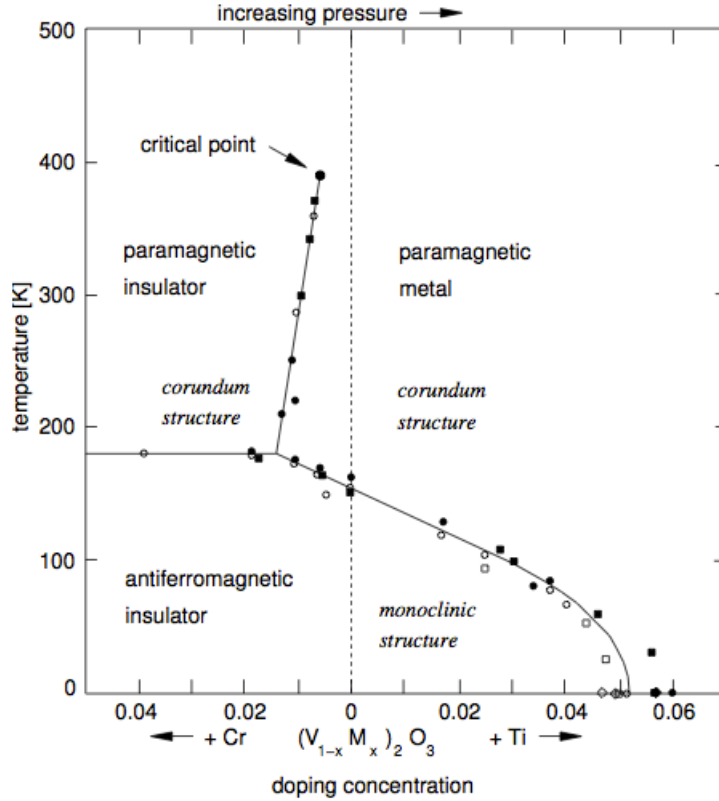
FIGURE 5.1: Experimental phase diagram for the Metal-to-Insulator transition in V_2O_3 as a function of chemical doping and pressure, [137].

advocated to explain the phase diagram of V_2O_3 on the basis of a DMFT-LDA calculation in Ref. [143], and seems supported by some experimental evidences [144]. Indeed, DMFT-LDA results have shown that the effective crystal field splitting Δ_{eff} between e_g^π and a_{1g} orbitals is enhanced by correlations from its bare value $\Delta \simeq 0.27$ eV due to the strength of the electron repulsion [143]. In addition, Δ_{eff} has been found to increase upon lowering temperature T, though only slightly [143] but, more importantly, it has been observed that the magnetic susceptibility of the e_g^π increases substantially with lowering T, while that of the a_{1g} stays constants [143] or even diminishes [145], precursor signals of a magnetic instability.

However, all calculations so far have not been pushed down to the Néel transition temperature to really uncover the proposed mechanism of a gradual depopulation of the a_{1g}-derived band and concomitant magnetic polarization of the e_g^π-derived ones. Here, we would like to address this issue by exploiting the finite temperature technique described in section 2.2 on a simplified model that we believe captures the essential physics. Instead of considering three t_{2g} orbitals split into two plus one and occupied on average by two electrons, we shall consider only two split orbitals occupied on average by one electron (quarter filling). In this way we miss the important role of Coulomb

exchange, which forces the two electrons on the e_g^π doublet to lock into a spin triplet state and might bring about relevant incoherence effects [146], but the gross features of the phase diagram, in particular the interplay between temperature, crystal field splitting, correlations and magnetism, should be maintained.

Specifically, we shall study the two-band Hamiltonian on a square lattice

$$
\begin{aligned}
\mathcal{H} &= \sum_{a=1}^{2} \sum_{\mathbf{k}\sigma} \epsilon_{\mathbf{k}}\, c_{\mathbf{k}a\sigma}^{\dagger} c_{\mathbf{k}a\sigma} + \sum_{\mathbf{k}\sigma} \gamma_{\mathbf{k}} \left(c_{\mathbf{k}1\sigma}^{\dagger} c_{\mathbf{k}2\sigma} + H.c. \right) \\
&+ \sum_{\mathbf{R}} \left[-\Delta \left(n_{\mathbf{R}1} - n_{\mathbf{R}2} \right) + \frac{U}{2} \left(n_{\mathbf{R}1} + n_{\mathbf{R}2} \right)^2 \right],
\end{aligned}
\tag{5.1}
$$

where $a = 1, 2$ labels the two orbitals, $\epsilon_{\mathbf{k}} = -2t\left(\cos k_x + \cos k_y \right)$ is the standard nearest neighbor tight-binding energy, U parametrizes the on-site repulsion and $\Delta > 0$ the crystal field splitting. We include an inter-orbital hopping $\gamma_{\mathbf{k}} = -4t' \sin k_x \sin k_y$ with a symmetry such that the local single-particle density matrix remains diagonal in the orbital indices 1 and 2, thus mimicking the a_{1g}-e_g^π hybridization in the corundum phase of V_2O_3 [143]. We shall further assume a density corresponding to one electron per site.

In spite of its simplicity, the model in Eq. (5.1) reproduces qualitatively the actual behavior of V_2O_3. If $\Delta \simeq t' \ll t$, which we shall consider hereafter, the model describes a two-band metal for small U. However, for very large U, we do expect a Mott insulating phase with the electrons localized mostly on the lowest orbital and antiferromagnetically ordered. Therefore a strong repulsion U can turn the two band metal into a single-band antiferromagnetic insulator, the two-band analogue of what is predicted in V_2O_3. The question we would like to address here is the behavior at finite temperature.

We first observe that the enhancement of the effective crystal field Δ_{eff} caused by U, which eventually leads to antiferromagnetism once the highest band is emptied, can be described also within Hartree-Fock. Indeed, if we neglect magnetism and assume the variational mean-field ansatz

$$
\langle n_{\mathbf{R}1} \rangle = \frac{1}{2} + \delta n, \quad \langle n_{\mathbf{R}2} \rangle = \frac{1}{2} - \delta n,
$$

then the Hartree-Fock energies of the orbitals are $\epsilon_1 = -\Delta + U\left(3 - 2\delta n\right)/2$, and $\epsilon_2 = \Delta + U\left(3 + 2\delta n\right)/2$, so that the effective crystal-field splitting is, within mean-field, $\Delta_{\text{eff}} = \Delta + U\,\delta n > \Delta$. As U increases, Δ_{eff} grows hence the highest band depopulates until it becomes completely empty. Beyond this point, only the lowest band remains occupied, specifically half-filled, which can lead to a Stoner-like antiferromagnetic instability, hence to an insulating state. In other words, an independent particle picture, like Hartree-Fock, is indeed able to explain the occurrence of an antiferromagnetic insulating state

at low temperature. However, no matter how large U is, Hartree-Fock will predict this insulating phase to turn metallic above the Néel temperature T_N. On the contrary, we expect that, for $T > T_N$ but U large enough, the phase should still be insulating, though paramagnetic.

Finite-T Gutzwiller approximation at work

We can improve the Hartree-Fock description at finite temperature by the Gutzwiller variational approach of section 2.2. By our choice, even though the inter-orbital hybridization t' is finite, hence the two orbital can mutually exchange electrons, still the local density matrix is diagonal by symmetry. It follows that the natural basis, see Eq. (2.50), coincides with the original one, a great simplification in the calculations. We identify the local Fock basis as

#	$\lvert\{n\}\rangle$	#	$\lvert\{n\}\rangle$
1	$\lvert 0, 0\rangle$	9	$\lvert \downarrow, \downarrow\rangle$
2	$\lvert \uparrow, 0\rangle$	10	$\lvert \uparrow\downarrow, 0\rangle$
3	$\lvert \downarrow, 0\rangle$	11	$\lvert 0, \uparrow\downarrow\rangle$
4	$\lvert 0, \uparrow\rangle$	12	$\lvert \uparrow\downarrow, \uparrow\rangle$
5	$\lvert 0, \downarrow\rangle$	13	$\lvert \uparrow\downarrow, \downarrow\rangle$
6	$\lvert \uparrow, \uparrow\rangle$	14	$\lvert \uparrow, \uparrow\downarrow\rangle$
7	$\lvert \downarrow, \uparrow\rangle$	15	$\lvert \downarrow, \uparrow\downarrow\rangle$
8	$\lvert \uparrow, \downarrow\rangle$	16	$\lvert \uparrow\downarrow, \uparrow\downarrow\rangle$

TABLE 5.1: Local Fock basis for the two-band model

Since we will search for simple two-sublattice Néel order, we can set, for any site $\mathbf{R}$ belonging to sublattice A, $\hat{\Phi}_\mathbf{R} = \hat{\Phi}_A \equiv \hat{\Phi}$ and $n^0_{\mathbf{R}a\sigma} = n^0_{Aa\sigma} \equiv n^0_{a\sigma}$ (see Eq. (2.50)), such that $\sum_{a\sigma} n^0_{a\sigma} = 1$. The variational matrix $\hat{\Phi}$ is defined in the local Fock space and is only invariant under spin-rotations around the magnetization axis, which we choose as the z axis. It follows that, for any site $\mathbf{R}$ belonging to the other other sublattice B, $\hat{\Phi}_\mathbf{R} = \hat{\Phi}_B = U^\dagger \hat{\Phi} U$ with $U = \exp\left(i\pi S_y/2\right)$ and S_y the y-component of the total local spin, while $n^0_{\mathbf{R}a\sigma} = n^0_{Ba\sigma} \equiv n^0_{a-\sigma}$. Because of Eq. (2.57), we must impose the constraint

$$\mathrm{Tr}\left(\rho_* c^\dagger_{\mathbf{R}a\sigma} c_{\mathbf{R}b\sigma'}\right) = \mathrm{Tr}\left(\hat{\Phi}^\dagger \hat{\Phi}\, c^\dagger_{a\sigma} c_{b\sigma'}\right) = \delta_{ab}\delta_{\sigma\sigma'}\, n^0_{a\sigma}, \tag{5.2}$$

for $\mathbf{R} \in A$, while, for $\mathbf{R} \in B$, $\hat{\Phi} \to U^\dagger \hat{\Phi} U$ and $n^0_{a\sigma} \to n^0_{a-\sigma}$.

Since natural and original bases coincide, the renormalization factors of Eq. (2.26) are diagonal and read, for $\mathbf{R} \in A$,

$$R^*_{\mathbf{R}\,a\sigma} = R^*_{a\sigma} = \frac{1}{\sqrt{n^0_{a\sigma}\left(1 - n^0_{a\sigma}\right)}} \mathrm{Tr}\left(\hat{\Phi}^\dagger\, c^\dagger_{a\sigma}\, \hat{\Phi}\; c_{a\sigma}\right), \tag{5.3}$$

while, for $\mathbf{R} \in B$, $R^*_{\mathbf{R}\,a\sigma} = R^*_{a-\sigma}$. We find that, at the optimized values of the variational parameters, $R_{\mathbf{R}\,a\sigma}$ are always real. Therefore, if we define $R_{a\sigma} \equiv R_a + \sigma\, S_a \in \Re e$, then the variational uncorrelated Hamiltonian $\mathcal{H}_*$, see Eq. (2.38), is

$$
\begin{aligned}
\mathcal{H}_*\left[\hat{\Phi}, n^0\right] &= \sum_{a=1}^{2}\sum_{\mathbf{k}\sigma} \epsilon_{\mathbf{k}a}\, c^\dagger_{\mathbf{k}a\sigma} c_{\mathbf{k}a\sigma} + \sum_{\mathbf{k}\sigma} \gamma'_{\mathbf{k}}\left(c^\dagger_{\mathbf{k}1\sigma} c_{\mathbf{k}2\sigma} + H.c.\right) + \sum_{\mathbf{k}\sigma} \sigma\, \gamma"_{\mathbf{k}}\left(c^\dagger_{\mathbf{k}1\sigma} c_{\mathbf{k}+\mathbf{Q}2\sigma} + H.c.\right) \\
&\quad + \mu \sum_{a\mathbf{k}\sigma} n_{\mathbf{k}a\sigma} + \mu_{\mathrm{CF}} \sum_{\mathbf{k}\sigma}\left(n_{\mathbf{k}1\sigma} - n_{\mathbf{k}2\sigma}\right) + \sum_{a=1}^{2}\sum_{\mathbf{k}\sigma} \sigma\, h_a\left(c^\dagger_{\mathbf{k}a\sigma} c_{\mathbf{k}+\mathbf{Q}a\sigma} + H.c.\right),
\end{aligned} \tag{5.4}
$$

where the Lagrange multipliers μ, μ_{CF}, h_1 and h_2 enforce the constraints (5.2), and

$$
\begin{aligned}
\epsilon_{a\mathbf{k}} &= \left(R_a^2 - S_a^2\right)\epsilon_{\mathbf{k}}, \\
\gamma'_{\mathbf{k}} &= \left(R_1 R_2 + S_1 S_2\right)\gamma_{\mathbf{k}}, \\
\gamma"_{\mathbf{k}} &= \left(R_1 S_2 + R_2 S_1\right)\gamma_{\mathbf{k}}.
\end{aligned}
$$

It follows that, if

$$F_*\left[\hat{\Phi}, n^0\right] = -\frac{T}{N} \ln \mathrm{Tr}\left(\mathrm{e}^{-\beta \mathcal{H}_*}\right), \tag{5.5}$$

where N in the number of sites, then we have to minimize

$$
\begin{aligned}
F\left[\lambda, \hat{\Phi}, n^0\right] &= F_*\left[\hat{\Phi}, n^0\right] + \frac{U}{2}\mathrm{Tr}\left(\hat{\Phi}^\dagger\left(n_1 + n_2\right)^2 \hat{\Phi}\right) - \Delta\mathrm{Tr}\left(\hat{\Phi}^\dagger\left(n_1 - n_2\right)\hat{\Phi}\right) \\
&\quad - \sum_{a\sigma} \lambda_{a\sigma}\left[\mathrm{Tr}\left(\hat{\Phi}^\dagger\hat{\Phi}\, n_{a\sigma}\right) - n^0_{a\sigma}\right] - T\, S\left(\hat{\Phi}^\dagger\hat{\Phi}||P^0\right),
\end{aligned} \tag{5.6}
$$

with the constraint $\sum_{a\sigma} n^0_{a\sigma} = 1$.

To minimize the variational free-energy (5.6) we find more convenient to minimize first with respect to all parameters except n^0 [64], thus obtaining the functional

$$F[n^0] = \min_{\lambda, \hat{\Phi}} F\left[\lambda, \hat{\Phi}, n^0\right]. \tag{5.7}$$

We calculate $F[n^0]$ in a two-steps cyclic process; first we fix $\hat{\Phi}$ and minimize $F[\lambda, \hat{\Phi}, n^0]$ with respect to the Lagrange multipliers in Eq. (5.4). Then, at fixed matrix elements $\langle c^\dagger_{\mathbf{R}a\sigma} c_{\mathbf{R}'b\sigma'}\rangle_{\rho_*}$, we minimize $F[\lambda, \hat{\Phi}, n^0]$ with respect to $\hat{\Phi}$ fulfilling the Gutzwiller constraints. This second non-linear constrained minimization is performed by the LANCELOT

B routine of the GALAHAD library [147]. This two-steps cycle is repeated until convergence. Finally a full minimization of $F[n^0]$ with respect to n^0 is performed.

5.2.1 $T = 0$ phase diagram

The results that follow are obtained setting $t = 1/8$ and the inter-orbital hybridization $t' = 0.3t$. The $t' = 0$ bandwidth $W = 8t = 1$ hence sets the unit of energy.

First we consider the $T = 0$ case of Eq. (5.6), which corresponds to the usual ground state Gutzwiller variational approach. In Fig. 5.16 we plot the zero temperature phase diagram in the paramagnetic sector as a function of U and Δ. Our results compare well with the DMFT phase diagram of Refs. [142] and [133]. In the limit $\Delta = 0$ the model undergoes a second order degenerate Metal-to-Insulator transition (MIT) at a critical value $U_c^{\Delta=0} \simeq 2.27W$ characterized by the disappearance of the renormalization factors $R_{1,2}$. In the opposite non interacting case, $U = 0$, upon increasing Δ the system crosses a Lifshitz transition from a two-band to a one-band metal. This critical value $\Delta_c = W/4$ in the hybridized case is slightly diminished by hybridization which acts as a small effective crystal field splitting. Moreover, we note that in this case the majority ($>$) and minority ($<$) bands do not have a unique orbital character; therefore the band polarization $n_> - n_<$, which saturates to 1 at the two-band $\rightarrow$ one-band transition, is in general different from the orbital polarization $n_1 - n_2$.

At finite U the Gutzwiller ground state can be determined in terms of an effective renormalized Hamiltonian. The effective bands are hence renormalized approximately as $R_a^2 W$, which implies that a smaller crystal field spitting is required to induce the two-band $\rightarrow$ one-band transition or, in other words, that the original bare crystal field splitting is enhanced by correlation. This is confirmed from the phase diagram in Fig. 5.16 in which we see that a smaller value of Δ is needed to drive the two-band $\rightarrow$ one-band transition. Above this transition, the ground state is a one-band metal which eventually undergoes a second order MIT at a critical value $U_c \simeq 1.68W$. In Fig. 5.3 (right panel) we show the details of these two subsequent transitions for a value of $\Delta = 0.15W$. For $U \leq 0.64W$, the two-band metal is stable but, increasing U, the minority band gradually empties and both renormalization factors, R_1 and R_2, decrease. At $U \simeq 0.64W$ the minority band completely depopulates and the leftover half-filled majority band is driven to the MIT at $U \simeq 1.68W$. Approaching the MIT, the renormalization factor R_1 of the lowest-energy orbital vanishes, while R_2 actually increases to one – the almost empty orbital undresses from correlations. For smaller Δ, the two-band $\rightarrow$ one-band transition becomes first order and approaches the one-band MIT point, ending in a multicritical point at $\Delta \simeq 0.028W$. In Fig. 5.3 (left panel) we plot the behavior of

R_1, R_2 and $n_> - n_<$ for $\Delta = 0.025W$; in this case the two renormalization factors are approximately equal and decrease monotonically with U. At the transition, the majority orbital occupation suddenly increases and the corresponding renormalization factor vanishes. We mention that a Mott insulator with partial occupation of both orbitals can not be stabilized within the Gutzwiller approximation, while more reliable DMFT calculations show that such a phase does exist for very small Δ [133]. We shall return on the details of this zero temperature Mott transition in the Section dedicated to the out-of-equilibrium dynamics.
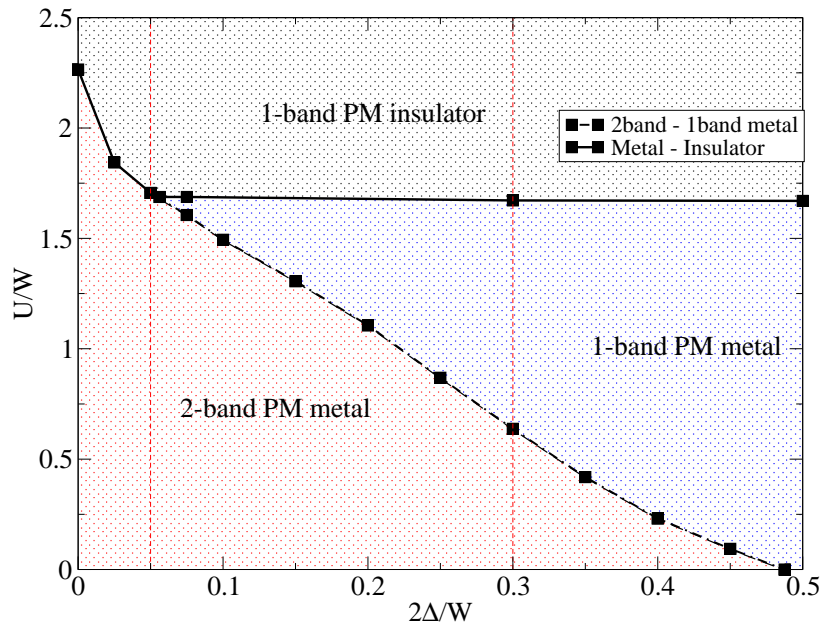

FIGURE 5.2: $T = 0$ phase diagram for model in Eq. (5.1). The solid line indicates the MIT transition; the dashed/dotted line separates the two-band paramagnetic metal (two-band PM metal) from the one-band PM metal. The vertical dashed red lines indicate the values of Δ which are used in Fig. 5.3.

If we allow for magnetism, the one-band phases, either metallic or Mott insulating, turn immediately into an antiferromagnetic insulator, see Fig. 5.4. The transition from the two-band paramagnetic metal to the one-band antiferromagnetic insulator (one-band AFI) is first order and accompanied by a jump in the orbital polarization and in the staggered magnetization, see inset of Fig. 5.4. This remains true apart for large values of the crystal field splitting and small interactions. In this case the two-band PM metal is first driven to a single band PM metal, and successively it undergoes a transition to an AFI at a finite value of the interaction. This is due to the presence of the small hybridization term which destroys the perfect nesting of the band dispersion. We mention moreover that in this regime the transition from the metal to the AFM insulator can take place through a narrow region in which an AFM metal sets in. Since this is irrelevant for the aims of the present work we overlooked this aspect.
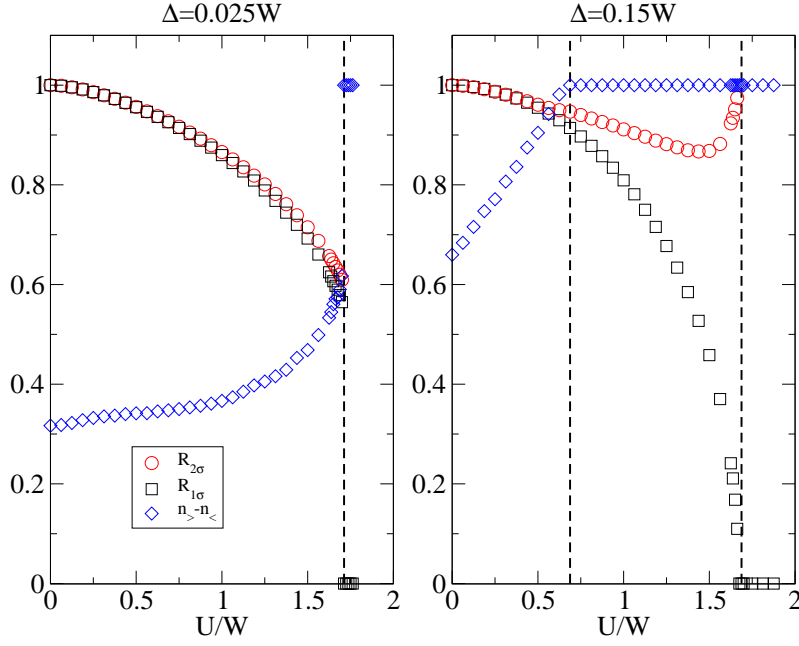
FIGURE 5.3: $n_> - n_<$ (blue diamonds), renormalization factors R_1 (black squares) and R_2 (red circles) as a function of U for fixed $\Delta = 0.025W$ (left panel) and $\Delta = 0.3W$ (right panel). The vertical dashed lines indicate the two-band $\rightarrow$ one-band metal transition and the MIT.
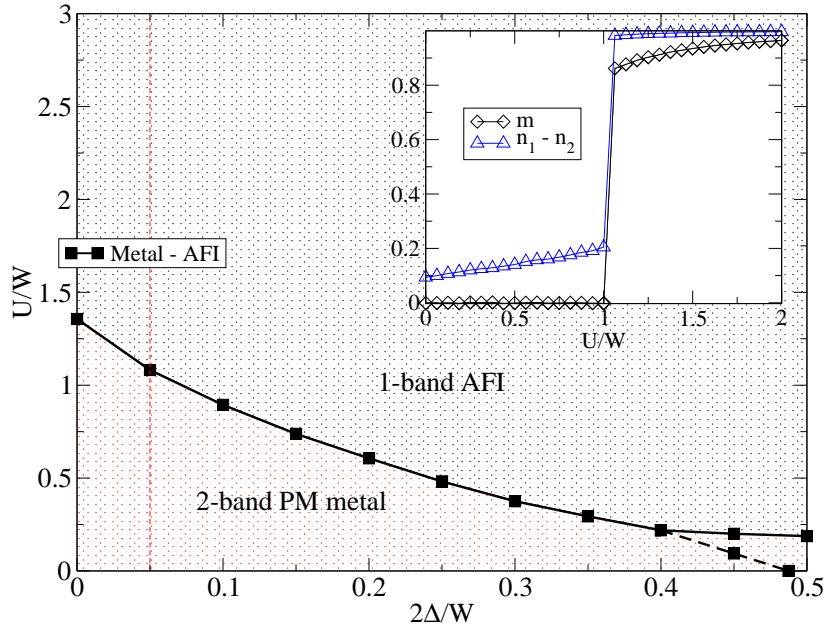

FIGURE 5.4: Zero temperature phase diagram allowing for magnetism. The black line separates the metal from the one-band antiferromagnetic insulator. In the inset we plot the orbital polarization $n_1 - n_2$ and the staggered magnetization for a fixed value of $\Delta = 0.025W$ (red dashed line). The dashed line at small values of U and large values of Δ, shows the transition line from a two-band to a single-band effective metal. This feature would not be present in the unhybridized case.

5.2.2 $T \neq 0$ phase diagram

We have seen that at zero temperature the ground state is either a one-band antiferromagnetic insulator or a two-band paramagnetic metal. Therefore, as we anticipated, the $T = 0$ Gutzwiller variational results are not dissimilar from the predictions of the Hartree-Fock approximation. Differences instead arise at finite temperature, where the Gutzwiller variational approach, as we are going to show, can describe melting of the Néel order without metallization, unlike Hartree-Fock.

We begin as before by restricting the analysis to the paramagnetic sector and consider the case of $\Delta = 0.025W$. At zero temperature we found that the model is a one-band PM insulator for values of $U \geq 1.7W$, while a two-band PM metal below, Fig. 5.2. At finite temperature, the entropic contribution may favor the paramagnetic insulating solution, like in the single band Hubbard model [69], thus leading to a finite T metal-insulator transition. This indeed occurs, as shown in Fig. 5.5 where we plot the phase diagram as a function of U and T (upper panel) and the temperature dependence of the majority orbital R_1 and the orbital polarization (lower panels). In the figure we observe that for values of $U \geq 1.7W$, increasing the temperature the orbital polarization decreases and the quasiparticle weight increase: the one-band PM insulator continuously evolves towards a two-band PM insulator. Instead, for smaller values of U, the system is initially a two-band metal and undergoes a first order transition to an insulating state which is accompanied by an abrupt fall-down of the renormalization factors and increase of orbital polarization. As in Ref. [81], we interpret the jump of the renormalization factor as the boundary of the PM Metal-to-Insulator transition. Notice that, differently from the $T = 0$ case, the orbital polarization does not saturate at the transition. Finally, for values of U smaller than $\sim 1.19W$, the quasiparticle weight and the orbital polarization evolve smoothly to the high temperature limit, displaying a dip that we interpret as the crossover regime. We estimate the end-point of the transition at $T \simeq 0.09W$. We note, in the lower panel of Fig. 5.5 and for $U = 1.1W$, the tiny discontinuity of R_1 and $n_1 - n_2$ at $T \approx 0.01W$, which is consequence of the aforementioned artificial discontinuity in the slope of the free energy caused by our not rigorous lower bound of the entropy.

When magnetism is allowed, at zero temperature and at large U the ground state is antiferromagnetic. At finite temperature the system remains ordered up to the Néel temperature. In Fig. 5.6 we plot for $\Delta = 0.025W$ the phase diagram, indicating by a dotted line the Metal-to-Insulator transition that we have found in the paramagnetic sector. We note that this transition line crosses the Néel temperature, roughly at $U \simeq 1.28W$, and extends above, unlike what happens in the single-band Hubbard model. For $U > 1.28W$, the Gutzwiller variational approach is able to describe melting of the AFI
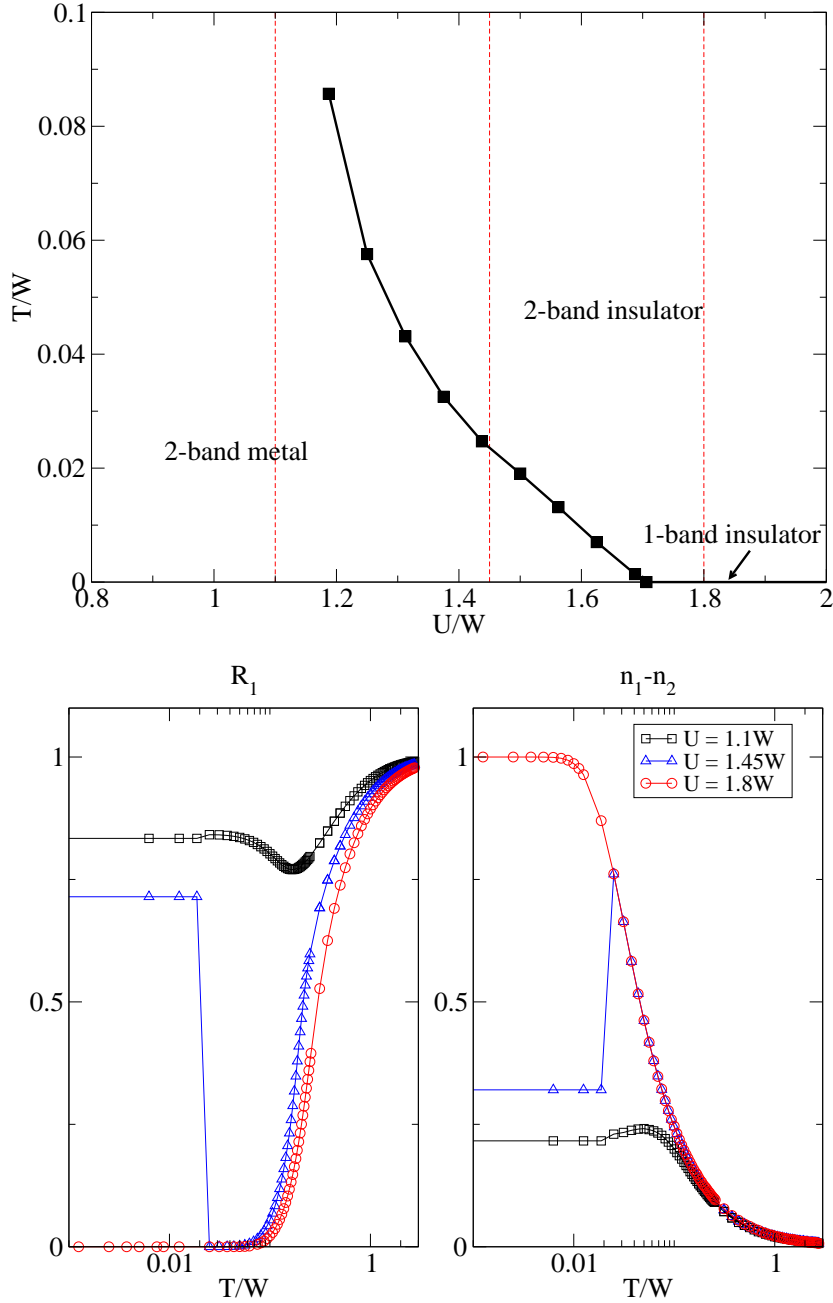
FIGURE 5.5: Upper panel: phase diagram in the paramagnetic domain. The black line separates the PM metal phase from the PM insulator. The red vertical lines indicate the values of U plotted in the lower panel. Lower panel: Temperature dependence of the quasiparticle weight for the majority orbital (left) and of the orbital polarization (right) for different values of U.

into a two-band PM insulator, which we mentioned is not accessible by Hartree-Fock. For smaller values of U, the magnetic insulator turns into a two-band PM metal that eventually undergoes a Mott transition at higher temperatures. In Fig. 5.7 we show more in detail the behavior of the physical quantities across the different transitions; in the low temperature AFI (blue area on the left) the orbital and magnetic polarizations are very weakly temperature dependent. Increasing T, the Néel order melts, the orbital

polarization decreases (red areas on the right), and the model turns into a two-band PM metal (left panel) or PM insulator (right panel) depending on the value of U. In the former case, left panel of Fig. 5.7, the two-band metal is eventually driven to the PM insulating state, transition that is signaled by the sudden vanishing of the renormalization factors and the jump of the orbital polarization $n_1 - n_2$. In the right panel, instead, the AFI melts directly in the PM insulator; the renormalization factor vanish at the transition and then smoothly increases from zero on raising T.

We observe that the finite-temperature phase diagram of Fig. 5.6 is not dissimilar to that of V_2O_3 as function of chemical/physical pressure, Fig. 5.1. Also the physical mechanism that controls the phase diagram, i.e. the correlation enhanced crystal-field splitting, is consistent with that proposed in Ref. [143] for V_2O_3, though in our case the number of orbitals involved is two and not three. We also note the discontinuous increase of the orbital polarization across the PM Metal-to-Insulator transition upon increasing temperature, see left panel in Fig. 5.7, which is consistent with X-ray adsorption spectra of V_2O_3 [139, 148], in which case the orbital polarization relates to the occupation of the e_g^π orbitals with respect to the a_{1g} one.
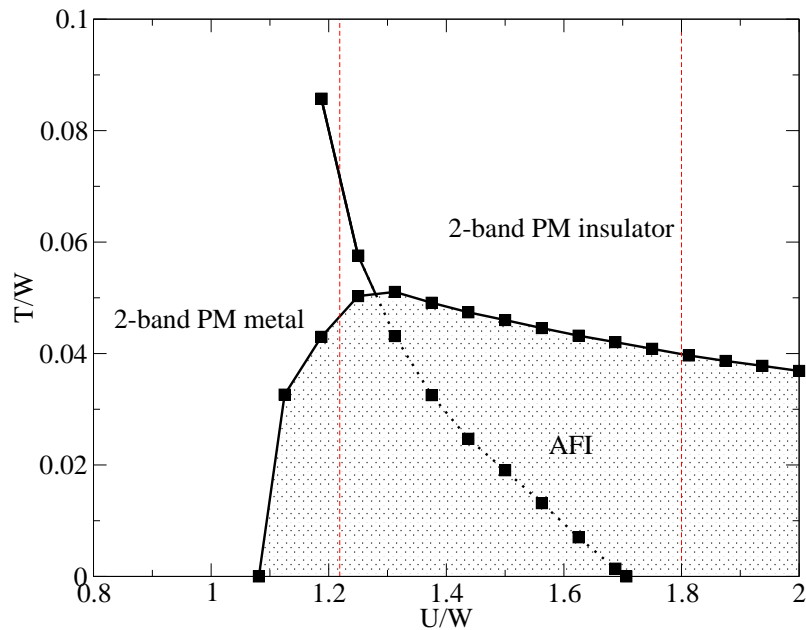

FIGURE 5.6: Finite temperature phase diagram as a function of U and T, for a fixed value of $\Delta = 0.025W$. The paramagnetic solution is continued also within the AFM domain (dotted line). The vertical red dashed line indicates the temperature cut represented in Fig.5.7.
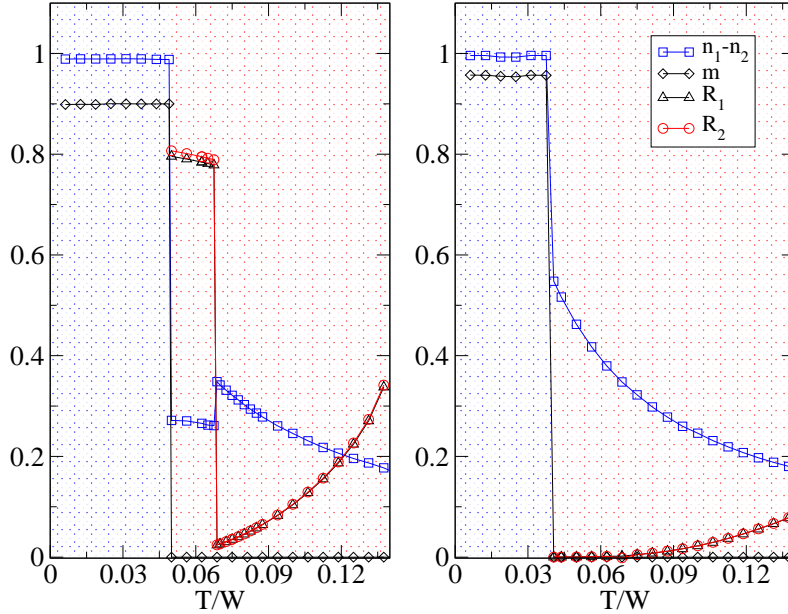
FIGURE 5.7: The blue and red areas indicate respectively the AFI phase and the paramagnetic phase as a function of temperature at fixed values of $U = 1.22W$ (left) and $U = 1.8W$ (right). At low temperatures the orbital polarization (blue squares) and the staggered magnetization (black squares) are practically equal to the zero temperature values and display a discontinuous jump at the AFI-PM transition. In the paramagnetic phase we show also the behavior of the renormalization factors whose jump indicates the PM Metal-to-Insulator transition.

5.3   Comparison with DMFT

In this section, we compare the quality of the finite temperature Gutzwiller approximation with exact DMFT results performed by Massimo Capone. In particular, we shall consider a simplified version of the model in Eq. (5.1) with vanishing inter-orbital hybridization, $t' = 0$, and on a Bethe lattice with only nearest neighbor hopping, which leads to a non-interacting semicircular density of states of bandwidth W. We choose a Bethe lattice (a Cayley tree with coordination number $z \to \infty$) because in this case DMFT is exact and, as previously discussed, the Gutzwiller approximation does provide a rigorous upper bound to the free energy, which therefore makes it possible to assess its accuracy with respect to exact results. The phase diagrams obtained by DMFT and by the Gutzwiller approximation in the U-T space for $\Delta = 0.025W$ are shown in Fig. 5.8.

DMFT maps the lattice model onto an impurity model, which, in the present calculation, is solved by means of exact diagonalization [149] in the finite-temperature implementation proposed in Ref. [150], which is particularly accurate at the low temperatures that we consider. Within the exact diagonalization approach, the bath is approximated by a finite number, N_b, of energy levels. Here we take $N_b = 10$ and
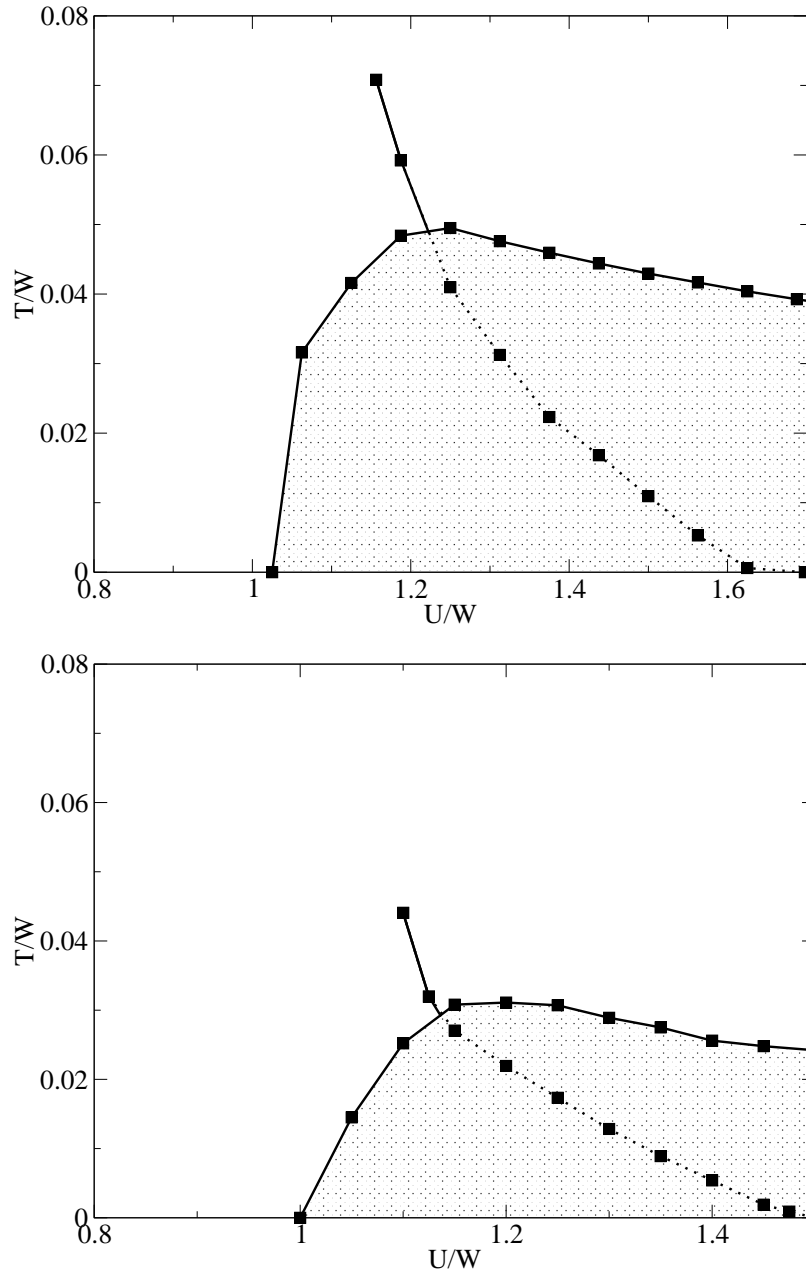
FIGURE 5.8: Top panel: finite T phase diagram within the Gutzwiller approximation at $\Delta = 0.025W$, $t' = 0$ and a semicircular DOS. Bottom panel: same as before but within DMFT, which is exact.

$N_b = 12$, i.e. 5 and 6 bath levels for each physical orbital. Only for $N_b = 10$ we could include a number of states sufficient to obtained converged results. Therefore data for $N_b = 12$ have only obtained for low temperatures, and used to prove that the discretization error only leads to minor corrections to the phase diagram. We consider both paramagnetic and antiferromagnetic solutions. As customary, we first determine the Mott transition line in the paramagnetic sector by comparing the free energies of the metallic and Mott insulating solutions. The transition is first-order at any finite temperature and ends in a finite-temperature critical point at $T \lesssim 0.05W$. If we allow

for long-range antiferromagnetic order, at $T = 0$ the system is metallic for $U \lesssim W$, and it turns into a single-band antiferromagnet for larger values of the interaction. The Néel temperature rapidly grows with U and reaches a maximum around $U \simeq 1.2W$, above which it monotonically decreases. However, differently from the single-band case, the first-order Mott line is not completely covered by the antiferromagnetic dome.

The DMFT phase diagram is thus very similar to that obtained by the finite-temperature Gutzwiller approach, qualitatively and to some extent quantitatively; see Fig. 5.8. As common with the Gutzwiller approximation, the $T = 0$ Mott transition in the paramagnetic sector occurs at larger $U/W \simeq 1.7$ than the exact DMFT value $U/W \simeq 1.5$. In addition, the Gutzwiller wavefunction seems to overestimate antiferromagnetism, which occupies a larger region in the phase diagram. However, quite remarkably, the endpoints of the PM Mott transition do not differ much, $U/W \simeq 1.175$ and $T/W \simeq 0.07$ in the Gutzwiller calculation, while $U/W \simeq 1.1$ and $T/W \simeq 0.05$ in DMFT. Concerning the relative performances of the Gutzwiller technique and of DMFT, we compared the CPU time required to calculate by both methods the free energy at given T and U on a machine with an Intel i7-3770 (3.40 GHz) quad-core processor. We find that the finite-T Gutzwiller approximation takes around 2–3 minutes in the paramagnetic sector and 10 minutes in the antiferromagnetic one, while DMFT using the finite-T implementation of the exact diagonalization impurity solver typically requires a time two orders of magnitude greater in both cases, which becomes even higher at high temperature but reduces to 10–15 times more at low temperature.

Conclusions on the equilibrium analysis

In this first part we have introduced a two-band toy model that we believe qualitatively captures the main physics of vanadium sesquioxide, V_2O_3. To corroborate this intuition we exploited the results of Sec. 2.2 on the extension of finite temperature of the Gutzwiller approach and we applied this technique to calculate the equilibrium phase diagram of this model. At zero temperature we find that a correlation-induced enhancement of the crystal field splitting plays a relevant role in determining a Metal-to-Insulator transition characterized by the depopulation of one band in accordance with DMFT picture [143, 151].

At finite temperature, in spite of being extremely simplified with respect to a complete description of V_2O_3, the model has a very similar phase diagram comprising a low-temperature antiferromagnetic insulating dome and high-temperature paramagnetic metal as well as Mott insulating phases separated by a first order line.

Finally we have tested the accuracy of our finite temperature Gutzwiller approximation

comparing the phase diagram of the model on a Bethe lattice with the exact one obtained by DMFT. The agreement is qualitatively very satisfying and partly also quantitatively. We believe therefore that this simple variational technique is very promising to attach correlated electron systems at finite temperature, and could be used whenever more reliable tools, like DMFT, become numerically too demanding.

5.4   Time dependent Gutzwiller for a two-band model

The previous part of this Chapter was devoted to the analysis of the equilibrium phase diagram within the GA of a two-band model which can reproduce the gross features of the actual phase diagram of V_2O_3. In order to proceed with the out-of-equilibrium investigation of this model it might be helpful to recall the zero temperature picture we obtained. This is sketched in the diagram of Figure 5.9. When the hopping is turned on (leftmost side of Fig. 5.9) the orbitals broaden in two bands that generally are both occupied, thus describing a quarter-filled two-band metal. Increasing the interaction, correlation induces a renormalization of the hopping with a consequent enhancement of the bare crystal field splitting, Δ. Eventually, as U is further increased, the upper band is left completely depopulated leaving the lower band half filled, which in turn can become Mott insulating, likely with the emergence of magnetism. The actual phase diagrams at zero temperature are reported in the previous Chapter, Fig. 5.2 and 5.4.

Two aspects that characterize this model are worth to be highlighted in comparison with the single band Hubbard model. First we notice that the Metal-to-Insulator transition in this case is not characterized by a genuine Mott-Hubbard gap that refers to the same orbital (as for the single band Hubbard model) but rather by an inter-band gap between an occupied Mott-localized band and a weakly correlated unoccupied one [133]. Moreover, for small values of the crystal field splitting, the metallic phase is predicted to disappear by a *first order transition*. This implies that close to the Mott transition a metastable paramagnetic metal phase is expected to exist even at zero temperature, an occurrence which is particularly interesting since one can envisage the possibility to stabilize this phase under nonequilibrium conditions, for instance by an external bias as in the phenomenological model proposed in Ref. [128]. Such possibility is very fascinating in view of recent pump-probe experiments on correlated materials where photoinduced Insulator-to-Metal transitions can be achieved [2].

In the remaining part of this Chapter we will address this issue by means of the time dependent Gutzwiller Approach. A complete analysis of the out-of-equilibrium physics for the two-band model requires a massive work due to the large number of competing degrees of freedom which can be changed. Therefore we will restrict on two different excitation protocols which we believe are particularly significant to highlight the differences between this two-band toy model and the single band Hubbard model so far considered.
We will start by analyzing the simplified situation in which the crystal field splitting Δ and the hybridization t' are set to zero and the excitation protocol is simulated by a sudden quench of the interaction U. This case simplifies to the dynamics of a two-band

degenerate model that we will study in the paramagnetic sector. In this way we extend the quench dynamics of the single band Hubbard model considered in Chapter 3. We will show that the gross features encountered there remain valid also for this model and in particular a separation between two different dynamical regimes appears as a function of the interaction quench.

In the second part of the Chapter we will instead highlight the differences that emerge when a redistribution of the orbital polarization is considered. By studying the evolution of an initial metallic state obtained by a sudden quench of the orbital polarization $n_1 - n_2$, we will foresee the possible existence of a metastable metallic phase in the insulating regime related to the occurrence of a first order Metal-to-Insulator transition. The existence of such metastable phase has no equilibrium counterpart.
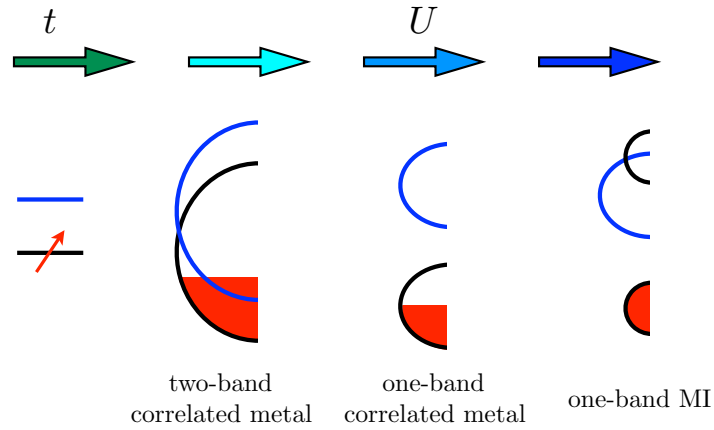

FIGURE 5.9: Sketch diagram which represents the mechanism of the Metal-to-Insulator transition for the two-band toy model as predicted by the GA.

t-GA equations of motion

The out-of-equilibrium dynamics of the two-band model is addressed here by means of the t-GA formalism so far introduced. We report for convenience the toy-model Hamiltonian introduced in (5.1),

$$
\begin{aligned}
\mathcal{H} &= \sum_{a=1}^{2} \sum_{\mathbf{k}\sigma} \epsilon_{\mathbf{k}}\, c_{a\mathbf{k}\sigma}^{\dagger} c_{a\mathbf{k}\sigma} + \sum_{\mathbf{k}\sigma} \gamma_{\mathbf{k}} \left(c_{1\mathbf{k}\sigma}^{\dagger} c_{2\mathbf{k}\sigma} + H.c. \right) \\
&+ \sum_{i} \left[-\Delta \left(n_{1i} - n_{2i} \right) + \frac{U}{2} \left(n_{1i} + n_{2i} \right)^{2} \right],
\end{aligned}
\tag{5.8}
$$

where $a = 1, 2$ labels the two orbitals, $\epsilon_{\mathbf{k}} = -2t \left(\cos k_x + \cos k_y \right)$ is the standard nearest neighbor tight-binding energy, U parametrizes the on-site repulsion and $\Delta > 0$ the

crystal field splitting. We have already noticed in the previous sections that the inter-orbital hopping $\gamma_{\mathbf{k}} = -4t'\sin k_x \sin k_y$ is such that the local single-particle density matrix remains diagonal in the orbital indices 1 and 2. Hence, in this case, the natural basis and the original one coincide.

Following the formalism presented in Chapter 2 we approximate the dynamics of an initial quantum state by a time dependent Gutzwiller wavefunction

$$|\Psi(t)\rangle = \prod_{\mathbf{R}} \mathcal{P}_{\mathbf{R}}(t) \, |\psi(t)\rangle, \tag{5.9}$$

and introduce a local basis for the Fock space in the natural basis (see Table 5.2)

$$|\mathbf{R}, \{n\}\rangle = \prod_{\alpha} (c_{\mathbf{R}\alpha}^{\dagger})^{n_\alpha}. \tag{5.10}$$

The dynamics of the Slater determinant and the Gutzwiller parameters is set by

$$i\partial_t |\psi(t)\rangle = \mathcal{H}_*[\hat{\Phi}(t)] \, |\psi(t)\rangle \tag{5.11}$$

$$i\partial_t \hat{\Phi}_{\mathbf{R}}(t) = \left(\hat{U}(t) + \hat{\Delta}(t)\right)\hat{\Phi}_{\mathbf{R}}(t) + \langle\psi(t)| \frac{\partial \mathcal{H}_*[\hat{\Phi}(t)]}{\partial \hat{\Phi}_{\mathbf{R}}(t)} |\psi(t)\rangle. \tag{5.12}$$

The renormalized Hamiltonian in presence of a Néel antiferromagnetic order is found by separating the bipartite square lattice into two sublattices A and B (see 4.2). Using the fact that

$$R_{\mathbf{R}_a\sigma} = R_{\mathbf{R}_{\bar{a}}-\sigma} \qquad (a \in \{A, B\}) \tag{5.13}$$

$\mathcal{H}_*$ reads

$$\begin{aligned} \mathcal{H}_* &= \sum_{\mathbf{k},a,\sigma} \epsilon_{\mathbf{k}} \Big[\Re(Z_{\mathbf{R}_A a}) c_{\mathbf{k}a\sigma}^{\dagger} c_{\mathbf{k}a\sigma} - i\Im(Z_{\mathbf{R}_A a}) c_{\mathbf{k}a\sigma}^{\dagger} c_{\mathbf{k}+\mathbf{Q}a\sigma}\Big] \\ &+ \sum_{\mathbf{k},\sigma} \gamma_{\mathbf{k}} \Big[Z_{\mathbf{R}_A\sigma}^S c_{\mathbf{k}1\sigma}^{\dagger} c_{\mathbf{k}2\sigma} + Z_{\mathbf{R}_A\sigma}^A c_{\mathbf{k}1\sigma}^{\dagger} c_{\mathbf{k}+\mathbf{Q}2\sigma} + H.c.\Big] \end{aligned} \tag{5.14}$$

where the vector $Q = (\pi, \pi)$. The following quantities are defined in order to simplify notations:

$$\begin{aligned} Z_{\mathbf{R}_A} &= R_{\mathbf{R}_A a\sigma}^* R_{\mathbf{R}_A a-\sigma} \\ Z_{\mathbf{R}_A\sigma}^S &= (R_{\mathbf{R}_A 1\sigma}^* R_{\mathbf{R}_A 2\sigma} + R_{\mathbf{R}_A 1-\sigma}^* R_{\mathbf{R}_A 2-\sigma})/2 \\ Z_{\mathbf{R}_A\sigma}^A &= (R_{\mathbf{R}_A 1\sigma}^* R_{\mathbf{R}_A 2\sigma} - R_{\mathbf{R}_A 1-\sigma}^* R_{\mathbf{R}_A 2-\sigma})/2 \, . \end{aligned} \tag{5.15}$$

5.5   Interaction quench in the degenerate case

Before considering the full dynamics of the model Hamiltonian (5.8) we begin our analysis in the simplified case in which both the inter-orbital hybridization, t', and crystal field splitting, Δ, are set to zero. At zero temperature, this model admits a two-band degenerate Metal-to-Insulator transition at a finite value of the interaction $U_c \approx 26.4\epsilon$, where ϵ is the hopping energy per site and per fermionic species. Within the GA, this transition is identified as usual by the vanishing of the renormalization factors and a corresponding vanishing of the occupation probabilities for the Fock states with occupation different from one [152].

In the following we restrict to the time evolution of an initial non-interacting ($U = 0$) state subject to a quench of the interaction, i.e. $U(t) = U_f\theta(t)$, where $\theta(t)$ is the Heaviside function. We shall return at end of this Section on the general case in which $U(t) = U_i + (U_f - U_i)\theta(t)$. Although this case reproduces a simplified dynamics of the full model Hamiltonian (5.8), this analysis is intended to confirm the presence of a dynamical separation between two regimes similar to that encountered by Schiró and Fabrizio in the single band Hubbard model [49].

The paramagnetic quench that we address here has recently been considered in Ref. [55] for the same model but at *half-filling*; it was shown that quenching the system at increasing values of U, the dynamics displays a crossover between two different regimes that resemble the weak and strong interacting regimes obtained in the single band model. The authors in Ref. [55] interpreted such crossover behavior as an "extended" dynamical Mott transition. Intriguing differences with respect to the single band one arose, in particular the singular Mott dynamical point encountered in Ref. [49] turns into an extended region characterized by the onset of a "chaotic-like" behavior in the physical quantities.

We concentrate here on the quarter-filling case and we show that a similar behavior is recovered also in this case.

First of all one can easily realize from eq. (5.14) that for $t' = 0$ the occupation probabilities $\langle\psi(t)|\ c^\dagger_{\mathbf{k}a}c_{\mathbf{k}a}\ |\psi(t)\rangle$ do not evolve in time, with the result that the dynamics is restricted to the solely evolution of the Gutzwiller parameters $\Phi_{\mathbf{R}\{n\}}$. The time evolution is then obtained by solving the equations of motions (5.12) for the Gutzwiller matrix $\hat\Phi$ whose elements we denote with Φ_n, where $n = 0, ..., 4$ indicates the electron occupation (the Gutzwiller parameters with equal occupation number are degenerate, for example $\Phi_{\uparrow,\uparrow} = \Phi_{\uparrow\downarrow,0} = \Phi_2$). The equations of motion for $\Phi_n(t)$ can be readily solved numerically.

As for the single band dynamics, the evolution within t-GA is characterized by un-damped oscillations without relaxation. It is therefore more effective to concentrate on the long time average of the main physical observables.

In Fig. 5.10 we plot the long time averages of $|R_{a\sigma}(t)|^2 \equiv |R(t)|^2$ and of the occupation probabilities $|\Phi_n(t)|^2$ as a function of U_f. One can notice that both the quasiparticle weight and the double occupation probability reproduce qualitatively the behavior found in the single band PM quench, Fig. 3.2. In particular three regimes can be distinguished: for small values of the quench, $\langle|R|^2\rangle_t$ and $\langle|\Phi_{n\neq1}|^2\rangle_t$ decrease, while the single occupied probability, $\langle|\Phi_1|^2\rangle_t$, shows an opposite trend. For values of $0.39 \lesssim U_f/U_c \lesssim 0.55$ (vertical red lines) the single-occupied probability shows a maximum indicating the tendency of the system to approach the zero temperature Mott insulating state. Finally, at large values of U_f, as expected, the occupation probabilities tend to their initial values, in accordance with the fact that the occupation probabilities remain trapped at very large values of the interaction due to energy constraints.

It is worth noticing that in the intermediate region the dynamics loses its regularity: time averages require very long times to converge and lack a smooth evolution as a function of U_f. The Fourier spectra of the time evolution display irregular and mostly noisy features as one can recognize from Fig. 5.11 (upper panel) in which we plot the Fourier power spectrum of $|R|^2(t) = Z(t)$ (i.e. $\Re^2 Z(w) + \Im^2 Z(w)$) as a function of the final value of the quench. These results are reminiscent of those obtained at half-filling in Ref. [55]; in fact one can identify a multiple-frequency level pattern in the limit of small and large values of the quench which breaks up in the intermediate region. For large values of the quench the dynamics is dominated by $1/U$-period oscillations typical of Mott insulating regime where the Hubbard term of the Hamiltonian is dominating. Such crossover behavior has been interpreted as an extended dynamical Mott transition.

To shade more light on this point we start by noticing from Fig. 5.10 (right panel) that the long time averages of the occupation probabilities for the Fock states with greater occupation number, i.e. $n = 3, 4$, are almost two orders of magnitude smaller than those for $n \leq 2$. This suggests to consider a Gutzwiller dynamics where the parameters $\Phi_{n=3,4}$ are discarded. In this case the equations of motion for the Gutzwiller dynamics read

$$
\begin{aligned}
i\partial_t \Phi_0 &= \frac{16}{\sqrt{3}}\epsilon R^* \Phi_1 + \frac{U}{2}\Phi_0 \\
i\partial_t \Phi_1 &= \frac{4}{\sqrt{3}}\epsilon R \Phi_0 + \frac{12}{\sqrt{3}}\epsilon R^* \Phi_2 \\
i\partial_t \Phi_2 &= \frac{8}{\sqrt{3}}\epsilon R \Phi_1 + \frac{U}{2}\Phi_2
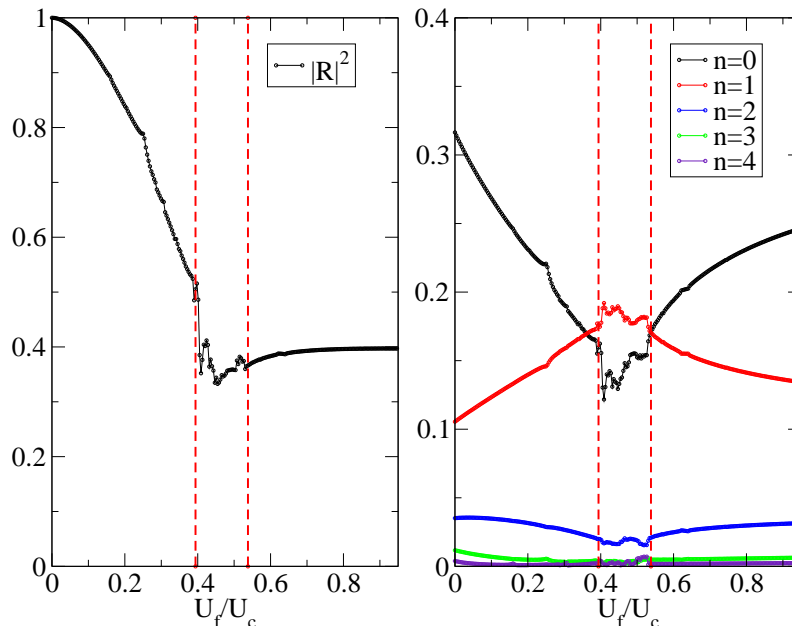\end{aligned}
\tag{5.16}
$$

FIGURE 5.10: Long time average of $|R|^2$ (left panel) and of the occupation probabilities $|\Phi_n|^2$ as a function of the quench interaction. The vertical red dashed lines represent the region in which the dynamics shows an irregular behavior.

with

$$R = \frac{4}{\sqrt{3}}\left(\Phi_0^*\Phi_1 + 3\Phi_1^*\Phi_2\right). \tag{5.17}$$

The time evolution conserves the total energy (L is the number of sites)

$$E/L = 4\epsilon|R|^2 + \frac{U}{2}(|\Phi_0|^2 + 6|\Phi_2|^2) \tag{5.18}$$

together with the Gutzwiller constraints

$$|\Phi_0|^2 + 4|\Phi_1|^2 + 6|\Phi_2|^2 = 1 \,,$$
$$4|\Phi_1|^2 + 12|\Phi_2|^2 = 1. \tag{5.19}$$

At equilibrium the renormalization factor R can always be chosen real and its vanishing signals the onset of the Mott insulator. Out-of-equilibrium, but in the half-filled single band model, $R(t)$ can still be chosen real and oscillates in time around a well defined mean value, which allows to identify a dynamical Mott transition when such a mean value vanishes, Sec. 3.2. In the present two-band model, $R(t)$ is unavoidably complex. Therefore, it is not as straightforward as in the single-band case to identify through its temporal evolution a dynamical transition. Nevertheless, there are signals that we believe can be associated to a dynamical transition. We observe that, as shown for the single band Hubbard model both in the PM and AFM quench, Sec. 3.2 and
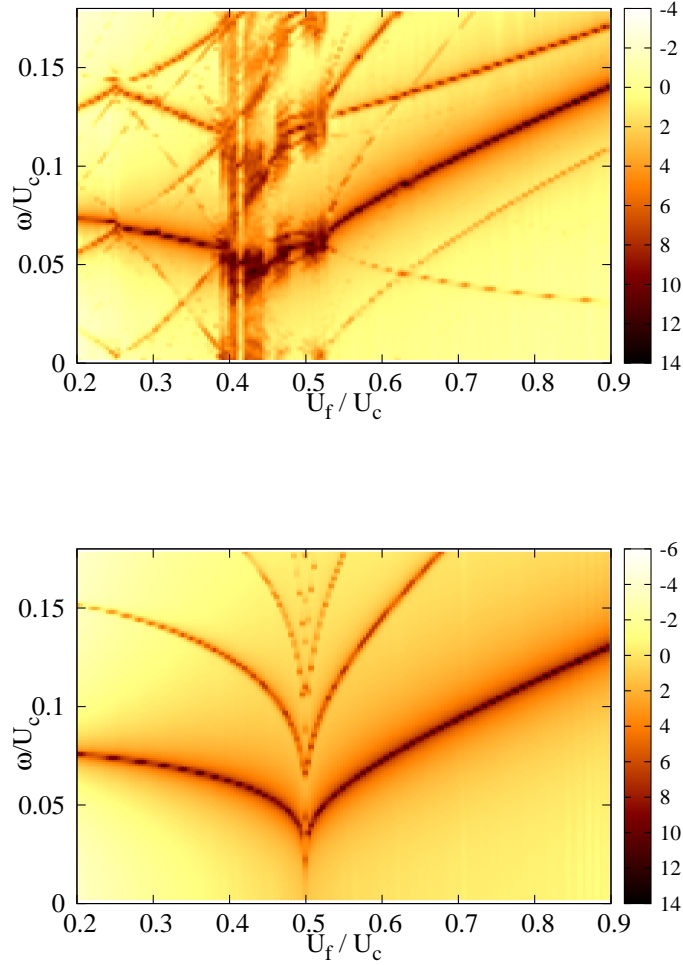
FIGURE 5.11: Discrete Fourier power spectrum (in logarithmic arbitrary units) of $|R|^2(t)$ as a function of U_f. In the upper panel the full dynamics is considered and the extended dynamical transition is clearly recognizable. In the lower panel the dynamics is restricted to the subspace $n \leq 2$ and the Fourier transform is peaked on a single frequency and its multiples; a dynamical transition occurs at $U_f/U_c = 0.5$.

4.3.2, upon rewriting the Gutzwiller parameters as

$$\Phi_n(t) = \rho_n e^{i\phi_n(t)}, \tag{5.20}$$

the Gutzwiller equations of motion can be recast in set of "classical" Hamiltonian equations where ϕ_n and ρ_n play the role of conjugate variables.

In the half-filled single band model, it is found that the time evolution of the phase

$$\phi = (\phi_0 + \phi_2)/2 - \phi_1 \tag{5.21}$$

is associated to the dynamics of the double occupation and reflects in a very transparent

way the dynamical metal-insulator transition. One can easily check that, also in the present case, this is the only angular variable which enters the Lagrangian (2.66). By means of (5.18) and (5.19) one can arrive to an equation of motion in terms of ϕ only,

$$\partial_t \phi = \pm \sqrt{U_f^2 - f(\cos(2\phi))} \qquad (5.22)$$

with

$$f(\cos(2\phi)) = \epsilon^2 \left(\frac{4}{\sqrt{3}}\right)^4 \left[\left(1 - \cos 2\phi\right)\left(\frac{5\sqrt{6}}{2} + 6\cos 2\phi\right)\right]. \qquad (5.23)$$

Hence ϕ displays a dynamical transition at $U_c^{dyn} = 4|\epsilon|(5 + 2\sqrt{6})/3 = U_c/2$ and can be considered a dynamical order parameter which displays small oscillations around zero below the critical point, while it precesses around the unit circle above. At the dynamical critical value the total energy after the quench is equal to zero and the dynamics flows to the stationary Mott insulator point characterized by the vanishing of the occupation probabilities $\Phi_{n \neq 1}$ and the renormalization factor, as one can see from Fig. 5.12.
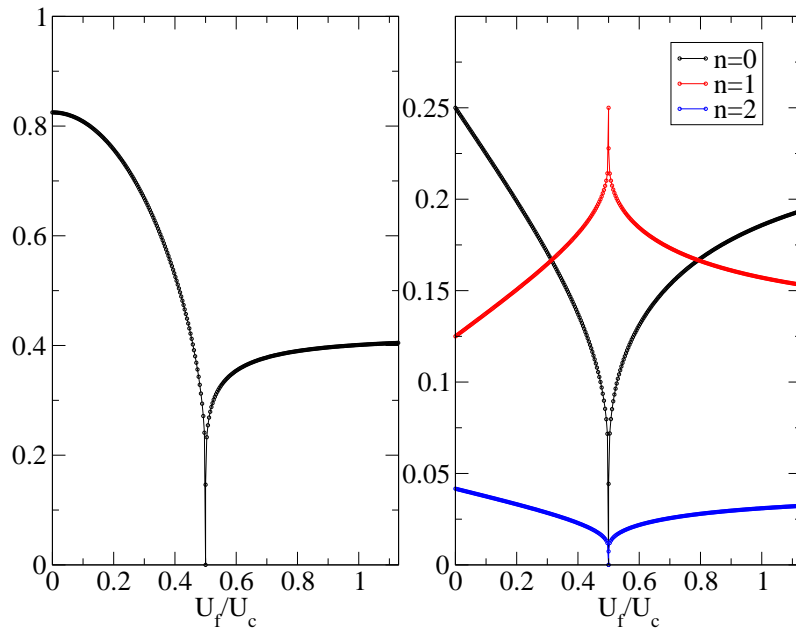

FIGURE 5.12: Long time average of $|R|^2$ (left panel) and $|\Phi_n|^2$ as a function of U_f for the dynamics restricted to the subspace $n \leq 2$. A dynamical phase transition occurs at $U_f = U_c/2$.

The nature of this transition is clearly reminiscent of the one found by Schiró and Fabrizio that we presented in Sec. 3.2. However a clear difference seems to arise. We have seen in Chapter 3 that for the single band Hubbard model the dynamical transition is characterized by the vanishing of the long time average of the renormalization factor, $\langle R \rangle_t = 0$, thus allowing to interpret it as the nonequilibrium counterpart of the

equilibrium Brinkmann-Rice transition. This could be seen even more clearly when the Hubbard model is reformulated in terms of a Z_2 slave spin theory. In this case, at equilibrium, the Mott insulating state corresponds to the unbroken symmetry state of the Ising model, i.e. $\langle \sigma^x \rangle = 0$. As a consequence, the dynamical transition at which Z_2 symmetry is dynamically restored, can be interpreted as a dynamical counterpart of the Metal-to-Insulator transition.

A natural question then arises: what symmetry is restored in the case under consideration? Or in other words, is this dynamical transition a counterpart of the equilibrium Metal-to-Insulator transition?

To answer this point we start by noticing from the constraints (5.19) that when the Fock states with electron occupation $n \geq 3$ are discarded, particle-hole symmetry is recovered, in the sense that the occupation probability of the states with $n = 0$ and $n = 2$ are equal, i.e. $|\Phi_0|^2 = 6|\Phi_2|^2$. This suggests to construct a Gutzwiller projector similar to the one introduced for the single band case, that is retaining only two degrees of freedoms that refer to the single occupied state and the Fock states with $n = 0, 2$. This projector reads

$$\mathcal{P}_{\mathbf{R}} = \Phi_{(1)} \frac{\mathcal{L}_{1\mathbf{R}}}{\sqrt{P_1^{(0)}}} + \frac{\Phi_{(2)}}{\sqrt{2}} \left(\frac{\mathcal{L}_{0\mathbf{R}}}{\sqrt{P_0^{(0)}}} + \frac{\mathcal{L}_{2\mathbf{R}}}{\sqrt{P_2^{(0)}}} \right) \tag{5.24}$$

where

$$\mathcal{L}_{n\mathbf{R}} = \sum_n \delta(n - \sum_{a\sigma} n_{\mathbf{R}a\sigma}) |\mathbf{R}, \{n\}\rangle\langle\mathbf{R}, \{n\}| \tag{5.25}$$

and $P_n^{(0)} = \langle \psi | \mathcal{L}_{n\mathbf{R}} | \psi \rangle$. The normalization condition implies that $|\Phi_{(1)}|^2 + |\Phi_{(2)}|^2 = 1$. One can verify that this is the most general projector which satisfies automatically the Gutzwiller constraints [68]; hence it is straightforward to calculate the expectation value of the Hamiltonian on the Gutzwiller wavefunction $|\Psi\rangle = \prod_{\mathbf{R}} \mathcal{P}_{\mathbf{R}} |\psi\rangle$ without requiring any additional constraint, obtaining

$$\langle \Psi | \mathcal{H} | \Psi \rangle / L = 4\epsilon |R|^2 + \frac{U}{2} |\Phi_{(1)}|^2 \tag{5.26}$$

with

$$R = \frac{2}{\sqrt{6}} \Phi_{(1)}^* \Phi_{(2)} + \Phi_{(2)}^* \Phi_{(1)}. \tag{5.27}$$

The advantage of the following reformulation is that one can interpret the parameters $\Phi_{(1)}$ and $\Phi_{(2)}$ as the components of a 1/2-pseudospin $|\Phi\rangle$. Eq. (5.26) turns out to be

equal to the mean field average value on $|\Phi\rangle$ of the anisotropic Heisenberg Hamiltonian

$$\mathcal{H}_S = 4\epsilon \sum_{\langle \mathbf{R},\mathbf{R}'\rangle} \left(\alpha^2 \sigma^x_{\mathbf{R}} \sigma^x_{\mathbf{R}'} + \beta^2 \sigma^y_{\mathbf{R}} \sigma^y_{\mathbf{R}'}\right) + \sum_{\mathbf{R}} \frac{U}{4}(1 - \sigma^z_{\mathbf{R}}) \tag{5.28}$$

with $\alpha, \beta = 1/2 \pm 1/\sqrt{6}$. As for the single band model, we arrive at an effective spin representation for the two-band degenerate model (where $n = 3, 4$ occupation states are discarded), in the sense that the Gutzwiller approximation is recovered in the mean field approximation of $\mathcal{H}_S$ [1]. Within this approximation $\mathcal{H}_S$ admits an equilibrium phase transition from a broken symmetry ferromagnetic state (i.e. $\langle \sigma^x \rangle \neq 0$) to a paramagnetic one at the critical value $U_c = 32|\epsilon|\alpha^2$. This transition corresponds to the two-band degenerate zero temperature MIT. If we then consider the mean field time evolution of $|\Phi(t)\rangle$ upon a sudden quench of U, this model Hamiltonian displays a dynamical transition at $U_c^{dyn} = U_c/2$ analogous to that encountered in the spin representation of the single band Hubbard model. For values of the quench above U_c^{dyn} the dynamical order parameter $\langle \sigma^x \rangle(t) = 2\rho_{(1)}\rho_{(2)} \cos(\phi_{(2)} - \phi_{(1)})$ oscillates between positive and negative values due to the precession of $\phi_{(2)} - \phi_{(1)}$ and symmetry is dynamically restored.
This dynamical critical point can be clearly seen considering the following parametrization for the semiclassical dynamics of (5.28)

$$\langle \sigma^x(t) \rangle = \cos(\theta)\cos(\phi) \tag{5.29}$$
$$\langle \sigma^y(t) \rangle = \cos(\theta)\sin(\phi) \tag{5.30}$$
$$\langle \sigma^z(t) \rangle = \sin(\theta) . \tag{5.31}$$

In Fig. 5.13 we plot the trajectories in phase space of θ and ϕ at different values of the total energy, for $U_f/U_c = 0.4$ and 0.6. One recognizes that the isoline $E = 0$ corresponds to a separatrix which drives the initial state into the stationary solution with $\langle \sigma^x(t) \rangle = \langle \sigma^y(t) \rangle = 0$. When the initial conditions $\theta = 0, \phi = 0$ are such that the total energy is less than zero, for example the case $U_f/U_c = 0.4$, the angle ϕ is bounded, while it precesses around the unit circle restoring the symmetry in the opposite case.
One can check that the angle ϕ corresponds to the one we introduced in (5.21). This confirms that the precession of ϕ can be related to the dynamical vanishing of the order parameter, hence indicating a dynamical counterpart of the transition from a metal to a Mott insulating state.

When the terms $\Phi_{n\geq 3}$ are not discarded and the full dynamics is considered we cannot determine anymore analytically a transition point. However, in Fig. 5.14 we

---

[1]We remark the for the single band Hubbard model at half filling the mapping to the Z_2 slave spin model is exact.
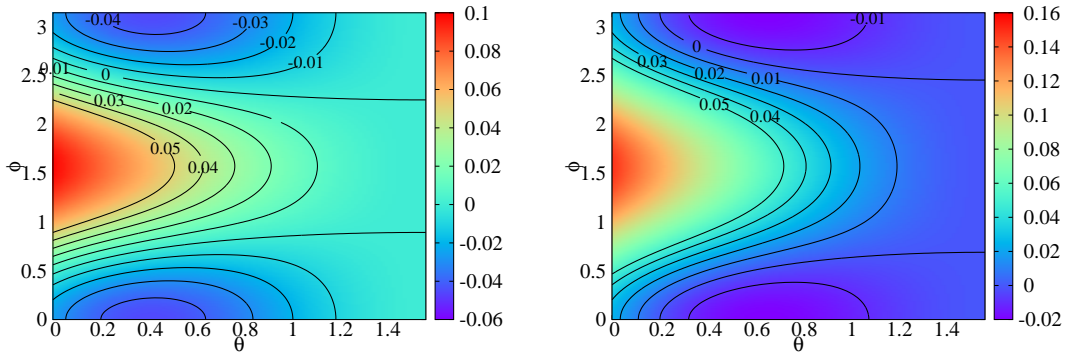
FIGURE 5.13: Phase space trajectories for the mean field dynamics of (5.28) at values of $U_f/U_c = 0.4, 0.6$ that lie below and above the dynamical critical point.

compare the long time average of $\cos\phi$ both in the restricted dynamics (left panel) and in the full one. As explained, for the restricted Hamiltonian $\cos\phi$ averages to zero above U_c^{dyn}; in the full dynamics an analogous behavior remains valid, with the long time average of $\cos\phi$ that stays finite for small values of the quench and vanishes in the opposite limit. In the crossover region a non regular behavior is found again with the long time averages that show an apparent incoherent pattern.

This confirms the existence of two different dynamical regimes which we interpret as a dynamical counterpart of the Metal-to-Insulator transition.
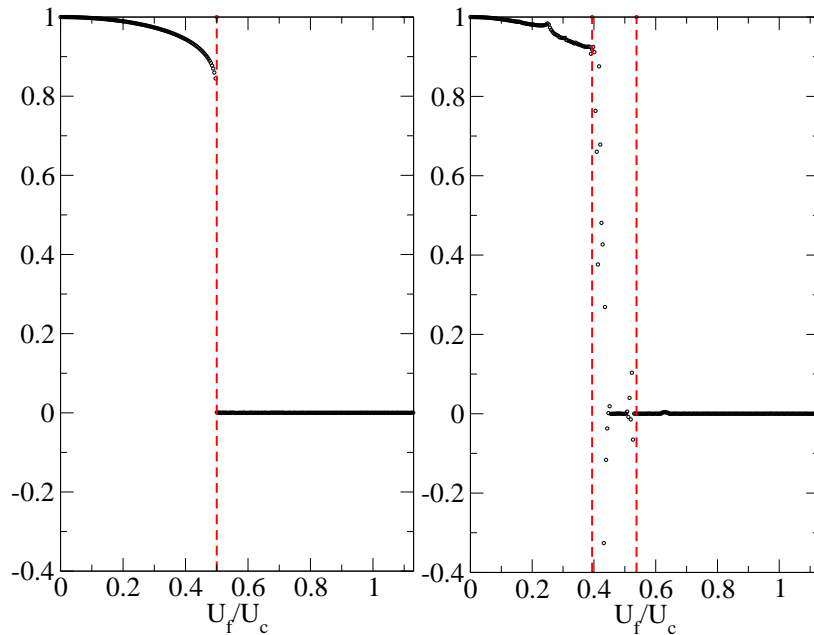

FIGURE 5.14: Long time average of $\cos\phi$ as a function of U_f for the restricted subspace (left panel) and unrestricted (right panel). The red dashed line indicates the dynamical transition point in the first case and the extended transition region in the second one.

We end this Section by considering what happens when the model is quenched from the ground state of an initial interacting Hamiltonian, that is $U(t) = U_i + (U_f - U_i)\theta(t)$ with $U_i > 0$. In this case, as U_i increases towards the equilibrium Mott transition point U_c, the Fock states with higher occupation number $n = 3, 4$ are systematically reduced [152]. Hence, the description in terms of the spin Hamiltonian (5.28) is increasingly well justified. In the limit $U_i \to U_c$, the extended dynamical transition becomes a truly dynamical critical point. As in the single band case [103], we can calculate the value of this dynamical critical point as a function of U_i by requiring that the initial conditions for the dynamics lie on the separatrix at $E = 0$. This condition gives

$$\frac{U_c^{dyn}}{U_c} = \frac{1}{2}\left(1 + \frac{U_i}{U_f}\right) \tag{5.32}$$

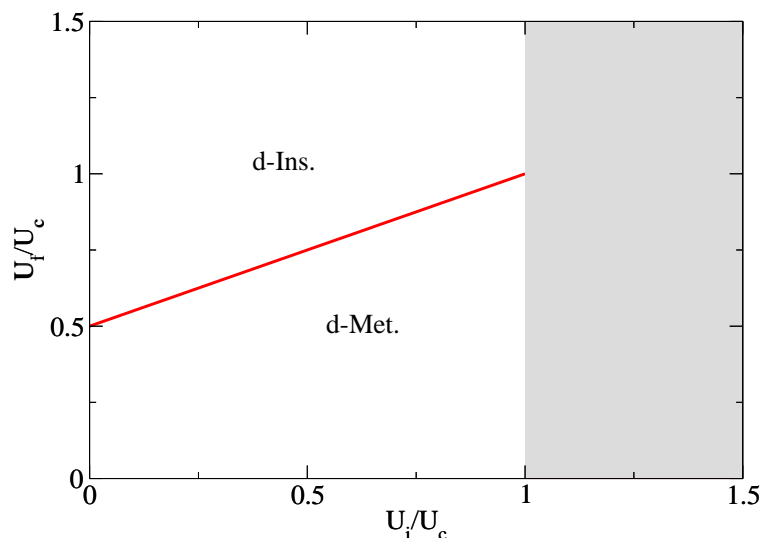which agrees with the result found in [103] for the single band Hubbard model.

FIGURE 5.15: Nonequilibrium phase diagram for the sudden quench in the degenerate two-band Hubbard model when Fock state with occupation $n = 3, 4$ are discarded. The gray region represents initial insulating solutions which are stationary with respect to the Gutzwiller equations of motion.

5.6   Emergence of a non-thermal metallic state

In the previous Section we have seen that the two-band degenerate Hubbard model at quarter filling, when driven out-of-equilibrium by quenching the interaction strength, displays essentially an extended dynamical Mott transition as found in the half filling case of Ref. [55] and bears many similarities with the dynamical phase transition for the half filled single band Hubbard model.

To this extent, an important aspect that one can recognize from the nonequilibrium phase diagram of Fig. 5.15 is that whenever a metallic state ($U_i < U_c$) is quenched in the equilibrium insulating phase ($U_f > U_c$), see blue arrow in Fig. 5.16, the corresponding dynamical phase is the one the we recognized as a dynamical Mott insulator. This excitation protocol aimed to investigate an idealized scenario in which a Mott insulator is excited by an external pulse: we describe the initial excited state as the ground state solution of the metallic Hamiltonian ($U_i < U_c$), thus mimicking the formation of doublons-holons pairs induced by photoexcitation, and we let it evolve under the effect of the strongly correlated insulating one ($U_f > U_c$).

Even though t-GA does not describe thermalization, the fact that the dynamical regime corresponds to the Mott insulating one is not surprising in a thermodynamic sense, since an excited state in the Mott insulating phase is expected to thermalize in a Mott insulator (or more properly a bad metal). In a way this suggest that the out-of-equilibrium physics of a two-band degenerate model displays no significant changes with respect to the single band Hubbard model.

The situation may instead change when we consider an excitation within the insulating phase in presence of a small crystal field splitting. The guiding idea is very simple. We have seen that at equilibrium correlation induces an enhancement of the bare crystal field splitting, with the consequent possibility to drive a two-band metal into a one-band Mott insulator, Fig. 5.16. We can imagine that a sudden reduction of the orbital polarization $m_i = n_1 - n_2$, induced for instance by an intense light pulse, could diminish the effective crystal field splitting to such an extent as to push temporarily the system in a stability region of the two-band metal by a collapse of the inter-band gap. The system could then remain trapped in a metallic phase, which is indeed not unlikely, as we are going to show.

We shall consider separately the case in which we force the system into the paramagnetic sector and the more realist one in which magnetic ordering is allowed.

5.6.1 Dynamics in the paramagnetic sector

First of all we recall that the ground state solution within the GA is determined by minimizing the energy functional (5.6). In the paramagnetic sector, this optimization can be performed in a two step process: first we minimize (5.6) with respect to the Slater determinant and the Gutzwiller parameters matrix $\hat{\Phi}$ for a fixed value of the orbital polarization $n_1 - n_2 = m_i$, obtaining the energy functional $E[m_i]$. Then, the resulting ground state is given by the global minimum of $E[m_i]$.

Since the energy can be written as

$$E[m_i] = E^{kin}[m_i] + E^{hub}[m_i] - \Delta\, m_i \tag{5.33}$$

where E^{kin} is the kinetic contribution and E^{hub} the Hubbard one, one can just calculate $E[m_i]$ for different values of U and m_i at $\Delta = 0$ and then subtract the contribution $\Delta\, m_i$. We find that, for a given value of the orbital polarization m_i, a Metal-to-Insulator transition appears at a critical value of the interaction, $U_c[m_i]$. We plot this value as a function of m_i in the right panel of Fig. 5.16. From this Figure one can evince that, in a region of strong correlation, a metallic or an insulating solution can be favored depending on the value of the crystal field splitting.

One notices that, since the kinetic contribution E^{kin} and the Hubbard one E^{hub} vanish in the insulating phase, from (5.33) it follows that a partially polarized insulator is never the ground state.

In other words, the Gutzwiller Approach does not predict the existence of a zero temperature partially polarized insulating phase. In turn, the two-band metal $\rightarrow$ one-band insulator transition is of first order. We describe this occurrence in Fig. 5.17 where we plot the energy functional $E[m_i]$ and the renormalization factors $R_{1,2}$ as a function of m_i for different values of Δ and at a fixed value of $U = 1.875W$. For $m_i > m_i^c \approx 0.9$ the state is a Mott insulator as one can clearly see from the behavior of the renormalization factors. We observe that there is a whole range of crystal field values where two minima coexist. The global minimum m_{eq}, can occur in the partially polarized metal, for values of $2\Delta/W = 0.0, 0.0125$, or in the fully polarized insulator, for greater values of Δ. The first order transition that we previously mentioned just corresponds to the crossing of the energies of these two minima.

It is important to notice that for values of Δ that correspond to the insulating phase, a metastable metallic minimum at m_* can still be present, as one can see for $2\Delta/W = 0.025$. We can therefore envisage that by suddenly reducing the orbital polarization, the system could indeed be trapped in the metastable metallic solution, as sketched in Fig. 5.17. This result is very suggestive since it predicts the possibility to excite a stationary

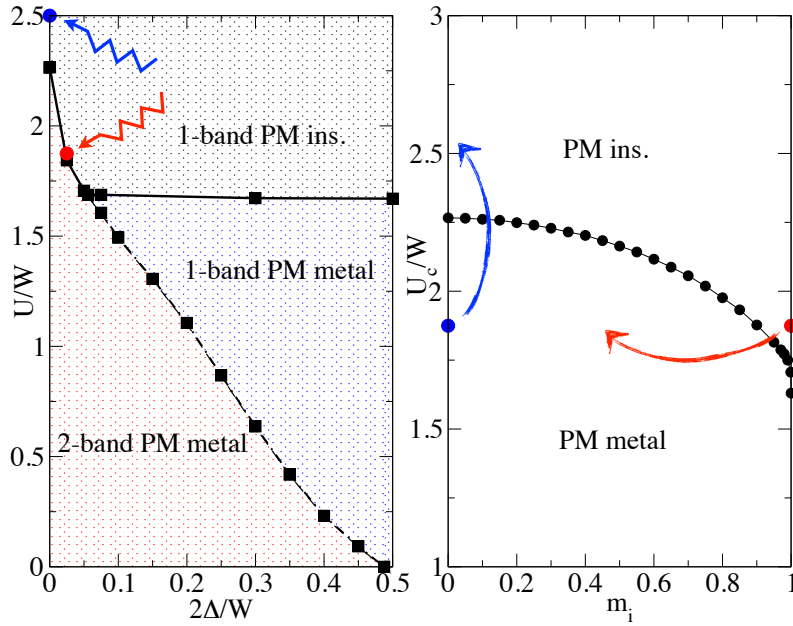metallic state in the insulating region of the phase diagram.

FIGURE 5.16: Left panel: $T = 0$ phase diagram for the model Hamiltonian (5.8) in the PM sector. The blue and red dots represent the values of Δ and U for which an insulator is driven out-of-equilibrium by a quench of the interaction or by a quench of the orbital polarization. Right panel: critical value of U for the Mott transition at fixed value of the orbital polarization m_i. The red bullet indicates the equilibrium value of m_{eq} for the parameters U and Δ shown in the phase diagram on the left. The arrows sketch the quench in the interaction and in the parameter m_i.
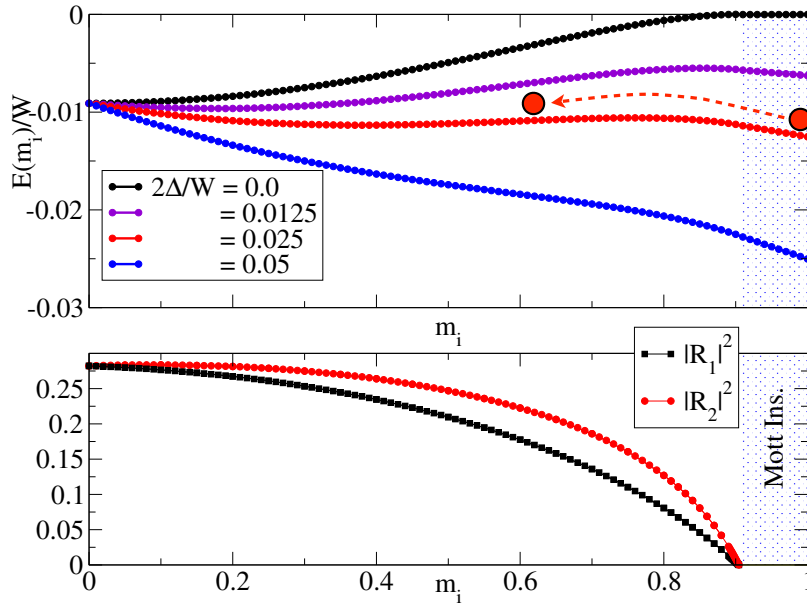

FIGURE 5.17: Upper panel: Ground state energy as a function of m_i at a fixed value of $U = 1.875W$ for different values of Δ. The arrow sketches the quench protocol adopted. Lower panel: $|R_{1,2}|^2$ as a function of m_i. Notice that they both vanish at $m_i \approx 0.9$.

To investigate this occurrence the first issue is how to initialize the state after the fast light pulse has transferred electrons from the lowest orbital to the highest one. We make here an adiabatic assumption that such initial state is the lowest energy one at fixed orbital polarization $m_i < m_{eq}$ and we fix the values of $U = 1.875W$ and $2\Delta = 0.025W$ constant in time (red bullet in Fig. 5.16). This assumption realizes just the process depicted in Fig. 5.17, where the system is instantaneously endowed with a value m_i of the orbital polarization that is not the one that minimizes the total energy.

In the entire region of values $m_i > m_i^c \approx 0.9$, the system is a zero temperature Mott insulator, hence the initial state is trivially stationary with respect to the Gutzwiller equations of motion due to the vanishing of the renormalization factors. This is a well known drawback of the Gutzwiller Approach, which cannot describe the dynamics of an initial Mott insulating state.

For smaller values of m_i instead, the initial out-of-equilibrium state is metallic (i.e., has finite renormalization weight) and evolves under eq. (5.11-5.12).

In Fig. 5.18 we show the time evolution of the orbital polarization, $m(t)$, and of the quasiparticle residue of the orbital 1, $|R_1|^2$, for different values of m_i's. We readily recognize that two regimes in the dynamics are well distinct. For small values of m_i, i.e. far from the equilibrium values $m_{eq} = 1$, both the orbital polarization and $|R_1|^2$ show damped coherent oscillations caused by the dephasing that occurs because of the summation on $\mathbf{k}$ subspace; the frequency oscillation of this amplitude mode is related to the dephasing time, while on top of this there are much faster oscillations (whose frequency scales as the bandwidth) which can hardly be distinguished. For $0.3 < m_i < 0.4$ there exists an initial state which is stationary with respect to the dynamics. This corresponds to the metastable minimum in Fig. 5.17, m_*, which, being a local minimum of the energy functional, is stationary with respect to the Gutzwiller equations of motion. Although the dynamics of the orbital polarization cannot be described as a classical variable where the energy functional $E[m_i]$ plays the role of the classic potential, we see that the tendency of the $m(t)$ is to move according the shape of the $E[m_i]$. In particular it tends to increase from the initial value for $m_i < m^*$ while the opposite happens for $m > m^*$.

This foresees that as m_i is increased (less energy is pumped in the system) and passes the top of the barrier which separates the insulating absolute minimum and the metallic relative one, the scenario should change. In this case, in fact, no relaxation is evident (see for example $m_i = 0.8$) and an undamped oscillating mode persists. Finally, when m_i is further increased the dynamics changes abruptly: $|R_1|^2$ approaches zero and the faster oscillations decouple from the slower becoming well visible.

The drastic change in the dynamics is reminiscent of the extended Mott dynamical transition encountered in the interaction quench of Sec. 5.5 and in Ref. [55]. To gain
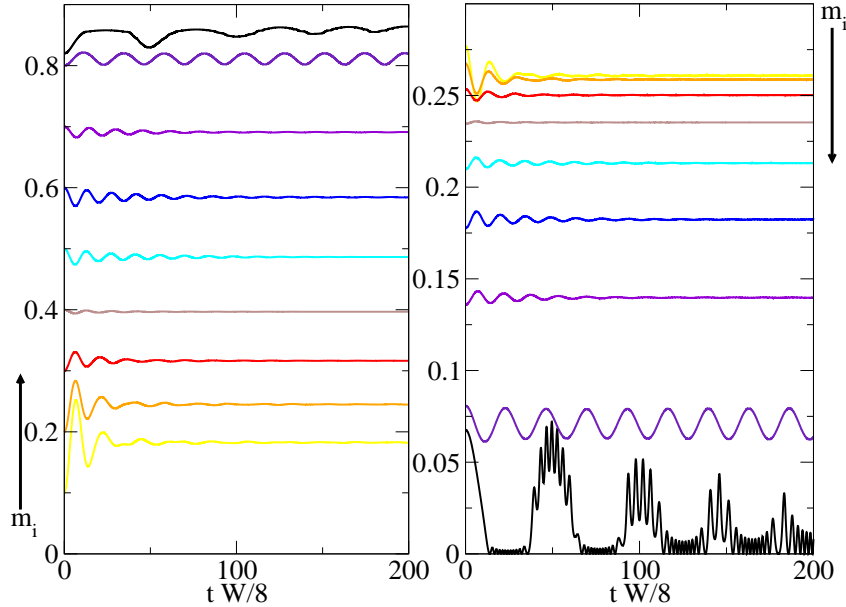
FIGURE 5.18: Time evolution of $m(t)$ (left panel) and $|R_1|^2(t)$ (right panel) for different values of m_i. In the left panel the order of the curves from the bottom is $m_i = 0.2, 0.3, ..., 0.8, 0.82$, while on the right panel the same order is from the top.

further insight in Fig. 5.19 (left panel) we plot the long time averages of m and $|R_1|^2$ as a function of m_i.

For small values of m_i, $\langle m \rangle_t$ and $\langle |R_1|^2 \rangle_t$ evolve smoothly and display no significant deviations from their initial values. This evidences the fact that the time evolution preserves essentially the nature of the initial non-equilibrium state. Approaching the critical region instead, the renormalization weight shows a non analyticity in its long time average which is typical of the dynamical Mott transitions so far studied in literature. As for the extended dynamical transition encountered in the previous Section, it is not possible to establish if a dynamical transition occurs at a single point or in a small extended region.

We can try to enforce this picture by adopting again the usual polar representation of the Gutzwiller parameters $\Phi_{\{n\}} = \rho_n e^{i\phi_n}$. Since we start from the one-band insulator, where the lowest orbital 1 is Mott localized, and we try to induce a nonequilibrium transition into the two-band metal, it is natural to focus on the same phase variable we encountered before pertaining just the orbital 1. In other words we shall concentrate on the dynamical evolution of the phase

$$2\tilde{\phi} = \phi_0 + \phi_{\{\uparrow\downarrow,0\}} - \sum_\sigma \phi_{\{\sigma,0\}} \ . \tag{5.34}$$

In Sec. 5.5 we showed that when the two bands are degenerate (hence the Gutzwiller

parameters can be indexed uniquely by the occupation number), we identified in $\phi = (\phi_0 + \phi_2)/2 - \phi_1$ a dynamical variable connected to the order parameter for the extended Mott transition. We shall therefore monitor the time evolution of $\cos(\tilde{\phi})$ with the belief that, if its time-average vanishes, the system is still in the Mott insulating regime. On the contrary, if the time-average of $\cos(\tilde{\phi})$ is finite and, at the meantime, the time-average of the orbital polarization is smaller than one, we shall conclude that the system has dynamically moved into the two-band metal regime.

In Fig. 5.19 we observe that the time average is essentially vanishing for large m_i's but, below $m_i \approx 0.82$, abruptly jumps to a finite value close to one. We take this as signature of a dynamical phase transition from the Mott insulator to the two-band metal.
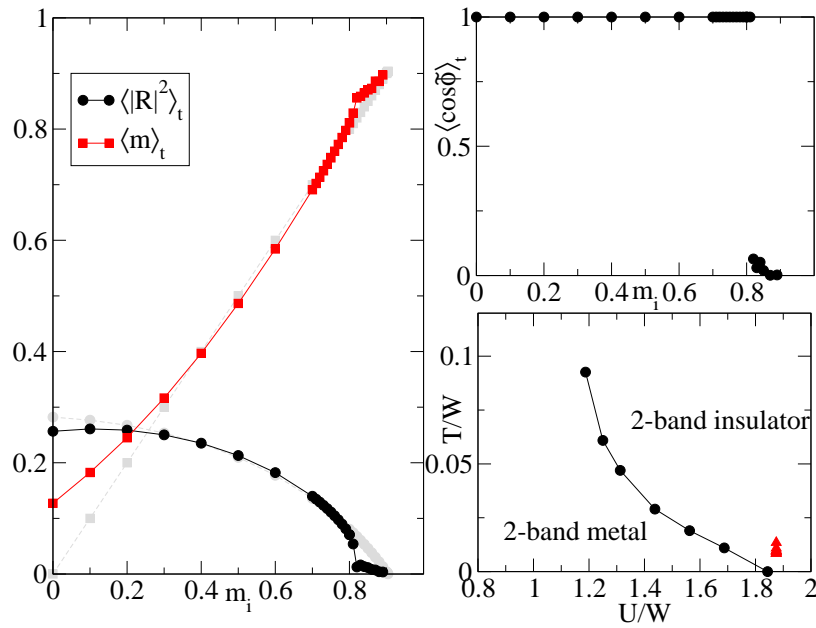
FIGURE 5.19: Left panel: long time averages for m (red squares) and $|R_1|^2$ as a function of m_i. The gray points represent the respective initial ($t = 0$) values. Right panel top: long time average of $\cos\tilde{\phi}$ as a function of m_i. Bottom: finite temperature phase diagram for (5.8) at fixed value of $\Delta = 0.025W$ as obtained by means of finite temperature GA. The red triangles show the effective temperature T_* for $m_i = 0.1, ..., 0.8$.

We note that such a metallic regime is not compatible with the hypothesis that the energy supplied to the system simply heats it. Indeed, if, following the thermalization hypothesis, we transform this excess energy into a temperature determined by imposing that the total energy, conserved in the unitary evolution, coincides with the internal energy at that temperature, we obtain the points shown in Fig. 5.19, all of which are inside the Mott insulating phase. In other words, the metal regime that seems to be stabilized in the dynamical evolution is incompatible with thermalization. Therefore the evidences seem to confirm the expectations that, when the Mott transition is of first

order it is possible to stabilize a metastable metal by properly driving off-equilibrium a Mott insulator.

5.6.2 Dynamics in the AFM sector

In this Section we repeat a similar analysis as before by considering the dynamics for the two-band model without enforcing spin symmetry. We have already recalled that at zero temperature and for large values of the interaction a first order transition from a two-band paramagnetic metal to a single band antiferromagnetic insulator occurs, as one can see in the $T = 0$ phase diagram reported in the left panel of Fig. 5.20. As for the PM case, in the right panel of the same Figure we show the behavior of the energy functional $E[m_i]$ as a function of the orbital polarization, for a value of the interaction $U = 1.125W$. We see that a PM minimum and an AFI one coexist, with their respective energies that cross as a function of the crystal field. We remark that in this case the insulating solution is not fully polarized, $m_{eq} \neq 1$, since the AFM insulator within the GA has finite renormalization factor with a consequent non vanishing of the hybridization term.

We are interested in studying the dynamics upon a sudden quench of the orbital polarization having in mind the effect of a possible external excitation that can trigger a redistribution of the electron population from the lower orbital to the upper one (see sketch in Fig. 5.20). We do expect that also in this case a stable paramagnetic metallic phase can emerge which eventually might not have a thermal counterpart. This possibility, to our knowledge, has not been investigated so far. Indeed, DMFT results on the dynamics of the AFM single band Hubbard model have shown the existence of non-thermal *ordered* states above the corresponding Néel temperature [11, 41], as we discussed in Chapter 4. Very recently, also time-dependent Slave Boson Mean Field Theory calculations considered the demagnetization of an initial AFM state for interaction quenches at lower values of U [153]. In this case the demagnetization mechanism is similar to what we found in the single band case, Chapter 4.

In the following we generalize the orbital polarization quench we introduced in the previous Section to study the evolution of an initial $T = 0$ AFM state at the fixed values of $2\Delta = 0.05W$ and $U = 1.125W, 1.375W, 1.625W$ (red bullets on Fig. 5.20). If we denote with $n^{eq}_{Aa\sigma}$ the equilibrium occupation for the sublattice A, orbital a and spin σ, we construct an initial nonequilibrium state by minimizing the Gutzwiller energy functional imposing that (in the next we discard the label A)

$$
\begin{aligned}
n^i_{1\sigma} &= \alpha \, n^{eq}_{1\sigma} \\
n^i_{2\sigma} &= n^{eq}_{2\sigma} + (1 - \alpha) \, n^{eq}_{1\sigma} \, .
\end{aligned}
\tag{5.35}
$$
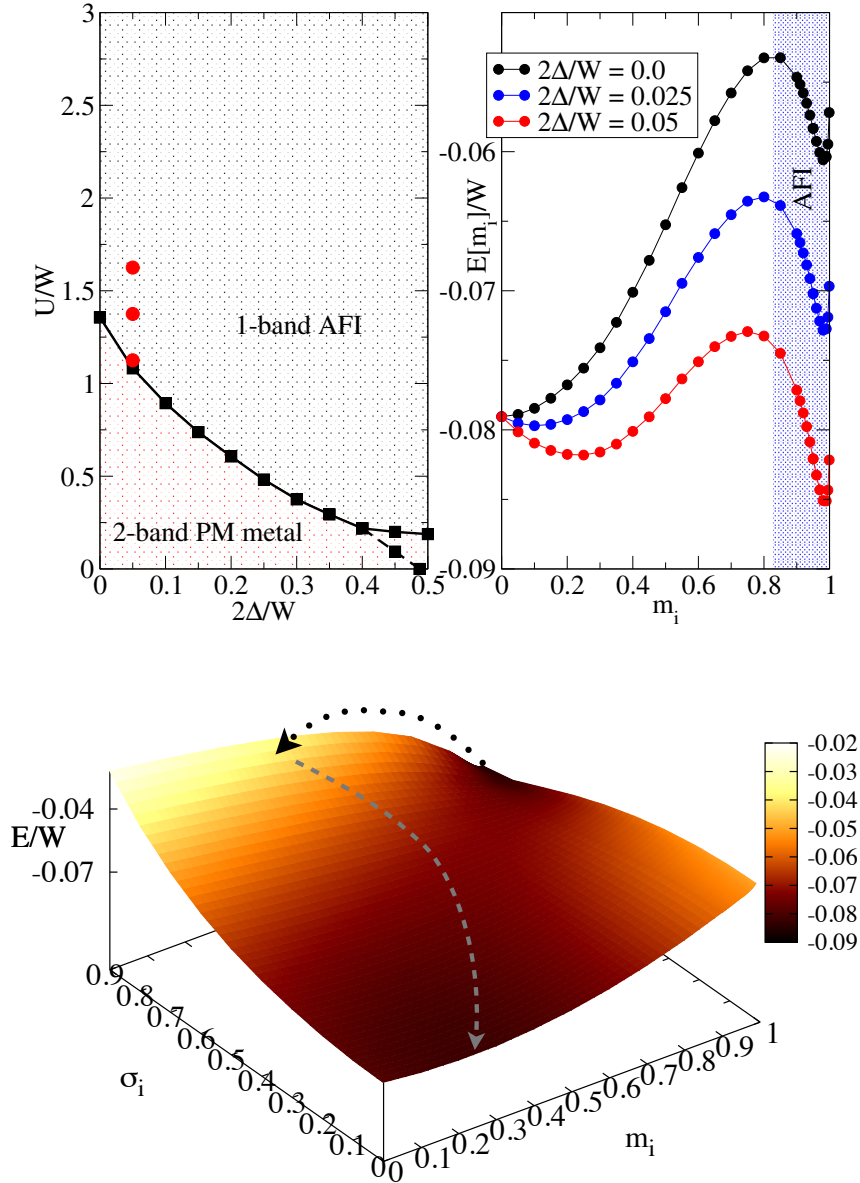
FIGURE 5.20: Left panel: $T = 0$ phase diagram when spin symmetry is not enforced. The red dots indicate the values of Δ and U considered for the dynamics. Right panel: Energy functional at fixed value of the orbital polarization, for different values of Δ at $U = 1.125W$. Lower panel: Energy functional at fixed value of the orbital polarization and of the total magnetization for a value of $2\Delta = 0.05W$. The black dotted line represents the quench in the orbital polarization, while the grey line sketches an approximate classical dynamics.

The state constructed in this way provides an initial excited configuration in which electrons from the lower orbital have been moved to the upper one. The case $\alpha = 1$ obviously corresponds to the equilibrium solution, while $\alpha = 0.5$ corresponds approximately to equally populated bands (it would be so in the unhybridized case where the AFM insulator is fully polarized).

An important difference with respect to the quench we applied in the previous Section is that, in this case, the initial total staggered magnetization remains equal to the equilibrium one, i.e. the external bias does not change the total magnetization, $\sigma^i = \sum_a n^i_{a\uparrow} - n^i_{a\downarrow} = \sum_a n^{eq}_{a\uparrow} - n^{eq}_{a\downarrow}$. Therefore, the initial magnetization does not correspond to the optimized one at the given value of the initial orbital polarization m_i. This is evident from the lower panel of Fig. 5.20 where we plot the energy functional where both the orbital polarization and the total magnetization are left as free parameters. From the Figure one can imagine that, as in the PM case, the dynamics of $m(t)$ and $\sigma(t)$ is approximately driven towards a minimum of the energy surface. This can be rationalized noticing that the equilibrium energy surface is obtained upon a minimization on the Gutzwiller parameters Φ for a fixed value of m_i and σ_i. Therefore, since the total energy is conserved during the dynamics, the initial change of $\Phi(t)$ results in an increase of the energy which has to be compensated by a change of $m(t)$ and $\sigma(t)$ towards a lower value in the energy surface. Of course this argument is qualitative, since $i)$ the energy surface is self-consistently coupled to the dynamics of the Gutzwiller parameters and hence not constant in time $ii)$ the evolving Slater determinant does not correspond in general to the ground state of the renormalized Hamiltonian at fixed values of $m(t)$ and $\sigma(t)$.

However, if one believes that this reasoning can capture at least the main behavior of the dynamics, one can expect that, as the initial orbital polarization is lowered (for smaller values of α), the dynamics will be driven towards a final state with vanishing magnetic order and finite orbital polarization, a two band paramagnet.

We find that this occurrence is met by plotting in Fig. 5.21 the dynamics for the population imbalance $m(t)$ and the total staggered magnetization $\sigma(t)$ as a function of time, for different values of α and for a fixed value of $U = 1.125W$. We first notice that, as in the PM case, two energy scales are well separated, with a high energy oscillating pattern on top of a much slower amplitude mode. Moreover, a further energy scale is associated to the presence of magnetic order and becomes evident in the dynamics of $\sigma(t)$. Upon decreasing the value of α, i.e. moving away from the equilibrium point, $\sigma(t)$ shows indeed a coherent oscillating mode with increasing period, that finally diverges around $\alpha = 0.8$ with a fast decay of the magnetization. This mechanism is actually the same encountered in the interaction quench of the single band Hubbard model in Chapter 4 and of Ref. [153], where the vanishing of the order parameter can be reconduced once again to dephasing. We extrapolate the oscillating period of the coherent mode associated to the presence of AFM order by taking the distance of the first maximum. From the bottom panel of Fig. 5.21 we see that the inverse of this period vanishes linearly at the transition to the PM phase. This agrees with the results we found in Chapter 4.

Above this transition point, $\sigma(t)$ displays very small oscillations around zero while the population imbalance $m(t)$ resembles the dynamics encountered in the PM case of the previous Section.

Overall, the picture that emerges is that the initial AFM state melts into a PM metal (this is confirmed also by the dynamics of the renormalization factors $R_{a\sigma}$ which remain finite and that we avoid to report for this case).
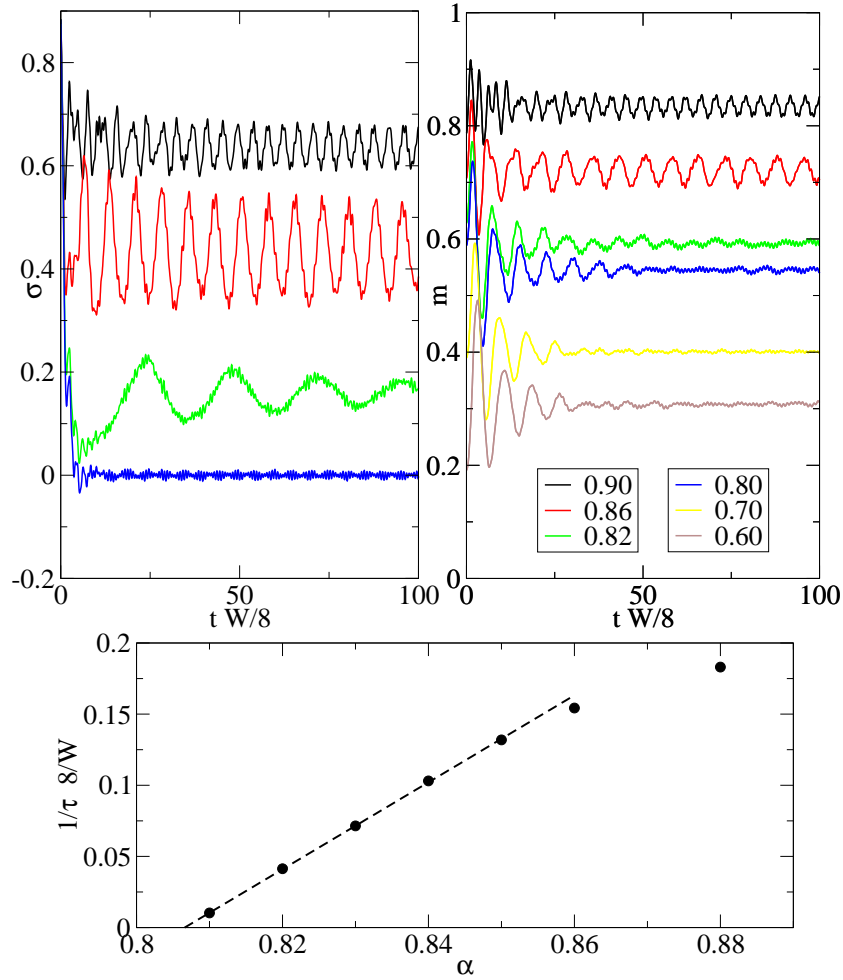
FIGURE 5.21: Upper panels: Time evolution of the staggered magnetization $\sigma(t)$ (left panel) and of the orbital polarization $m(t)$ (right panel) for different values of α at a fixed value of $U = 1.125W$. Lower panel: Inverse of the period oscillation for the AFM coherent mode as a function of the quench parameter α.

The vanishing of the magnetic order rises a second important aspect regarding the nature of the final PM state. Indeed, from the finite temperature diagram that we reproduce for convenience in Fig. 5.22, one would expect that at large enough values of U, the AFM state melts into a PM insulator. It is therefore natural to investigate if the nonequilibrium dynamics is able to capture this aspect.

We have already pointed out that, even though t-GA is not able to describe thermalization, it might be useful to compare the results of the long time dynamics with the corresponding thermal state at an effective temperature such that the initial internal energy equates the thermal one. However, since in this case the equilibrium phase transition is of first order, the two solutions whose free energies cross at the transition lead to a discontinuity in the equilibrium internal energy. This implies the existence of a window of initial energies for which we cannot find a corresponding thermal counterpart. In principle this problem might be solved by following the metastable solutions through the first order transition. This requires to track the local minima in the space of the Gutzwiller variational parameters and of the uncorrelated densities for the Slater determinant. However, since t-GA does not provide thermalization and these arguments are somehow qualitative, we leave this aspect to future work and just consider that if a dynamic PM metallic phase emerges in the correspondent equilibrium insulating one, this could be indicative of a phase that has no equilibrium counterpart.
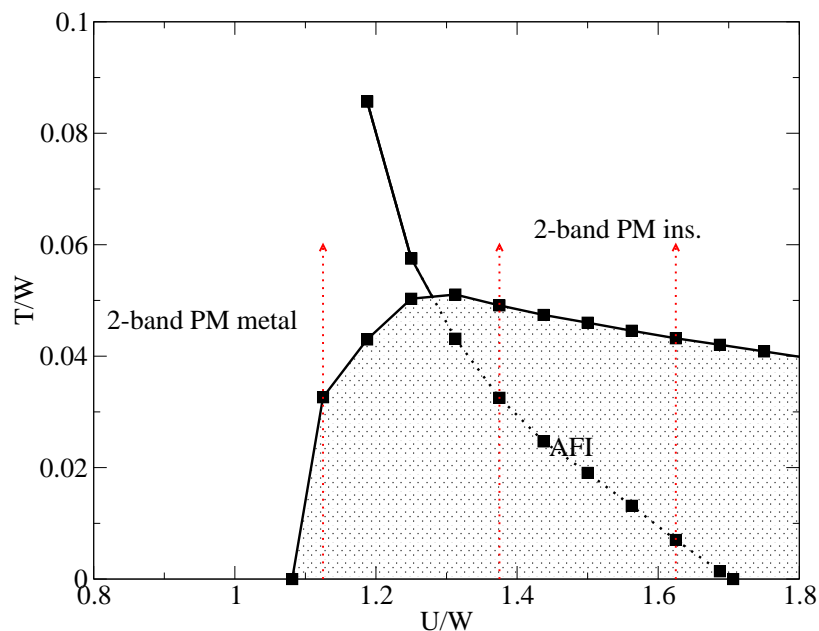
FIGURE 5.22: Equilibrium phase diagram as obtained by means of finite temperature GA for $2\Delta = 0.05W$. The red arrows show the values of U considered for the dynamics.

To verify this guess we consider the time evolution at larger values of the interaction $U = 1.375W$ and $U = 1.625W$, which are respectively evidenced by the red vertical arrows of Fig. 5.22, where the final PM state would correspond to a two-band PM insulator. In Fig. 5.23 we display all the quantities which are of interest in this problem for the two different values of the Coulomb interaction. We recognize that for $U = 1.375W$ we recover a dynamics which is similar to that encountered at the smaller value of U,

with the magnetic order that vanishes for a sufficiently low value of α and a corresponding finite value of the orbital polarization and of the renormalization factors. This is compatible with the emergence of a PM metallic phase with no thermal counterpart.

To substantiate this finding we consider what happens increasing further the value of the interaction. A different scenario is encountered. Upon exciting the system, the dynamics displays an irregular behavior typical of the extended Mott transition previously described. This is once again well captured by the behavior of the renormalization factors, which approach zero, as one can see from Fig. 5.23. For $\alpha > 0.7$ the AFM order averages to zero in the long time limit, even though the dynamics of the Slater determinant is strongly suppressed by the decrease of the renormalization factors. This scenario suggests a dynamical transition to an insulating out-of-equilibrium PM state, a picture that is enforced by considering the evolution of the angle $\tilde{\phi}$ introduced in (5.34). Indeed, as on can see from the bottom panel of Fig. 5.23, the angle $\tilde{\phi}$ oscillates around zero in the metallic regime, while it precesses around the unit circle above the dynamical transition.
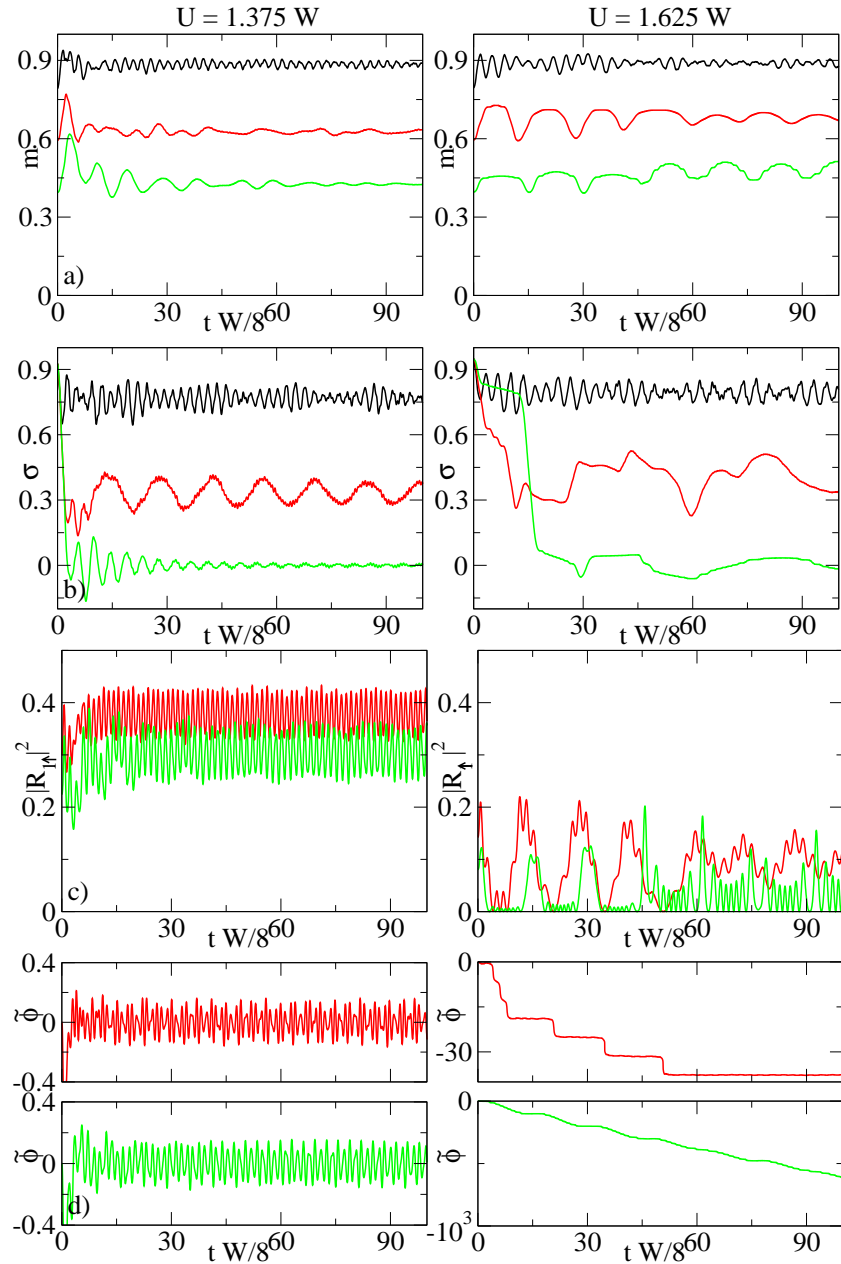
FIGURE 5.23: Left panels refer to the dynamics at $U/W = 1.375$ while right panels at $U/W = 1.625$. The plots respectively represent, as a function of time, a) orbital polarization; b) total magnetization; c) renormalization factor of the most occupied orbital; d) angle $\tilde{\phi}$, for different values of $\alpha = 0.9$ (black), 0.8 (red), 0.7 (green).

5.7   Conclusions

In this Chapter we studied by means of the Gutzwiller Approach a two-band model that we believe captures the main physical mechanisms of the Metal-to-Insulator transition in vanadium sesquioxide.

At equilibrium we confirmed that the phase diagram of the model resembles the actual one of V_2O_3. In particular we pointed out the importance of a correlation-induced enhancement of the crystal field splitting which is responsible for a Metal-to-Insulator transition different from the one encountered in the single-band Hubbard model. In particular, at zero temperature, this transition is of first order and separates a two-band paramagnetic metal from a single-band Mott insulator (either paramagnetic or antiferromagnetic if spin symmetry is not forced). The presence of metastable metallic minima in the energy functional envisaged the possibility that, upon properly exciting an initial zero temperature Mott insulator, a metallic phase can be stabilized which does not correspond simply to a finite temperature Mott insulator.

We provided evidence for this occurrence by considering two paradigmatic excitation protocols. We first considered the case in which the two-band degenerate model ($\Delta = 0$) is driven out-of-equilibrium by a sudden quench of the interaction strength (U). We found that the gross features encountered in the single band Hubbard model remain valid, with an "extended dynamical transition" that separates a metal from an insulator. This situation is therefore not very different from the picture that emerges in the single band case where the dynamics in the insulating regime of the phase diagram is dominated by the atomic excitations.

Differently, if we assume that, at a finite value of the crystal field Δ, an external bias is such to excite the fully polarized Mott insulator moving electrons from the lower to the upper band, we found that such an initial metallic state is stable with respect to the Gutzwiller dynamics and has no equilibrium counterpart. This metallic phase is compatible with an out-of-equilibrium state where the interband Mott energy gap has collapsed. Such scenario is completely different from the ones considered so far for the single band Hubbard model, for which an excited Mott insulator could be essentially described in terms of photo-excited carriers from the lower to the upper Hubbard band.

Some considerations on the method are in order in these concluding remarks. The time dependent GA, even though is able to couple the dynamics of atomic degrees of freedom with the evolution of the Gutzwiller quasiparticles, poorly accounts for all dissipative processes and cannot provide relaxation towards thermal equilibrium. In particular, the quasiparticle Hamiltonian $\mathcal{H}_*(t)$ does not couple subspaces at different values of the momentum $\mathbf{k}$, hence it is ineffective in describing equilibration of the electrons between the two bands that should take place on longer times. This probably leads

to an incorrect increased stability of the metastable metallic phase thus leaving open the issue on its life-time. A possible way to go beyond the Gutzwiller Approximation would be to quantize the degrees of freedom represented by the variational parameters $\Phi_{\mathbf{R}\{n\}}$ and to treat quantum mechanically the coupling to the low energy quasiparticles.

Another open question regards the extension of the quench we considered here to initial states at finite temperature. This would necessitate a generalization of the time-dependent GA to treat initial mixed states, which has not yet been achieved.

Overall, apart from the improvements we proposed above, t-GA has nevertheless provided good qualitative agreement with more sophisticated methods both in describing different relaxation regimes for the single band Hubbard model (Chapter 3) and the presence of non-thermal AFM states (Chapter 4). Therefore we believe that the results presented in this Chapter are important since they provide at least a qualitative evidence of non trivial out-of-equilibrium phenomena emerging in multi-band models.

Conclusions

In this Thesis we analyzed the out-of-equilibrium dynamics of some prototypical model Hamiltonians which are believed to describe the main physical aspects attributable to strong Coulomb correlation in electronic systems.

We adopted the time dependent extension of the Gutzwiller Variational Approach (t-GA) as recently introduced by Schiró and Fabrizio. This method describes the dynamics in terms of a non-interacting renormalized Hamiltonian which is self-consistently coupled, in a mean field fashion, to the evolution of the local degrees of freedom. t-GA, therefore, is not an exact method, with the main drawback being the lack of enough dissipation channels to predict stationarization and eventually thermalization. Nevertheless it is a non perturbative approach, hence it can interpolate well between the itinerant and Mott localized regime, an important property if one intends to address dynamical phenomena for systems that display an equilibrium Mott Metal-to-Insulator transition. It has indeed shown to be a cheap and intelligible technique which can reproduce some main results obtained with more sophisticated methods, such as DMFT. In particular, from the analysis of the single band Hubbard model subject to a sudden quench of the interaction, t-GA provides a qualitative and in some cases also quantitative description for *i)* long lived non thermal states and *ii)* dynamical critical points.

This result motivated our interest in extending the method to more complex situations and models to approach a closer description of real compounds.

In Chapter 2 we introduced the method and in particular we presented a finite temperature extension of the Gutzwiller Approach that we recently developed. This turned out to be necessary if out-of-equilibrium dynamics is intended to be compared with equilibrium average values in order to assess the possible existence of non-thermal phases.

Chapter 3 has been mainly devoted to extending the analysis for the interaction quench in the single Hubbard model. This was essentially motivated by the interest in understanding with greater detail the dynamical phase transition encountered in the sudden quench case. To this extent we considered a linear ramp of the interaction U and we showed that a dynamical phase transition exists at any final value of ramp time which

smoothly evolves into the equilibrium Mott Metal-to-Insulator transition in the adiabatic limit. This confirms that within t-GA the dynamical phase transition corresponds to the out-of-equilibrium counterpart of the Brinkmann Rice transition, thus leaving open the puzzle on its interpretation within DMFT. Moreover, we considered the role of spatial fluctuations beyond mean field and we showed that a dynamical critical region remains.

In Chapter 4 we focused on the dynamics of an initial AFM state for the single band Hubbard model. This quench protocol, in the thermalization hypothesis, would allow to explore the $UvsT$ phase diagram and eventually cross the equilibrium phase transition from the AFM to the PM. In this case we showed that, in agreement with DMFT, non-thermal ordered states survive more than expected, thus confirming the ability of t-GA to capture this aspect. We also found evidence for the existence of two different types of nonequilibrium antiferromagnets separated by a dynamical transition that can be interpreted as the magnetic analogue of the Mott dynamical transition. This dynamical point has no equilibrium counterpart, hence it represents an intriguing direction for future studies.

Finally, in the last Chapter we approached a more realistic modeling of the paradigmatic correlated material vanadium sesquioxide, V_2O_3. To this extent we introduced a two-band model for which we showed that the equilibrium phase diagram captures many aspects of the actual one for the compound. Moreover, the equilibrium analysis highlighted the importance of a correlation-induced enhancement of the crystal field splitting in driving the Metal-to-Insulator transition. Specifically, being this transition of first order, metallic metastable minima are present in a whole region of the zero temperature insulating phase. Upon properly exciting the insulating phase, we showed that a coherent two-band metallic state survives in the dynamics, an occurrence which has no thermal counterpart. Differently from the single band cases considered in the other chapters, where a comparison with DMFT was possible, these results represent a first intriguing evidence that multi-band models can display nonequilibrium behaviors significantly different from the paradigmatic single band Hubbard model so far adopted.

In this Thesis we focused on simplified model situations and excitation protocols which we believe are important for a first understanding of non trivial behavior that might emerge in the novel field of out-of-equilibrium correlated systems.

Further improvements, maintaining the time dependent Gutzwiller Approach as it is, can be reached in several ways. A possible route would be to move from infinitely extended systems (which is the case we considered in this Thesis) to finite layered structures. This has already been considered in some recent works for the single band Hubbard model [67]. It would be interesting to extend these analyses to the two-band model proposed

in the last Chapter of the Thesis.

Starting always from Ref. [67], a second major contribution would be to couple the dynamics of the electrons in the two-band model to phononic degrees of freedom. In this way the transfer of energy from the excited electrons to the lattice could be investigated, a process that might be particularly sensitive in proximity of a dynamical transition. A final important step would be reached by coupling t-GA equations of motion with an external electromagnetic field. This would allow a more accurate description of the pump-and-probe excitation protocol which does not rely on the sudden quench approximation that we adopted in this work.

The present formulation of the method should be considered a valid representation to describe short-to-intermediate times phenomena. The characterization of long time relaxation regimes, where eventually thermalization may occur, necessitates an extension of the t-GA. An important progress on this front, as mentioned in the last Chapter, would be obtained by quantizing the Gutzwiller variational parameters Φ and coupling them quantum mechanically to the low energy degrees of freedom of the renormalized Hamiltonian $\mathcal{H}_*$. We moved in this direction in Chapter 3, where the local degrees of freedom could be mapped into a slave spin Hamiltonian. For a general Hamiltonian however, this represents an open issue which hopefully will be addressed in the future.

Ringraziamenti

Giunto alla fine di questi quattro anni a Trieste ringrazio in primo luogo Michele Fabrizio per la disponibilitá che mi ha sempre dimostrato e per le molte cose che mi ha insegnato. Lo ringrazio soprattutto per la pazienza, il supporto e l'incoraggiamento col quale mi ha condotto ad affrontare il mondo della ricerca.

Un ringraziamento particolare lo dedico a Marco Schiró e a Massimo Capone con i quali ho avuto il piacere di poter collaborare. A loro va la mia gratitudine per tutta la fisica che mi hanno insegnato e per tutti i preziosi consigli che mi hanno dato nelle scelte che ho affrontato.

Non penso che un semplice grazie basti per Adriano Amaricci che non mi ha mai negato un minuto del suo tempo. Grazie Adriano!!

Ringrazio anche Giacomo Mazza che penso sia una delle poche persone con cui ho potuto condividere gioie e dolori del Gutzwiller, e Gianluca Giovannetti e Daniel Grieger per i molti pareri che mi hanno dato.

Un ringraziamento particolare va a tutti gli amici che hanno reso indimenticabili questi anni a Trieste. Ringrazio Nicola e Guglielmo con i quali ho condiviso ben piú di quattro lunghi anni in ufficio assieme ed i vecchi amici importati da Padova, Cristiano ed Andrea. Ringrazio anche gli amici di nuova data, Cristina, Ivan e Aurora ed i miei coinquilini Michele, Stefano ed Andrea.

Infine ringrazio la mia famiglia e Lucia. Per loro non ci sono abbastanza parole per esprimere la mia gratitudine.

Appendix A

Some useful proofs for the Gutzwiller Approach

A.1 Vanishing of the contraction terms with $n \geq 4$ fermionic lines

In the following we shall show that the term

$$\langle \psi | \prod_{\mathbf{R'} \neq \mathbf{R}} \left(\mathcal{P}_{\mathbf{R'}}^{\dagger} \mathcal{P}_{\mathbf{R'}} \right) \mathcal{O}_{\mathbf{R}} | \psi \rangle_{\text{connected}} \tag{A.1}$$

where more than four fermionic lines connect $\mathcal{P}_{\mathbf{R'}}^{\dagger} \mathcal{P}_{\mathbf{R'}}$ with $\mathcal{O}_{\mathbf{R}}$ disappear in the limit of infinite coordination number z. This can be easily seen if $\mathbf{R}$ and $\mathbf{R'}$ are nearest neighbors. In fact, Metzner and Vollhardt [154] realized that in the limit of infinite coordination the hopping strength between nearest neighbors has to scale as $t' \propto t/\sqrt{z}$. Being z the number of nearest neighbors, this scaling property implies that the average value of the hopping operator vanishes in the limit of $z \to \infty$ as

$$\langle \psi | c_{\mathbf{R}}^{\dagger} c_{\mathbf{R'}} | \psi \rangle \propto \frac{1}{\sqrt{z}}. \tag{A.2}$$

Therefore, multiplying four contractions terms and summing over all the possible nearest neighbors, one obtains that the term (A.1) vanishes as $\propto 1/z$. Obviously contracting more than four fermionic lines vanishes even faster in the infinite coordination limit. This argument can be extended also for further neighbors sites, for which one finds that the connected term vanishes as $1/z^l$ where l is the Manhattan distance between the sites.

A.2   Derivation of the Lagrangian for the t-GA

In this section we report the derivation of (2.66) and (2.69) following Ref. [68]. We need to evaluate

$$\mathcal{S}[|\Psi\rangle] = \int_0^t d\tau \overbrace{\langle\Psi(\tau)|\, i\partial_\tau - \mathcal{H}(\tau)\,|\Psi(\tau)\rangle}^{\mathcal{L}(\tau)} \tag{A.3}$$

where $|\Psi(t)\rangle = \mathcal{P}(t)\,|\psi(t)\rangle$ is a time-dependent Gutzwiller wavefunction. The Lagrangian $\mathcal{L}(t)$ can be split in three terms that we can evaluate separately,

$$\mathcal{L}(t) = \overbrace{i\langle\psi(t)|\,\mathcal{P}^\dagger(t)\mathcal{P}(t)\,\partial_t|\psi(t)\rangle}^{(1)} + \overbrace{i\langle\psi(t)|\,\mathcal{P}^\dagger(t)\partial_t\mathcal{P}(t)\,|\psi(t)\rangle}^{(2)}$$
$$- \overbrace{\langle\psi(t)|\,\mathcal{P}^\dagger(t)\mathcal{H}\mathcal{P}(t)\,|\psi(t)\rangle}^{(3)} \tag{A.4}$$

The term (1) can be evaluated noticing that since $|\psi(t)\rangle$ is a Slater determinant, its evolution is in general set by a Scrödinger equation

$$i\partial_t|\psi(t)\rangle = \Big(\sum_{\mathbf{R}} \mathcal{V}_{\mathbf{R}}(t) + \sum_{\mathbf{R}\neq\mathbf{R}'} \mathcal{V}_{\mathbf{R}\mathbf{R}'}(t)\Big)|\psi(t)\rangle \tag{A.5}$$

where $\mathcal{V}_{\mathbf{R}}$ is a general single particle local operator and $\mathcal{V}_{\mathbf{R}\mathbf{R}'}$ is an intersites hopping operator.

Due to the Gutzwiller constraints (2.64) and (2.65)

$$\langle\psi(t)|\,\mathcal{P}^\dagger(t)\mathcal{P}(t)\,\mathcal{V}_{\mathbf{R}}(t)|\psi(t)\rangle = \prod_{\mathbf{R}'\neq\mathbf{R}} \overbrace{\langle\psi(t)|\,\mathcal{P}^\dagger_{\mathbf{R}'}(t)\mathcal{P}_{\mathbf{R}'}(t)\,|\psi(t)\rangle}^{=1}\langle\psi(t)|\,\mathcal{P}^\dagger_{\mathbf{R}}(t)\mathcal{P}_{\mathbf{R}}(t)\mathcal{V}_{\mathbf{R}}(t)\,|\psi(t)\rangle$$
$$+ \langle\psi(t)|\prod_{\mathbf{R}'\neq\mathbf{R}} \mathcal{P}^\dagger_{\mathbf{R}'}(t)\mathcal{P}_{\mathbf{R}'}(t)\mathcal{P}^\dagger_{\mathbf{R}}(t)\mathcal{P}_{\mathbf{R}}(t)\mathcal{V}_{\mathbf{R}}(t)\,|\psi(t)\rangle_{\text{connected}}$$
$$= \langle\psi(t)|\,\mathcal{V}_{\mathbf{R}}(t)|\psi(t)\rangle. \tag{A.6}$$

$$\langle\psi(t)|\,\mathcal{P}^\dagger(t)\mathcal{P}(t)\,\mathcal{V}_{\mathbf{R}\mathbf{R}'}(t)|\psi(t)\rangle = \prod_{\mathbf{R}''\neq\mathbf{R},\mathbf{R}'} \langle\psi(t)|\,\mathcal{P}^\dagger_{\mathbf{R}''}(t)\mathcal{P}_{\mathbf{R}''}(t)\,|\psi(t)\rangle \times$$
$$\times \langle\psi(t)|\,\mathcal{P}^\dagger_{\mathbf{R}}(t)\mathcal{P}_{\mathbf{R}}(t)\mathcal{P}^\dagger_{\mathbf{R}'}(t)\mathcal{P}_{\mathbf{R}'}(t)\mathcal{V}_{\mathbf{R}\mathbf{R}'}(t)\,|\psi(t)\rangle$$
$$+ \text{connected}$$
$$= \langle\psi(t)|\,\mathcal{P}^\dagger_{\mathbf{R}}(t)\mathcal{P}_{\mathbf{R}}(t)\,|\psi(t)\rangle\langle\psi(t)|\,\mathcal{P}^\dagger_{\mathbf{R}'}(t)\mathcal{P}_{\mathbf{R}'}(t)\,|\psi(t)\rangle\langle\psi(t)|\,\mathcal{V}_{\mathbf{R}\mathbf{R}'}(t)\,|\psi(t)\rangle$$
$$+ \text{connected}$$
$$= \langle\psi(t)|\,\mathcal{V}_{\mathbf{R}\mathbf{R}'}(t)\,|\psi(t)\rangle \tag{A.7}$$

so that

$$i\langle\psi(t)|\,\mathcal{P}^\dagger(t)\mathcal{P}(t)\,\partial_t|\psi(t)\rangle = i\langle\psi(t)|\,\partial_t|\psi(t)\rangle. \tag{A.8}$$

Let us consider now the term (2). Also in this case the Gutzwiller constraints allow a simplification in the calculation,

$$
\begin{aligned}
\langle\psi(t)|\,\mathcal{P}^\dagger(t)\partial_t\mathcal{P}(t)\,|\psi(t)\rangle &= \sum_{\mathbf{R}}\langle\psi(t)|\prod_{\mathbf{R}'\neq\mathbf{R}}\mathcal{P}^\dagger_{\mathbf{R}'}(t)\mathcal{P}_{\mathbf{R}'}(t)\,\mathcal{P}^\dagger_{\mathbf{R}}(t)\partial_t\mathcal{P}_{\mathbf{R}}(t)\,|\psi(t)\rangle \\
&= \sum_{\mathbf{R}}\langle\psi(t)|\,\mathcal{P}^\dagger_{\mathbf{R}}(t)\partial_t\mathcal{P}_{\mathbf{R}}(t)\,|\psi(t)\rangle + \cancel{\text{connected}} \tag{A.9}
\end{aligned}
$$

Combining together (A.8) and (A.9) we obtain eq. (2.66) of the main text. We need next to evaluate terms (2) and (3) in the matrix formulation using the parametrization for the local projector

$$\mathcal{P}_{\mathbf{R}}(t) = \sum_{\Gamma n}\frac{\Phi_{\mathbf{R};\Gamma n}(t)}{\sqrt{P^{(0)}_{\mathbf{R};n}(t)}}\,|\mathbf{R};\Gamma\rangle\langle\mathbf{R};n|. \tag{A.10}$$

From (A.10) we have that (A.9)

$$
\begin{aligned}
\langle\psi(t)|\,\mathcal{P}^\dagger_{\mathbf{R}}(t)\partial_t\mathcal{P}_{\mathbf{R}}(t)\,|\psi(t)\rangle &= \sum_{\Gamma n}\Phi^\dagger_{\mathbf{R};n\Gamma}\partial_t\Phi_{\mathbf{R};\Gamma n} - \frac{1}{2}\sum_{\Gamma n}\cancel{\Phi^\dagger_{\mathbf{R};n\Gamma}\Phi_{\mathbf{R};\Gamma n}\frac{\partial_t P^{(0)}_{\mathbf{R};n(t)}}{P^{(0)}_{\mathbf{R}n}(t)}} \\
&= \text{Tr}\big(\hat{\Phi}^\dagger_{\mathbf{R}}\partial_t\hat{\Phi}_{\mathbf{R}}\big) \tag{A.11}
\end{aligned}
$$

The vanishing of the second term in (A.11) can be proved by the following argument. Due to the Gutzwiller constraint (2.64)

$$\partial_t\langle\psi(t)|\,\mathcal{P}^\dagger_{\mathbf{R}}(t)\mathcal{P}_{\mathbf{R}}(t)\,|\psi(t)\rangle \stackrel{GC}{=} 0 \tag{A.12}$$

which implies that

$$0 = \langle\psi(t)|\,\partial_t\Big(\mathcal{P}^\dagger_{\mathbf{R}}\mathcal{P}_{\mathbf{R}}\Big)|\psi(t)\rangle + \overbrace{\partial_t\langle\psi(t)|\,\mathcal{P}^\dagger_{\mathbf{R}}\mathcal{P}_{\mathbf{R}}\,|\psi(t)\rangle + \langle\psi(t)|\,\mathcal{P}^\dagger_{\mathbf{R}}\mathcal{P}_{\mathbf{R}}\,\partial_t|\psi(t)\rangle}^{\diamond} \tag{A.13}$$

where $\diamond$ can be proved to vanish repeating a reasoning similar to the one we used to reach (A.8). We are left therefore with

$$0 = \langle\psi(t)|\,\partial_t\Big(\mathcal{P}^\dagger_{\mathbf{R}}\mathcal{P}_{\mathbf{R}}\Big)|\psi(t)\rangle = \cancel{\partial_t\text{Tr}\big(\hat{\Phi}^\dagger_{\mathbf{R}}(t)\hat{\Phi}_{\mathbf{R}}(t)\big)} + \sum_{\Gamma n}\Phi^\dagger_{\mathbf{R};n\Gamma}\Phi_{\mathbf{R};\Gamma n}P^{(0)}_{\mathbf{R};n(t)}\partial_t\left(\frac{1}{P^{(0)}_{\mathbf{R};n(t)}}\right)$$

which proves the vanishing term in (A.11).

Finally the term (3) in (A.4) can be easily computed by repeating the same argument we used for the equilibrium case. In fact, upon introducing the time-dependent renormalization factors $R_{ab}(t)$ defined through

$$
\begin{aligned}
\langle\psi(t)|\,\mathcal{P}^\dagger_{\mathbf{R}}(t)\,c^\dagger_{\mathbf{R}a}\,\mathcal{P}_{\mathbf{R}}(t)\,d_{\mathbf{R}b}\,|\psi(t)\rangle &= \sum_c R^*_{\mathbf{R}ac}\langle\psi(t)|\,d^\dagger_{\mathbf{R}c}d_{\mathbf{R}b}\,|\psi(t)\rangle \\
&= R^*_{\mathbf{R}ab}(t)\,n^{(0)}_{\mathbf{R}b}(t)
\end{aligned}
\tag{A.14}
$$

one finds that

$$
\begin{aligned}
\langle\psi(t)|\,\mathcal{P}^\dagger(t)\mathcal{H}\mathcal{P}(t)\,|\psi(t)\rangle &= \sum_{\mathbf{R},\mathbf{R}'}\sum_{cd}\Big(R^*_{\mathbf{R}ac}R_{\mathbf{R}'bd}\langle\psi(t)|\,d^\dagger_{\mathbf{R}c}d_{\mathbf{R}'d}\,|\psi(t)\rangle + H.c.\Big) \\
&\quad + \sum_{\mathbf{R}}\mathrm{Tr}\big(\hat{\Phi}^\dagger_{\mathbf{R}}(t)\hat{H}_{\mathbf{R}}\hat{\Phi}_{\mathbf{R}}(t)\big)
\end{aligned}
\tag{A.15}
$$

Terms (A.8), (A.11) and (A.15) sum up to give the final form of the Lagrangian in the main text (2.69).

A.3 Quasiparticle weight and discontinuity at the Fermi surface

In this Section we show that the Gutzwiller quasiparticle weight in the single band paramagnetic Hubbard model corresponds to the jump in the occupation probability $n_{\mathbf{k}} = \langle\Psi|c^\dagger_{\mathbf{k}}c_{\mathbf{k}}|\Psi\rangle$ at the Fermi surface. We start from the equilibrium renormalized Hamiltonian which, as shown in Sec. 3.2, reads

$$
-Z(D)\,t\sum_{\langle\mathbf{R},\mathbf{R}'\rangle,\sigma}c^\dagger_{\mathbf{R}\sigma}c_{\mathbf{R}'\sigma} + H.c.
\tag{A.16}
$$

where $Z(D) = |R|^2 = 8D(1-2D)$ has been identified with the quasiparticle weight. In this case simple case, the Slater determinant which corresponds to the ground state of (A.16) is simply the Fermi sea at half filling, $|\psi_0\rangle$. Following the discussion of Sec. 2.1 the corresponding momentum distribution for the Gutzwiller quasiparticles is simply given by

$$
n^{(0)}_{\mathbf{k}} = \langle\psi_0|\zeta^\dagger_{\mathbf{k}}\zeta_{\mathbf{k}}|\psi_0\rangle = \theta(k_F - |\mathbf{k}|).
\tag{A.17}
$$

The occupation distribution of the original fermionic operators can be easily computed remembering the definition of the quasiparticle renormalization factor (2.23) and reads

$$
\langle\Psi|c^\dagger_{\mathbf{k}\sigma}c_{\mathbf{k}\sigma}|\Psi\rangle = \langle\psi_0|\mathcal{P}^\dagger\,c^\dagger_{\mathbf{k}\sigma}c_{\mathbf{k}\sigma}\,\mathcal{P}|\psi_0\rangle
$$

$$
\begin{aligned}
&= \frac{1}{N} \sum_{\mathbf{R} \neq \mathbf{R}'} Z e^{i\mathbf{k}\cdot(\mathbf{R}-\mathbf{R}')} \langle \psi | c_{\mathbf{R}\sigma}^{\dagger} c_{\mathbf{R}'\sigma} | \psi \rangle + \frac{1}{N} \sum_{\mathbf{R}} \langle \psi | c_{\mathbf{R}\sigma}^{\dagger} c_{\mathbf{R}\sigma} | \psi \rangle \\
&= Z\theta(k_F - |\mathbf{k}|) + \frac{(1-Z)}{2}.
\end{aligned}
\tag{A.18}
$$

Therefore the occupation distribution displays a jump at the Fermi surface (k_F) equal to Z, in agreement with Landau's theory for a normal metal. We notice that from the definition of the renormalization factor for a time dependent Gutzwiller wavefunction (A.14), the above derivation remains valid and $Z(t)$ represents the jump at Fermi surface of the evolving momentum distribution $\langle \Psi(t) | c_{\mathbf{k}\sigma}^{\dagger} c_{\mathbf{k}\sigma} | \Psi(t) \rangle$. In this sense the quasiparticle weight can be compared with the non equilibrium DMFT results of Ref. [10].

Appendix B

Quantum Fluctuations plus feedback

B.1 Classical Adiabatic Dynamics and Slow Quantum Fluctuations for long ramps

Here we discuss the classical dynamics of the Gutzwiller variational parameters in the limit of slow ramps and the small quantum fluctuations around it. We start from the equations of motions

$$\dot{D} = \frac{\epsilon}{2} \frac{\partial Z}{\partial \phi} \tag{B.1}$$

$$\dot{\phi} = \frac{U(t)}{2} - \frac{\epsilon}{2} \frac{\partial Z}{\partial D} \tag{B.2}$$

where $\epsilon = \frac{U_c}{8}$ is the kinetic energy of the Fermi Sea in units of the critical repulsion U_c for the zero temperature equilibrium Mott transition, while $Z[D, \phi] = 8D \left(1 - 2D\right) \cos^2 \phi$ is the time dependent quasiparticle weight at half-filling. The above dynamics derives from a classical Hamiltonian which reads

$$E[D, \phi] = \frac{U(t)}{2} D - \frac{\epsilon}{2} Z[D, \phi] \tag{B.3}$$

When $U(t) \equiv U_f / U_c = u_f \leq 1$ the equilibrium solution

$$D_{gs} = \frac{1 - u_f}{4} \qquad \phi_{gs} = 0 \tag{B.4}$$

is a stationary point of the Hamiltonian. For slow variations of $U(t)$, that is for $\tau \to \infty$, we can assume to leading order the trajectory D, ϕ to follow the instantaneous minimum

$D_{gs}(u(t/\tau)), 0$ plus small oscillations that we want to compute. To this extent we expand E around D_{gs}, ϕ_{gs} up to the quadratic order (the first non vanishing). The result takes the form

$$E = E_{gs} + \frac{1}{2m(s)}\phi^2 + \frac{1}{2}\,m(s)\,\omega^2(s)\,(D - D_{gs}(s))^2 \qquad (B.5)$$

where we have introduced $s = t/\tau$ as well as the slowly varying mass and frequency which read

$$m(s) = \frac{8}{1 - (u_f\,s)^2} \qquad \omega(s) = \frac{1}{2}\sqrt{1 - (u_f\,s)^2} \qquad (B.6)$$

We notice that for $u_f < 1$ the frequency is always positive definite, while for ramps that cross the critical points it exists a time $t^\star = \tau/u_f < \tau$ at which the harmonic approximation breaks down. Let's consider the case $u_f < 1$. Then using results from classical adiabatic dynamics we can write to leading order

$$D_\tau(s) = D_{gs}(s) - \frac{1}{\tau}D'_{gs}(0)\sqrt{\frac{m(0)}{m(s)\omega(s)\omega(0)}}\,\sin\left(\tau\Omega(s)\right) \qquad (B.7)$$

and

$$\phi_\tau(s) = \frac{m(s)\,D'_{gs}(s)}{\tau} - \frac{D'_{gs}(0)}{\tau}\sqrt{\frac{m(s)\,m(0)\omega(s)}{\omega(0)}}\,\cos\left(\tau\Omega(s)\right) \qquad (B.8)$$

where we have defined $\Omega(s) = \int_0^s ds'\,\omega(s')$

$$\Omega(s) = \frac{1}{4u_f}\left(u_f s\,\sqrt{1 - (u_f s)^2} + \arcsin(u_f s)\right) \qquad (B.9)$$

After simple algebra we get for

$$D_\tau(s) = D_{gs}(s) + \frac{u_f}{2\tau}\left(1 - (u_f s)^2\right)^{1/4}\sin\Omega(s)\tau \qquad (B.10)$$

as well as

$$\phi_\tau(s) = \frac{1}{\tau}\left(-\frac{2u_f}{1 - (u_f s)^2} + \frac{2u_f}{(1 - (u_f s)^2)^{1/4}}\cos\Omega(s)\tau\right) \qquad (B.11)$$

The excitation energy $\Delta E(\tau) = E(t = \tau) - E_{gs}(u_f)$ can be easily evaluated in terms of $D_\tau(s = 1)$ and $\phi_\tau(s = 1)$ and the result gives the scaling $\Delta E_{exc} \sim 1/\tau^2$ quoted in the main text.

Let's now consider the effect of harmonic quantum fluctuations (QF) around the Gutzwiller dynamics in the regime of slow ramps [121]. The Hamiltonian of QF describe a set of harmonic oscillators with time dependent mass $m(t)$ and frequency $\omega_\mathbf{q}(t)$. In the limit of slow ramps, using the results just obtained for the mean field variational

parameters and the definition of $m(t), \omega_{\mathbf{q}}(t)$ in terms of θ, ϕ, we can write

$$m(t) = m^{gs}(u(t/\tau)) + \frac{\delta m_\tau(t)}{\tau^\delta} \tag{B.12}$$

$$\omega_{\mathbf{q}}(t) = \omega_{\mathbf{q}}^{gs}(u(t/\tau)) + \frac{\delta \omega_{\mathbf{q}\tau}(t)}{\tau^\delta} \, . \tag{B.13}$$

In order to discuss the dynamics of quantum fluctuations in the limit of slow ramps, we will for simplicity drop the index $\mathbf{q}$ since, at the gaussian level we are considering here each mode evolves independently. Hence, considering just a single mode we have

$$H(t) = \frac{p^2}{2m(t)} + \frac{1}{2} m(t) \, \omega^2(t) \, x^2 \tag{B.14}$$

Let's define the (explicitly time-dependent) annihilation/creation operators as

$$a = \sqrt{\frac{m(t)\omega(t)}{2}} \, x - i \sqrt{\frac{1}{2m(t)\omega(t)}} \, p \tag{B.15}$$

$$a^\dagger = \sqrt{\frac{m(t)\omega(t)}{2}} \, x + i \sqrt{\frac{1}{2m(t)\omega(t)}} \, p \tag{B.16}$$

which satisfy the coupled equations

$$\dot{a} = -i\omega \, a + \frac{1}{2}\eta(t) \, a^\dagger \tag{B.17}$$

$$\dot{a}^\dagger = i\omega \, a^\dagger + \frac{1}{2}\eta(t) \, a^\dagger \tag{B.18}$$

with $\eta = \partial_t \, (log \, m \, \omega)$. While a formal solution of this equations can be written in terms of time-ordered exponential we can perturbative expand the equation in power of η, the leading order term reading

$$\begin{aligned} a(t) &= e^{-i \int_0^t \omega(t')dt'} \, a(0) \\ &+ e^{-i \int_0^t \omega(t')dt'} \int_0^t dt' \, e^{2i \int_0^{t'} dt''\omega(t'')} \, \eta(t') \, a^\dagger(0) \end{aligned} \tag{B.19}$$

Using this result and the definitions (B.15) we can easily obtain the expression for coordinate and momentum operators, $x(t), p(t)$ in term of their initial values. Then, assuming the initial state to be in the ground state of $H(t = 0)$ we can obtain the results quoted in the main text for $\langle x^2 \rangle_t, \langle p^2 \rangle_t$.

B.2 Quantum Fluctuations plus feedback

In this Appendix we present a treatment of quantum fluctuations above the mean field dynamics that goes beyond the spin wave (gaussian) approximation of Ref. [103] and that leads to the the dynamical equations (B.26-B.27) we used in the main text.

As shown in [103] and recalled in the main text, in the approximation that the evolving state is a product of fermions and spins wavefunctions, the Hamiltonian (3.36), upon introducing the Fourier transform of the Ising spins

$$\sigma_{\mathbf{q}}^a = \sum_{\mathbf{R}} e^{-i\mathbf{q}\cdot\mathbf{R}} \sigma_{\mathbf{R}}^a$$

reads (in units of U_c)

$$\mathcal{H}_I = \frac{u}{4}\sigma_0^z - \frac{1}{8V}\sigma_0^x\sigma_0^x - \frac{1}{8V}\sum_{\mathbf{q}\neq 0}\gamma_{\mathbf{q}}\sigma_{\mathbf{q}}^x\sigma_{-\mathbf{q}}^x. \tag{B.20}$$

V is the number of sites and $\gamma_{\mathbf{q}} = \sum_{\mathbf{a}} e^{i\mathbf{q}\mathbf{a}}$, with $\mathbf{a}$ a vector which connects two nearest neighbor sites. The spin operators in momentum space satisfy the commutation relations

$$[\sigma_{\mathbf{q}}^a, \sigma_{-\mathbf{q}'}^b] = 2i\varepsilon_{abc}\sigma_{\mathbf{q}-\mathbf{q}'}^c. \tag{B.21}$$

In the same spirit of the spin-wave approximation we assume that the evolved state has a *condensate* component, which means that $\langle \sigma_0^a \rangle \sim V$ while, for any $\mathbf{q} \neq 0$, $\langle \sigma_{\mathbf{q}}^a \rangle = 0$ because of translational symmetry and $\langle \sigma_{\mathbf{q}}^a \sigma_{-\mathbf{q}}^b \rangle \sim V$. If the dynamics is able to drive the system towards equilibrium, we expect a damping of the $\mathbf{q} = 0$ sector.

Within such an approach and at the leading order in V, the only non-vanishing commutation relations are

$$\begin{aligned}
\left[\sigma_0^a, \sigma_0^b\right] &= 2i\varepsilon_{abc}\sigma_0^c \\
\left[\sigma_{\mathbf{q}}^a, \sigma_{-\mathbf{q}}^b\right] &= 2i\varepsilon_{abc}\sigma_0^c \\
\left[\sigma_{\mathbf{q}}^a, \sigma_0^b\right] &= 2i\varepsilon_{abc}\sigma_{\mathbf{q}}^c.
\end{aligned}$$

We evaluate then the equations of motions

$$i\partial_t \sigma_{\mathbf{q}}^a = \left[\sigma_{\mathbf{q}}^a, \mathcal{H}_I\right]$$

using the above approximate commutators. We find

$$i\partial_t \sigma_0^x = i\frac{u}{2}\sigma_0^y \tag{B.22}$$

$$i\partial_t \sigma_0^y = -i\frac{u}{2}\sigma_0^x + \frac{i}{4V}\left(\sigma_0^z \sigma_0^x + h.c.\right)$$

$$+\frac{i}{4V}\sum_{\mathbf{q}\neq 0}\gamma_{\mathbf{q}}\left(\sigma_{\mathbf{q}}^z \sigma_{-\mathbf{q}}^x + \sigma_{\mathbf{q}}^x \sigma_{-\mathbf{q}}^z\right)$$

$$i\partial_t \sigma_0^z = -\frac{i}{4V}\left(\sigma_0^x \sigma_0^y + h.c.\right)$$

$$-\frac{i}{4V}\sum_{\mathbf{q}\neq 0}\gamma_{\mathbf{q}}\left(\sigma_{\mathbf{q}}^x \sigma_{-\mathbf{q}}^y + \sigma_{\mathbf{q}}^y \sigma_{-\mathbf{q}}^x\right)$$

for the $\mathbf{q} = 0$ components, while for the $\mathbf{q} \neq 0$ ones

$$i\partial_t \sigma_{\mathbf{q}}^x = i\frac{u}{2}\sigma_{\mathbf{q}}^y \tag{B.23}$$

$$i\partial_t \sigma_{\mathbf{q}}^y = -i\frac{u}{2}\sigma_{\mathbf{q}}^x + \frac{i}{2V}\sigma_{\mathbf{q}}^z \sigma_0^x + \frac{i}{2V}\gamma_{\mathbf{q}}\sigma_{\mathbf{q}}^x \sigma_0^z$$

$$i\partial_t \sigma_{\mathbf{q}}^z = -\frac{i}{2V}\sigma_{\mathbf{q}}^y \sigma_0^x - \frac{i}{2V}\gamma_{\mathbf{q}}\sigma_{\mathbf{q}}^x \sigma_0^y.$$

We let then evolve the condensate component as a mean field, i.e. we assume for the $\mathbf{q} = 0$ spins the classical values

$$\sigma_0^x = VN\sin\theta\cos\phi \tag{B.24}$$

$$\sigma_0^y = VN\sin\theta\sin\phi$$

$$\sigma_0^z = VN\cos\theta$$

while for the $\mathbf{q} \neq 0$ we introduce the following quantity

$$\Delta_{ab}(\mathbf{q}, t) \equiv \frac{1}{2}\langle\sigma_{\mathbf{q}}^a \sigma_{-\mathbf{q}}^b + \sigma_{\mathbf{q}}^b \sigma_{-\mathbf{q}}^a\rangle. \tag{B.25}$$

From eq. (B.22) and (B.23) the dynamics of these quantities is easily derived and amounts to a set of non-linear coupled differential equations; the condensate dynamics satisfies

$$\dot{\theta} = \frac{N}{2}\sin\theta\cos\phi\sin\phi \tag{B.26}$$

$$+\frac{1}{2NV^2}\sum_{\mathbf{q}\neq 0}\gamma_{\mathbf{q}}\left(\sin\theta\Delta_{xy}(\mathbf{q}) + \cos\theta\sin\phi\Delta_{xz}(\mathbf{q})\right)$$

$$\sin\theta\dot{\phi} = -\frac{u}{2}\sin\theta + \frac{N}{2}\sin\theta\cos\theta\cos^2\phi$$

$$+\frac{1}{2NV^2}\cos\phi\sum_{\mathbf{q}\neq 0}\gamma_{\mathbf{q}}\Delta_{xz}(\mathbf{q})$$

$$\dot{N} = \frac{1}{2V^2}\sum_{\mathbf{q}\neq 0}\gamma_{\mathbf{q}}\left(-\cos\theta\Delta_{xy}(\mathbf{q}) + \sin\theta\sin\phi\Delta_{xz}(\mathbf{q})\right)$$

while the $\mathbf{q} \neq 0$ terms

$$
\begin{aligned}
\dot{\Delta}_{xx}(\mathbf{q}) &= u\Delta_{xy}(\mathbf{q}) \qquad\qquad\qquad\qquad\qquad\qquad\text{(B.27)}\\
\dot{\Delta}_{xy}(\mathbf{q}) &= \frac{1}{2}\left(-u + N\gamma_{\mathbf{q}}\cos\theta\right)\Delta_{xx}(\mathbf{q})\\
&\quad + \frac{N}{2}\sin\theta\cos\phi\Delta_{xz}(\mathbf{q}) + \frac{u}{2}\Delta_{yy}(\mathbf{q})\\
\dot{\Delta}_{xz}(\mathbf{q}) &= -\frac{N}{2}\gamma_{\mathbf{q}}\sin\theta\sin\phi\Delta_{xx}(\mathbf{q})\\
&\quad - \frac{N}{2}\sin\theta\cos\phi\Delta_{xy}(\mathbf{q}) + \frac{u}{2}\Delta_{yz}(\mathbf{q})\\
\dot{\Delta}_{yy}(\mathbf{q}) &= \left(-u + N\gamma_{\mathbf{q}}\cos\theta\right)\Delta_{xy}(\mathbf{q}) + N\sin\theta\cos\phi\Delta_{yz}(\mathbf{q})\\
\dot{\Delta}_{yz}(\mathbf{q}) &= -\frac{N}{2}\gamma_{\mathbf{q}}\sin\theta\sin\phi\Delta_{xy}(\mathbf{q})\\
&\quad + \frac{1}{2}\left(-u + N\gamma_{\mathbf{q}}\cos\theta\right)\Delta_{xz}(\mathbf{q})\\
&\quad - \frac{N}{2}\sin\theta\cos\phi\Delta_{yy}(\mathbf{q}) + \frac{N}{2}\sin\theta\cos\phi\Delta_{zz}(\mathbf{q})\\
\dot{\Delta}_{zz}(\mathbf{q}) &= -N\gamma_{\mathbf{q}}\sin\theta\sin\phi\Delta_{xz}(\mathbf{q}) - N\sin\theta\cos\phi\Delta_{yz}(\mathbf{q})
\end{aligned}
$$

By inspection of (B.26) one recognizes that if the feedback of the $\mathbf{q} \neq 0$ terms is neglected, the condensate dynamics is the same we obtained in the Gutzwiller approximation. In that approach indeed, N remained fixed during the dynamics ($N(t) = 1$), so that no damping was present for the condensate sector with a consequent impossibility of energy conservation. With respect to the results of Ref. [103], this new approach has the main advantage to conserve the mean value of energy during the dynamics,

$$
\partial_t\langle\mathcal{H}\rangle = 0
$$

as one can easily verify from eq (B.26-B.27).

In this work we considered quenches from the non-interacting system ($u_i = 0$); the initial conditions are then readily found from the solution of an Ising model in absence of transverse field and read:

$$
\begin{cases}
N(0) = & 1\\
\theta(0) = & \pi/2\\
\phi(0) = & 0
\end{cases}
\qquad
\begin{cases}
\Delta_{yy}(\mathbf{q},0) = & V\\
\Delta_{zz}(\mathbf{q},0) = & V\\
\Delta_{ab}(\mathbf{q},0) = & 0
\end{cases}
\qquad\text{(B.28)}
$$

Bibliography

[1] S. Iwai, M. Ono, A. Maeda, H. Matsuzaki, H. Kishida, H. Okamoto, and Y. Tokura. Ultrafast optical switching to a metallic state by photoinduced mott transition in a halogen-bridged nickel-chain compound. *Phys. Rev. Lett.*, 91:057401, Jul 2003.

[2] L. Perfetti, P. A. Loukakos, M. Lisowski, U. Bovensiepen, H. Berger, S. Biermann, P. S. Cornaglia, A. Georges, and M. Wolf. Time evolution of the electronic structure of $1t$-tas$_2$ through the insulator-metal transition. *Phys. Rev. Lett.*, 97:067402, Aug 2006.

[3] A. L. Cavalieri, N. Muller, Th. Uphues, V. S. Yakovlev, A. Baltuska, B. Horvath, Schmidt, L. Blumel, R. Holzwarth, S. Hendel, M. Drescher, U. Kleineberg, P. M. Echenique, R. Kienberger, F. Krausz, and U. Heinzmann. Attosecond spectroscopy in condensed matter. *Nature*, 449:1029, 2007.

[4] B. Mansart, D. Boschetto, S. Sauvage, A. Rousse, and M. Marsi. Mott transition in cr-doped V2O3 studied by ultrafast reflectivity: Electron correlation effects on the transient response. *EPL (Europhysics Letters)*, 92(3):37007, November 2010. ISSN 0295-5075.

[5] S. Dal Conte, C. Giannetti, G. Coslovich, F. Cilento, D. Bossini, T. Abebaw, F. Banfi, G. Ferrini, H. Eisaki, M. Greven, A. Damascelli, D. van der Marel, and F. Parmigiani. Disentangling the electronic and phononic glue in a high-tc superconductor. *Science*, 335(6076):1600–1603. ISSN 0036-8075, 1095-9203.

[6] D. Fausti, R. I. Tobey, N. Dean, S. Kaiser, A. Dienst, M. C. Hoffmann, S. Pyon, T. Takayama, H. Takagi, and A. Cavalleri. Light-induced superconductivity in a stripe-ordered cuprate. *Science*, 331(6014):189–191, 2011.

[7] A. Cavalleri, Th. Dekorsy, H. H. W. Chong, J. C. Kieffer, and R. W. Schoenlein. Evidence for a structurally-driven insulator-to-metal transition in vo2: A view from the ultrafast timescale. *Phys. Rev. B*, 70:161102, Oct 2004.

[8] Martin Eckstein and Marcus Kollar. Theory of time-resolved optical spectroscopy on correlated electron systems. *Phys. Rev. B*, 78:205119, Nov 2008.

[9] Martin Eckstein and Philipp Werner. Thermalization of a pump-excited mott insulator. *Phys. Rev. B*, 84:035122, Jul 2011.

[10] Martin Eckstein, Marcus Kollar, and Philipp Werner. Thermalization after an interaction quench in the hubbard model. *Phys. Rev. Lett.*, 103:056403, Jul 2009.

[11] Philipp Werner, Naoto Tsuji, and Martin Eckstein. Nonthermal symmetry-broken states in the strongly interacting hubbard model. *Phys. Rev. B*, 86:205101, Nov 2012.

[12] Immanuel Bloch, Jean Dalibard, and Wilhelm Zwerger. Many-body physics with ultracold gases. *Rev. Mod. Phys.*, 80:885–964, Jul 2008.

[13] Markus Greiner, Olaf Mandel, Theodor Hansch, and Immanuel Bloch. Collapse and revival of the matter wave field of a Bose-Einstein condensate. *Nature*, 419: 51, 2002.

[14] Toshiya Kinoshita, Trevor Wenger, and David S. Weiss. A quantum newton's cradle. *Nature*, 440:900, 2006.

[15] Hideo Aoki, Naoto Tsuji, Martin Eckstein, Marcus Kollar, Takashi Oka, and Philipp Werner. Nonequilibrium dynamical mean-field theory and its applications. *Rev. Mod. Phys.*, 86:779–837, Jun 2014.

[16] Anatoli Polkovnikov, Krishnendu Sengupta, Alessandro Silva, and Mukund Vengalattore. *Colloquium*: Nonequilibrium dynamics of closed interacting quantum systems. *Rev. Mod. Phys.*, 83:863–883, Aug 2011.

[17] Pasquale Calabrese and John Cardy. Time dependence of correlation functions following a quantum quench. *Phys. Rev. Lett.*, 96(13):136801, Apr 2006.

[18] J. M. Deutsch. Quantum statistical mechanics in a closed system. *Phys. Rev. A*, 43:2046–2049, Feb 1991.

[19] Mark Srednicki. Chaos and quantum thermalization. *Phys. Rev. E*, 50:888–901, Aug 1994.

[20] Marcos Rigol, Vanja Dunjko, and Maxim Olshanii. Thermalization and its mechanism for generic isolated quantum systems. *Nature*, 452, 2008.

[21] Marcos Rigol. Breakdown of thermalization in finite one-dimensional systems. *Phys. Rev. Lett.*, 103:100403, Sep 2009.

[22] Marcos Rigol. Quantum quenches and thermalization in one-dimensional fermionic systems. *Phys. Rev. A*, 80:053607, Nov 2009.

[23] Corinna Kollath, Andreas M. Läuchli, and Ehud Altman. Quench dynamics and nonequilibrium phase diagram of the bose-hubbard model. *Phys. Rev. Lett.*, 98: 180601, Apr 2007.

[24] S. R. Manmana, S. Wessel, R. M. Noack, and A. Muramatsu. Strongly correlated fermions after a quantum quench. *Phys. Rev. Lett.*, 98:210405, May 2007.

[25] M. C. Bañuls, J. I. Cirac, and M. B. Hastings. Strong and weak thermalization of infinite nonintegrable quantum systems. *Phys. Rev. Lett.*, 106:050405, Feb 2011.

[26] Giuseppe Carleo, Federico Becca, Marco Schiró, and Michele Fabrizio. Localization and glassy dynamics of many-body quantum systems. *Sci. Rep.*, 2, 2012.

[27] Ehsan Khatami, Marcos Rigol, Armando Relaño, and Antonio M. García-García. Quantum quenches in disordered systems: Approach to thermal equilibrium without a typical relaxation time. *Phys. Rev. E*, 85:050102, May 2012.

[28] Marcos Rigol, Vanja Dunjko, Vladimir Yurovsky, and Maxim Olshanii. Relaxation in a completely integrable many-body quantum system: An *Ab Initio* study of the dynamics of the highly excited states of 1d lattice hard-core bosons. *Phys. Rev. Lett.*, 98:050405, Feb 2007.

[29] M. A. Cazalilla. Effect of suddenly turning on interactions in the luttinger model. *Phys. Rev. Lett.*, 97:156403, Oct 2006.

[30] Martin Eckstein and Marcus Kollar. Nonthermal steady states after an interaction quench in the falicov-kimball model. *Phys. Rev. Lett.*, 100:120404, Mar 2008.

[31] Marcus Kollar and Martin Eckstein. Relaxation of a one-dimensional mott insulator after an interaction quench. *Phys. Rev. A*, 78:013626, Jul 2008.

[32] Amy C. Cassidy, Charles W. Clark, and Marcos Rigol. Generalized thermalization in an integrable lattice system. *Phys. Rev. Lett.*, 106:140405, Apr 2011.

[33] Simone Ziraldo and Giuseppe E. Santoro. Relaxation and thermalization after a quantum quench: Why localization is important. *Phys. Rev. B*, 87:064201, Feb 2013.

[34] D. M. Gangardt and M. Pustilnik. Correlations in an expanding gas of hard-core bosons. *Phys. Rev. A*, 77:041604, Apr 2008.

[35] B. Pozsgay, M. Mestyán, M. A. Werner, M. Kormos, G. Zaránd, and G. Takács. Correlations after quantum quenches in the XXZ spin chain: Failure of the generalized gibbs ensemble.

[36] J. Berges, Sz. Borsányi, and C. Wetterich. Prethermalization. *Phys. Rev. Lett.*, 93:142002, Sep 2004.

[37] Michael Moeckel and Stefan Kehrein. Crossover from adiabatic to sudden interaction quenches in the hubbard model: prethermalization and non-equilibrium dynamics. *New Journal of Physics*, 12(5):055016, 2010.

[38] Marcus Kollar, F. Alexander Wolf, and Martin Eckstein. Generalized gibbs ensemble prediction of prethermalization plateaus and their relation to nonthermal steady states in integrable systems. *Phys. Rev. B*, 84:054304, Aug 2011.

[39] Matteo Marcuzzi, Jamir Marino, Andrea Gambassi, and Alessandro Silva. Prethermalization in a nonintegrable quantum spin chain after a quench. *Phys. Rev. Lett.*, 111:197203, Nov 2013.

[40] Jürgen Berges, Alexander Rothkopf, and Jonas Schmidt. Nonthermal fixed points: Effective weak coupling for strongly correlated systems far from equilibrium. *Phys. Rev. Lett.*, 101:041603, Jul 2008.

[41] Naoto Tsuji, Martin Eckstein, and Philipp Werner. Nonthermal antiferromagnetic order and nonequilibrium criticality in the hubbard model. *Phys. Rev. Lett.*, 110:136404, Mar 2013.

[42] Steven R. White and Adrian E. Feiguin. Real-time evolution using the density matrix renormalization group. *Phys. Rev. Lett.*, 93:076401, Aug 2004.

[43] Robert Jördens, Niels Strohmaier, Kenneth Günter, Henning Moritz, and Tilman Esslinger. A mott insulator of fermionic atoms in an optical lattice. 455(7210): 204–207. ISSN 0028-0836.

[44] M. Eckstein, A. Hackl, S. Kehrein, M. Kollar, M. Moeckel, P. Werner, and F.A. Wolf. New theoretical approaches for correlated systems in nonequilibrium. 180 (1):217–235, . ISSN 1951-6355, 1951-6401.

[45] Michael Moeckel and Stefan Kehrein. Interaction quench in the hubbard model. *Phys. Rev. Lett.*, 100:175702, May 2008.

[46] Simone A. Hamerla and Götz S. Uhrig. Interaction quenches in the two-dimensional fermionic hubbard model. *Phys. Rev. B*, 89:104301, Mar 2014.

[47] Naoto Tsuji, Peter Barmettler, Hideo Aoki, and Philipp Werner. Nonequilibrium dynamical cluster theory. *Phys. Rev. B*, 90:075117, Aug 2014.

[48] Florian Goth and Fakher F. Assaad. Time and spatially resolved quench of the fermionic hubbard model showing restricted equilibration. *Phys. Rev. B*, 85: 085129, Feb 2012.

[49] Marco Schiró and Michele Fabrizio. Time-dependent mean field theory for quench dynamics in correlated electron systems. *Phys. Rev. Lett.*, 105:076401, Aug 2010.

[50] Simone A. Hamerla and Götz S. Uhrig. Dynamical transition in interaction quenches of the one-dimensional hubbard model. *Phys. Rev. B*, 87:064304, Feb 2013.

[51] Bruno Sciolla and Giulio Biroli. Quantum quenches and off-equilibrium dynamical transition in the infinite-dimensional bose-hubbard model. *Phys. Rev. Lett*, 105 (22):220401, 2010.

[52] A. Gambassi and P. Calabrese. Quantum quenches as classical critical films. *EPL (Europhysics Letters)*, 95(6):66007, 2011.

[53] Bruno Sciolla and Giulio Biroli. Dynamical transitions and quantum quenches in mean-field models. *J. Stat. Mech.*, page 11003, August 2011.

[54] Giacomo Mazza and Michele Fabrizio. Dynamical quantum phase transitions and broken-symmetry edges in the many-body eigenvalue spectrum. *Phys. Rev. B*, 86: 184303, Nov 2012.

[55] Malte Behrmann, Michele Fabrizio, and Frank Lechermann. Extended dynamic mott transition in the two-band hubbard model out of equilibrium. *Phys. Rev. B*, 88:035116, Jul 2013.

[56] Martin Eckstein, Takashi Oka, and Philipp Werner. Dielectric breakdown of mott insulators in dynamical mean-field theory. 105(14):146404, .

[57] Takashi Oka and Hideo Aoki. Ground-state decay rate for the zener breakdown in band and mott insulators. 95(13):137601, .

[58] Naoto Tsuji and Philipp Werner. Nonequilibrium dynamical mean-field theory based on weak-coupling perturbation expansions: Application to dynamical symmetry breaking in the hubbard model. *Phys. Rev. B*, 88:165115, Oct 2013.

[59] Martin Eckstein and Philipp Werner. Nonequilibrium dynamical mean-field calculations based on the noncrossing approximation and its generalizations. *Phys. Rev. B*, 82:115115, Sep 2010.

[60] Martin C. Gutzwiller. Effect of correlation on the ferromagnetism of transition metals. *Phys. Rev.*, 134:A923, 1964.

[61] Martin C. Gutzwiller. Correlation of electrons in a narrow s band. *Phys. Rev.*, 137:A1726, 1965.

[62] W. F. Brinkman and T. M. Rice. Application of Gutzwiller's Variational Method to the Metal-Insulator Transition. *Phys. Rev. B*, 2:4302, 1970.

[63] Walter Metzner and Dieter Vollhardt. Analytic calculation of ground-state properties of correlated fermions with the gutzwiller wave function. *Phys. Rev. B*, 37: 7382–7399, May 1988.

[64] Nicola Lanatà, Hugo U. R. Strand, Xi Dai, and Bo Hellsing. Efficient implementation of the gutzwiller variational method. *Phys. Rev. B*, 85:035133, Jan 2012.

[65] XiaoYu Deng, Lei Wang, Xi Dai, and Zhong Fang. Local density approximation combined with gutzwiller method for correlated electron systems: Formalism and applications. *Phys. Rev. B*, 79:075114, Feb 2009.

[66] Giovanni Borghi. *Gutzwiller Approximation applied to inhomogeneous lattice models and solid-state systems*. PhD thesis, International School for Advanced Studies (SISSA), 2011.

[67] Patrice André, M. Schiró, and Michele Fabrizio. Lattice and surface effects in the out-of-equilibrium dynamics of the hubbard model. *Phys. Rev. B*, 85:205118, May 2012.

[68] Michele Fabrizio. The out-of-equilibrium time-dependent gutzwiller approximation. In Veljko Zlatic and Alex Hewson, editors, *New Materials for Thermoelectric Applications: Theory and Experiment*, NATO Science for Peace and Security Series - B: Physics and Biophysics, pages 247–272. Springer, 2013.

[69] Antoine Georges, Gabriel Kotliar, Werner Krauth, and Marcelo J. Rozenberg. Dynamical mean-field theory of strongly correlated fermion systems and the limit of infinite dimensions. *Rev. Mod. Phys.*, 68:13, 1996.

[70] J. Hubbard. Electron correlations in narrow energy bands. *Proc. R. Soc. Lond.*, 276, 1963.

[71] J. Kanamori. Electron correlation and ferromagnetism of transition metals. *Progr. Theor. Phys.*, 30:275, 1963.

[72] Frank Lechermann, Antoine Georges, Gabriel Kotliar, and Olivier Parcollet. Rotationally invariant slave-boson formalism and momentum dependence of the quasiparticle weight. *Phys. Rev. B*, 76:155102, Oct 2007.

[73] Jörg Bünemann, Florian Gebhard, and Rüdiger Thul. Landau-gutzwiller quasiparticles. *Phys. Rev. B*, 67:075103, Feb 2003.

[74] J. Bünemann, F. Gebhard, T. Ohm, R. Umstätter, S. Weiser, W. Weber, R. Claessen, D. Ehm, A. Harasawa, A. Kakizaki, A. Kimura, G. Nicolay, S. Shin, and V. N. Strocov. Atomic correlations in itinerant ferromagnets: Quasi-particle bands of nickel. 61(5):667. ISSN 0295-5075.

[75] V. Eyert. vo$_2$: A novel view from band theory. *Phys. Rev. Lett.*, 107:016401, Jun 2011.

[76] G. Sangiovanni, A. Toschi, E. Koch, K. Held, M. Capone, C. Castellani, O. Gunnarsson, S.-K. Mo, J. W. Allen, H.-D. Kim, A. Sekiyama, A. Yamasaki, S. Suga, and P. Metcalf. Static versus dynamical mean-field theory of mott antiferromagnets. *Phys. Rev. B*, 73:205121, May 2006.

[77] Matteo Sandri, Massimo Capone, and Michele Fabrizio. Finite-temperature gutzwiller approximation and the phase diagram of a toy model for V$_2$O$_3$. *Phys. Rev. B*, 87:205108, May 2013.

[78] Dénes Petz. A survey of certain trace inequalities. In *Functional analysis and operator theory*, pages 287–298. Banach Center Publications, 1994.

[79] Sandro Sorella. Wave function optimization in the variational Monte Carlo method. *Phys. Rev. B*, 71(24):241103, Jun 2005.

[80] J. Bünemann, W. Weber, and F. Gebhard. Multiband gutzwiller wave functions for general on-site interactions. *Phys. Rev. B*, 57:6896–6916, Mar 1998.

[81] Wan-Sheng Wang, Xiang-Mei He, Da Wang, Qiang-Hua Wang, Z. D. Wang, and F. C. Zhang. Finite-temperature gutzwiller projection for strongly correlated electron systems. *Phys. Rev. B*, 82:125105, Sep 2010.

[82] P.A.M. Dirac. Note on exchange phenomena in the thomas atom. *Proc. Cambridge Philos. Soc.*, 26:376, 1930.

[83] Nicola Lanatà, Paolo Barone, and Michele Fabrizio. Fermi-surface evolution across the magnetic phase transition in the kondo lattice model. *Phys. Rev. B*, 78:155127, Oct 2008.

[84] Nicola Lanatà, Yong-Xin Yao, Cai-Zhuang Wang, Kai-Ming Ho, Jörg Schmalian, Kristjan Haule, and Gabriel Kotliar. The y-α iso-structural transition in cerium, a critical element. arXiv:1305.3950, 2013.

[85] David Chen, Matthew White, Cecilia Borries, and Brian DeMarco. Quantum quench of an atomic mott insulator. *Phys. Rev. Lett.*, 106:235304, Jun 2011.

[86] Giulio Biroli, Corinna Kollath, and Andreas M. Läuchli. Effect of rare fluctuations on the thermalization of isolated quantum systems. *Phys. Rev. Lett.*, 105(25): 250401, Dec 2010.

[87] Elena Canovi, Davide Rossini, Rosario Fazio, Giuseppe E. Santoro, and Alessandro Silva. Quantum quenches, thermalization, and many-body localization. *Phys. Rev. B*, 83:094431, Mar 2011.

[88] Michael Moeckel and Stefan Kehrein. Real-time evolution for weak interaction quenches in quantum systems. *Annals of Physics*, 324(10):2146 – 2178, 2009.

[89] Takuya Kitagawa, Adilet Imambekov, Jörg Schmiedmayer, and Eugene Demler. The dynamics and prethermalization of one-dimensional quantum systems probed through the full distributions of quantum noise. *New Journal of Physics*, 13(7): 073018, 2011.

[90] Anatoli Polkovnikov and Vladimir Gritsev. Breakdown of the adiabatic limit in low-dimensional gapless systems. *Nature Physics*, 4:477, 2008.

[91] Max Born and Vladimir Fock. *Z. Phys.*, 51:165, 1928.

[92] Lev Davidovich Landau. *Phys. Z. Sowjetunion*, 2:46, 1932.

[93] Clarence Zener. *Proc. R. Soc.*, 137(833):696, 1932.

[94] Ettore Majorana. Atomi orientati in campo magnetico variabile. *Il Nuovo Cimento (1924-1942)*, 9:43–50, 1932. ISSN 1827-6121. 10.1007/BF02960953.

[95] E. C. G. Stueckelberg. *Helvetica Physica Acta.*, 5:369, 1932.

[96] P. Nozieres. *Theory of Interacting Fermi Systems*. Advanced Book Classics, 1997.

[97] Anatoli Polkovnikov. Universal adiabatic dynamics in the vicinity of a quantum critical point. *Phys. Rev. B*, 72:161201, Oct 2005.

[98] C. De Grandi, V. Gritsev, and A. Polkovnikov. Quench dynamics near a quantum critical point. *Phys. Rev. B*, 81:012303, Jan 2010.

[99] Nikolai Eurich, Martin Eckstein, and Philipp Werner. Optimal ramp shapes for the fermionic hubbard model in infinite dimensions. *Phys. Rev. B*, 83:155122, Apr 2011.

[100] Armin Rahmani and Claudio Chamon. Optimal control for unitary preparation of many-body states: Application to luttinger liquids. *Phys. Rev. Lett.*, 107:016402, Jul 2011.

[101] Jean-Sébastien Bernier, Guillaume Roux, and Corinna Kollath. Slow quench dynamics of a one-dimensional bose gas confined to an optical lattice. *Phys. Rev. Lett.*, 106:200601, May 2011.

[102] Stefan S. Natu, Kaden R. A. Hazzard, and Erich J. Mueller. Local versus global equilibration near the bosonic mott-insulator˘superfluid transition. *Phys. Rev. Lett.*, 106:125301, Mar 2011.

[103] Marco Schiró and Michele Fabrizio. Quantum quenches in the hubbard model: Time-dependent mean-field theory and the role of quantum fluctuations. *Phys. Rev. B*, 83:165105, Apr 2011.

[104] F Gebhard. *The Mott Metal-Insulator Transition.* Springer, 1997.

[105] Michael Stark and Marcus Kollar. Kinetic description of thermalization dynamics in weakly interacting quantum systems.

[106] Martin Eckstein, Marcus Kollar, and Philipp Werner. Interaction quench in the hubbard model: Relaxation of the spectral function and the optical conductivity. *Phys. Rev. B*, 81:115131, Mar 2010.

[107] Bruno Sciolla and Giulio Biroli. Quantum quenches, dynamical transitions and off-equilibrium quantum criticality. *arXiv:1211.2572 [cond-mat, physics:quant-ph]*, November 2012.

[108] Martin Eckstein and Marcus Kollar. Near-adiabatic parameter changes in correlated systems: influence of the ramp protocol on the excitation energy. *New Journal of Physics*, 12(5):055012, 2010.

[109] Jacek Dziarmaga. Dynamics of a quantum phase transition: Exact solution of the quantum ising model. *Phys. Rev. Lett.*, 95:245701, Dec 2005.

[110] Wojciech H. Zurek, Uwe Dorner, and Peter Zoller. Dynamics of a quantum phase transition. *Phys. Rev. Lett.*, 95:105701, Sep 2005.

[111] Michael Kolodrubetz, Bryan K. Clark, and David A. Huse. Nonequilibrium dynamic critical scaling of the quantum ising chain. *Phys. Rev. Lett.*, 109:015701, Jul 2012.

[112] Anushya Chandran, Amir Erez, Steven S. Gubser, and S. L. Sondhi. Kibble-zurek problem: Universality and the scaling limit. *Phys. Rev. B*, 86:064304, Aug 2012.

[113] Victor Bapst and Guilhem Semerjian. On quantum mean-field models and their quantum annealing. *Journal of Statistical Mechanics: Theory and Experiment*, 2012(06):P06007, June 2012. ISSN 1742-5468.

[114] Guilhem Semerjian. (private communication).

[115] A. P. Itin and P. Törmä. Dynamics of quantum phase transitions in dicke and lipkin-meshkov-glick models. *arXiv:0901.4778 [cond-mat]*, January 2009.

[116] Frank Pollmann, Subroto Mukerjee, Andrew G. Green, and Joel E. Moore. Dynamics after a sweep through a quantum critical point. *Phys. Rev. E*, 81:020101, Feb 2010.

[117] S. D. Huber and A. Rüegg. Dynamically generated double occupancy as a probe of cold atom systems. *Phys. Rev. Lett.*, 102:065301, 2009.

[118] A. Rüegg, S. D. Huber, and M. Sigrist. Z2-slave-spin theory for strongly correlated fermions. *Phys. Rev. B*, 81:155118, 2010.

[119] L. de'Medici, A. Georges, and S. Biermann. Orbital-selective mott transition in multiband systems: Slave-spin representation and dynamical mean-field theory. *Phys. Rev. B*, 72(20):205124, Nov 2005.

[120] S. R. Hassan and L. de' Medici. Slave spins away from half filling: Cluster mean-field theory of the hubbard and extended hubbard models. *Phys. Rev. B*, 81(3): 035106, Jan 2010.

[121] Spyros Sotiriadis and John Cardy. Quantum quench in interacting field theory: A self-consistent approximation. *Phys. Rev. B*, 81:134305, Apr 2010.

[122] P. Beaud, S. L. Johnson, E. Vorobeva, U. Staub, R. A. De Souza, C. J. Milne, Q. X. Jia, and G. Ingold. Ultrafast structural phase transition driven by photoinduced melting of charge and orbital order. *Phys. Rev. Lett.*, 103:155702, Oct 2009.

[123] Andrei Kirilyuk, Alexey V. Kimel, and Theo Rasing. Ultrafast optical manipulation of magnetic order. *Rev. Mod. Phys.*, 82:2731–2784, Sep 2010.

[124] R. Chitra and G. Kotliar. Dynamical mean field theory of the antiferromagnetic metal to antiferromagnetic insulator transition. *Phys. Rev. Lett.*, 83:2386–2389, Sep 1999.

[125] Michael Brunner, Fakher F. Assaad, and Alejandro Muramatsu. Single-hole dynamics in the $t - j$ model on a square lattice. *Phys. Rev. B*, 62:15480–15492, Dec 2000.

[126] C. Zhou, D. M. Newns, J. A. Misewich, and P. C. Pattnaik. A field effect transistor based on the mott transition in a molecular layer. 70(5):598–600. ISSN 0003-6951, 1077-3118.

[127] M. Nakano, K. Shibuya, D. Okuyama, T. Hatano, S. Ono, M. Kawasaki, Y. Iwasa, and Y. Tokura. Collective bulk carrier delocalization driven by electrostatic surface charge accumulation. 487(7408):459–462. ISSN 0028-0836.

[128] Pablo Stoliar, Laurent Cario, Etiene Janod, Benoit Corraze, Catherine Guillot-Deudon, Sabrina Salmon-Bourmand, Vincent Guiot, Julien Tranchant, and Marcelo Rozenberg. Universal electric-field-driven resistive transition in narrow-gap mott insulators. 25(23):3222–3226. ISSN 1521-4095.

[129] Martin Eckstein and Philipp Werner. Photoinduced states in a mott insulator. *Phys. Rev. Lett.*, 110:126401, Mar 2013.

[130] Takashi Oka, Ryotaro Arita, and Hideo Aoki. Breakdown of a mott insulator: A nonadiabatic tunneling mechanism. 91(6):066406.

[131] Takashi Oka and Hideo Aoki. Dielectric breakdown in a mott insulator: Many-body schwinger-landau-zener mechanism studied with a generalized bethe ansatz. 81(3):033103, .

[132] F. Heidrich-Meisner, I. González, K. A. Al-Hassanieh, A. E. Feiguin, M. J. Rozenberg, and E. Dagotto. Nonequilibrium electronic transport in a one-dimensional mott insulator. 82(20):205110.

[133] Alexander I. Poteryaev, Michel Ferrero, Antoine Georges, and Olivier Parcollet. Effect of crystal-field splitting and interband hybridization on the metal-insulator transitions of strongly correlated systems. *Phys. Rev. B*, 78:045115, Jul 2008.

[134] G. Kotliar, S. Y. Savrasov, K. Haule, V. S. Oudovenko, O. Parcollet, and C. A. Marianetti. Electronic structure calculations with dynamical mean-field theory. *Rev. Mod. Phys.*, 78:865–951, Aug 2006.

[135] S. Biermann, F. Aryasetiawan, and A. Georges. First-principles approach to the electronic structure of strongly correlated systems: Combining the *gw* approximation and dynamical mean-field theory. *Phys. Rev. Lett.*, 90:086402, Feb 2003.

[136] D. B. McWhan, A. Menth, J. P. Remeika, W. F. Brinkman, and T. M. Rice. Metal-insulator transitions in pure and doped V_2O_3. *Phys. Rev. B*, 7:1920–1931, Mar 1973.

[137] D. B. McWhan and J. P. Remeika. Metal-insulator transition in $(V_{1-x}Cr_x)_2O_3$. *Phys. Rev. B*, 2:3734–3750, Nov 1970.

[138] R. M. Moon. Antiferromagnetism in V_2O_3. *Phys. Rev. Lett.*, 25:527–529, Aug 1970.

[139] J.-H. Park, L. H. Tjeng, A. Tanaka, J. W. Allen, C. T. Chen, P. Metcalf, J. M. Honig, F. M. F. de Groot, and G. A. Sawatzky. Spin and orbital occupation and phase transitions in V_2O_3. *Phys. Rev. B*, 61:11506–11509, May 2000.

[140] L. Paolasini, C. Vettier, F. de Bergevin, F. Yakhou, D. Mannix, A. Stunault, W. Neubeck, M. Altarelli, M. Fabrizio, P. A. Metcalf, and J. M. Honig. Orbital occupancy order in V_2O_3: Resonant x-ray scattering results. *Phys. Rev. Lett.*, 82: 4719–4722, Jun 1999.

[141] L F Mattheiss. Band properties of metallic corundum-phase V_2O_3. *Journal of Physics: Condensed Matter*, 6(32):6477, 1994.

[142] Nicola Manini, Giuseppe E. Santoro, Andrea Dal Corso, and Erio Tosatti. Sensitivity of the mott transition to noncubic splitting of the orbital degeneracy: Application to $NH_3K_3C_{60}$. *Phys. Rev. B*, 66:115107, Sep 2002.

[143] Alexander I. Poteryaev, Jan M. Tomczak, Silke Biermann, Antoine Georges, Alexander I. Lichtenstein, Alexey N. Rubtsov, Tanusri Saha-Dasgupta, and Ole K. Andersen. Enhanced crystal-field splitting and orbital-selective coherence induced by strong correlations in V_2O_3. *Phys. Rev. B*, 76:085127, Aug 2007.

[144] M. K. Stewart, D. Brownstead, S. Wang, K. G. West, J. G. Ramirez, M. M. Qazilbash, N. B. Perkins, I. K. Schuller, and D. N. Basov. Insulator-to-metal transition and correlated metallic state of V_2O_3 investigated by optical spectroscopy. *Phys. Rev. B*, 85:205113, May 2012.

[145] Daniel Grieger, Christoph Piefke, Oleg E. Peil, and Frank Lechermann. Approaching finite-temperature phase diagrams of strongly correlated materials: A case study for V_2O_3. *Phys. Rev. B*, 86:155121, Oct 2012.

[146] Luca de' Medici, Jernej Mravlje, and Antoine Georges. Janus-faced influence of hund's rule coupling in strongly correlated materials. *Phys. Rev. Lett.*, 107:256401, Dec 2011.

[147] N. I. M. Gould, D. Orban, and Ph. L. Toint. Galahad, a library of thread-safe fortran 90 packages for large-scale nonlinear optimization. *ACM Trans.actions on Mathematical Software*, 29:353, 2003.

[148] F. Rodolakis, P. Hansmann, J.-P. Rueff, A. Toschi, M. W. Haverkort, G. Sangiovanni, A. Tanaka, T. Saha-Dasgupta, O. K. Andersen, K. Held, M. Sikora, I. Alliot, J.-P. Itié, F. Baudelet, P. Wzietek, P. Metcalf, and M. Marsi. Inequivalent routes across the mott transition in V_2O_3 explored by x-ray absorption. *Phys. Rev. Lett.*, 104:047401, Jan 2010.

[149] Michel Caffarel and Werner Krauth. Exact diagonalization approach to correlated fermions in infinite dimensions: Mott transition and superconductivity. *Phys. Rev. Lett.*, 72:1545–1548, Mar 1994.

[150] Massimo Capone, Luca de' Medici, and Antoine Georges. Solving the dynamical mean-field theory at very low temperatures using the lanczos exact diagonalization. *Phys. Rev. B*, 76:245116, Dec 2007.

[151] P. Hansmann, A. Toschi, G. Sangiovanni, T. Saha-Dasgupta, S. Lupi, M. Marsi, and K. Held. Mott–hubbard transition in v2o3 revisited. 250(7):1251–1264. ISSN 1521-3951.

[152] Claudio Attaccalite and Michele Fabrizio. Properties of gutzwiller wave functions for multiband models. *Phys. Rev. B*, 68:155117, Oct 2003.

[153] Malte Behrmann and Frank Lechermann. Spin oscillations triggered by strongly correlated t_{2g} electrons at the timescale of electron-electron interactions.

[154] Walter Metzner and Dieter Vollhardt. Correlated lattice fermions in d=∞ dimensions. *Phys. Rev. Lett.*, 62:324–327, Jan 1989.